Instituto de Física de Cantabria (IFCA), CSIC-Universidad de Cantabria

Patrones de circulación atmosférica y cambio climático: un análisis exhaustivo de la clasificación de Jenkinson-Collison para su aplicación en la evaluación de modelos basada en procesos.

Atmospheric Circulation Patterns and Climate Change: A Comprehensive Analysis of the Jenkinson-Collison Classification for Its Application in Process-based Model Evaluation

Programa de Doctorado en Ciencia y Tecnología

Presentada por:

Juan Antonio Fernández de la Granja

Bajo la dirección de:

Ana Casanueva Vicente

Joaquín Bedia Jiménez

Julio 2025

Patrones de circulación atmosférica y cambio climático: un análisis exhaustivo de la clasificación de Jenkinson-Collison para su aplicación en la evaluación de modelos basada en procesos.

Atmospheric Circulation Patterns and Climate Change: A Comprehensive Analysis of the Jenkinson-Collison Classification for Its Application in Process-based Model Evaluation

Juan Antonio Fernández de la Granja

Santander Meteorology Group

Institute of Physics of Cantabria

(CSIC–University of Cantabria)

Santander, Spain

July 2025

'La tecnología por sí sola no basta. También tenemos que poner el corazón..."

– Jane Goodall

Acknowledgements

This PhD Thesis has been developed in the framework of the national project "*Contribucion española al ATLAS del IPCC-AR6: Desarrollo y problemas cientificos*" (ATLAS, PID2019-111481RB-I00), through a grant from the FPI program (PRE2020-094728), funded by the *Ministerio de Ciencia e Innovación – Agencia Estatal de Investigación* (MCIN/AEI/10.13039/501100011033) and ESF investing in your future. I also benefited from a 3-months long stay in the Institute of Atmospheric Physics (IAP) of the Czech Academy of Sciences (CAS) in Prague (Czech Republic); within the FPI program (PRE2020-094728). I acknowledge funding from the Project INDECIS, part of European Research Area for Climate Services Consortium (ERA4CS) with co-funding by the European Union Grant 690462, for funding me in the previous months before the start of this Thesis. I also gratefully acknowledge the support of the CSIC's Interdisciplinary Thematic Platform Clima (PTI-Clima), funded by the Spanish Ministry for the Ecological Transition and the Demographic Challenge (MITECO) and the European Commission's NextGenerationEU programme (Regulation EU 2020/2094), for providing financial assistance to attend some of the conferences listed in this thesis (Sec. 7.2).

Data availability is the basic premise for research. In this regard, I acknowledge the World Climate Research Programme's Working Group on Coupled Modelling, which is responsible for CMIP, and I thank the climate modelling groups (listed in Tables 5.1 and 6.1) for producing and making available their model output, used in Chapters 5 and 6. Also, I would like to acknowledge the Earth System Grid Federation (ESGF) for the implementation and maintenance of a robust data infrastructure that enables open and efficient access to CMIP datasets, which was essential for the development of this Thesis.

I am grateful to Sixto Herrera (University of Cantabria), for sharing the Blocking Index Data used in this study and the NOAA Climate Prediction Center for making publicly available the monthly teleconnection indices; to José M. Gutiérrez, who provided useful comments along the different stages of this Thesis; to the Santander Climate Data Service (http://scds.es) and our colleagues Antonio Cofiño and Ezequiel Cimadevilla for their support in data management. I am deeply grateful to Radan Huth and Jan Stryhal for their invaluable guidance, insightful teaching, and generous support during my research stay at the Institute of Atmospheric Physics

in Prague. Their mentorship greatly enriched both the scientific and personal dimensions of this experience. I also thank the various anonymous reviewers who provided insightful comments on the early versions of the published manuscripts that conform the main body of this PhD Thesis, listed in Section 7.2.

A continuación, de una forma más personal, y en español, me gustaría expresar mi más profundo agradecimiento, en primer lugar, a mis directores, Ana Casanueva y Joaquín Bedia, no solo por su valiosa guía científica a lo largo de esta Tesis Doctoral, sino, sobre todo, por haber roto con todos los estereotipos que suelen rodear este proceso. Muy lejos de sentir soledad o abandono, ellos siempre estuvieron cerca, con una implicación constante y un acompañamiento que muchas veces trascendió lo profesional para convertirse en un apoyo genuinamente amistoso. Supieron ver en mí un potencial que ni yo mismo reconocía, motivándome a desarrollarlo con confianza y perseverancia. Me han enseñado no solo habilidades prácticas esenciales, sino también formas de pensar y afrontar la vida profesional que sin duda llevaré conmigo. Gracias a ellos, he redescubierto el valor de la rigurosidad y el compromiso con el trabajo bien hecho, una motivación que siento más viva que nunca.

Quiero dar las gracias a mi familia, especialmente a mis padres, que me han apoyado incondicionalmente todos estos años y han hecho posible que haya llegado a donde estoy ahora.

Quiero también agradecer a mis abuelos todo el amor y ayuda proporcionados estos 11 años de andadura universitaria de Grado, Máster y Doctorado, en la que me han acogido en su casa durante los primeros años. Habéis sido unos padres para mí. Ojalá estuvieras aquí aún abuelo...

A Inés. Es imposible expresar con palabras lo mucho que me das, enseñas y haces mejor cada día, y más aún, todo lo que te quiero (no te imaginas lo que te espera el día de la Defensa...)

Y no con menos importancia, a mis hermanos, amigos, compañeros del *Santander Meteorology Group*, etc., por poder contar siempre con todos ellos y ser un apoyo fundamental para mi. No puedo terminar sin una mención especial a Óscar, el universo no me ha podido conceder un mejor compañero de despacho que él.

También agradecer a todas aquellas personas que de distinta manera me han ayudado a la realización de esta Tesis...

Contents

List of Figures

List of Tables

Acronyms

AAO Antarctic Oscillation. x, 57

AR4 Fourth Assessment Report. viii, 11

AR5 Fifth Assessment Report. viii, 11

AR6 Sixth Assessment Report. viii, 12

ATL Atlantic Blocking Region. ix, 50

BI Blocking Index. 31

CMIP Coupled Model Intercomparison Project. 6

CMIP5 Coupled Model Intercomparison Project Phase 5. xiii, 80

CMIP6 Coupled Model Intercomparison Project Phase 6. xiii, 80

CORDEX Coordinated Regional Downscaling Experiment. 14

CT Circulation Types. 24

DJF December–January–February or boreal winter. ix, 47, 80

EA East Atlantic. 18

EAIS East Antarctic Ice Sheet. 67

ECA Extratropical Cyclone Activity. 26

ECMWF European Centre for Medium-Range Weather Forecasts. 4

ECS Equilibrium Climate Sensitivity. 9

ERA-20C ECMWF 20th Century Reanalysis. 29

ERA-Interim ECMWF ERA Interim Reanalysis. 29

ERA5 ECMWF Reanalysis 5. 29

EUR Western Europe Blocking Region. ix, 50

FAR First Assessment Report. viii, 11

GCMs Global Climate Models. 6

GSAT Global Surface Air Temperature. 39

GWL Global Warming Level. 39

IPCC Intergovernmental Panel on Climate Change. 3

ITCZ Intertropical Convergence Zone. 48

JC-WT Jenkinson–Collison Weather Type. 25

JJA June–July–August or boreal summer. ix, 47, 81

JMA Japan Meteorological Agency. 30

JRA-55 Japanese 55-year Reanalysis. 30

LWT Lamb Weather Type. 25

MAE Mean Absolute Error. 80

MAM March–April–May or boreal spring. 80

NAO North Atlantic Oscillation. 18

NCEP NCEP–NCAR Reanalysis 1. 30

PID Persistent Identifier. xvii, 99

PMFs Probability Mass Functions. 37

PNA Pacific–North American Pattern. x, 57

RCMs Regional Climate Models. 14

RCPs Representative Concentration Pathways. 10

RUS Eastern Europe Blocking Region. ix, 50

SAR Second Assessment Report. viii, 11

SCAND Scandinavian Pattern. 18

SLP Sea Level Pressure. 16

SOM Self-Organizing Map. 25

SON September–October–November or boreal autumn. 86

SRES Special Report on Emissions Scenarios. viii, 12

SSPs Shared Socioeconomic Pathways. 11

SST Sea Surface Temperature. 22

TAR Third Assessment Report. viii, 11

ToE Time of Emergence. 40

TPM Transition Probability Matrix. 38

TPMS Transition Probability Matrix Score. 38

UN United Nations. 3

WCRP World Climate Research Programme. 14

WT Weather Types. 24

Resumen en Español

Contexto y motivación

El cambio climático es una realidad que nos afecta a todos. Según el Panel Intergubernamental de Expertos sobre Cambio Climático (IPCC[1] por sus siglas en inglés), la temperatura media de la superficie global aumentó aproximadamente 1.1°C entre 2011 y 2020 en comparación con el período preindustrial 1850–1900, mayormente provocado por las emisiones de gases de efecto invernadero derivadas de actividades socioeconómicas humanas. Este calentamiento da lugar a eventos meteorológicos extremos cada vez más frecuentes e intensos (p. ej. olas de calor, lluvias torrenciales o sequías), con impactos en los ecosistemas, las economías y las comunidades a nivel mundial (IPCC, 2021). No obstante, las diferentes regiones del planeta no están afectadas de igual manera por el cambio climático. Algunas zonas son más vulnerables que otras debido a variaciones regionales en la geografía, los diferentes sistemas climáticos y otros factores socioeconómicos. Los informes de evaluación más recientes del IPCC indican que las variaciones en temperatura y precipitación en el futuro no se producirán de forma uniforme en todo el globo. El IPCC reconoce estas diferencias y subraya la importancia de contar con datos climáticos regionales con amplio detalle para guiar eficazmente en los planes políticos de adaptación y mitigación (véase la Fig. 1.1).

Las proyecciones de cambio climático del IPCC son posibles gracias al uso de un amplio volumen de modelos climáticos globales (GCMs, por sus siglas en inglés, véase Sec. 1.2.1). Estos modelos son herramientas computacionales muy populares en el estudio del cambio climático, ya que son capaces de reproducir condiciones pasadas y proyectar el clima futuro basándose en una representación física del sistema climático. Los GCMs han evolucionado desde los años 60 (Manabe and Wetherald, 1967), desde simples esquemas atmosféricos a complejos *Earth System Models* (ESMs), incluyendo componentes relacionadas con océanos, criosfera, biogeoquímica y química atmosférica (Mcguffie and Henderson-Sellers, 2005; Edwards, 2011). El desarrollo de los GCMs ha sido impulsado por iniciativas como el proyecto CMIP (*Coupled Model Intercom-*

[1]El IPCC es un organismo de las Naciones Unidas que proporciona evaluaciones sobre el estado del arte en materia del cambio climático, con el fin de orientar en decisiones políticas de mitigación del cambio climático y acción global.

parison Project en inglés), cuya sexta fase (CMIP6) supone el estado del arte en modelización climática, mejorando notablemente en resolución espacial y en la representación de procesos físicos clave (Eyring et al., 2016). Sin embargo, a pesar de estos avances, los GCMs aún presentan limitaciones importantes, como errores sistemáticos e incertidumbres en sus proyecciones (Maraun et al., 2010) o, en su mayoría, una resolución espacial demasiado grosera como para simular fielmente el clima regional y local.

En relación a la limitación de la resolución grosera de los GCMs (muchos de ellos en torno a 100km× 100km), los investigadores en este campo, bajo iniciativas coordinadas como CORDEX (COordinated Regional Downscaling EXperiment en inglés; Giorgi et al., 2009; Jones et al., 2011) han desarrollado una serie de técnicas para regionalizar estos modelos globales, pudiendo convertir las proyecciones climáticas globales en predicciones a mayor resolución (típicamente 25km×25km ó 12km×12km) o incluso a nivel puntual. Estas técnicas de regionalización, o *downscaling* son esenciales para comprender cómo el cambio climático afectará específicamente a distintas regiones, y así que comunidades enteras y responsables políticos puedan tomar decisiones que salven vidas y el medio ambiente.

En el contexto del *downscaling*, existen enfoques dinámicos, mediante modelos regionales anidados a GCMs; y estadísticos, que utilizan relaciones empíricas entre predictores de larga escala de los GCMs, como la presión a nivel del mar (*Sea Level Pressure* en inglés, SLP), y variables locales, como precipitación o temperatura a alta resolución (McSweeney et al., 2015; Evin et al., 2021). En ambos casos, la calidad de la circulación atmosférica simulada por los GCMs es esencial, pues errores en la representación de patrones sinópticos pueden propagar errores a las proyecciones regionales (Addor et al., 2016; Maraun et al., 2017). Además, está bien documentado en la literatura reciente que los GCMs presentan discrepancias e incertidumbres importantes tanto en sus proyecciones futuras del clima como en sus simulaciones históricas (i.e. Dawson et al., 2012; Chang et al., 2012a; Colle et al., 2013; Zappa et al., 2013; Masato et al., 2013; Maraun et al., 2010; Maraun, 2016; Hochman et al., 2019), lo cual complica los esfuerzos de CORDEX para obtener proyecciones regionales fidedignas. Asimismo, las tareas del IPCC de extraer conclusiones del cambio climático con un nivel de confianza estadística suficiente se ven condicionadas por estas discrepancias entre los GCMS.

Ante estas necesidades, la evaluación de modelos globales mediante variables de circulación atmosférica de larga-escala, como la SLP, se ha considerado una práctica crucial (Jones et al., 2011; McSweeney et al., 2015; Maraun et al., 2017). Esta evaluación basada en procesos permite seleccionar GCMs físicamente plausibles para su aplicación en estudios de impactos climáticos y regionalización del clima, y está siendo ampliamente adoptada por CORDEX (Sobolowski

et al., 2023) y los informes del IPCC (IPCC, 2021). En este contexto, cobran una importancia clave los datos de reanálisis, que combinan observaciones con modelos numéricos para reconstruir pseudo-realidades climáticas pasadas (Fujiwara et al., 2017). Estos productos permiten una comparación objetiva entre simulaciones históricas de los GCMs y condiciones observadas (pseudo-observaciones), aunque también pueden introducir incertidumbres debido a las diferencias en cobertura, resolución y sistemas de asimilación (Sterl, 2004).

Esta evaluación basada en procesos está poniendo en el punto de mira a la clasificación sinóptica en tipos de tiempo (o *Weather Types* en inglés, WTs) mediante técnicas de *clustering*, como herramienta para reducir la dimensionalidad del problema y evaluar de forma objetiva los patrones de circulación atmosférica simulados (Sobolowski et al., 2023). En este contexto, el análisis de agrupamiento o *clustering* puede suponer una herramienta útil y potente, ya que puede resumir y reducir el volumen de los datos climáticos (Littmann, 2000; Huth et al., 2008). Estas técnicas clasifican todas las muestras disponibles en un número determinado de grupos (o *clusters*) siguiendo unas reglas de similitud, con el objetivo de que las observaciones dentro de un mismo clúster sean más similares entre sí que a las de otros clústeres (Anderberg, 1973; Cherkassky and Mulier, 1998). Su ventaja principal es que reduce sustancialmente la dimensionalidad de los datos, lo cual simplifica su tratamiento desde un punto de vista estadístico.

Entre las técnicas de *clustering* disponibles para esta aplicación, destaca la clasificación en tipos de tiempo de Jenkinson and Collison (1977), que es una versión automatizada y objetiva del método de Lamb (1972), basada en la SLP y ampliamente utilizada en el campo de la climatología. Esta metodología permite identificar patrones representativos de circulación atmosférica en la mayoría de regiones del planeta, lo que facilita su uso en una comparativa o evaluación de modelos, así como en la detección de cambios proyectados en la circulación atmosférica bajo diferentes escenarios de cambio climático. A continuación se definen detalladamente los principales objetivos de esta Tesis, que van en sincronía con la resolución de la problemática expuesta hasta ahora.

Objetivos de la Tesis

El objetivo principal de esta Tesis es ampliar el conocimiento sobre la representación, evaluación y proyección futura de la circulación atmosférica de larga escala por parte de los Modelos Climáticos Globales (GCMs) de las generaciones de CMIP5 y CMIP6, en el contexto del cambio climático. Para ello, se emplea la clasificación de tipos de tiempo como herramienta para la evaluación basada en procesos de los GCMs, junto con la estimación de cambios futuros en la circulación atmosférica. Específicamente, la Tesis se estructura en torno a tres objetivos

principales:

1. Evaluar el potencial y los límites de la metodología de classificación sinóptica de Jenkinson-Collison *Weather Typing* (JC-WT) como herramienta de diagnóstico basada en procesos para evaluar la circulación atmosférica de los GCMs.

    - Analizar de forma global la aplicabilidad del método de clasificación JC-WT en el extratrópico (incluyendo el Hemisferio Sur).
    - Encontrar conexiones entre los JC-WTs y los principales modos de variabilidad atmosférica (como índices de teleconexión y bloqueos atmosféricos), con el fin de evaluar la coherencia física, relevancia y capacidad diagnóstica del los JC-WTs.

2. Evaluar la capacidad de la nuevos GCMs de CMIP5/6, desarrollados para el Quinto y Sexto Informe de Evaluación del IPCC (AR5 y AR6, respectivamente), para representar los patrones de circulación atmosférica de larga escala. Esta evaluación basada en procesos incluye:

    - Analizar la incertidumbre observacional en base a la clasificación en JC-WT.
    - Cuantificar la capacidad de los modelos CMIP5/6 de reproducir las clasificaciones históricas de JC-WTs en el extratrópico, utilizando una serie de métricas de evaluación basadas en características de los JC-WTs.

3. Estimar los cambios futuros en los patrones de circulación atmosférica a escala *sinóptica* (mediante clasificaciones JC-WTs) proyectados por los modelos, considerando así un vínculo más cercano con la variabilidad climática a escala local, relevante para estudios de impactos climáticos. Esto se realizará para las regiones extratropicales a partir de un ensemble de modelos de CMIP5/6.

    - Identificar cambios robustos en los JC-WT que emerjan sobre la variabilidad interna del *ensemble* multi-modelos.
    - Generar un catálogo global de JC-WTs de más de 50 GCMs basado tanto en sus simulaciones históricas como para en proyecciones futuras.

Conclusiones principales

Los resultados principales de esta Tesis demuestran los vínculos entre la circulación atmosférica en superficie y de larga-escala, probando el potencial del método JC-WT para detectar la influencia de los principales modos de variabilidad atmosférica de baja frecuencia en la circulación

regional. Además, se desarolla satisfactoriamente la evaluación de modelos basada en procesos, no sin antes haber analizado en detalle la incertidumbre observacional de las clasificaciones de JC-WT para diferentes reanálisis. Finalmente, se analizan las tendencias futuras de los JC-WT principales. A continuación, se resumen las principales conclusiones para cada uno de los objetivos descritos en la sección anterior (en *cursiva*), para mayor claridad. Aunque esta sección recoja las conclusiones más relevantes, se remite al lector a los Capítulos 3, 4, 5 y 6 para mayor detalle.

1. *Evaluar el potencial y los límites de la metodología JC-WT como herramienta de diagnóstico basada en procesos para evaluar la circulación atmosférica de los GCMs.*

   - *Analizar de forma global la aplicabilidad del método de clasificación JC-WT en el extratropico (incluyendo el Hemisferio Sur).*

     En el Capítulo 3 (Sec. 3.1), se estudian sus límites de aplicabilidad de JC-WTs, proporcionando una extensión de este método que lo justifica como una herramienta potente y útil para la evaluación de modelos climáticos basada en procesos. Se muestra que los JC-WTs pueden aplicarse de forma fiable en la mayoría de las zonas globales comprendidas entre las latitudes 23.5° y 80° en ambos hemisferios. Éste es el primer estudio que aborda la aplicación global de los JC-WTs.

     En la mayor parte de esta zona de aplicabilidad, se observa una gran diversidad de tipos de tiempo, y baja frecuencia del tipo U (que representa las situaciones sinópticas sin gradiente de presión). Como advertencia a una pérdida de aplicabilidad por parte del método, se observa una transición brusca a partir de la cual la diversidad de WTs disminuye al mismo tiempo que el tipo U se convierte en el tipo dominante. Esta transición marca un umbral empírico de aplicabilidad regional en torno a una variedad de 16 WTs.

   - *Encontrar conexiones entre los JC-WTs y los principales modos de variabilidad atmosférica (como índices de teleconexión y bloqueos atmosféricos), con el fin de evaluar la coherencia física, relevancia y capacidad diagnóstica del los JC-WTs.*

     Según los resultados del Capítulo 3, Sec. 3.2, el método JC-WT, basado en la circulación en superficie, permite generar WTs que se correlacionan significativamente con los principales modos de variabilidad de baja frecuencia, incluyendo el índice de bloqueos atmosféricos. Esta evaluación regional es físicamente coherente con la huella que dejan estos modos de variabilidad en la variable geopotencial, en la mitad de la troposfera, operando a escalas más grandes.

La metodología JC-WT reproduce teleconexiones y bloqueos bien conocidos y documentados, con tipos de circulación físicamente interpretables en cuanto a sus patrones espaciales y su ciclo estacional. Además, es posible que se estén descubriendo también algunas relaciones no documentadas anteriormente, como la asociación entre tipos ciclónicos en el desierto del Sahara occidental y Anatolia con el índice SCAND (activo en DJF y JJA). De forma similar, y sin haber encontrado alguna documetación previa sobre ello, en el caso de los eventos de bloqueo en el Atlántico Norte (ATL) y el continente euroasiático (RUS) que afectan al clima europeo, la predominancia del tipo puramente anticiclónico (A) no se expande más allá de la región fuente de detección del bloqueo. Del mismo modo, el tipo A domina una fracción del Atlántico Norte subtropical, describiendo un puente circumpolar zonal que permite delimitar objetivamente el área de influencia de estos eventos de bloqueo en términos de circulación en superficie (JC-WTs).

Estos resultados proporcionan una comprensión más detallada y matizada de los mecanismos atmosféricos subyacentes que dan lugar a las diferentes configuraciones de JC-WTs, y refuerzan la aplicabilidad y consistencia de esta clasificación como herramienta útil para la evaluación de modelos y la investigación sobre impactos climáticos. El análisis realizado en este capítulo podría aplicarse a otras regiones del mundo donde teleconexiones o eventos de bloqueo jueguen un papel fundamental en el clima regional, extendiendo así los resultados aquí presentados sobre sus vínculos con la circulación en superficie.

2. *Evaluar la capacidad de la nuevos GCMs de CMIP5/6, desarrollados para el Quinto y Sexto Informe de Evaluación del IPCC (AR5 y AR6, respectivamente), para representar los patrones de circulación atmosférica de larga escala. Esta evaluación basada en procesos implica:*

   - *Analizar la incertidumbre observacional en base a la clasificación en JC-WT.*

     El TPMS (Capítulo 4), que proporcionan una medida del grado de acuerdo en las probabilidades de transición entre WTs, revelan una consistencia general entre reanálisis dentro de este rango de aplicabilidad. En los resultados del Capítulo 4, se busca encontrar un equilibrio entre aplicabilidad de los JC-WTs y la incetidumbre asociada a la observación. Por un lado, hay regiones donde el método JC-WT, en principio, es aplicable pero su uso práctico se ve limitado por una gran incertidumbre entre reanálisis, como el Mediterráneo en JJA, y Madagascar y África austral oriental en DJF. Por otro lado, existen regiones donde el método JC-WT es menos

adecuado independientemente de la incertidumbre del reanálisis, como la Península Arábiga y el Sahara en JJA, y África austral occidental y el centro de Australia en DJF. Asimismo, en regiones con orografía compleja, la aplicación de la clasificación JC-WT requiere atención, ya que la SLP se estima mediante algoritmos de reducción de presión, diferentes en cada conjunto de datos. Las diferencias derivadas del algoritmo de reducción de presión se confirman con las discrepancias encontradas entre reanálisis en: Groenlandia, Antártida, América Central norte, América del Norte occidental, América del Norte central, Asia central, Asia del Sur y la meseta tibetana. Tanto el umbral de diversidad de 16 tipos (mencionado anteriormente) como las áreas con valores altos de TPMS muestran un desplazamiento hacia los polos durante el verano del hemisferio correspondiente. Este desplazamiento es especialmente marcado para el TPMS durante JJA (verano boreal).

- *Cuantificar la capacidad de los modelos CMIP5/6 para reproducir las clasificaciones históricas de JC-WTs en el extratrópico, utilizando una serie de métricas de evaluación basadas en características de los JC-WTs.*

  En los resultados (Capítulo 5) se observa una mejora general de CMIP6 respecto a CMIP5 en varias métricas de evaluación relacionadas con las frecuencias simuladas de los JC-WTs y sus secuencias temporales (probabilidad de persistencia y de transición entre tipos). Los GCMs que mostraron un buen rendimiento en CMIP5 (como EC-EARTH y HadGEM2-ES) también lo mantienen en CMIP6. Se encuentran grandes mejoras para IPSL-CM5A-LR y GFDL-ESM4, mientras que permanecen sesgos importantes en otros modelos de CMIP6 (como NorESM2-LM), debido a su limitada capacidad para reproducir correctamente las probabilidades de transición observadas, especialmente en ciertas estaciones del año.

  En general, los GCMs muestran buena habilidad para representar las probabilidades de transición entre JC-WTs. A pesar de diferencias significativas para ciertas transiciones, la imagen conjunta de las matrices de transición indica que los modelos son capaces de reproducir de forma razonable los patrones más probables según los reanálisis, incluso en los modelos con peor rendimiento. Además, estos resultados son consistentes entre los productos de reanálisis considerados.

  No es posible emitir una recomendación general sobre qué modelos concretos utilizar, ya que esto depende de las aplicaciones específicas, que suelen centrarse en una estación del año concreta o en determinados tipos de tiempo (como los que generan eventos extremos en una región). En este sentido, los resultados permiten identi-

ficar qué estaciones y JC-WTs no reproduce correctamente un modelo en particular, lo cual es útil en enfoques de *downscaling* estadístico. Sin embargo, en el *downscaling* dinámico, debe buscarse un rendimiento general (todos los JC-WTs, todas las estaciones).

3. *Estimar los cambios futuros en los patrones de circulación atmosférica a escala sinóptica (mediante clasificaciones JC-WTs) proyectados por los modelos, considerando así un vínculo más cercano con la variabilidad climática a escala local, relevante para estudios de impactos climáticos. Esto se realizará para las regiones extratropicales a partir de un ensemble de modelos de CMIP5/6.*

   - *Identificar cambios robustos en los JC-WT que emerjan a la variabilidad interna del ensemble multi-modelos.*

     Al aplicar la clasificación JC-WT a escala global, se ofrece un marco completo para entender los impactos del cambio climático en la circulación de larga-escala (Capítulo 6). Gracias a la metodología basada en niveles de calentamiento global (*Global Warming Levels* en inglés, GWL), se ha podido analizar la relación lineal entre respuestas regionales y calentamiento global, así como estimar el Tiempo de Emergencia (*Time of Emergence*, ToE) de señales robustas. Estos resultados tienen implicaciones prácticas para investigadores en impactos climáticos, particularmente en regiones donde los cambios en la circulación atmosférica pueden jugar un papel fundamental.

     Los resultados revelan tendencias significativas en los JC-WTs en regiones climáticas clave, con cambios estadísticamente significativos en patrones de circulación reconocidos de las zonas extratropicales. Por ejemplo, se detectan tendencias positivas significativas en regiones influidas por la teleconexión NAO y de ambos signos en la zona afectada por la PNA. El tipo Ciclónico presenta tendencias robustas de ambos signos en Groenlandia y el Ártico canadiense. Además, el tipo Anticiclónico (A) muestra tendencias negativas notables en el Mediterráneo en JJA y positivas en DJF, así como tendencias robustas mayormente positivas en JJA para una amplia franja del hemisferio sur (correspondiente al cinturón subtropical de altas presiones) y de ambos signos para DJF. El tipo Oeste (*Westerly*) presenta cambios robustos positivos en su frecuencia en zonas subantárticas, mientras que el tipo No-Clasificado (U) exhibe variaciones positivas destacadas en el Mediterráneo o cerca de los trópicos.

     La emergencia de señales del cambio climático está estrechamente relacionada con

la robustez de las tendencias encontradas. Aunque la mayoría de señales emergen con claridad en torno a la década de 2070, algunas regiones, como el Mediterráneo, muestran señales emergentes tan tempranas como en las décadas actuales (2020s), en particular para los tipos A y U. Esta variabilidad temporal refleja la interacción entre la variabilidad natural del ensemble multi-modelo y la creciente influencia del forzamiento antropogénico sobre la circulación atmosférica en los modelos.

La intensificación de las señales emergentes hacia finales del siglo XXI subraya la importancia de estas tendencias para entender los escenarios climáticos futuros. Hay evidencias de que los cambios en las frecuencias de los JC-WTs serán más importantes que la variabilidad interna histórica en cada GCM, reforzando la solidez y relevancia de estos cambios. Esto destaca el papel crucial de los patrones de circulación de larga-escala en la configuración de las respuestas climáticas regionales, aportando información de gran valor para responsables políticos e investigadores que enfrentan los desafíos del cambio climático.

- *Generar un catálogo global de JC-WTs de más de 50 GCMs tanto para sus simulaciones históricas como para sus proyecciones futuras.*

  Como resultado del logro de los diferentes objetivos de esta Tesis, y con el fin de apoyar futuros estudios que puedan beneficiarse de las clasificaciones de JC-WTs, se han creado varios repositorios de datos en línea y de acceso abierto. Estos repositorios contienen catálogos de JC-WTs derivados de múltiples GCMs y reanálisis. Se describen en detalle en las Secciones 7.4 y 7.3.2, e incluyen clasificaciones JC-WTs en una resolución 6-horaria para 61 modelos en el periodo histórico (1979–2005), y 41 modelos en escenarios futuros (2005–2100), así como para 5 reanálisis cubriendo el periodo 1979–2005.

Publicaciones y Contribuciones

Las principales contribuciones de esta Tesis han dado lugar a varias publicaciones en revistas científicas internacionales de alto impacto que incluyen proceso de revisión por pares, así como en actas de congresos relevantes en los campos de la climatología y la meteorología. Más concretamente, tres artículos ya han sido publicados y otro se encuentra actualmente en proceso de revisión, además de un capítulo de libro en las actas del *XII Congreso de la Asociación Española de Climatología (AEC)*. La información detallada de estas publicaciones puede encontrarse en la Sección 7.2

Part I

State of the art and methods

1

Introduction

1.1 Context and motivation

Climate change is a present reality that affects every region of the world. According to the Intergovernmental Panel on Climate Change (IPCC)[1], mean global surface temperature has increased by approximately 1.1°C between 2011 and 2020 compared to the pre-industrial period of 1850–1900, mainly due to greenhouse gas emissions from human activities. This warming has led to more frequent and intense extreme weather events, such as heatwaves, heavy rainfall, and droughts, impacting ecosystems, economies, and communities worldwide (IPCC, 2021).

However, not all regions of the world are equally affected by climate change. Some areas are more vulnerable than others due to regional variations in geography, climatic systems, and socioeconomic factors. For example, recent IPCC assessments show that changes in temperature and precipitation will not occur uniformly across the world. Instead, regional climate responses to a given level of global warming (such as 1.5°C, 2°C, or 4°C above pre-industrial levels) are expected to vary substantially depending on geographic location, with some areas experiencing amplified warming, shifts in rainfall patterns (Fig. 1.1), flooding in coastal areas due to sea-level rise or severe droughts over extensive inland areas, among other expected impacts. The IPCC acknowledges these differences and emphasizes the importance of comprehensive regional climate data to guide successful adaptation and mitigation plans.

These statements and projections provided by the IPCC are possible thanks to the use of a great volume of Global Climate Models (GCMs, Sec. 1.2.1). GCMs are popular computational tools in the field of climate change studies that are capable of reproducing the past climate and projecting future climate conditions based on a faithful description of the climate system. However, some models have coarse spatial resolution, which is not sufficient to simulate the regional climate. To do so, scientists employ a variety of techniques to downscale these global

[1]The IPCC is a United Nations (UN) body that provides scientific assessments on climate change to inform policy and global action.

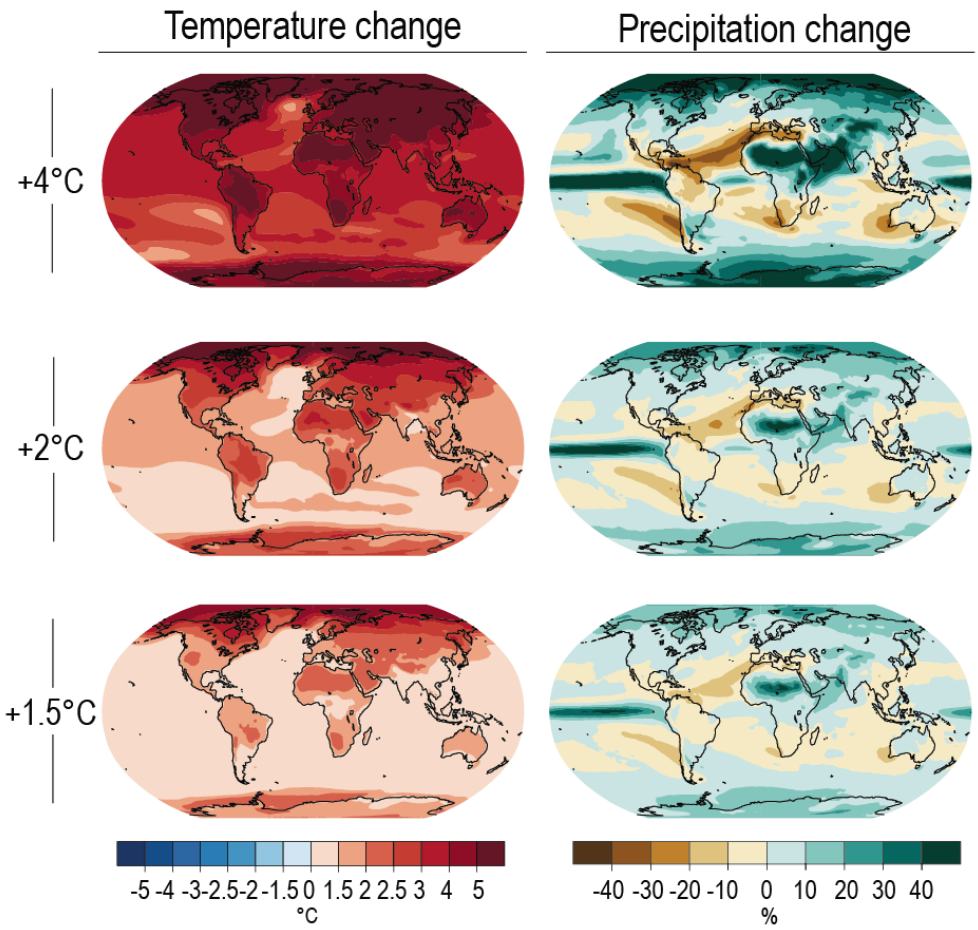

Figure 1.1: *Future projected changes of temperature (in °C) and precipitation (in %) for different levels of mean global warming relative to mean global temperature in 1850–1900. These results are based on multi-model ensembles of climate models (Sec. 1.2.1). Source: IPCC 2021, https://www.ipcc.ch/report/ar6/wg1/figures/technical-summary/*

climate models, translating global climate projections into more local information. In order to help communities and policymakers make well-informed decisions to safeguard lives and the environment, downscaling techniques are essential to comprehend how climate change will specifically affect specific regions.

In recent decades, climate change studies, along with the fields of weather forecasting and climate modeling, have experienced an unprecedented surge in data production. Scientific institutions worldwide aim to simulate and predict atmospheric processes with an ever-growing resolution and complexity to improve the representation of the climate system. For example, the daily production of meteorological and climate data worldwide is considerable. For example, the European Centre for Medium-Range Weather Forecasts (ECMWF) produces approximately 144 TeraBytes (TB = 10^{12} bytes) of data per day, which is nearly 1 PB per week (Hawkes et al., 2020). These amounts include both raw data and post-processed products. Moreover,

there are more than 100 climate models from nearly 50 modeling centers available worldwide encompassing more than 20 PetaBytes (PB = 10^{15} bytes) of climate-related data (Petrie et al., 2021). Additionally, the improvement of existing GCMs and the development of new ones will very likely increase this data volume. This abundance of data entails an unprecedented opportunity to build a deeper understanding of the Earth's climate system (as the IPCC does), but it also presents an urgent problem: how to properly interpret all these data, as well as how to assess and filter them for use in impact studies, policy creation, and adaptation planning.

In this context, *clustering analysis* may emerge as a useful and powerful tool for the purpose to summarize and reduce the volume and variety of climate data (Littmann, 2000; Huth et al., 2008). The *clustering analysis* refers to a set of techniques that aim to classify all samples into a predefined number of groups (referred to as clusters) based on similarity rules. The objective is to define groups (i.e. clusters) so that the observations within the same cluster are more similar to each other than to those in other clusters (Anderberg, 1973; Cherkassky and Mulier, 1998). The main advantage of clustering techniques is the substantial reduction in the dimensionality of the samples, simplifying their use from a statistical point of view. For that reason, *clustering* techniques have found wide applicability in numerous fields, including engineering, computer science, medicine, social and earth sciences or economics (Hartigan, 1975; Everitt et al., 2011). This broad scope of applications highlights the central role that *clustering* occupies within scientific research. In climate science, this Thesis can be framed in the field of Synoptic Climatology[2], a discipline which, broadly speaking, determines distinct categories (*clusters*) of synoptic weather (or circulation) patterns, and then usually undertakes an assessment of the weather conditions associated with these patterns (Lee and Sheridan, 2015) (Sec. 1.5.1).

There is a wide range of clustering techniques, which can be classified according to numerous criteria beyond the specific domain or field of application. One general approach to categorize clustering methods is based on the nature of their "similarity" rules. Under this criterion, clustering techniques are typically divided into *objective* and *subjective* approaches. Objective techniques rely solely on the intrinsic properties of the data to define the rules that generate the clusters. In contrast, subjective techniques incorporate domain-specific expert knowledge to establish the classification rules applied to the data.

Even interpreting, handling, and understanding a single climate model requires considerable computational resources and expert knowledge to properly distill its outputs. In fact, the

[2]Synoptic circulation refers to large-scale atmospheric flow patterns, typically spanning hundreds to thousands of kilometers, that govern weather systems such as cyclones, anticyclones, and fronts, and are commonly analyzed using pressure and wind fields at specific levels.

complexity, diversity, and specialization of these models can be considered a challenge itself. In another vein, GCMs show substantial spread in their future climate projections (Maraun et al., 2010), as well as discrepancies in their historical simulations (e.g. Dawson et al., 2012; Chang et al., 2012a; Colle et al., 2013; Zappa et al., 2013; Masato et al., 2013; Maraun, 2016; Hochman et al., 2019) when contrasting them with observations. This complicates the efforts of the scientific community to draw conclusions and key messages about climate change with a certain level of statistical significance or confidence. In light of these model uncertainties, the development of an objective and efficient method for the physical evaluation and interpretation of the model outputs emerges as a key step, in order to extract meaningful insights from them (IPCC, 2021; Sobolowski et al., 2023).

Throughout this Thesis, clustering analysis is used to identify, evaluate and project common circulation patterns in state-of-the-art GCMs. The following Sections of this Chapter provide the necessary background for this topic, which supports the overall objectives of the Thesis, outlined in Section 1.6.

1.2 Modeling the climate system

An overview of the tools and datasets used to simulate and evaluate the climate system is key to understand how climate projections are generated. This section introduces Global Climate Models (GCMs), the core part of modern climate science, and describes their historical evolution, basic components, and known limitations. It also reviews the Coupled Model Intercomparison Project (CMIP) and the improvements that have progressively led to CMIP6. Additionally, the role of reanalysis datasets (gridded reconstructions that merge observations with numerical models) as pseudo-observational references to assess the historical plausibility of GCM simulations is introduced. Lastly, the section highlights the importance of process-based GCM evaluation to support robust regional climate projections.

1.2.1 Global Climate Models (GCMs)

Global Climate Models (GCMs), also known as General Circulation Models, set the ground for modern climate science research. They constitute a sophisticated and complex software tool to simulate both past and future global climate conditions by solving, numerically and computationally, physical equations about how Earth's climate evolves (Fig. 1.2). GCMs have been under development since the 1960s (Manabe and Wetherald, 1967), when they assimilated only atmosphere-based components. More components were gradually added to the GCMs in order to simulate more accurately interactions between different key components of the climate sys-

tem (Fig. 1.3). Components such as the ocean (coupled ocean-atmosphere circulation models) and sea-ice play an important role in seasonal forecasts; and land and vegetation, the carbon and nitrogen cycles and atmospheric chemistry do it so for decadal and multi-decadal predictions (Mcguffie and Henderson-Sellers, 2005; Edwards, 2011). The latter recent developments of GCMs have promoted the emergence of more comprehensive Earth System Models (ESMs, Eyring et al., 2016). ESMs integrate various components of the Earth's system, including the atmosphere, oceans, land surface, biogeochemical cycles and other biosphere processes, to provide a more comprehensive and holistic understanding of climate dynamics and interactions. By incorporating these diverse elements, ESMs offer enhanced predictive capabilities and insights into the complex processes driving climate change.

In practice, GCMs and ESMs give a detailed framework to analyze past climate variability, as well as project future changes on different temporal scales (seasons, decades and centuries) under different natural and anthropogenic forcing scenarios, based on emission of different levels of greenhouse gases[3]. For simplicity, throughout this Thesis the acronym GCM will be used to refer to both GCMs and ESMs interchangeably, considering that more recent models generally feature higher resolution, greater complexity, and more interactive components compared to previous ones (see Sec. 1.2.2).

In order to solve the pertinent processes on a specific scale, these components (e.g. atmosphere, ocean, land or vegetation) and their interactions are simplified versions of their real-world counterparts, that operate on a discretized representation of the Earth (Figure 1.2). The architecture of a GCM is built on a four-dimensional grid of longitude, latitude, vertical layers, and time, with spatial resolutions ranging from $\sim$ 50 km to $\sim$ 300 km, around 10 and 20 atmospheric layers in the vertical axis and time steps from 1 to 6 hours. This gridded structure facilitates numerical simulations of climate variables in a standard format, as well as their spatial analysis and visualization.

Despite their growing complexity and resolution, GCMs are still constrained by some manlimitations. Due to their grids' relatively coarse resolution, they are not able to resolve small-to-mesoscale processes like fog formation, sea breezes, orographic effects, and local convection, occurring on spatial scales below grid spacing. In order to represent the net effect of unresolved subgrid phenomena on such rough scales, parameterization schemes (through empirical or semiempirical formulations) must be used to approximate these processes (Stensrud, 2007; McFarlane, 2011). The problem of these parameterizations is that they add systematic biases to the GCM, and their choice leads to more uncertainties. For example, in areas with complex to-

[3]Greenhouse gases, such as carbon dioxide and methane, are gases that have the ability to trap heat in the Earth's atmosphere.

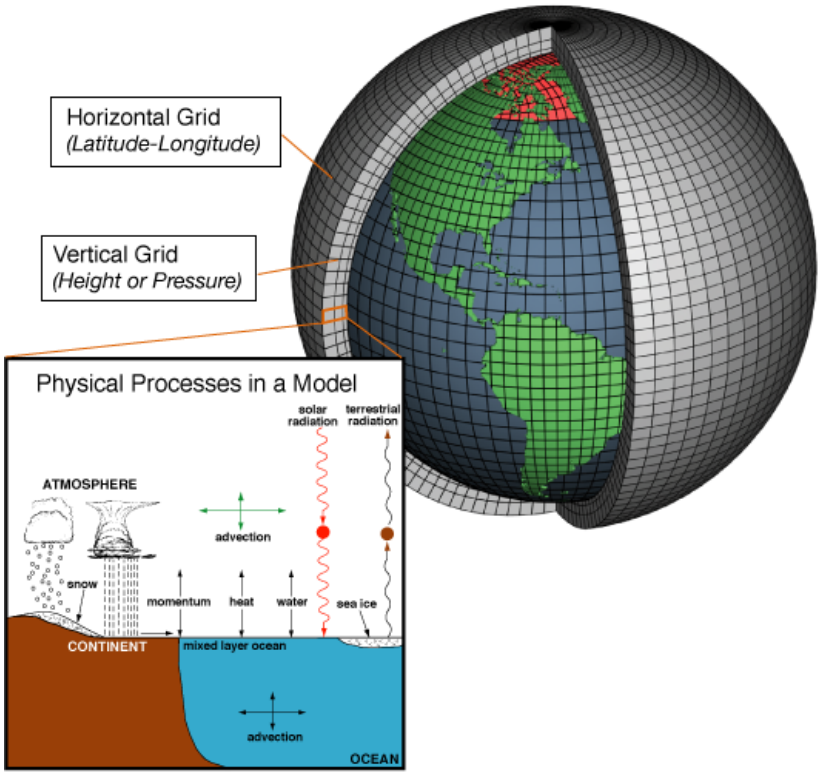

Figure 1.2: *Scheme of a typical grid-based representation of the Earth system used in the numerical computation of a GCM. Source: NOAA, http://celebrating200years.noaa.gov/breakthroughs/climate_model/AtmosphericModelSchematic.png*

pography such as the Andes or the Himalayas, convective precipitation is often underestimated or misplaced (Tost et al., 2006). Furthermore, differences in the parameterizations among models (i.e. grid structure and physics) lead to significant spread in climate projections, even under the same forcing scenarios (Maraun et al., 2010).

To address these limitations, multi-model ensembles are useful to quantify projections' uncertainty. Over the past decades, new and more refined models have been developed in order to create ensembles, as well as to improve their resolutions (Fig. 1.4) and evolve in represented components (Fig. 1.3). These advances have been possible thanks to the improvement of modern computational tools and systems, and they have turned into consecutive generations of GCMs.

1.2.2 Overview of the Coupled Model Intercomparison Project

The Coupled Model Intercomparison Project (CMIP) has coordinated different standardized generations of GCM experiments. CMIP was launched in 1995 with support of the Working Group on Coupled Modelling (WGCM) and the World Climate Research Programme (WCRP), with the goal of producing a publicly available dataset composed of an ensemble of models adhering to specific standards and experimental protocols. CMIP is therefore the primary

source of data for impact and adaptation studies, as well as for the description of the physical risks of climate change by providing climate projections to understand past, present and future climate changes (Meehl et al., 2000; Eyring et al., 2016). The large ensemble of models within CMIP offers the advantage of quantifying uncertainty in climate simulations and projections (IPCC, 2013).

Since its inception, CMIP has undergone multiple phases. The development of GCMs is closely related to these different stages. The main focus of the first three generations, namely CMIP1, CMIP2, and CMIP3, was to coordinate experiments using increasingly complex coupled models. CMIP3 was the first generation to incorporate multi-model ensembles of fully coupled atmosphere–ocean GCMs, and comprised 24 GCMs. The IPCC's Fourth Assessment Report (AR4; IPCC, 2007) concluded, for the first time with a confidence level greater than 90% that anthropogenic greenhouse gas emissions were more likely to be responsible for most of the warming observed since the middle of the 20th century.

CMIP5, the fifth phase, included 29 models and marked a significant change in experimental design and model diversity towards experiments on near-term decadal prediction, carbon cycle feedbacks, and regional climate modeling (Taylor et al., 2012) thanks to new computational advances. The IPCC Fifth Assessment Report (AR5; IPCC, 2013), relied on CMIP5 and showed greater integration of processes and impacts affecting at regional level, enhanced attribution of observed changes, and advanced the assessment of Equilibrium Climate Sensitivity (ECS). The ECS is the expected long-term warming following a doubling of atmospheric CO_2 concentrations compared to pre-industrial levels, and it is measured in degrees Celsius (°C). It is among the most significant predictors of the severity of the effects of future warming.

The sixth phase, known as CMIP6, was intended to be more modular, thorough and process-oriented, building on the lessons learned in AR5. It is organized around a number of approved Model Intercomparison Projects and a core set of DECK (Diagnostic, Evaluation and Characterization of Klima) experiments (Eyring et al., 2016). CMIP6 consisted of more than 100 models developed by 49 different modeling centers around the world. Furthermore, CMIP6 models have better coupling between biogeophysical and biogeochemical components, higher resolution, and a more realistic representation of cloud and aerosol processes (Eyring et al., 2016).

Additionally, each generation of models has defined its own simulation time coverage. For example, all models included in the CMIP5 and CMIP6 experiments comprise future projections of climate variables at least until 2100 (throughout the 21st century), and they cover the historical period with simulations from 1850 to 2005 for CMIP5, and up to 2014 for CMIP6.

Historical simulations are commonly used to evaluate model performance and assess their ability to represent key climate processes and features.

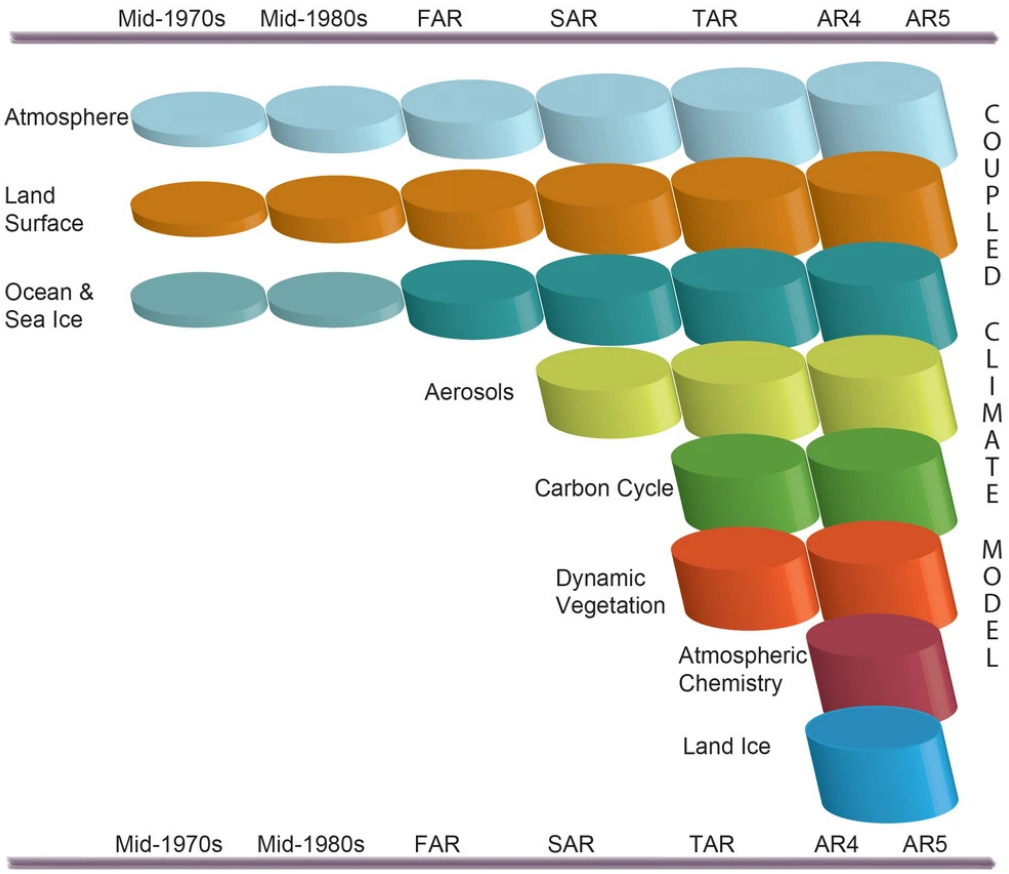

Figure 1.3: *Development of climate models over the last 50 years showing how the different components were coupled into comprehensive climate models over time. In each aspect (e.g., the atmosphere, which comprises a wide range of atmospheric processes) the complexity and range of processes has increased over time (illustrated by growing cylinders). Note that the horizontal and vertical resolution has increased considerably at the same time. For instance, for spectral models from T21L9 (roughly 500 km horizontal resolution and 9 vertical levels) in the 1970s to T95L95 (roughly 100 km horizontal resolution and 95 vertical levels) at AR5. Source: IPCC wiki, http://ipcc.wikia.com/wiki/151.5.2_Capabilities_in_Global_Climate_Modelling*

Each generation of CMIP has incorporated its own set of future scenarios, customized to reflect the scientific and political priorities of each time. The CMIP3 ensemble was the first generation of models to introduce different long-term climate projections, derived from the Special Report on Emissions Scenarios (SRES; Nakicenovic et al., 2000) such as A1F1, A2, A1B, B2 or B1. These are ordered by more economical aggressive and less environmental aware to the opposite. In other words, these scenarios are socio-economically sensitive. Later, CMIP5 introduced the Representative Concentration Pathways (RCPs) as new standardized future emission scenarios (van Vuuren et al., 2011). These scenarios (e.g., RCP2.6, RCP4.5, RCP6.0, and RCP8.5) focus on the radiative forcing levels that would result from different emission

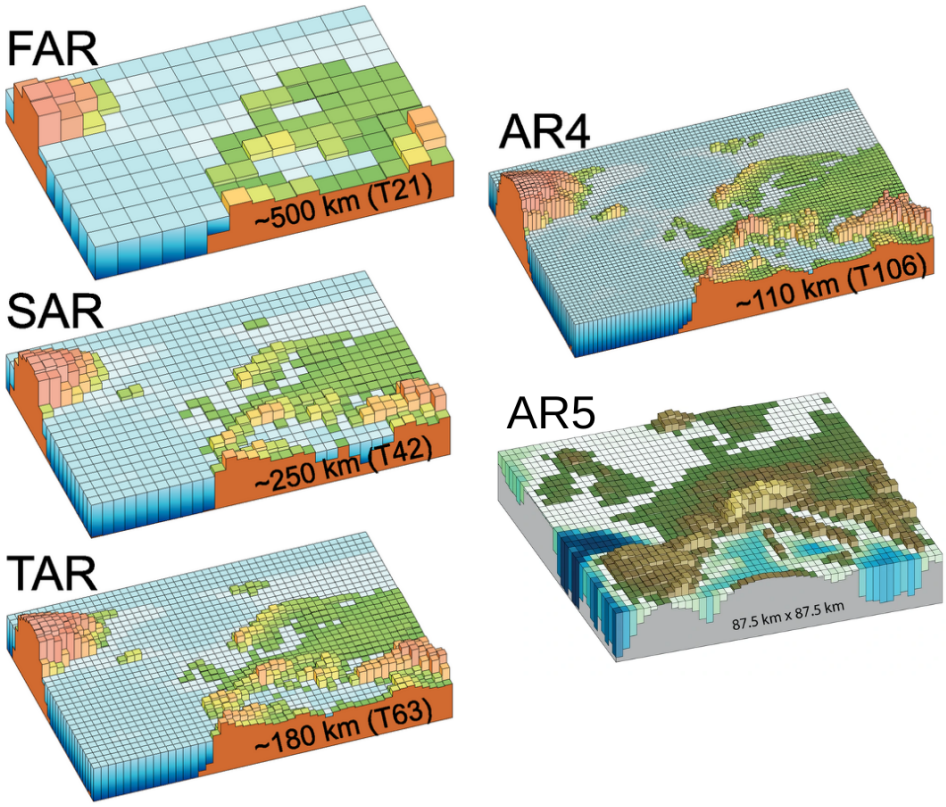

Figure 1.4: *Geographic characteristic and spatial resolution of the generations of climate models used in the IPCC Assessment Reports: First Assessment Report, FAR (Houghton et al., 1990); Second Assessment Report, SAR (Houghton et al., 1996); Third Assessment Report, TAR (Houghton et al., 2001), AR4 (IPCC, 2007) and AR5 (IPCC, 2013). The figures above show how successive generations of these global models improved on the representation of Europe. These illustrations are representative of the most detailed horizontal resolution. Vertical resolution in both atmosphere and ocean models is not shown, but it has increased comparably with the horizontal resolution, beginning typically with a single-layer slab ocean and ten atmospheric layers in the FAR and progressing to about thirty levels in both atmosphere and ocean. Source: IPCC, https://archive.ipcc.ch/publications_and_data/ar4/wg1/en/ch1s1-5.html and http://ipcc.wikia.com/wiki/151.5.2_Capabilities_in_Global_Climate_Modelling.*

pathways. In order to increase the relevance of projections for mitigation and adaptation policy, CMIP6 adopted the Shared Socioeconomic Pathways (SSPs), which reconnect emission scenarios with narratives about global development trajectories (O'Neill et al., 2016; Riahi et al., 2016). For example, RCP8.5 and SSP5-8.5 represent high emission futures (reaching a radiative forcing of 8.5 W/m^2 by the end of the century), whereas RCP2.6 and SSP1-2.6 reflect significant mitigation efforts (reaching an associated radiative forcing of 2.6 W/m^2). These standardized scenarios are essential for comparing projections from different models and time periods.

Figure 1.5 illustrates the projected evolution of atmospheric CO_2 concentration throughout the 21st century, based on 14 different scenarios from the IPCC's AR4, AR5, and AR6 reports. These different projected trajectories on CO_2 concentrations are critical to determining the ex-

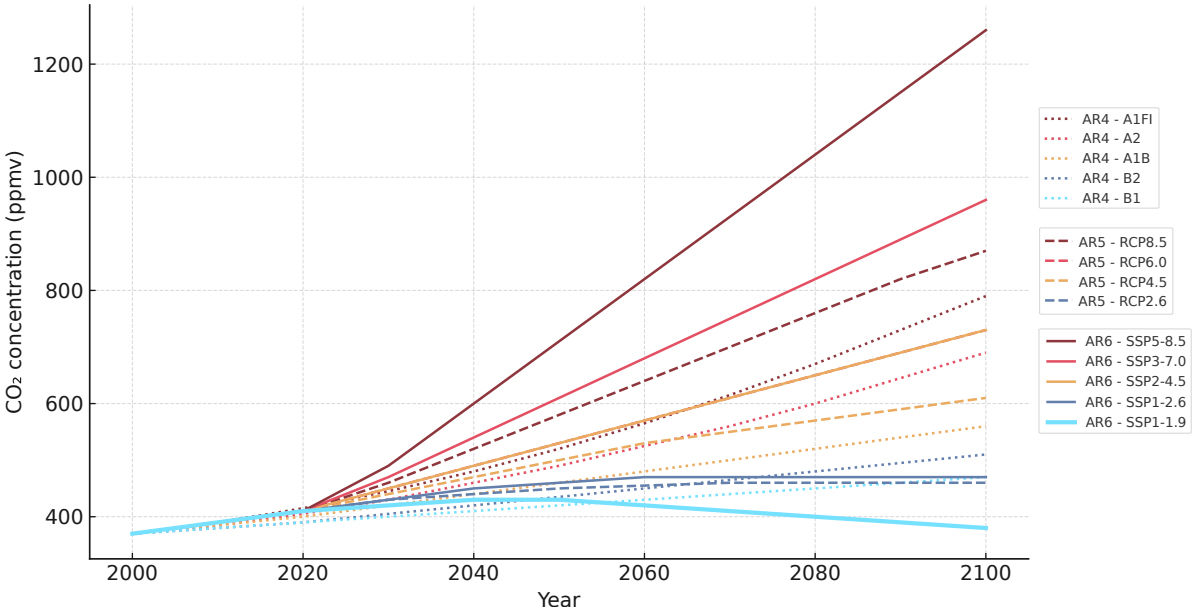

Figure 1.5: *Comparison of projected atmospheric CO_2 concentrations in different SSPs (AR6), RCPs (AR5) and SRESs (AR4) in 2000-2100. The data showed is approximate and based on interpolations of the trends described in IPCC (2007), IPCC (2013) and IPCC (2021).*

pected radiative forcing and global warming levels, directly influencing estimates of Equilibrium Climate Sensitivity (ECS) and the magnitude of associated impacts. This summary emphasizes the importance of the emission pathway, socio-economic development narratives and the model generation in shaping our understanding of possible future climate outcomes.

In summary, the different IPCC Assessment Reports have served as a roadmap for upcoming research projects, and as a summary of the current knowledge available. For example, the uncertainties in aerosol–cloud interactions were highlighted in AR4, the need for better depiction of decadal variability and short-term climate projections was highlighted in AR5 because CMIP5 models exhibited significant biases in their projections (IPCC, 2013), and regional-scale processes, extreme events, and narratives were given additional attention as risk assessment tools in AR6 (Zappa and Shepherd, 2017). The design and priorities of the upcoming CMIP generation have been shaped by each report, establishing an iterative feedback loop between model development and scientific evaluation. The development of GCMs from CMIP1 to CMIP6 demonstrates the ongoing change towards more comprehensive, high-resolution, and policy-relevant climate modeling frameworks. These developments, when combined with the IPCC's recommendations, are crucial for improving the reliability and applicability of climate projections for planning regional climate adaptation and Earth system diagnostics, as well as for understanding the world climate at once.

1.2.3 Reanalysis

A reanalysis project involves integrating observational data with numerical simulation models to generate datasets that accurately represent the atmospheric state, featuring variable vertical and horizontal spatial resolutions and covering an extensive historical period of several decades or more (Fujiwara et al., 2017). Hence, the resulting analysis is considered to be the "best" estimate of the state of the atmosphere at a particular moment in time. The outputs from reanalysis can be utilized in meteorological and climatological research, such as analyzing past climate variations and changes, and more (see e.g. https://reanalyses.org for an overview). Reanalyses ease the lack of observations for certain variables, at the surface and on vertical levels, across large areas of the globe, producing a homogeneous record of past atmospheric evolution, free from spurious non-climatic signals introduced by changes in model formulation, assimilation systems, or data availability (Sterl, 2004). For this reason, they are commonly referred to as *pseudo-observations* by climatologists. As a result, reanalyses provide physically consistent multivariate datasets that would otherwise be difficult (or impossible) to obtain through conventional observational methods with comparable spatial and temporal resolution. As it builds upon assimilated observations, there is a rather good temporal correspondence with real climatic conditions. Thus, they are valuable tools for understanding climate variability and change, and for monitoring current climate conditions.

Reanalyses are often available on a six-hourly to hourly timescale, they can extend several decades into the past and incorporate a massive amount of observations from extensive networks of surface stations, ships, buoys, aircraft, satellites, etc. (Kalnay et al., 1996; Dee et al., 2011; Hersbach et al., 2020). The representation of climate signals across different reanalysis products is inevitably affected by temporal and spatial biases when assimilating these observations, as well as changes in the global observing system, numerical model grid resolution, etc., leading to reanalysis-related uncertainties (Brands et al., 2013; Fujiwara et al., 2017). Furthermore, the density of the assimilated observations is a crucial factor in determining how realistic the simulated atmospheric states are. If observations are available, the reanalyzed atmospheric states are realistic and the system is consistent with them. When there are few or no observations at all, the model creates its own "unbound" variability. This might be implausible and differ significantly between different reanalysis systems (Sterl, 2004), leading to inhomogeneities that exacerbate the problem of reanalysis uncertainty. As a result, there are well-known discrepancies between reanalyses in specific regions and periods (see e.g. Brands et al., 2013). Some examples of these discrepancies are the reconstruction of historical records of climate impact indices (e.g. Bedia et al., 2012), forecast verification (Ramon et al., 2024) or downscaling approaches (Maraun

and Widmann, 2018). In the latter, the selection of reanalysis predictors emerges as a critical step in model performance (Brands et al., 2012a) and the associated plausibility of future climate projections (Manzanas et al., 2015). Indeed, one of the main sources of uncertainty in the evaluation of GCMs lies in the choice of reanalysis dataset used as the pseudo-observational reference, an aspect that is specifically addressed in this Thesis (Sec. 1.6).

1.2.4 From global to regional climate projections: Downscaling

The application of GCM outputs at local scales is not straightforward due to their coarse horizontal resolution (on the order of hundreds of kilometers), which challenges their direct application in many climate impact applications. To overcome this limitation, downscaling is aimed to refine and enhance the resolution of climate model outputs to provide more detailed and localized climate information. Two main broad types of techniques exist, namely dynamical and statistical downscaling. Dynamical downscaling relies on Regional Climate Models (RCMs), which simulate the physical characteristics of the climate at higher resolution over a specific region (e.g. continental-size domain), using the initial and boundary conditions provided by GCMs (Figure 1.6). However, RCM outputs often exhibit substantial regional biases partly inherited from their driving GCMs, and to date, no method has been able to fully correct these biases (Christensen et al., 2008; Maraun, 2012). Secondly, statistical downscaling methods (SDMs) are based on empirical statistical models that link large-scale variables or predictors, e.g. sea-level pressure (SLP, Sec. 1.3.1) with local-scale surface variables, e.g. precipitation, which serve as dependent variables in the model (see, for example, Benestad et al., 2008).

In this context, a reference international downscaling initiative stands out, named the Coordinated Regional Downscaling Experiment (CORDEX). CORDEX (Giorgi et al., 2009; Jones et al., 2011) is a project of the World Climate Research Programme (WCRP) and aims to provide regionalized climate projections in all continental regions (at a common resolution of 50km×50km or 25km×25km worldwide and 12km×12km in Europe). Currently, it constitutes the most comprehensive initiative for GCM–RCM (Giorgi, 2006; Feser et al., 2011) coupling experiments. In particular, the EURO-CORDEX branch (Jacob et al., 2014, 2020) is specifically responsible for delivering regional projections on the European continent. Moreover, within CORDEX, Flagship Pilot Studies[4] were developed to conduct RCMs simulations in domains smaller than continental scales, at higher spatial resolutions (2–3 km), in order to investigate specific processes such as urban heat islands or convection in high mountain regions.

Both dynamical and statistical downscaling techniques rely heavily on climate variables

[4]https://cordex.org/strategic-activities/flagship-pilot-studies/finished-flagship-pilot-studies/

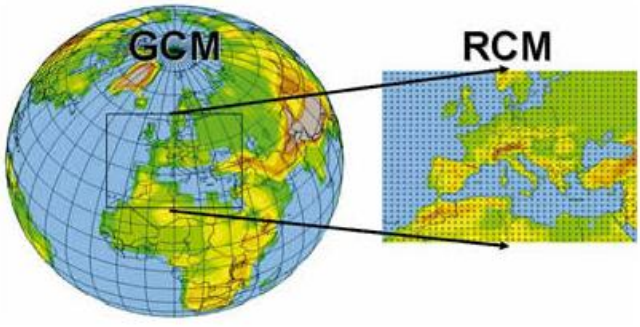

Figure 1.6: *Illustration of the increase in grid resolution of a Regional Climate Model (RCM). Source: WMO, https://www.wmo.int/pages/themes/climate/climate_models.php*

from GCMs related to atmospheric circulation (e.g. Sea-Level Pressure, SLP, Sec. 1.3.1), which serve as initial and boundary conditions for dynamical downscaling, and as predictors in statistical downscaling, to produce climate projections. For this reason, the selection of driving GCMs for RCM is necessary in the design of downscaling experiments. GCM selection for downscaling purposes is usually a two-step process (McSweeney et al., 2015), which requires, first, the plausibility of the GCMs (historical and future) projections and, second, that the selected GCMs cover a large fraction of the climate alternatives spanned by the full ensemble. The selection of GCMs based on their ability to adequately simulate particular local surface variables, such as temperatures or precipitation, is inadequate and may result in a suboptimal selection of driving GCMs given the known discrepancies in how these variables are represented by GCMs (Addor et al., 2016; Maraun et al., 2017). In the presence of systematic biases, a sensible bias correction approach can substantially improve raw model fields from a statistical point of view, and is recommended for specific variables and threshold-dependent climate indices (see e.g. Dosio, 2016; Iturbide et al., 2020a). However, fundamental model errors may persist after bias adjustment (Kim et al., 2024), and therefore a proper process-based validation is required in order to identify poorly performing GCMs. Even though RCMs can add value in this sense, by improving the misrepresentation of the driving data (Jones et al., 1995), this improvement is incomplete, particularly when there are large errors in the driving GCM (Diaconescu and Laprise, 2013). Moreover, even when bias correction methods improve the applicability of climate simulations, in general, it cannot improve low model credibility, and may even hide the lack of reliability of model output when applied inadequately (Maraun et al., 2017), eventually resulting in poorly informed adaptation decisions. For this reason, a robust evaluation of GCMs considering fundamental climate features, such as atmospheric circulation, is a fundamental step in the design of downscaling experiments.

The selection of the driving GCM has a large effect on the performance of RCM simulations

(as shown e.g. by Prein et al., 2019, in North America), which also has an impact on the projected climate change signal (Turco et al., 2013). Thus, the choice of GCM is an issue of paramount importance in GCM-RCM intercomparison experiments and climate change impact applications. Until now, most downscaling efforts conducted an *ad hoc* GCM selection, which led to unbalanced GCM-RCM matrices, with some GCMs being under/overrepresented. In order to guarantee both physical realism and RCM ensemble diversity, the EURO-CORDEX CMIP6 GCM selection framework suggests an objective set of criteria, which combine data availability and process-based plausibility criteria with a proper representation of the full-ensemble future spread and model independence (Sobolowski et al., 2023). The growing consensus that informed, process-aware GCM selection is crucial to provide trustworthy climate information for impact studies and adaptation planning is supported by this structured, multi-criteria approach, which is a significant improvement over earlier methods (McSweeney et al., 2015; Evin et al., 2021).

In order to gain a deeper understanding of the evaluation and selection of GCMs based on large-scale processes, it is necessary to describe one of the main variables representing atmospheric circulation (SLP) and the main modes of atmospheric variability. Later, Section 1.3.4 describes the influence of large-scale atmospheric circulation on the overall variability of local surface climate, which helps to understand the usefulness and effectiveness of process-based evaluation.

1.3 Large-scale climate variables and indices

In this Section, some key large-scale atmospheric variables and indices that play a fundamental role along this Thesis are introduced and defined. Characterization of large-scale atmospheric circulation is essential to understand regional climate variability and its projected changes under anthropogenic forcing. Among the most relevant variables related to atmospheric circulation, Sea Level Pressure (SLP) is considered. In addition, some large-scale circulation indices based on geopotential height at 500 hPa (Z500) are introduced, such as atmospheric blocking events and teleconnection indices, as they represent fundamental dynamical processes and drive regional climate.

1.3.1 Sea-Level Pressure

Sea-Level Pressure (SLP) is a key meteorological variable that represents atmospheric pressure at sea-level. It is derived from surface pressure measurements that are adjusted using factors such as altitude, temperature, and humidity; allowing a standardized comparison of pressure data in different topographies and elevations (Wallace and Hobbs, 2006). The SLP is particularly

relevant in weather and climate studies because it serves as a near-surface proxy for larger-scale atmospheric circulation. In this way, the SLP can help experts in identifying and analyzing large-scale circulation patterns and features, such as cyclones (marked by areas of low SLP and often associated with precipitation), anticyclones (marked by areas of high SLP, diverging winds and generally clear skies), and the pressure gradients that drive surface winds. The way in which SLP patterns are spatially distributed is closely related to geostrophic flow, providing a solid indicator to assess atmospheric dynamics at the surface level (Peixoto et al., 1992).

Another relevant feature of the SLP is its relative stability under global warming (Bhend and Whetton, 2013; Xiong et al., 2020), especially compared to geopotential height at fixed pressure levels. Since the total mass of the atmosphere tends to remain constant even with climate change, SLP patterns maintain their physical reliability across climate models and observational data (Trenberth and Smith, 2005). As a result, SLP has become a trusted input for process-based evaluation of climate models (see Sec. 1.5). Furthermore, SLP data can be summarized into a reduced set of patterns using classification techniques such as *Clustering Analysis* (Sec. 1.5.1), yielding a synoptic classification of representative SLP states for a particular location or region of interest.

Although SLP is the primary and most essential tool for conducting a process-based evaluation, it shows certain limitations that must be explicitly taken into account. The first drawback arises from the nature and definition of the variable itself. Essentially, SLP is an estimated variable in reanalyses and GCMs following a procedure highly sensitive to altitude and to the original resolution of the orography of the dataset. Its reduction process is especially susceptible to uncertainties in regions of complex orography, where large elevation differences, steep gradients, and variable surface temperatures challenge the general agreement among datasets. This hinders a meaningful comparison of datasets based on SLP over these regions, which should be also taken into account in model evaluation.

1.3.2 Atmospheric Blockings

Atmospheric blocking constitutes a major source of low-frequency variability in mid-latitudes. They are associated with large-scale high-pressure systems, lasting several days to weeks, that substantially modify the zonal flow by interrupting the eastward-travelling extratropical cyclones in the North Atlantic or by displacing their trajectories towards the north or south (Rex, 1950; Schwierz et al., 2004; Jury et al., 2019). Blocking episodes interrupt the typical westerly flow, often leading to extreme weather events such as prolonged droughts, heatwaves, or cold spells (Barriopedro et al., 2006). Their identification requires a dedicated methodology, such as

the Blocking Intensity (BI) index, which relies on meridional gradients of Z500 over specific latitude bands. Given their regional impacts and links to persistent circulation anomalies, blockings are a crucial element in this Thesis. Since the first subjective definition of atmospheric blocking by Rex (1950), there is no universally accepted criterion for their detection (Lupo, 2021), and several objective methods are in use nowadays (see e.g. Pinheiro et al., 2019, for an overview).

1.3.3 Teleconnection patterns

Teleconnection patterns are a persistent and recurrent large-scale anomalies in atmospheric circulation that link climate variability between distant regions of the globe (Wallace and Gutzler, 1981). The North Atlantic Oscillation (NAO), East Atlantic (EA), and Scandinavian Pattern (SCAND) are some examples of teleconnection patterns affecting the European Climate, encapsulating recurrent and spatially coherent patterns of atmospheric variability (Barnston and Livezey, 1987). These indices are typically derived through principal component analysis (PCA) of standardized Z500 anomalies (Hurrell et al., 2003), and they represent dominant modes of mid-tropospheric variability across the extratropics. The teleconnection indices considered in this Thesis are briefly introduced next. Further details can be found in the references provided.

North Atlantic Oscillation (NAO) The NAO pattern consists of a north-south dipole of SLP anomalies with two centers located over Iceland and the North Atlantic respectively (Barnston and Livezey, 1987). The NAO is the strongest variability mode in winter and summer in Europe. It can modulate the intensity and location of the North Atlantic jet stream and storm track (Hurrell, 1995), which in turn affects temperature and precipitation (Trigo et al., 2002) often extending from eastern North America to western and central Europe (Van Loon and Rogers, 1978; Rogers, 1997). The positive phase of the NAO tends to be associated with above average temperatures in the eastern United States and across northern Europe and below average temperatures in Iceland, southern Europe and the Middle East. It is also related to increased precipitation over northern Europe and Scandinavia and dry conditions over southern and central Europe in winter (Bladé et al., 2011; Brands et al., 2012b; Casanueva et al., 2014). Responses of opposite sign are typically found during its negative phase.

East Atlantic Pattern (EA) The EA pattern was originally defined by Wallace and Gutzler (1981) and later reformulated by Barnston and Livezey (1987). The spatial structure of EA is still a matter of debate (Comas-Bru and Hernández, 2018), and different authors provide alternative descriptions. While some authors regard it as a north-south dipole of anomaly centres, others characterize it as a SLP monopole south of Iceland and west of Ireland. In

either case, it has a similar spatial structure to the NAO, although shifted slightly to the south, together with the corresponding storm track in between (Comas-Bru and Hernández, 2018). Its lower-latitude center contains a strong subtropical link in association with modulations in the subtropical ridge intensity and location. This subtropical link makes the EA pattern distinct from its NAO counterpart, which prevents simplistic relationships of natural proxies with NAO (Mellado-Cano et al., 2019). The positive phase of EA is associated with above average temperatures in southwestern Europe (Sáenz et al., 2001; Rodríguez-Puebla et al., 2010) and below average in some parts of north America. It is also connected to enhanced winter precipitation over the Atlantic watershed and weakening over southeastern Europe (Casanueva et al., 2014).

Scandinavian pattern (SCAND) Also referred to as "Eurasia-1" by Barnston and Livezey (1987), this pattern consists of a primary center of action over Scandinavia, with weaker centers of opposite sign over western Europe and eastern Russia/western Mongolia (Bueh and Nakamura, 2007). Its positive phase is characterized by increased Z500 over Scandinavia and western Russia. This suppresses anticyclonic activity and below average temperatures are found over central Russia and western Europe (in particular, a reduction of warm days in the Iberian Peninsula; Rodríguez-Puebla et al., 2010). Also, above average precipitation and more wet spells tend to occur over central and southern Europe, whereas the opposite occurs for Scandinavia across all seasons (Zveryaev, 2009; Casanueva et al., 2014).

1.3.4 Climate impacts induced by large-scale atmospheric dynamics

Regional climate variability is largely determined by large-scale atmospheric circulation (Soares et al., 2019), which, particularly in the extratropics, exhibits recurrent spatial patterns operating at multiple scales. Within the context of atmospheric circulation, SLP (Sec. 1.3.1) is considered a fundamental variable, as it serves as a near-surface proxy of large-scale circulation. The seasonal variability of large-scale mean sea-level pressure patterns exerts a direct influence on the regional European climate. Different mechanisms explain this relationship, such as the influence of some teleconnection indices, e.g. the NAO (Hurrell et al., 2003; Folland et al., 2009), which is characterized by a seasonal-shift dipole system of high-low pressures, and then is related to extreme seasonal temperature events (Favà et al., 2015), precipitation dry/wet spells and extremes (Trigo et al., 2004; Busuioc et al., 2001; Casanueva et al., 2014), droughts (Bladé et al., 2011), snow cover (Brands et al., 2014a), river flow (Massei and Fournier, 2012) or cereal production (Rodríguez-Puebla et al., 2007). Other teleconnections, such as the Scandinavian Pattern (SCAND) or the East Atlantic Pattern (EA, Wallace and Gutzler, 1981), also play an

important role influencing precipitation and temperature variability in Europe (Sáenz et al., 2001; Ramos et al., 2010; Casanueva et al., 2014; Comas-Bru and Hernández, 2018).

In addition to these recurrent patterns, the European climate is also affected by large-scale anomalous situations caused by atmospheric blocking (characterized by persistent high pressure systems, see Sec. 1.3.2). Recent studies show that precipitation anomalies are closely related to the longitudinal position of the blocking centers (Sousa et al., 2017), which modify the storm tracks. Also, the occurrence of these blocking situations has been associated with changes in the precipitation distribution, and may result in drought or flood events in summer (Lupo, 2021), due to its ability to disturb the predominant cyclonic westerly flow (Sillmann and Croci-Maspoli, 2009). Temperature extreme events have also been attributed to atmospheric blocking situations (Buehler et al., 2011). One example is the severe heat wave which affected eastern Europe and large parts of Russia in 2010 (Barriopedro et al., 2011). The strong linkage between warm temperature extremes and the atmospheric blocking mechanism (Pfahl and Wernli, 2012) is also involved in the positive heatwave trends observed in western Europe (Rousi et al., 2022), having an impact on ecosystems and societies, including excess mortality, wildfires and droughts, among others (Kautz et al., 2022). As a result, an adequate representation of atmospheric circulation and high/low pressure variability becomes essential for a proper representation of the main regional climate features, although current GCMs exhibit substantial errors in this sense (Vial and Osborn, 2012; Dawson et al., 2012; Masato et al., 2013).

Bhend and Whetton (2013) conducted a global assessment of the ability CMIP3 and CMIP5 climate models to reproduce observed regional SLP trends. Their research uncovered a widespread tendency to underestimate changes in observed SLP, particularly in tropical regions and during winter in high-latitude areas. These inconsistencies were evident for both generations of models and observation-based datasets, pointing to structural biases in the representation of SLP dynamics. As a consequence, errors in the SLP fields tend to propagate into other meteorological variables. In other words, if two models or reanalyses show differences in their pressure patterns, those discrepancies will inevitably translate into differences in other surface variables (Sterl, 2004). SLP biases affect the spatial patterns as well as the frequency and duration of the main Euro-Atlantic wintertime weather regimes (Dawson et al., 2012; Fabiano et al., 2020) and Atlantic and European winter blocking events (Vial and Osborn, 2012; Anstey et al., 2013). For instance, the frequency of the latter are systematically underestimated, by CMIP5 GCMs (Taylor et al., 2012). The representation of the Northern Hemisphere storm tracks has improved in CMIP5 GCMs with respect to previous model versions (Zappa et al., 2013), but they still underestimate cyclone intensity and present location biases (Chang et al.,

2012a; Colle et al., 2013). Likewise, CMIP5 GCMs are able to capture eastern Mediterranean weather regimes qualitatively, although they fail in reproducing quantitative features (Dawson et al., 2012; Hochman et al., 2019). The most recent generation of GCMs (CMIP6, Eyring et al., 2016) shows substantial improvements with respect to CMIP5 in the representation of atmospheric circulation worldwide (Cannon, 2020), although more focused analyses are still needed to adequately assess the implications at a regional scale for downscaling purposes (Addor et al., 2016; Perez et al., 2014; Otero et al., 2018).

1.4 Observed variability and projected changes in atmospheric circulation

In this Section, previous studies' conclusions regarding past and future projections of atmospheric circulation and related variables are addressed. Sea-level pressure, unlike geopotential, is generally insensitive to the general heating of the troposphere imposed by greenhouse gas emissions since the total mass of the atmosphere is not expected to increase (Xiong et al., 2020). However, horizontal temperature gradients driving thermal circulation cells have been reported to change on multiple scales or are projected to do so in the future. Such *thermodynamic* circulation changes include, for instance, a general strengthening of summer monsoon systems in the northern hemisphere due to growing land-sea temperature gradients (Turner and Annamalai, 2012; Eyring et al., 2021), a relative cooling of the Mediterranean Sea compared to surrounding land areas (Tuel and Eltahir, 2020), and more frequent blocking events over Greenland associated with surface feedback processes (Hanna et al., 2018).

Superimposed on these regional thermodynamic effects are the own dynamics of the large-scale atmospheric circulation, operating at hemispheric scale. It is commonly described by the number of circumpolar planetary waves (referred to as Rossby waves) in the geopotential height field or jet streams, influenced by the hemispheric meridional temperature gradient. The properties of these waves (length, amplitude and displacement) are largely considered to be stochastic, even on decadal to multidecadal time-scale, in what is commonly referred to as *internal* or *unforced* climate variability (Deser et al., 2012).

Several studies have shown that the dynamic components of atmospheric circulation are more important to local-scale climate variability than the thermodynamic ones (Elbaum et al., 2022), and that internal variability is of paramount importance in the extratropics (Maher et al., 2019; Deser et al., 2020), particularly in the North Atlantic - European sector (Deser et al., 2017). This variability complicates the detection of any externally forced change in the circulation, for instance, induced by greenhouse gas emissions or low-frequency natural sea-surface temperature variations. A remarkable exception from this is the response of the Southern Hemisphere circu-

lation to ozone depletion during the 1980s and 90s, and the subsequent ozone recovery, achieved by reducing the concentrations of inorganic halogens in the stratosphere agreed in the Montreal protocol in 1987. Ozone depletion caused an increase in the hemispheric meridional temperature gradient that drove a poleward shift and an intensification of the southern hemisphere westerlies during austral summer. This trend reversed around 2000 due to ozone recovery, but is now re-emerging in observations and projected to manifest in models along the 21st century, not because of ozone depletion but due to the effects of greenhouse gas emissions (Thompson et al., 2011; Banerjee et al., 2020; Goyal et al., 2021). Considering large internal variability, this is to date the one circulation change in the extratropics that has been most clearly attributed to an external forcing (Thomas et al., 2015).

Other continental to hemispheric-wide circulation observed changes can be less robustly attributed to external forcings. These include:

1. A poleward expansion of the Hadley cell in both hemispheres driven by ozone depletion, multi-decadal Sea Surface Temperature (SST) variability, and greenhouse gas emissions (in the Southern Hemisphere, only) (Grise et al., 2019).

2. Contrasting findings concerning the Hadley cell *intensity* ranging from a forced strengthening to a forced weakening (Zaplotnik et al., 2022; Chemke and Yuval, 2023).

3. A northern hemisphere jet stream and storm track strengthening during winter, (Blackport and Fyfe, 2022; Woollings et al., 2023; Franzke and Harnik, 2023) and weakening during summer (Coumou et al., 2015; Chang et al., 2016; Gertler and O'Gorman, 2019; Dong et al., 2022; Cox et al., 2024), with a forced response to Arctic sea-ice loss emerging at the end of the 21st century (Barnes and Screen, 2015; Coumou et al., 2018; Kang et al., 2023).

4. A weak *forced* poleward shift of the jet stream *position* on both hemispheres during both the summer and winter seasons (Woollings et al., 2023).

For a comprehensive overview on continental to hemispheric wide atmospheric circulation changes in observations and model projections, and the sources thereof, the interested reader is referred to Shaw et al. (2024). In essence, all of the aforementioned studies focus on atmospheric circulation changes at continental to hemispheric scale, looking, for instance, at zonal mean values for specific seasons of the year. Both issues are currently acknowledged as "knowledge gaps" (Shaw et al., 2024) and will be further examined in this Thesis. By addressing these gaps, this Thesis aims to provide a better understanding of the expected changes in near-surface circulation patterns across different seasons.

1.5 Process-based evaluation of climate models

The evaluation of the performance of Global Climate Models (GCMs) is a fundamental step in ensuring the credibility and robustness of future climate projections, especially when such models are used as boundary conditions for downscaling experiments (Sec. 1.2.4). Several criteria have been applied to assess GCM performance at both global and regional scales, in order to determine which models represent key processes in a plausible way when compared to observations. Some examples of globally applicable criteria include observationally constrained metrics such as the Transient Climate Response (TCR; Ribes et al., 2021; Tokarska et al., 2020; IPCC, 2021), models' historical performance based diagnostics (Brunner et al., 2020), or the consistency of future global temperature projections with observational constraints (Qasmi and Ribes, 2022). At the regional scale, particularly over Europe, some examples of indices used to assess model credibility are the position of the North Atlantic jet stream (Oudar et al., 2020), large-scale processes performance of historical simulations (Palmer et al., 2023), or the sea surface temperature (SST) anomaly for European surrounding water areas (Sobolowski et al., 2023). These evaluation metrics serve as a benchmark for model selection in coordinated downscaling frameworks like CORDEX.

In more detail, Palmer et al. (2023) proposed a CMIP6-based revision of the McSweeney et al. (2015) scoring system tailored to Europe, integrating circulation-specific diagnostics into the selection process. In fact, *process-based evaluation* of GCMs is a common denomination for the validation of models based on their representation of certain processes, for instance, related to atmospheric circulation. The idea of evaluating GCM performance by means of atmospheric circulation started long time ago (Jones et al., 1993; Hulme et al., 1993), although process-based GCM performance assessments have recently emerged, particularly within the downscaling community (Sec. 1.2.4; Giorgi et al., 2009; Jones et al., 2011; McSweeney et al., 2015; Maraun et al., 2017) in the framework of CORDEX, and the IPCC Assessment Reports (Sec. 1.2.2). One of the common goals of CMIP and IPCC is enabling a systematic evaluation of GCM performance in order to inform model developers and provide them essential inputs for the assessment of climate change within IPCC reports (Eyring et al., 2016, 2019).

This type of GCM evaluation compares the historical model simulations with pseudo-observations or reanalysis datasets (Sec. 1.2.3) in terms of the representation of atmospheric processes or dynamics, such as storm tracks, blocking events, jet streams or synoptic circulation patterns (Brands et al., 2013; Addor et al., 2016). Then, deviations between the models and observed reference datasets are quantized using some statistical evaluation metric. The fundamental premise in process-based evaluations is that more reliable future projections will result

from models that replicate more accurately important atmospheric processes in a historical period and their climate drivers.

In this context, atmospheric circulation variables (such as sea-level pressure) or main modes of atmospheric variability (like teleconnections or atmospheric blockings) are brought into focus as key driving resources for process-based evaluation. The rationale behind using large-scale atmospheric variables instead of local scale ones (e.g. temperature of precipitation) for evaluation is two-fold. First, because regional climate variability is largely determined by large-scale atmospheric circulation (Soares et al., 2019), and second, because such local-scale variables emerge as an important source of uncertainty in climate projections of GCMs (Maraun et al., 2010).

All in all, the IPCC and the CORDEX community have come to the common conclusion that process-based evaluation is not only a desirable practice, but also a crucial step for the advance of climate modeling. It serves as an essential link between understanding the performance of current models and trusting future climate projections. Assessing how well models represent key dynamical processes, especially those driving regional climate such as atmospheric circulation, blockings or storm tracks, becomes a requirement for climate simulations plausibility, at the same time that models increase in complexity and output volume. These assessments are essential for developing physically credible GCM projections that can be used in impact studies and downscaling, as well as to guide the evolution of future CMIP generations. In this context, synoptic scale classification techniques based on clustering analysis present a promising way to address this need in climate modeling: to find effective, impartial, and interpretable configurations to evaluate dynamical model performance by reducing and simplifying the high dimensionality of the "problem".

1.5.1 Synoptic climatology and atmospheric circulation classification

The use of different *clustering* techniques is common in geosciences, particularly in synoptic climatology (Lee and Sheridan, 2015), building upon the extensive collection of meteorological data across the globe. Clustering techniques are mainly used to define Circulation Types (CT) and Weather Types (WT). In this context, different atmospheric states represented by time series of one or more meteorological variables are grouped into clusters (each corresponding to a CT or WT) based on their similarity. Specifically, CTs often refer to clusters formed from climate variables such as surface pressure and other upper-air variables (e.g., geopotential, humidity), whereas WTs refer to clusters formed from surface-level climate variables (e.g., precipitation, surface temperature). International initiatives (e.g. Tveito et al., 2016) have

defined and detailed CTs and WTs in a multitude of studies since 2005.

The application of circulation and weather type classifications has provided novel insights into climatological trends and projections, turning them into practical and meaningful analytical tools in this field. For example, Littmann (2000) employs WTs/CTs to classify mid-troposphere atmospheric circulation over the Mediterranean Sea into 20 clusters. The daily sequence of cluster occurrences is used to explain precipitation variability in the region. Moreover, Huth et al. (1993) analyze daily winter climatic conditions (December–February) in Prague, identifying 44 weather types. This study uses up to eight variables to characterize the climatic conditions (such as daily mean temperature, relative humidity, wind speed, etc.), effectively scaling the data volume by a factor of eight. In a follow-up study, Huth et al. (2008) investigate the evolution of these techniques within the COST733 Action, presenting a three-fold approach for CTs and WTs: the historical climatological analysis, the analysis of present climate variability, and the evaluation of GCMs. In this way, the usefulness of CTs and WTs in process-based model evaluation aligns with the needs previously identified by the IPCC and the CORDEX initiative.

Synoptic weather types are a useful tool as they summarize the whole range of variability of the data into a few construable patterns (Huth et al., 2008; Littmann, 2000; Stryhal and Huth, 2017). A well-known circulation classification method is the Lamb Weather Type (LWT) Classification. The LWT classification is a *subjective* clustering approach defined by the climatologist Hubert H. Lamb (Lamb, 1972) with the aim of studying the synoptic climatology over the British Isles. The LWT classification is based on a number of rules which rely on meteorological expert knowledge. This differs from objective clustering algorithms, such as K-means or Self-Organizing Map (SOM), which are data driven. Therefore, LWT classification is deterministic and has a straightforward and well-defined physical interpretation. This is an advantage since the results obtained can be interpreted in terms of actual meteorological conditions, and there is no source of added uncertainty as in stochastic clustering algorithms, whose results are initialization-dependent. Later in the computer era, Jenkinson and Collison (1977) developed a more *objective* scheme following Lamb's principles, known as the Jenkinson–Collison Weather Type (JC-WT) classification. The JC-WT approach is an automated procedure using a set of equations based upon SLP (Sec. 2.2) and is able to reproduce circulation types with negligible differences from the original LWT catalogue (Jones et al., 1993, 2013). Furthermore, unlike the original LWT approach, the JC-WT scheme has the advantage of being automatically applicable to different geographical locations through the introduction of some adjustment parameters to account for changes in the relative grid spacing as a function of latitude. Taking all of this into account, the JC-WT classification methodology emerges as a strong candidate among clustering

techniques to perform a process-based evaluation of GCMs.

The JC-WT classification provides a robust Eulerian framework for characterizing daily synoptic-scale circulation patterns, based on geostrophic wind and vorticity diagnostics derived from SLP fields (Sec. 2.2). Unlike Lagrangian storm-tracking methods (e.g. Hodges, 1994), which offer detailed insights into individual cyclone trajectories and intensities (Priestley et al., 2020; Priestley and Catto, 2022), JC-WT captures broader atmospheric regimes, including anti-cyclonic and directional flows, that may not manifest as distinct low-pressure centers. Similarly, other popular Eulerian approaches like the Extratropical Cyclone Activity Extratropical Cyclone Activity (ECA) index (Wallace et al., 1988) or similar monthly variance statistics, can effectively quantify storm track variability (see e.g, Chang et al., 2012b, 2016), but they lack the categorical structure needed to assess regime shifts or blocking patterns. In contrast, JC-WT enables the detection of persistent circulation changes through the aggregation of daily types into broader categories, making it particularly suitable for long-term climatological analyses (Trigo and DaCamara, 2000) and model intercomparison of historical simulations (Brands, 2022b,c; Brands et al., 2023a). For these reasons, the JC-WT classification provides a particularly suitable and interpretable framework for evaluating projected changes in atmospheric circulation.

1.6 Objectives

Building on the previous context and motivation exposed, the main goal of this Thesis is to expand the knowledge on the representation, assessment, and future projection of large-scale atmospheric circulation of Global Climate Models (GCMs) from CMIP5 and CMIP6 experiments in the context of climate change. For this purpose, weather typing classification is used for process-based GCM evaluation, along with the estimation of future changes in the atmospheric circulation. Specifically, the Thesis is structured following three primary objectives:

1. Assess the potential and limits of the JC-WT methodology as a process-based diagnostic tool to evaluate the atmospheric circulation of GCMs.

    - Examine the global extratropical applicability of the JC-WT classification method (including the Southern Hemisphere).
    - Connect the JC-WTs to the main modes of climate variability (such as predominant teleconnection indices and atmospheric blockings), as a way to evaluate the physical consistency, meaningfulness and diagnostic capability of the classification scheme.

2. Evaluate the ability of the new generation of GCMs from CMIP5/6, developed for the IPCC Fifth and Sixth Assessment Report (AR5 and AR6, respectively), on their ability to represent observed large-scale atmospheric circulation patterns. This process-based evaluation involves to:

    - Analyze the observational uncertainty in the JC-WT classification.
    - Quantify the ability of CMIP5/6 models to reproduce historical JC-WTs classifications in the extratropics, focusing on a diversity of WTs features and evaluation metrics.

3. Estimate projected future changes in the atmospheric circulation patterns on the *synoptic* scale (by means of the JC-WTs classification) globally, thus considering a closer link to local-scale climate variability relevant for impact studies.

    - Identify emerging changes of JC-WT from model ensemble internal variability.
    - Generate a catalog of global JC-WT from more than 50 GCMs for both their historical simulations and future CMIP5 and CMIP6 projections.

1.7 Structure

This Thesis is organized into three main parts, comprising seven chapters, each of them aiming to address the objectives outlined in the previous section.

Part I (State of the art and methods) is made up of two introductory chapters. Chapter 1 introduces the motivation, objectives, and structure of the Thesis. This chapter sets the ground for the topic by presenting the current context of the Global Climate Models (GCMs), their evolution, reanalysis datasets, large-scale atmospheric circulation of GCMs and the need for their process-based evaluation. To close this chapter, the main objectives of this Thesis are introduced.

Chapter 2 explains the data sources and the methodological background necessary to support the subsequent analyses. It describes the details of the main methodological tool, the Jenkinson–Collison Weather Type (JC-WT) classification, its application and its relationship with the main modes of climate variability, the metrics used to evaluate model performance and to examine their future changes.

Part II (Contributions) contains the main contributions of the Thesis. It is divided into four chapters where the fundamental scientific objectives are addressed, including the results of four scientific papers, led by the PhD candidate. Chapter 3, based on results from Fernández-Granja

et al. (2023) and Fernández-Granja et al. (2024), explores the global suitability of the JC-WT classification scheme, including its limitations and physical interpretability through links with large-scale atmospheric modes. Chapter 4, based on results from Fernández-Granja et al. (2023) assesses the uncertainty associated with reanalysis products. Chapter 5, based on results from Fernandez-Granja et al. (2021), presents a process-based evaluation of GCMs, through their ability to reproduce JC-WT characteristics, to support model selection in regional downscaling frameworks. Chapter 6, based on results from Fernández-Granja et al. (2025) analyzes projected changes in JC-WT frequencies under under climate change conditions, evaluating the emergence of circulation changes in extratropical regions.

Finally, Part III (Concluding Remarks) presents the conclusions and future perspectives in Chapter 7, summarizing the key findings of the Thesis, as well as discussing implications for climate change impact assessments and model selection, software tools and datasets developed during the Thesis, related contributions, and avenues for future research.

2

Methodological and data framework

2.1 Data sources

This section describes the atmospheric circulation data used in this Thesis to support the achievement of the objectives outlined in Section 1.6.

2.1.1 Reanalysis datasets

In this Thesis, reanalyses serve as a pseudo-observational reference to evaluate the performance of Global Climate Models (GCMs). The premise is that the closer the GCMs reproduce the reanalysis, the better their performance (Sec. 1.5). Up to five different reanalyses are taken into account in this Thesis to adequately encompass the widest possible range of reanalysis uncertainty, namely: ERA-Interim (Dee et al., 2011), ERA5 (Hersbach et al., 2020), ERA-20C (Poli et al., 2016), JRA-55 (Kobayashi et al., 2015; Harada et al., 2016) and NCEP-NCAR (Kalnay et al., 1996).

ECMWF ERA Interim Reanalysis (ERA-Interim) is one of the most popular datasets in the contemporary atmospheric sciences, as it has received more than 20,000 citations to date. However, the ECMWF Reanalysis 5 (ERA5) has recently replaced ERA-Interim. Whereas the ERA-Interim covers the period 1979-2019 in a 3-hourly time resolution (not the case for some variables, such as sea-level pressure (SLP), which is only available 6-hourly), ERA5 extends from 1950 onwards and it is continuously updated in hourly time-steps. Their spatial resolutions are approximately 79 km for ERA-Interim and 31 km for ERA5 ($1° \approx 100km$ in the Equator), with 60 vertical levels (from the surface up to 10 Pa) for ERA-Interim and with 137 vertical levels (from the surface up to 1 Pa) for ERA5[1]. ECMWF 20th Century Reanalysis (ERA-20C) is ECMWF's first atmospheric reanalysis covering the entire 20th century, from 1900 to 2010 (in a 6-hourly time resolution for SLP), with a 1.13° two-dimensional instantaneous

[1] https://www.ecmwf.int/en/newsletter/159/meteorology/global-reanalysis-goodbye-era-interim-hello-era5

diagnostic fields and 37 pressure levels vertically. However, this reanalysis only assimilates observations of surface pressure and surface marine winds, thus assimilating less components than other reanalyses. The Japanese 55-year Reanalysis (JRA-55), implemented by the Japan Meteorological Agency (JMA), covers from 1958 to 2013 in a 3-hourly time resolution, and has a 1.25° longitudinal-latitudinal spatial resolution. It also assimilates regular radiosonde observations. Finally, the NCEP–NCAR Reanalysis 1 (NCEP), developed by the National Oceanic and Atmospheric Administration (NOAA) Earth System Research Laboratory, consists of a 6-hourly dataset covering from 1948 to near present, with a global spatial coverage of 2.5° × 2.5° resolution and 28 vertical layers. The main characteristics of these reanalyses are summarized in Table 2.1.

Reanalysis	**Nom. res. (°)**	**Modelling Center**	**Reference**
ERA-20C	1.13	ECMWF	Poli et al. (2016)
ERA-Interim	0.75	ECMWF	Dee et al. (2011)
ERA5	0.25	ECMWF	Hersbach et al. (2020)
JRA-55	1.25	JMA	Kobayashi et al. (2015); Harada et al. (2016)
NCEP Reanalysis 1	2.50	NCEP-NCAR	Kalnay et al. (1996)

Table 2.1: *Reanalyses used in this Thesis, their nominal resolution at the Equator (in °) and modelling centers producing them. ECMWF: European Center for Medium Range Weather Forecasts; JMA: Japanese Meteorological Agency; NCEP-NCAR: National Centers for Environmental Prediction / National Center for Atmospheric Research.*

2.1.2 Sea-Level Pressure data

For this Thesis, a significant computational effort was devoted to the download and handling of 6-hourly sea-level pressure (SLP) data from five different reanalyses and more than forty GCMs. The main characteristics of the reanalyses (see also Sec. 2.1.1 for an overview) are summarized in Table 2.1, and characteristics of the GCMs can be found in Tables 5.1 and 6.1. SLP data for the historical period covering 1979–2005 for reanalysis and CMIP5 GCMs and up to 2014 for CMIP6 were retrieved; as well as RCP8.5/SSP5-8.5 scenarios from CMIP5/6, respectively, until 2100. All these data were directly downloaded from the ESGF[2] nodes (Cinquini et al., 2012; Williams et al., 2016). Altogether, this corresponds to an estimated total of approximately 1500 GB of SLP data (1.5 TB).

Regridding of Sea-Level Pressure

As reanalyses and climate models operate at different native resolutions (Tables 2.1 and 6.1), any validation or intercomparison exercise necessarily requires regridding them to a common

[2]The Earth System Grid Federation (ESGF) is a globally distributed data infrastructure that provides access to climate model output and observational datasets for research and policy support: https://esgf.llnl.gov/nodes.html.

spatial grid. This step is crucial to ensure a fair and consistent comparison among datasets. Several interpolation methods can be applied for this purpose, such as nearest-neighbor, bilinear, or conservative remapping, among others.

In this Thesis, regridding by spatial averaging (*upscaling* hereafter) is performed for the different datasets to match a common 2.5° resolution grid. This *upscaling* is designed to preserve the smoothness and spatial consistency of the variable during the interpolation process onto a coarser grid. It applies an aggregation function (the mean in this case) across the neighboring points that fall within the new larger (coarser) gridbox. After upscaling, bilinear interpolation is used (only if 2.5° is not a multiple of the original resolution).

2.1.3 Atmospheric Blockings data

The Blocking Index (BI) detection methodology introduced by Barriopedro et al. (2006) is used for the atmospheric blocking estimation. BI is based on meridional differences of geopotential height at 500 hPa (Z500, Z in the equations) over a 2.5×2.5° latitude-longitude grid encompassing the latitudinal range between 55 and 65°N. A blocking situation is identified when the criteria on Eq. 2.1–2.3 are fulfilled for at least one of the five Δ values $\{-5.0°, -2.5°, 0°, 2.5°, 5°\}$ and for five consecutive longitudes (i.e. spanning at least 12.5°) for at least five consecutive days:

$$\frac{Z(\lambda, \Phi_0) - Z(\lambda, \Phi_S)}{\Phi_0 - \Phi_S} \geq 0 \tag{2.1}$$

$$\frac{Z(\lambda, \Phi_N) - Z(\lambda, \Phi_0)}{\Phi_N - \Phi_0} \leq -10 \;\; m/deg \tag{2.2}$$

$$Z(\lambda, \Phi_0) - \overline{Z(\lambda, \Phi_0)} > 0 \tag{2.3}$$

where:

$$\Phi_N = 77.5°\mathrm{N} + \Delta$$

$$\Phi_0 = 60.0°\mathrm{N} + \Delta$$

$$\Phi_S = 40.0°\mathrm{N} + \Delta$$

using for the calculation the daily Z500 at latitude Φ and longitude λ, and the climatological mean $\overline{Z}$ for that particular day.

In this Thesis, the BI dataset used for the European domain was shared upon request by

Jury et al. (2019). Their calculation is based on the ERA-Interim Z500 field and encompasses the period 1981-2005. The interested reader is referred to Jury et al. (2019) and the more detailed description of the BI detection algorithm in Barriopedro et al. (2006).

For a meaningful representation of the signature of blocking on the JC-WT classification for Europe, BI data over the Euro-Atlantic region are divided into three longitudinal subdomains covering the western, central and eastern parts: the Eastern Atlantic (ATL, 30°W–0°E), western-central continental Europe (EUR, 0°E–30°E) and eastern Europe (Russia RUS, 30°E–60°E). For each subdomain, data consists on an aggregated single binary daily time series, identifying the blocking days (1) according to the BI detection methodology; the rest of the days were classified as non-blocking days (0).

2.1.4 Teleconnection patterns data

Data from teleconnection indices such as the North Atlantic Oscillation (NAO), East Atlantic (EA), and Scandinavian (SCAND) are considered in order to achieve the objectives from this Thesis. More details on the spatial patterns and influence of these teleconnections can be found in Sec. 1.3.3. Monthly series for the main teleconnection indices affecting Europe were retrieved from the NOAA Climate Prediction Center (https://www.cpc.ncep.noaa.gov/data/teledoc/telecontents.shtml). These indices are derived from a rotated principal component analysis of monthly mean standardized anomalies of Z500, with a 3-month moving window, from 1950 to the present. In this work, the period 1979-2005 was used, which is common to the considered reanalyses.

2.2 Jenkinson-Collison Weather Type (JC-WT) classification

The Jenkinson–Collison Weather Types (JC-WT) classification method is a widely used circulation-typing scheme to characterize atmospheric patterns at the synoptic scale. Originally developed as an objective reformulation of the Lamb Weather Types (LWT, Sec. 1.5.1) by Jenkinson and Collison (1977), it was designed to automate and generalize Lamb's manually applied classification over the British Isles (Lamb, 1972). The system relies on a deterministic classification of weather types based on a number of rules requiring meteorological expert knowledge for the interpretation of daily SLP charts, providing a straightforward and well-defined physical interpretation of SLP patterns.

LWTs were originally developed centered in the British Isles (55°N, 5°W). The efforts of Jenkinson and Collison (1977) to automatize LWTs made it possible to easily apply the classification at any centering point over mid-latitudes (Jones et al., 1993, 2013). The original JC-WT

method is based on instantaneous 12 UTC SLP fields, extracting a grid of 16 points to compute geostrophic wind direction and vorticity. Each couple of points has a separation of 5° latitude by 10° longitude between them, making a grid of points covering 30° longitude by 20° latitude (Fig. 2.1).

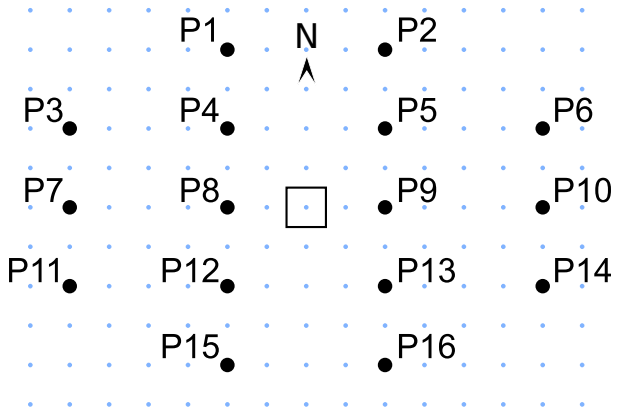

Figure 2.1: *Spatial distribution of the grid point pattern ("cross") of 16 points (in black) used in the JC-WT classification scheme for any location worldwide. The background grid (in blue) represents a* 2.5° *regular underlying grid, to which all datasets have been interpolated. The square indicates the central grid cell of the cross, located at latitude* ψ *(see equations in Table 2.2).*

The formulation of the JC-WT classification uses six parameters related to wind-flow characteristics: southerly flow, westerly flow, total flow, southerly shear vorticity, westerly shear vorticity and total shear vorticity (see equations in Table 2.2). Depending on their values, the SLP is classified in a given weather type following these rules defined by Jenkinson and Collison (1977):

1. The direction of flow is $\tan^{-1}(W/S)$, where W and S are the westerly and southerly flows, respectively. 180° is added if W is positive. The appropriate direction is calculated on an eight-point compass allowing 45° per sector. For example, the *Westerly* type occurs between 247.5° and 292.5°.

2. If $|Z|$ (total shear vorticity) is less than F (resultant flow), flow is essentially straight and corresponds to a JC-WT pure directional type.

3. If $|Z|$ is greater than $2F$, then the pattern is strongly cyclonic ($Z > 0$) or anticyclonic ($Z < 0$). This corresponds to JC-WT's pure cyclonic and anticyclonic types.

4. If $|Z|$ lies between F and $2F$ then the flow is partly (anti-)cyclonic and this corresponds to one of JC-WT's synoptic/direction hybrid types, e.g., anticyclonic easterly (AE) and cyclonic northerly (CN).

5. If F is less than 6 and $|Z|$ is less than 6, there is light indeterminate flow corresponding to JC-WT's unclassified type U. The choice of 6 is dependent on the grid spacing and would need tuning if used with a finer grid resolution.

The implementation requires an explicit inversion of the signs of the constants involved in the calculation of geostrophic flow and vorticity terms, as well as a reversal in the spatial ordering of the 16-point cross used as input (see Table 2.2). These adaptations are necessary to ensure a physically consistent interpretation of directional flow and rotational features under SH dynamics.

In the end, the JC-WT classification results in a set of 27 different weather types, including one pure cyclonic (C), one pure anticyclonic (A), eight directional types (N, NE, E, SE, S, SW, W, NW), sixteen hybrid types (directional + cyclonic/anticyclonic), and one unclassified (U) type (Fig. 2.2). The latter represents weak or chaotic flows with no dominant geostrophic tendency. Some state-of-the-art studies opt for different configurations of the JC-WT methodology by reducing the number of weather types obtained from the SLP classification. For instance, studies such as Trigo and DaCamara (2000) and Herrera-Lormendez et al. (2023) simplify the classification into 11 types: the anticyclonic and cyclonic types, the eight directional types and the unclassified type.

Param.	**Northern hemisphere**	**Southern hemisphere**	**Wind-flow characteristics**
W	$\frac{P_{12}+P_{13}}{2}-\frac{P_4+P_5}{2}$	$\frac{P_4+P_5}{2}-\frac{P_{12}+P_{13}}{2}$	Westerly flow
S	$s\left(\frac{P_5+2P_9+P_{13}}{4}-\frac{P_4+2P_8+P_{12}}{4}\right)$	$s\left(\frac{P_4+2P_8+P_{12}}{4}-\frac{P_5+2P_9+P_{13}}{4}\right)$	Southerly flow
D	$\arctan\frac{W}{S}$		Flow direction
F	$\sqrt{W^2+S^2}$		Resultant flow
Z_W	$z_w^-\left(\frac{P_{15}+P_{16}}{2}-\frac{P_8+P_9}{2}\right)$ $-z_w^+\left(\frac{P_8+P_9}{2}-\frac{P_1+P_2}{2}\right)$	$z_w^+\left(\frac{P_1+P_2}{2}-\frac{P_8+P_9}{2}\right)$ $-z_w^-\left(\frac{P_8+P_9}{2}-\frac{P_{15}+P_{16}}{2}\right)$	Westerly shear vorticity
Z_S	$z_s\left(\frac{P_6+2P_{10}+P_{14}}{4}-\frac{P_5+2P_9+P_{13}}{4}\right.$ $\left.-\frac{P_4+2P_8+P_{12}}{4}+\frac{P_3+2P_7+P_{11}}{4}\right)$	$z_s\left(\frac{P_3+2P_7+P_{11}}{4}-\frac{P_4+2P_8+P_{12}}{4}\right.$ $\left.-\frac{P_5+2P_9+P_{13}}{4}+\frac{P_6+2P_{10}+P_{14}}{4}\right)$	Southerly shear vorticity
Z	Z_W+Z_S		Total shear vorticity

where $s=\frac{1}{\cos\psi}$; $z_w^-=\frac{\sin\psi}{\sin(\psi-5°)}$; $z_w^+=\frac{\sin\psi}{\sin(\psi+5°)}$; $z_s=\frac{1}{2\cos^2\psi}$

Table 2.2: *Equations of the different circulation parameters of the JC-WT classification, for Northern (Jenkinson and Collison, 1977) and Southern Hemispheres (Sarricolea et al., 2018). Crosses in Fig. 2.1 displays the relative position of the points $i=1,\ldots,16$, for any location worldwide where SLP values P_i are considered.*

The advantages of this circulation typing method have been exploited in different studies in the Northern Hemisphere (NH). For instance, JC-WTs have been centered in the Iberian Peninsula in $[10°W, 40°N]$ (Trigo and DaCamara, 2000) and $[5°W, 40°N]$ (Ramos et al., 2014a),

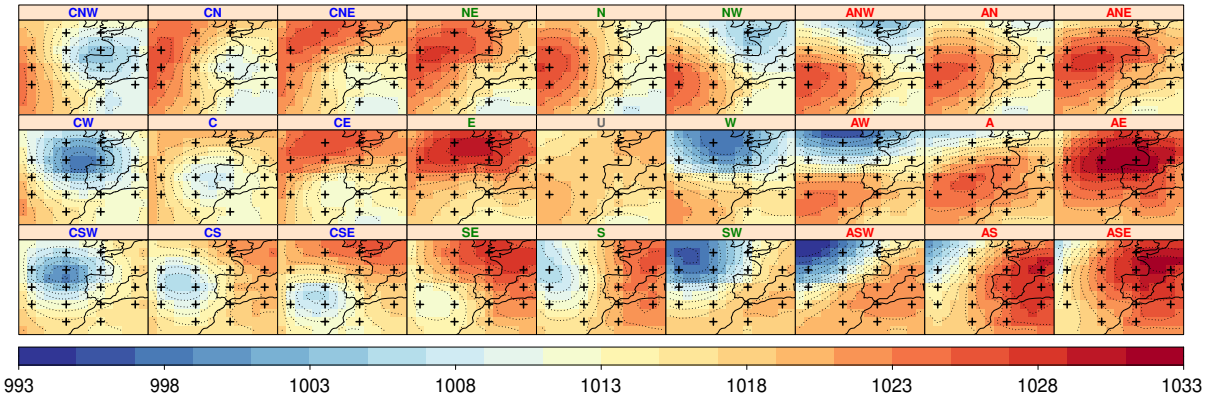

Figure 2.2: *Composite maps of SLP (hPa) and isobars for the 27 JC-WTs centroids for a classification centered over south-western Europe (40° N, 10° W), as an example. Note that the WTs are arranged in 3 groups of 9 WTs around the cyclonic (left panels and blue labels) and anticyclonic types (right panels and red labels) making a similar distribution to Self-Organized Maps (Kohonen, 1982) while following the cardinal directions (this explains that pure directional types, in green label, are beside its corresponding hybrid directional type, in blue or red). Purely directional types are arranged in the center, around the U type.*

in the western Mediterranean basin $[5°E, 40°N]$ (Grimalt-Gelabert et al., 2013), in southern Scandinavia $[15°E, 60°N]$ (Chen, 2000), in Central Europe $[10°E, 50°N]$ (Donat et al., 2010), in south-west Russia $[55°E, 55°N]$ (Spellman, 2017), in Ireland $[10°W, 55°N]$ (Fealy and Mills, 2018a), in Serbia $[20°E, 42.5°N]$ (Putnikovic et al., 2016) and in southeastern China (Wang and Sun, 2020; Wu et al., 2020). Otero et al. (2018) obtained, for the first time, a spatially continuous application of the JC-WT classification throughout Europe $[13°W - 34°E, 34°N - 71°N]$ and, in an unprecedented study, Brands (2022a) derived JC-WTs on every grid-box covering the majority of the NH extratropical region to evaluate GCM performance. However, to the best of my knowledge, the JC-WT classification has seldom been used in the southern hemisphere (SH), by Sarricolea et al. (2018) in southern Chile $[72.5°W, 42.5°S]$ and Brands et al. (2023b) in the course of this Thesis. These cases required an adaptation of the JC-WT equations to the SH circulation.

The JC-WT classification, built upon SLP fields only, is somewhat limited in its ability to infer other atmospheric features related to atmospheric circulation in a broad context. However, important information regarding low-level circulation physics can also be inferred from the analysis of the JC intermediate parameters, such as air flows and shear vorticities. The relatively easy interpretation of these airflow indices and the simplicity of the JC method, which allows transferability to other regions with a simple implementation, make it the preferred classification scheme in previous studies (e.g. Otero et al., 2018). Moreover, as shown by Conway and Jones (1998), circulation patterns fundamentally control meteorological characteristics on the surface, whereby the use of SLP has many advantages.

The above-mentioned teleconnection patterns and blocking events, however, operate on spatial scales covering entire continents, ocean basins and even the entire hemisphere. This scale is too coarse to capture the whole variability range of extratropical low and high pressure systems, whose relative positions determine the origin and properties of the air masses reaching a given location. In other words, any link between continental-to-hemispheric phenomena and local-scale climate variability is expected to materialize via atmospheric circulation anomalies on an *intermediate* scale, here referred to as "regional" or "synoptic". An approach to account for this can be the JC-WT classification, which, to date, has not been applied in this sense.

One of the goals of this Thesis is to contribute to the understanding and extension of the JC-WT classification methodology. Despite the fact that the JC-WTs are recommended to be applied in a limited range from middle to high latitudes (approximately from 30° to 70°) by Jones et al. (2013), the limits of applicability of JC-WTs are explored here, by obtaining them systematically in all locations of the globe, even in the Southern Hemisphere (Sec. 3.1). Additionally, the meaningfulness of the obtained JC-WTs is addressed, associating them with main teleconnection indices for different regions of the world (Sec. 3.2). Such analysis is inspired by previous studies such as Sarricolea et al. (2018), who investigated the JC-WTs associated with the teleconnections affecting central-southern Chile, namely El Niño - Southern Oscillation (Trenberth, 1997), Pacific Decadal Oscillation (Mantua and Hare, 2002) and Antarctic Oscillation (Limpasuvan and Hartmann, 1999) also known as Southern Annular Mode (Gong and Wang, 1999).

2.3 Measures for JC-WTs evaluation

2.3.1 Relative bias

One salient feature of a weather type is its probability of occurrence, which can be estimated by the relative *frequency of occurrence* in a sample, i.e. the proportion of records classified in a particular category over the complete time series length. From the historical record of observed weather types occurring at discrete T time steps $X_1, X_2, \ldots, X_T$, the frequency of occurrence of the JC-WT ℓ per season s is denoted as $f(\ell, s)$ and calculated as the number of time steps falling in type ℓ divided by the total number of time steps in the season $s \in \{DJF, MAM, JJA, SON\}$. Thus the relative bias ε is considered to compute the deviation of the JC-WT frequency with respect to a reference data set:

$$\varepsilon_m(\ell, s) = \frac{f_m(\ell, s) - f_o(\ell, s)}{f_o(\ell, s)} \tag{2.4}$$

where $f_m(\ell, s)$ refers to the frequency in the model m and $f_o(\ell, s)$ is the reference observed (in this case, reanalysis) frequency. The model (m) can be any of the considered GCMs or any of the reanalyses other than that used as observational reference. The relative bias is a non-dimensional measure, which is zero for a perfect agreement of frequencies.

2.3.2 Kullback–Leibler divergence

This measure (KL; Kullback and Leibler, 1951), also known as relative entropy, is used to quantify the degree of disparity between a GCM and the reanalysis in the representation of the different JC-WT probabilities. For this purpose, the JC-WT classifications obtained by the GCMs and reanalysis are handled as discrete Probability Mass Functions (PMFs), whose dissimilarity is measured through KL divergence (see e.g. Jiang et al., 2011; Sharma and Seal, 2019). The use of KL divergence in the comparison of two PMFs is more appropriate than using a distance function on a metric space (e.g. Euclidean distance) due to multiple facts: the PMFs may be differently distributed, have different sample sizes, different geometric centers or contain extreme probabilities that may disrupt the comparison negatively (Weijs et al., 2010; Jiang et al., 2011). Therefore, the KL divergence is not symmetric and it is not affected by any biases derived from the probability of the samples, thus avoiding the more frequent JC-WTs unduly influencing the evaluation results.

The KL divergence of a discrete probability distribution, $P(x)$, with respect to another, $Q(x)$, both defined on the same probability space X (in our case, spanned by the JC-WTs) is defined within the Information Theory (Cover and Thomas, 2006) as:

$$KL(P \parallel Q) = \sum_{x \in X} P(x) \log \frac{P(x)}{Q(x)} \tag{2.5}$$

The KL divergence is a measure of the statistical "distance" of the model distribution ($P(x)$) with respect to the reanalysis one ($Q(x)$). It is zero for a perfect match ($P(x) = Q(x)\, \forall x \in X$) and takes positive values without an upper bound for increasingly different distributions.

2.3.3 Transition Probability Matrix Score

JC-WT persistence or, more generally, transition probabilities between two different types are also important. They determine key temporal features such as spell duration, serving as an effective tool for the assessment of the model's ability to reproduce circulation pattern sequences (Gibson et al., 2016; Hochman et al., 2019; Fernandez-Granja et al., 2021). In order to estimate the differences among datasets (either among reanalyses or to evaluate GCMs), the probability

of transition of one type into another is assessed and analyzed using a Transition Probability Matrix (TPM), briefly described next. Let the discrete random variable X_t represent a particular JC-WT at time t, whose values $x_t \in \{1, \ldots, K\}$, where $K = 27$ is the total number of WTs. This variable is considered at two consecutive time steps, X_{t-1} and X_t, to construct the $K \times K$ transition probability matrix A, where $A_{ij} = p(X_t = j \mid X_{t-1} = i)$, representing the probability of transitioning from WT i to WT j. Hence, each row of the matrix adds one, $\sum_j A_{ij} = 1$. The TPM thus provides a visual "fingerprint" on how a given dataset represents the JC-WT classification centered on a given grid cell.

In order to summarize the TPM information, the Transition Probability Matrix Score (TPMS) is introduced. The TPMS allows assessing model performance (compared to reanalysis) based on their TPM fingerprint, defined as:

$$TPMS = \sum_{p \in A^*} |p_m - p_o| \tag{2.6}$$

where p_m and p_o are the transition probabilities in the model and in the observational reference (reanalysis), respectively, whose (absolute) difference is calculated considering the subset of transition probabilities A^* from the complete matrix (A), that are significantly different from the reanalysis, following the two-proportion Z-Test. In order to include the "missing" transitions in the score (i.e. either transitions that exist in the reanalysis but are never simulated by the model, or transitions that are simulated by the model but do not occur in the reanalysis), these are assigned a zero probability (i.e. either $p_m = 0$ or $p_o = 0$) and included in the A^* subset. As a result, the larger the departure from zero (perfect agreement), the larger the dissimilarity of the TPM fingerprints between the GCM and the reanalysis.

2.3.4 Two-Proportions Z-Test

The Two-Proportions Z-Test is used to assess statistically significant differences between models and reanalysis. It is used for proportions, which in this case arise from relative frequencies (proportion of time steps classified in a given JC-WT) and transition probabilities (proportion of time steps in JC-WT i with transition to JC-WT j). The test statistic takes into account the potentially different sample size in the model and reanalysis data. This test was performed for each combination of JC-WT ℓ, season s and model m, using a 95% confidence to establish significant probability or relative frequency differences. This parametric test is used to identify significant differences in their resulting weather type frequencies.

2.4 Estimates of future climate change

2.4.1 Global Warming Levels

Global Warming Levels (GWLs) are the basis for a climate change approach that quantifies impacts and responses as a function of specific thresholds in Global Surface Air Temperature (GSAT) relative to a pre-industrial baseline, typically 1850–1900. This method differs from traditional fixed period-based analyses by using a temperature increment axis instead, allowing a more direct and policy-relevant connection to climate targets such as those specified in the Paris Agreement (Iturbide et al., 2022; Seneviratne et al., 2021). This framework enhances comparability across emission pathways, climate models and disciplines, thus enabling inter-disciplinary assessments of risks and responses. For example, in Chapter 1 of the IPCC AR6 report ("Framing, Context and Methods", IPCC, 2021), GWLs are introduced to support a single analytical structure across Working Groups I, II and III, that facilitates homogeneous risk assessments and the synthesis of their reported outcomes.

Methodologies based on GWLs typically obtain the 20 or 30-year running means of GSAT during the 21st century (Vautard et al., 2014; Nikulin et al., 2018), and identify the first time slice that it surpasses predefined warming levels (e.g. +1.5°C, +2°C, +3°C or +4°C) above the pre-industrial period, for each individual model. Once these time slices are estimated, they are used to extract anomalies of regional climate variables (e.g., precipitation, temperature extremes, circulation indices) compared to a defined common baseline period (Seneviratne and Hauser, 2020; Diez-Sierra et al., 2023). In order to implement these GWLs from GCMs, GSAT data is retrieved from the public IPCC ATLAS github repository (https://github.com/SantanderMetGroup/ATLAS/tree/devel/datasets-aggregated-regionally/data/CMIP5/CMIP5_tas_landsea for CMIP5 and https://github.com/SantanderMetGroup/ATLAS/tree/devel/datasets-aggregated-regionally/data/CMIP6/CMIP6_tas_landsea for CMIP6). Note that the GSAT signal over land and sea is estimated.

An advantage of this methodology comes from the empirical scaling relationships found between regional climate impacts and global warming, which has been found for multiple variables for both CMIP5 and CMIP6 model ensembles. Although GWLs are calculated globally, Seneviratne and Hauser (2020) introduced the concept of "regional climate sensitivity" as the change rate of a regional climate variable (e.g. precipitation) per degree of global warming. This approach reveals quasi-linear and often robust relationships across world regions. However, the literature also notes significant multi-model spread in these responses, especially for circulation patterns, highlighting the need for robust statistics for multi-model ensembles and detection of

emergent signals (James et al., 2021).

In the context of this Thesis, near-surface circulation changes are analyzed using a GWL approach. *Regional climate sensitivity* plots are used to illustrate the relationship between a specific climate variable or derived climate index (in this case, future anomalies in the WTs frequencies) and global warming, as described by Seneviratne and Hauser (2020) and Diez-Sierra et al. (2023). These plots have also been used by the IPCC to assess the regional sensitivity to global warming in the Interactive Atlas (Gutiérrez et al., 2021, http://interactive-atlas.ipcc.ch), referred to as *GWL scaling plots* (or simply GWL plots hereafter).

2.4.2 Time of Emergence

Time of Emergence (ToE) is a widely used concept in climate science that refers to the point at which a climate change signal becomes statistically prominent from the background noise of natural climate variability (Hawkins and Sutton, 2012). That is, the signal would show an anthropogenically driven trend for the specific variable. Following Seneviratne et al. (2016), ToE is defined as the first time a projected anomaly exceeds a threshold related to the standard deviation of historical variability, and remains consistently beyond that threshold over time. This criterion ensures that the emergence is not simply a transient excursion due to variability, but reflects a sustained shift.

As introduced in IPCC AR6 (IPCC, 2021), ToE is closely related to the concepts of detection and attribution. It shows the point in time when the "forced" climate signal emerges from the envelope of internal variability. In this context, "signal" refers to long-term trends driven by external forcings (e.g., greenhouse gas emissions), and "noise" refers to the internal and unforced variability of the climate system. This concept can be applicable to a wide range of climate variables, from global temperature anomalies to regional-scale precipitation patterns, extreme events, or circulation changes. For example, Kirchmeier-Young et al. (2019) use ToE to identify the GWL at which a significant anthropogenic signal appears first in the probability of the occurrence of extreme temperature and precipitation events, based on large ensembles of climate models. Kirchmeier-Young et al. (2019) also address the importance of spatial and temporal scale in determining ToE. They demonstrate, using perfect-model large ensembles, that emergence tends to occur earlier for variables averaged over larger areas or longer periods, due to improved signal-to-noise ratios. For instance, large-scale temperature metrics show earlier emergence compared to local precipitation extremes, which are noisier and more subject to internal variability. ToE is applied in this Thesis to evaluate the emergence of signals of JC-WTs frequencies.

2.5 Software and computing resources

All the software used and implemented to achieve the objectives of this Thesis relies on R programming language (R Core Team, 2020). In addition to some libraries and functions, this Thesis builds mainly on `climate4R` (C4R; Iturbide et al., 2019), a bundle of R packages developed by the Santander Meteorology Group. C4R is an open-source software framework available on GitHub[3]. GitHub is a web-based platform used for version control and collaborative software development, and is also the main tool to contribute to the C4R framework. It allows multiple people to work on projects simultaneously, track changes, and manage different versions of their code. Software developers use it extensively to host and review code, manage projects, and build software together. It integrates with Git, a distributed version control system, to provide powerful collaboration features and tools for developers.

The C4R framework emerged as an increasingly used R-based environment (R Core Team, 2020), oriented towards climate services. It aims to gather under a single software the various procedures needed in climate studies, from data access to processing and visualization, designed for a broad range of climate data users.

The structure of the C4R environment is outlined in Figure 2.3. This environment is compatible with two basic types of climate data structures: gridded (or *grid-boxes*) and station-based (point locations). All datasets or grids (whether observational, reanalyses, seasonal forecasts, or climate projections) accessible through C4R follow a consistent and compatible metadata structure. Moreover, C4R is compatible with NetCDF (Network Common Data Form), which is a data format widely used in climate science to store and share information. NetCDF allows researchers to organize gridded climate data in a structured way, including helpful metadata (as units or coordinates), making them standard and reusable.

Thus, C4R constitutes a powerful framework for handling climate data, offering nearly 100 functions distributed across four core packages: `loadeR` (Cofiño et al., 2018; Iturbide et al., 2019), mainly focused on climate data access; `transformeR` (Iturbide et al., 2019), which provides tools for data transformation, manipulation, and conversion, among other capabilities; `downscaleR` (Bedia et al., 2020), which focuses on statistical downscaling and bias correction techniques; and `visualizeR` (Frías et al., 2018), for visualizing climate data. Moreover, several additional packages are fully integrated into C4R for specific application domains, such as species distribution modeling for ecological studies (Iturbide et al., 2018), the calculation of climate indices for drought or fire risk analysis (e.g. Bedia et al., 2018), and a specialized module for metadata annotation of climate products (Bedia et al., 2019). In particular, this

[3]https://github.com/SantanderMetGroup/climate4R

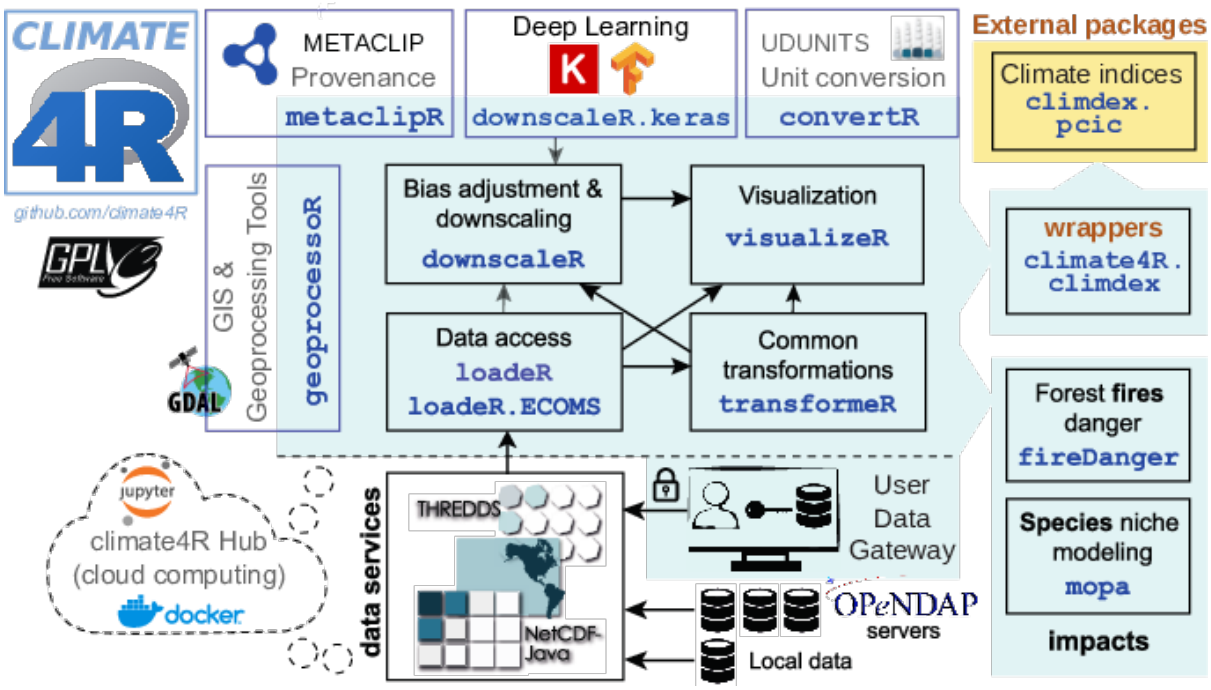

Figure 2.3: *Schematic overview of the* `climate4R` *(C4R) working environment, which consists of three layers: (a) Climate Data Services based on NetCDF-Java and THREDDS to load local or remote data, including datasets from the Santander Climate Data Service (User Data Gateway, UDG); (b) A core of basic R packages for data access and post-processing, composed of four main packages for data loading, transformation, downscaling and bias adjustment, and visualization. These core packages form the foundation for additional sector-specific impact study packages, thereby extending C4R functionalities to specific applications. (c) External packages, connected via functions adapted to the C4R data model. (d) Additional climate packages that provide extended functionality, including metadata tracking ("provenance") and unit control and transformation (based on the UDUNITS software). Arrows indicate possible data flows, and blue shading highlights internal developments. All components are distributed under the GNU General Public License. Logos of THREDDS, NetCDF-Java, and UDUNITS are courtesy of UCAR / Unidata. The R logo is © 2016 The R Foundation. The RDF icon used by METACLIP is © 1994–2006 W3C. This figure is taken from the official C4R repository at https://github.com/SantanderMetGroup/climate4R.*

Thesis makes extensive use of `loadeR`, `transformeR`, `geoprocessoR` (for data geo-processing) and `visualizeR`.

Regarding the computing resources used in this Thesis, large computing and storage resources were required for the data curation, calculation of JC-WTs classifications and postprocessing. The research group hosting this Thesis, i.e. the Santander Meteorology Group, has access to its own computing and storage infrastructure, the Santander Climate Data Service (SCDS). This service, which includes a node of the Earth System Grid Federation (ESGF) and is part of the Spanish node of the IPCC Data Distribution Center, makes use of the high performance infrastructure owned by the University of Cantabria (with a computing capacity of 512 cores and 2PB of storage) and allows external users to transparently access and process climate data.

Part II

Contributions

3

Contribution to the JC-WT methodology

Section 2.2 introduces the concept of JC-WTs, explaining its methodological basis, historical evolution, and providing examples of its applications, as well as emphasizing their relevance in the broader context of atmospheric variability and climate change research. In this Chapter, my contributions to the Jenkinson-Collison Weather Typing (JC-WT) classification method for atmospheric circulation are presented, which are based on two manuscripts: Fernández-Granja et al. (2023) and Fernández-Granja et al. (2024).

3.1 Exploring the limits of the JC-WTs applicability

3.1.1 Experiment setup

The first part of this Chapter (Sec. 3.1) examines the applicability and limitations of the method on a global scale, including the Southern Hemisphere. This alone constitutes a contribution to the method, as no previous study has applied JC-WTs comprehensively over all global locations, particularly in the Southern Hemisphere where their application has seldom been explored (Sec. 2.2). These results are based on SLP from ERA-5 reanalysis in 1979-2005 and global coverage, which has been interpolated to a 2.5° regular grid (Sec. 2.1.2). In order to produce the classification for the entire globe, the center of the cross is displaced from one grid-box to another through all points of the reference 2.5° regular SLP grid within a band from 80°S to 80°N. Note that grid-boxes within 90°S − 80°S and 80°N − 90°N are beyond the range of computational applicability of the JC-WT method since the cross extends 10° north-south from its center (Fig. 2.1). Note also that the $z_w^{\mp}$ coefficients from the JC-WTs equations (Table 2.2), included in the westerly shear vorticity estimation, are undefined at $\psi = \pm 5°$ cross center latitudes, and take nonphysical, negative values in between. Therefore, this latitudinal band has been excluded from our calculations. Here, the method is intentionally pushed to its limits in order to explore whether it can be applied anywhere between 30 and 70 degrees North or

South, as was estimated by Jones et al. (2013), or even beyond (Fig. 3.1).

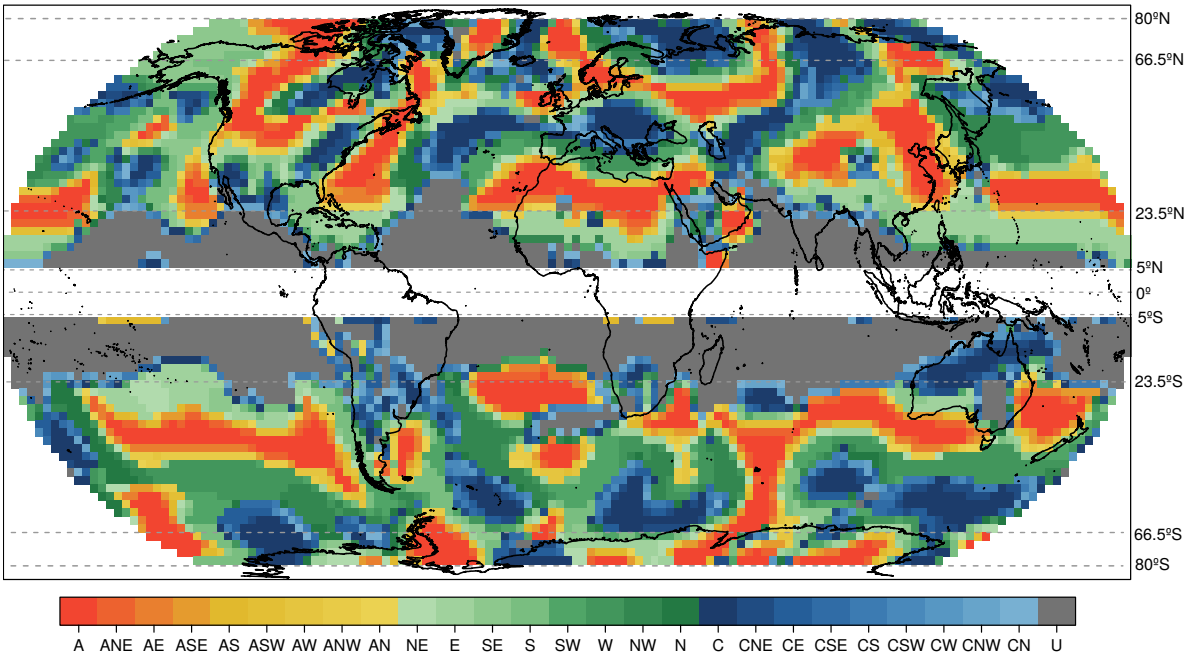

Figure 3.1: *Example of a single, 6-hourly record of the Jenkinson-Collison Weather Type catalogue obtained from ERA-5, corresponding to the SLP state at {1979-01-01} 00:00:00 UTC. The 26 JC-WT circulation types are indicated in the legend, ranging from purely anticyclonic (A) and its hybrids (ANE to AN), pure directional (NE to N) and purely cyclonic (C) and its hybrids (CNE to CN). Type 27, unclassified (U), is depicted in grey. For reference, dashed grey lines depict some latitudes such as the Equator, the Tropic of Cancer (23.5° N) and Capricorn (23.5° S) and the Arctic and Antarctic Circles (± 66.5°), and they are also included in subsequent figures.*

Two main aspects are addressed in order to investigate the suitability of the method for all regions of the world: (1) the number of different weather types, accounting for the regional circulation's *diversity*, and (2) the occurrence of the unclassified (U) type, showing weak pressure gradient with no clear vorticity behaviour, also known as *barometric swamp* (Grimalt-Gelabert et al., 2013). For the diversity criterion, weather types attaining relative frequencies above 0.1% are considered. This means that the specific WT must have 40 or more occurrences in the total record of nearly 40,000 time steps (6-hourly data over 27 years, equivalent to approximately 1.5 annual occurrences). This threshold is consistent with Brands (2022b), who applied the same criterion since some JC-WTs were found to occur with relative frequencies as small as 0.47% even in "optimal" conditions, such as over the British Isles, where the method was originally formulated (Perry and Mayes, 1998). In light of both measures (weather type diversity and type U frequency) jointly considered, the aim is to obtain empirical evidence of the global geographical boundaries for the applicability of the JC-WT classification.

3.1.2 *Worldwide diversity of the JC-WTs and presence of unclassified days*

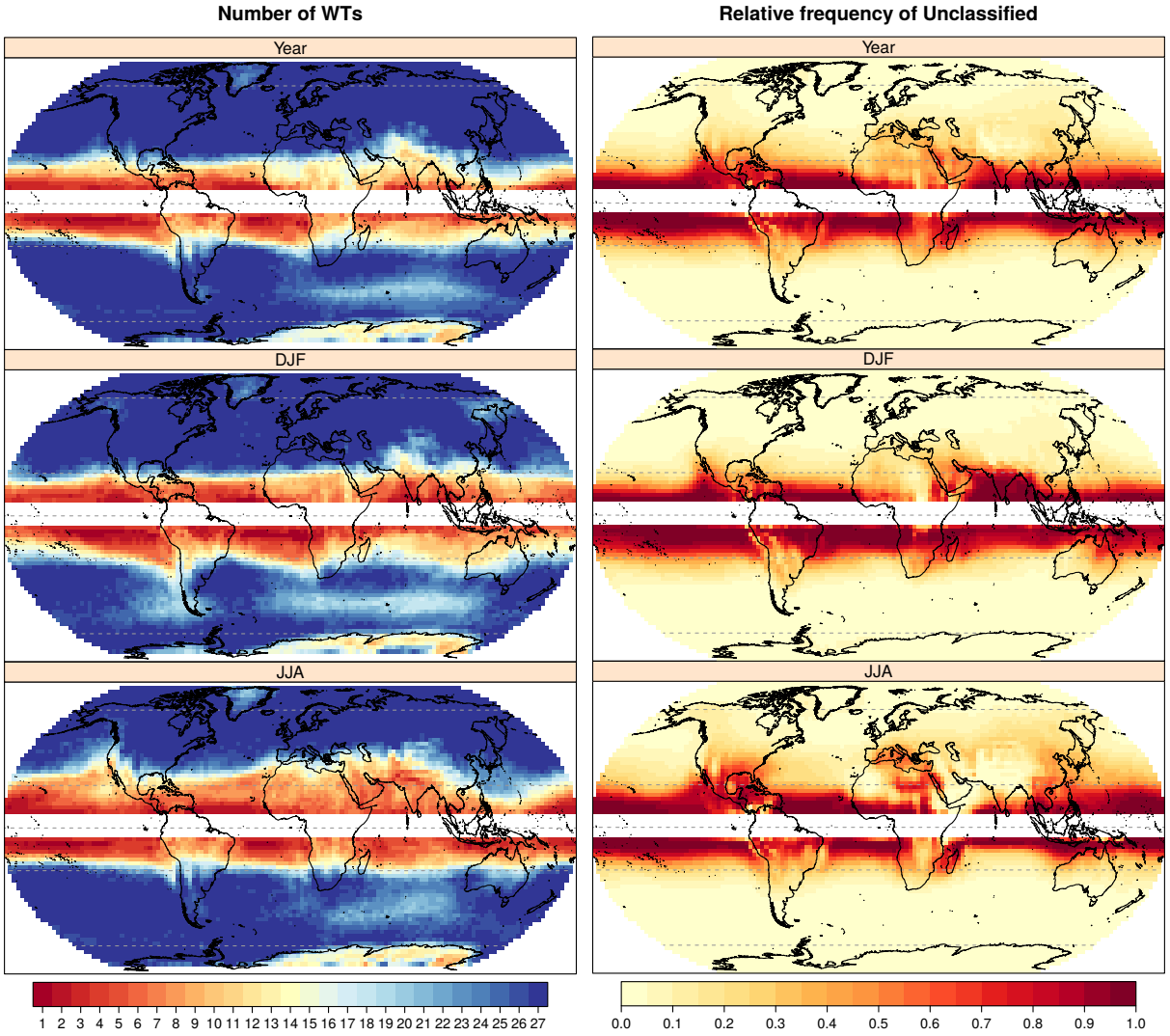

Figure 3.2: *Summary of the Jenkinson-Collison global classification calculated upon the SLP from ERA-5 (6-hourly, 1979-2005), considering the whole annual series (top row) and DJF and JJA seasons (rows 2–3 respectively). Left column: Number of weather types per grid-box with a relative frequency of occurrence above* 0.1%*. Right column: Relative frequency of the Unclassified type (U) per grid-box.*

Low diversity of WTs and frequent barometric swamp are here assumed to be indicative of the method working at its theoretical limits. The global distribution of the total number of distinct WTs (Fig. 3.2, left) shows a marked latitudinal gradient, with a decreasing diversity of types towards the tropics. Conversely, the frequency of the U type (Fig. 3.2, right) exhibits a sudden increase in the tropics, following a pattern similar to weather types diversity (left). In general, the lower the diversity of types, the higher the frequency of the U type, with a few regional exceptions, where reduced diversity coincides with small U-type frequencies. Such exceptions are found year-round over Antarctica and the Tibetan Plateau; and to a lesser degree also over Greenland and the southern Indian Ocean at mid-latitudes.

Figure 3.2 reveals a remarkable empirical threshold of around 16 different types corresponding to at least half the temporal records falling into the U type. This threshold is interpreted as an applicability criterion in the following and is generally met polewards at the Tropics latitudes on both hemispheres (±23.5°), which extends the range of application suggested by Jones et al. (2013), from 30° to 70°.

The aforementioned thresholds exhibit seasonal excursions which affect the Mediterranean, Middle-East and southwestern United States during JJA season (boreal summer), as well as the mid-latitude eastern South Atlantic and eastern South Pacific for DJF (boreal winter). These seasonal fluctuations go hand in hand with the seasonal shifts of the monsoon region and the Intertropical Convergence Zone (ITCZ; Barry and Carleton, 2013), where local scale processes of deep convection are predominant and may alter to some extent the applicability of the JC-WT classification beyond the extra-tropics. Applying the method under these circumstances makes little sense, since synoptic variability is, either missing at the considered scale, or it is represented by other variables than SLP.

In the Mediterranean Basin, for instance, suitability is optimal during DJF (maximum JC-WT diversity and a negligible U-type frequency), which is due to a southward shift of the Atlantic storm tracks in combination with autochthonous cyclogenesis over the Mediterranean Sea (see e.g. Fita et al., 2007). In JJA, however, the U-type frequency increases hand in hand with a shrinking type diversity, hence compromising the usefulness of the classification during this season.

Miró et al. (2020) used a modified version of the JC method, which combines the JC classification at the surface with an upper air classification based on 500 hPa geopotential height, obtaining a better differentiation within the U type, for a small region in the Pyrenees. Further research is needed for an overall and systematic application of the cited modified version, since expert local knowledge is needed to fine-tune the parameters, hence preventing its automated application in large-scale assessments.

In summary, for both hemispheres, the favourable area of application widens towards the Equator in winter and retreats towards the respective pole in summer (Fig. 3.2).

3.2 Signature of JC-WTs in large-scale atmospheric circulation dynamics

3.2.1 Experiment setup

The second part of the Chapter presents an in-depth analysis of the physical links of the JC-WT classification with major modes of atmospheric circulation (Sec. 3.2). In such analysis,

intermediate links are found between continental-to-hemispheric and local scales of climate variability, by means of the JC-WTs. We hypothesize that there is a significant link between these indices and the JC-WTs. As they modulate large-scale circulation, they could influence the frequency and configuration of JC-WTs. Therefore, incorporating them into the analysis improves the physical interpretability of the classification results and supports the use of JC-WTs in the process-based evaluation of GCMs (one of the goals of this Thesis).

Firstly, the influence of the Blocking Index (BI, Sec. 2.1.3) on JC-WTs is analyzed. For every grid-cell in the previously described subdomains (ATL, EUR and RUS; Sec. 2.1.3), the most frequent WT given a blocking day is selected. It is then tested whether this conditional frequency is significantly different from the climatological (unconditioned) frequency for that WT. To this aim, the two proportions Z-test implemented in the `prop.test` function from the R package `stats` (v3.6.3, R Core Team, 2020) is used, considering a 95% confidence level. For this matter, JC-WTs at 12-UTC from the 6-hourly series from ERA-Interim are retrieved (because BI is calculated daily) for 1981-2005 at the domains previously described in Sec. 2.1.3. Secondly, the association between teleconnection indices (Sec. 1.3.3) and JC-WTs is assessed by performing a correlation analysis. For this purpose, monthly time series of teleconnection indices (Sec. 2.1.4) and monthly frequencies for each WT are considered. For every grid-cell, the WT with the highest significant Spearman's correlation coefficient with a given teleconnection index is selected, at annual, JJA (boreal summer) and DJF (boreal winter) timescales. Statistical significance is tested by using the `cor.test` function from the R package `stats` (v3.6.3, R Core Team, 2020), using a 95% confidence level. These results are based in 6-hourly JC-WTs obtained from ERA-Interim in the region from 20°N to 80°N and 75°W to 75°E for the time period 1979-2005.

3.2.2 Sensitivity of JC-WTs to blocking events

Blocking events may, in theory, be captured by the JC-WT methodology as the size of the high-pressure anomaly produced by the blocking situation is comparable to the size of the input "cross" of 16 SLP points used in the JC-WT approach (Fig. 2.2). Figure 3.3 shows the composites of SLP anomalies conditioned on each of the three blocking centers (Sec. 2.1.3), indicating distinct surface high-pressure signatures around the blockings in all cases. According to Jury et al. (2019), the climatological probabilities of the ATL, EUR and RUS blockings in the period 1981-2005 are around 0.13, 0.14 and 0.10, respectively.

In general, the characteristic spatial distribution of blocking frequencies has been described in the literature as a bimodal geographical distribution with major peaks over the North Atlantic

and eastern North Pacific in all four seasons (Croci-Maspoli et al., 2007; Pfahl and Wernli, 2012), with some secondary longitudinal discrepancies depending on the blocking detection methodology and input variables (e.g. Pelly and Hoskins, 2003).

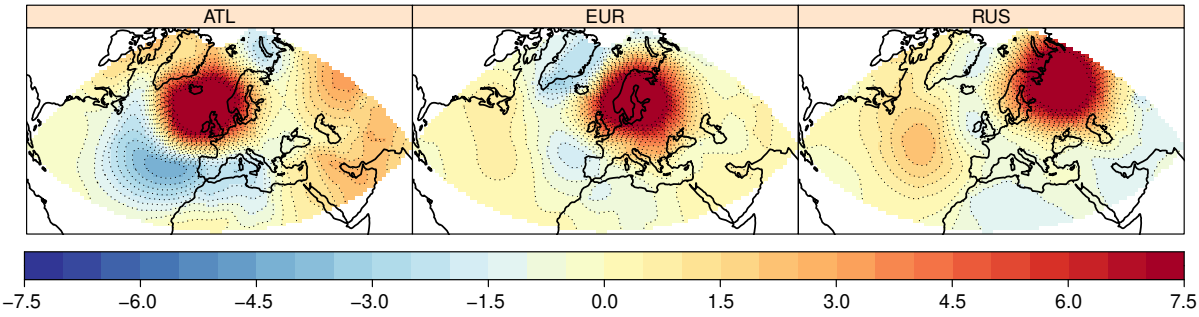

Figure 3.3: *SLP anomaly (hPa) during blocking conditions in the three subdomains considered in this analysis, namely Atlantic (ATL, 30° W-0° E), western Europe (EUR, 0° E-30° E) and continental Europe (RUS, 30° E-60° E). See Sec. 2.1.3 for more details on the three subdomains and blockings detection.*

Figure 3.4 shows the spatial "fingerprint" of blocking on the JC-WT classification, as represented by the most frequent type in each grid-box of the Euro-Atlantic region conditioned on blocking occurrence. It is then tested whether this conditional frequency is significantly different from the climatological (unconditioned) frequency of that WT. If not statistically significant, the result is hatched. As a result, the purely anticyclonic (A) type is most frequent in the three subdomains under blocking conditions. In all of them (ATL, EUR and RUS panels of Fig. 3.4), blocking events break the prevailing subpolar low-pressure conditions with the dominance of type A ridges, that penetrates poleward. The low pressure situation is found in the upper left panel of Fig. 3.4 (overall climatology of the most frequent JC-WT under no blocking conditions) within the two parallel lines (indicating the latitudinal band 55°N-65°N) where blocking centers are searched.

However, the A type predominance is not confined to these "source regions" but rather forms a *zonal circumpolar belt* located at mid-to-high latitudes over the European continent, which shifts southward to the sub-tropics over the Atlantic, thereby describing pronounced latitudinal variations. This pattern is consistent with the spatial extent of the blocking centers previously described in the literature (Croci-Maspoli et al., 2007; Pfahl and Wernli, 2012). For EUR blocking events, anomalously positive A-type occurrence along this belt is significant mainly over the eastern Atlantic-European region. For ATL and RUS blocking events, A-type frequency is significantly positive in central-to-eastern Europe and around the Azores. During RUS blocking events, E-NE type frequency is significantly positive over western Asia, transitioning from hybrid anticyclonic types in this area (ASE, AS in Fig. 3.4-RUS).

Results show a significantly increased frequency of the purely anticyclonic (A) type condi-

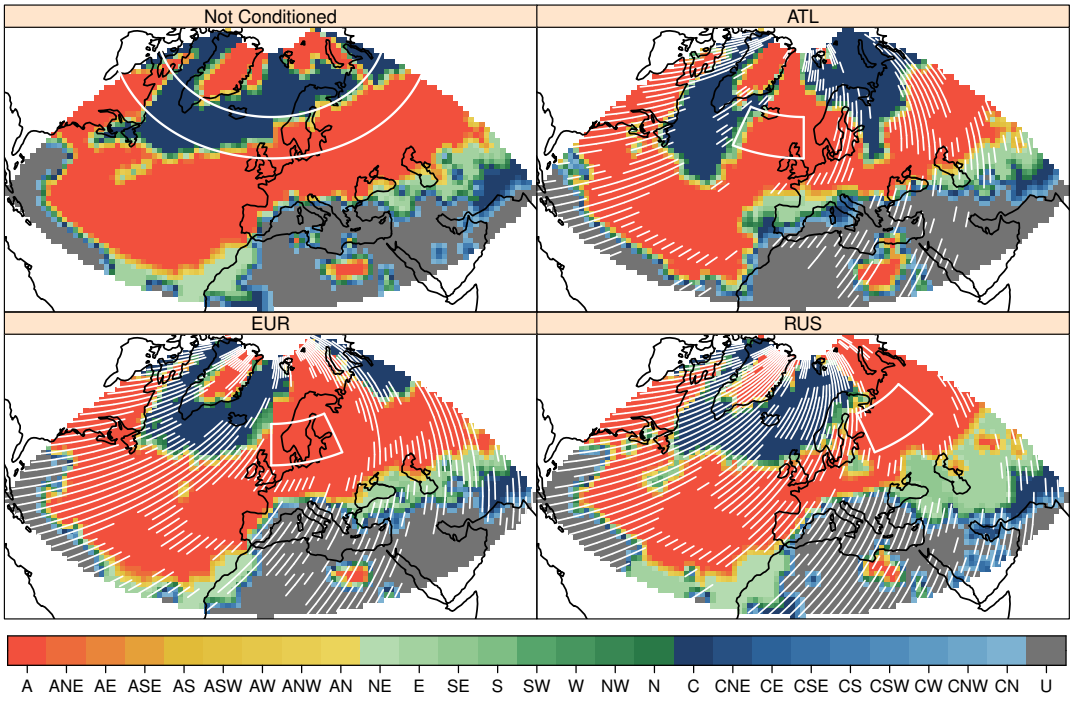

Figure 3.4: *Climatological maps of the most frequent daily Jenkinson-Collison weather type under different blocking conditions (period 1981-2005). Top left: Overall climatology of the most frequent JC-WT, under no blocking conditions. Two parallel lines indicate the latitudinal band (55°N-65°N) where blocking centers are searched for in the BI methodology (Sec. 2.1.3). Top right: most frequent JC-WT conditioned on blocking events centered on the Eastern Atlantic (ATL). Bottom left: Same as before but for the European subdomain (EUR). Bottom right: Same as before, but for the Eastern Europe subdomain (RUS). White hatched pixels exhibit frequencies that are not significantly different from the climatological (un) frequency after two-sided Z-test of proportions with a confidence level of 95%. White rectangles show the three blocking subdomains (more details in Sec. 2.1.3).*

tioned on the different blocking situations (32, 38 and 38% of days for ATL, EUR and RUS, respectively) as compared to the A-type climatological (unconditioned) frequencies (around 14-20% of days in the three subdomains, Fig. 3.5). Also, the purely cyclonic type (C) drops to a marginal probability during the blocking events in the three subdomains.

Regarding the seasonal cycle of these JC-WT frequencies (Fig. 3.6), blocking events simultaneously enhance the A-type and reduce the C-type monthly frequencies, respectively. For example, the probability of A type conditioned to blocking occurrence is 0.38 in September for ATL, and this frequency is reduced to less than its 25% when taking into account all days in the dataset (climatological, unconditioned frequency).

Additionally, considering their seasonal cycle, blocking events in ATL and EUR are more likely to correspond to non-summer events, while blocking situations over RUS are relatively more frequent in summer and therefore more closely associated with heat and drought-related events. This is in agreement with other analyses on the seasonal distribution of blocking situations (Barriopedro et al., 2006; Lupo, 2021), which show a reduced activity during summer in the Euro-Atlantic region, and an increase in the blocking frequency over eastern Europe (RUS)

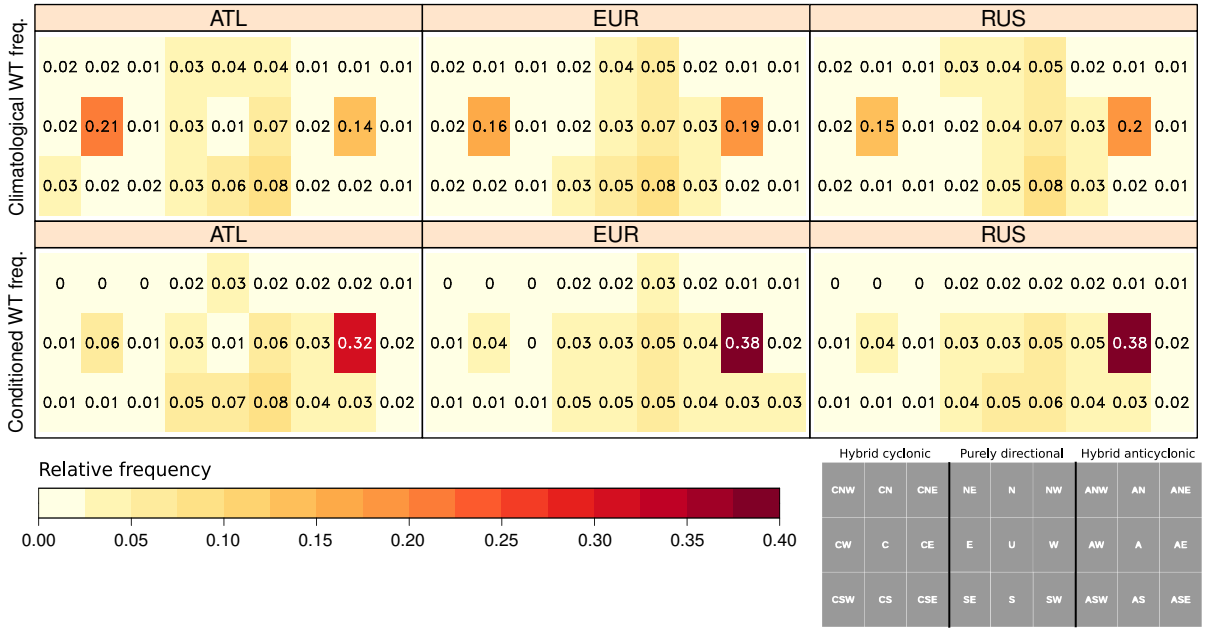

Figure 3.5: *JC-WT frequencies for the three considered blocking domains: ATL, EUR and RUS. Upper row: Climatological (unconditioned) frequencies for each JC-WT. Bottom row: JC-WT frequencies conditioned on the three blocking events. Frequencies are calculated as the mean of all grid-cells within each subdomain in the period 1981-2005. Panels within each blocking are arranged as in Fig. 2.2; see the key in the lower right panel.*

and western Asia (commonly referred to as the continental blocking sector). Here, it is shown that this characteristic blocking seasonality has a direct influence on the prevailing monthly JC-WTs, as illustrated in Fig. 3.6 for the pure types A and C.

These characteristic JC-WT configurations can be linked to specific regional climate events. For example, the prevalence of cyclonic conditions in southwestern Europe and E-NE flow over that part of the continent, as indicated by the most frequent JC-WT (Fig. 3.4-ATL), may be often related to extreme cold events in winter. This pattern is well supported by the connection between eastern North Atlantic blocking (ATL) and cold extremes in Europe, induced by the northerly advection on the eastern flank of the block (see e.g. Sillmann et al., 2011; Buehler et al., 2011). On the other hand, the increased relative frequency of continental blocking events and increased anticyclonic (A type) frequencies over the RUS subdomain in summer (Fig.3.6) can trigger heatwaves that affect vast areas of continental Europe and western Asia. A well-studied example is the unprecedented Russian heat event of summer 2010, associated with a persistent blocking event of these characteristics (Grumm, 2011).

Overall, these results highlight the sensitivity of the JC-WT classification to blocking events, that leads to characteristic spatial and temporal patterns with a direct physical interpretation in the resulting atmospheric configurations.

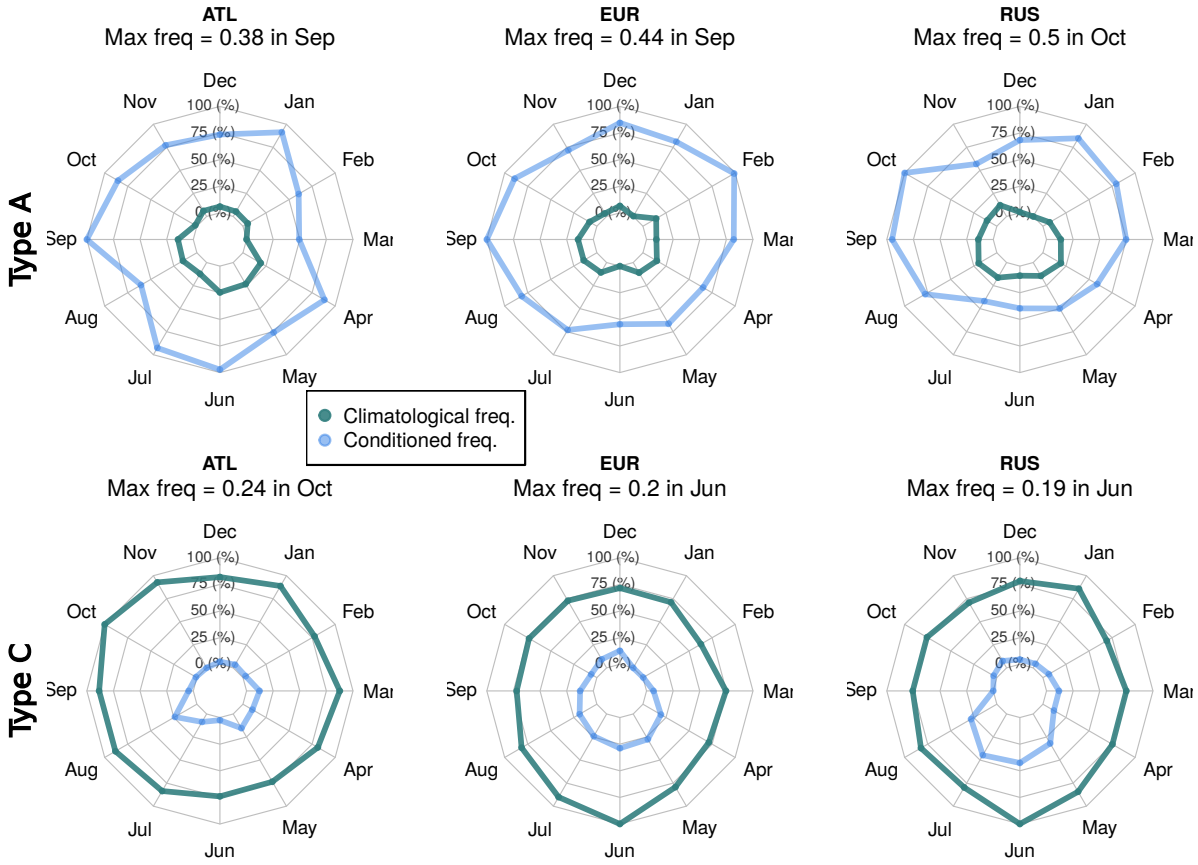

Figure 3.6: *Monthly JC-WT frequencies of types A (purely anticyclonic, upper row) and C (purely cyclonic, lower row) for ATL, EUR and RUS subdomains (left, center and right columns respectively). Frequencies are calculated similarly to Fig.3.5. The green line in each subplot corresponds to climatological (unconditioned) frequencies and blue line corresponds to blocking-conditioned frequencies. These monthly frequencies are relative to the maximum in each panel, indicated in the corresponding titles.*

3.2.3 Sensitivity of JC-WTs to teleconnection patterns

The main modes of atmospheric variability in Europe (Sec. 1.3.3) also present distinct surface pressure patterns, as shown, for instance, by the SLP anomalies during their positive phase (Fig. 3.7). Annual anomalies exhibit the characteristic dipoles of NAO and SCAND patterns, and the EA monopole west of the British Isles, with extended anomalies of opposite sign over subtropical areas. Their seasonal cycle entails a northward shift of the patterns during the summer season.

As with blockings, the JC-WT classification shows a remarkable sensitivity to teleconnection patterns. The spatial distribution of the most correlated JC-WT exhibits a strong seasonal variability and distinct relationships with the three analyzed teleconnection indices, further reinforcing the idea of their complementarity in describing different aspects of European climate variability (Fig. 3.8). JC-WTs capture the predominant spatial modes in each case providing a characteristic signature for each mode of variability. For example, the characteristic dipole

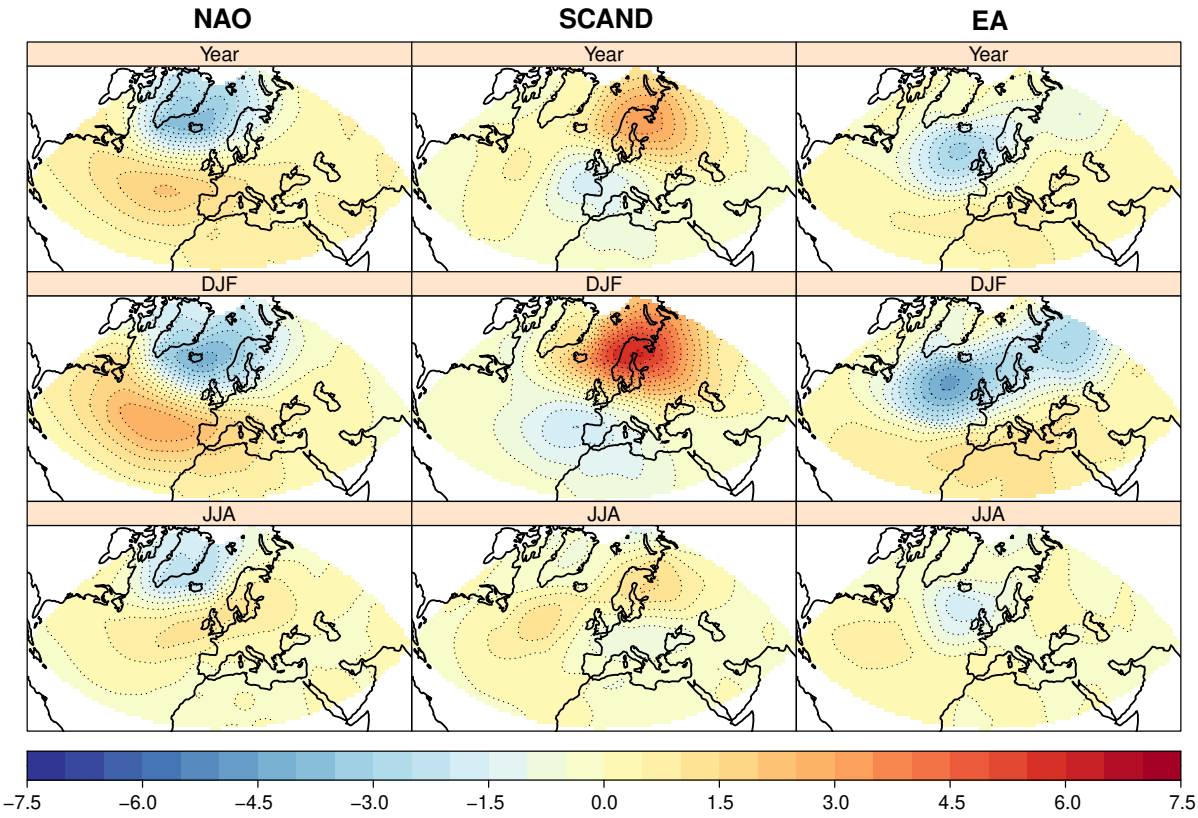

Figure 3.7: *SLP anomalies (hPa) during positive NAO, SCAND and EA (in columns) phases for year-round or season-specific values (annual, DJF and JJA, in rows) calculated from the ERA-Interim reanalysis for 1979-2005.*

structure of the NAO, with a low-pressure centre over Iceland, is well captured through the highest correlation with the purely cyclonic type (C) over its centre and its associated hybrid types in the surroundings (Hurrell, 1995). The same holds for the Azores high centre, represented by the anticyclonic type (A) and its related hybrids. At an intermediate latitude between both centres, a predominance of the purely directional type W and associated types occurs, characterizing the prevailing westerlies across the storm track. Correlations are statistically significant over almost the entire Euro-Atlantic region if year-round data are considered (Fig. 3.8, upper left panel). Furthermore, the NAO systematically contracts northward in summer and expands southward in winter (Barnston and Livezey, 1987), a displacement that is accordingly captured by the spatial pattern of the prevailing JC-WTs in those seasons (Fig. 3.8, see JJA and DJF). During winter, the links over eastern North America, the North Atlantic Ocean and Europe (the *core NAO region* hereafter) remain significant (compare with https://www.cpc.ncep.noaa.gov/products/precip/CWlink/pna/nao.loading.shtml). During summer, the remote links over the subtropical area right below the core NAO region are lost, as well as the significant links in Eastern Europe/Western Asia. Additionally, unclassified (U) type becomes more frequent (as shown in Sec. 3.1 and in line with the findings by Otero

et al., 2018) and significantly stands out as the most correlated with summer NAO over the central-eastern part of the Mediterranean Sea.

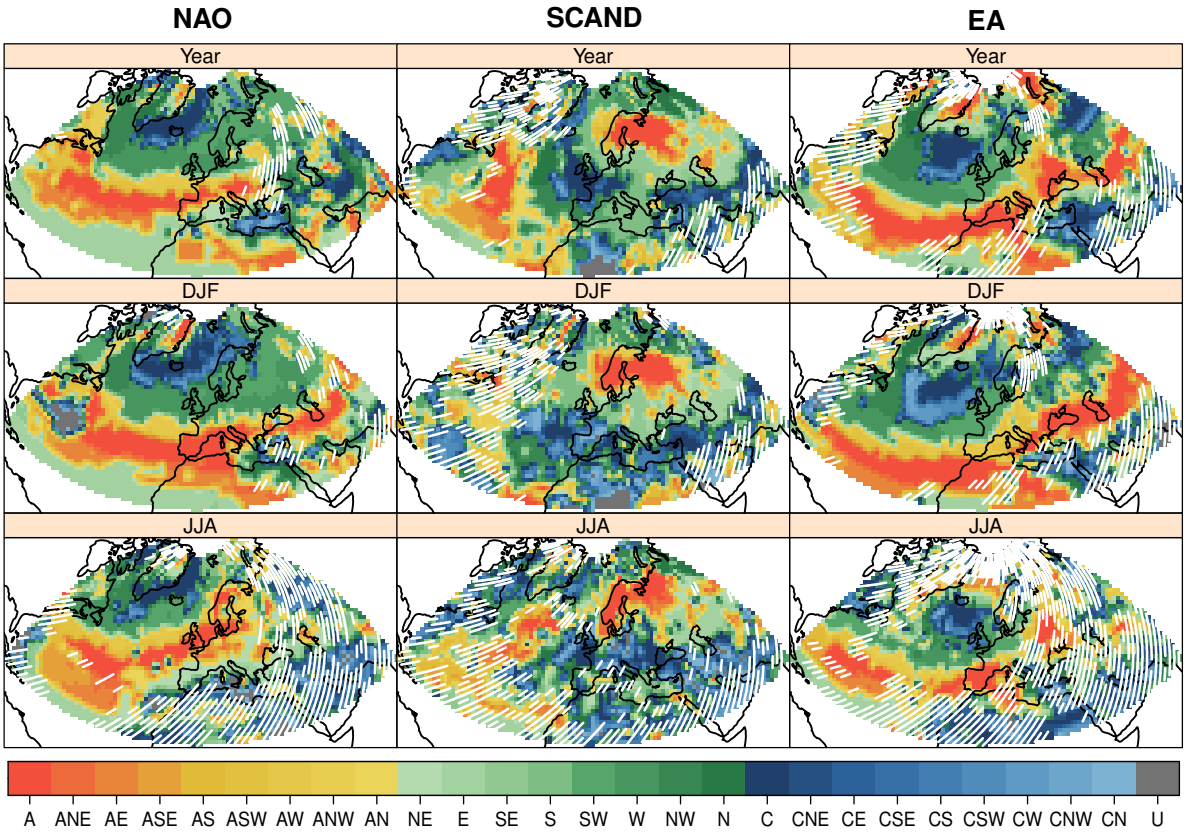

Figure 3.8: *JC-WT yielding the highest positive Spearman product-moment correlation coefficient with the North Atlantic Oscillation (NAO), Scandinavian pattern (SCAND) and East Atlantic pattern (EA). The correlations are obtained on a monthly basis considering the index value for each month and the monthly frequencies for each WT. Results are displayed for the annual series, winter (DJF) and summer (JJA). White hatching hides grid points with non-significant correlation for a confidence level of 95%.*

Interestingly, the association of EA and SCAND indices with the JC-WTs is restricted to a smaller region than for NAO (Fig. 3.8, central column). The JC-WTs associated the strongest with the SCAND likewise reflect the core area for this index, forming a tripole of cyclonic types located in southwestern Europe and west Siberia, contrasted by anticyclonic types over Scandinavia. This pattern can be found in any of the seasons considered, showing a characteristic seasonal displacement, consistent with the SCAND seasonal cycle (Bueh and Nakamura, 2007). In addition, significant centers of action as depicted by JC-WT cyclonic types are detected over Anatolia and the western Sahara desert. This center appears in all seasons and, to the best of my knowledge, has no direct reflection in the Z500 loading patterns Barnston and Livezey (1987) (compare with https://www.cpc.ncep.noaa.gov/data/teledoc/scand_map.shtml). A secondary SCAND center of action, found only in summer, consists of anticyclonic types to the south and southwest of Iceland.

The spatial pattern of EA is well represented by the predominant JC-WTs depicted in Fig. 3.8 (right column). The statistically significant correlation progressively declines in summer over Europe and western Asia, in turn unveiling a significant link with the classification over the North Atlantic Ocean. The correlation pattern depicts a southward-shifted NAO-like pattern having its largest extension during winter, revealing, on the one hand, a zonal belt of anticyclonic types ranging from the subtropical North Atlantic to eastern Europe, and, on the other hand, a cyclonic belt further north, extending from the central North Atlantic to western Siberia. In summer, this pattern is largely reduced and restricted to the subtropical North Atlantic and south of Iceland.

Overall, these results demonstrate physically consistent and interpretable links between NAO, SCAND and EA teleconnection indices with the synoptic-scale variability as described by the JC-WT classification, as reflected by characteristic weather type configurations associated with specific states of these major modes of atmospheric variability.

Similarly, as an extrapolation of the previous analysis to regions out of the Euro-Atlantic domain, high and consistent correlations with JC-WTs are also found for teleconnections affecting the North Pacific and the Southern Hemisphere (Fig. 3.9). Teleconnections like the Pacific–North American Pattern (PNA; Hurrell, 1995) and the Antarctic Oscillation (AAO; Gong and Wang, 1999) show strong significant correlation with JC-WTs in the core area for these indices. In particular, PNA forms a dipole of anticyclonic-cyclonic types located in the North Pacific Ocean; and, AAO is constructed by a westerly-type-belt around the Antarctic Circle.

This outcome reinforces the robustness and consistency of the JC-WT classification in capturing large-scale patterns across different regions in both hemispheres, thereby strengthening the Euro-Atlantic-focused findings discussed above. Although these results fall outside the main scope of this chapter, which is primarily oriented towards GCM selection activities within EURO-CORDEX, it is worthwhile to highlight the strong performance of the method in other regions of the globe.

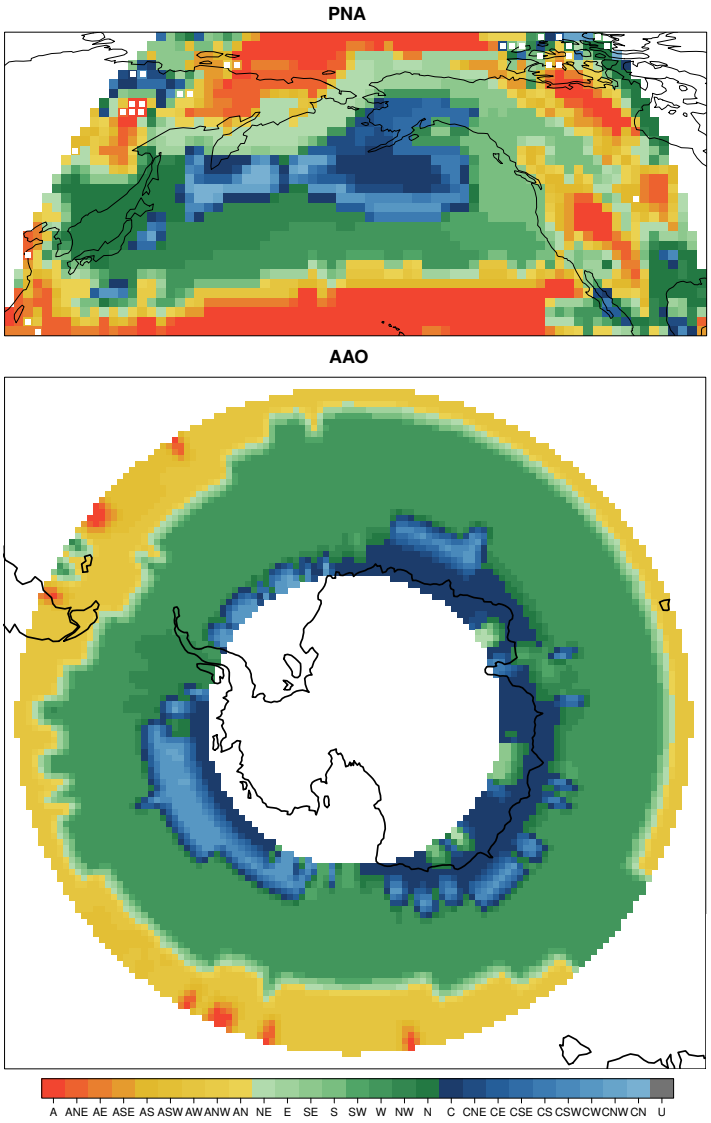

Figure 3.9: *Jenkinson-Collison weather type yielding the strongest positive correlation coefficient with the PNA and AAO indices at each grid-box of the North Pacific region and between 50° and 70° South, respectively. PNA data were retrieved from https://www.cpc.ncep.noaa.gov/data/teledoc/pna.shtml, and AAO data were extracted from https://www.cpc.ncep.noaa.gov/products/precip/CWlink/daily_ao_index/aao/aao_index.html. Non-statistically significant correlations (at a confidence level of 95 %) are marked in white. Monthly JC-WT frequencies and index values are taken into account. Here JC-WTs are derived from the ERA-5 reanalysis (1979-2005).*

4

Observational uncertainty in atmospheric circulation

Given the sparse network of stations measuring large-scale atmospheric circulation variables (such as pressure at different height levels) worldwide, reanalyses stand out as the best tools to analyze climate variability and change (Sec. 1.2.3). This Chapter describes the main results of Fernández-Granja et al. (2023) and Fernandez-Granja et al. (2022) about the effect of the choice of the reanalysis dataset in the JC-WT classification.

4.1 Experiment setup

The global JC-WT classification is estimated from five reanalysis products (Sec. 2.1.1) using the 6-hourly SLP data. Table 2.1 summarizes their features and provides references for further details. Prior to the JC-WT calculation and in order to intercompare all reanalyses, their SLP fields are interpolated to a common 2.5° regular longitude-latitude (Sec. 2.1.2). Their common 27-year period 1979-2005, coincident with the AR5 CMIP5 historical baseline (Taylor et al., 2012), is considered. Bear in mind that ERA-20C is produced through the assimilation of just SLP and marine winds, being therefore not fully comparable to the others, which assimilate a wider range of surface, upper-air and satellite observations. However, it has also been included in the intercomparison experiment for the sake of diversity. The reanalysis uncertainty is here analyzed by following an "all-against-all" validation scheme, so every reanalysis have been validated against each other.

The JC-WT method was conceived for extratropical applications since significant pressure gradients within the cross, required for a meaningful classification, are expected to occur mainly in these latitudes. Consequently, Jones et al. (2013) recommended the JC-WT classification for any mid-to-high latitude region (approximately from 30° to 70°). However, the JC-WT classification is obtained here beyond this range, following the results in Chapter 3, in order to achieve a more complete picture of the observational uncertainty worldwide.

Discrepancies in the resulting JC-WT classification among reanalyses are estimated considering the relative bias of their WT frequencies (Sec. 2.3.1). Annual and seasonal relative biases for each WT are computed between all pairs of reanalyses in Table 2.1. The statistical significance of these differences is taken into account using a two-proportions Z-test, with the null hypothesis that the relative frequencies of a given type for two different reanalyses are the same.

Moreover, reanalysis differences in their representation of transition probabilities are evaluated with the TPM Score (Sec. 2.3.3), envisaged to provide a quantitative measure of dissimilarity between two transition probability matrices. As a result, the larger the TPMS departure from zero (perfect agreement), the larger the dissimilarity of the TPM fingerprints between the reanalyses for a given center grid cell.

4.1.1 Regional synthesis

A regional assessment is presented using the latest set of climatic reference regions defined by the IPCC (Iturbide et al., 2020b) in order to provide a synthesized overview of the results of this Chapter (Fig. 4.1). In favor of avoiding the inclusion of unsuitable areas for the application of the JC-WT methodology (based on the findings presented in Chapter 3) and providing a more meaningful summary for regional intercomparison, the intertropical range ($23.5°S - 23.5°N$) is excluded from the original polygon dataset. As a result, some of the original IPCC regions are modified to exclude this area (see the blue polygons in Fig. 4.3). The IPCC regions affected by this modification are indicated with an asterisk throughout the text. The modified polygon layer is included for reproducibility of the results (https://doi.org/10.5281/zenodo.15847558, more details in Sec. 7.3.2).

4.2 Sensitivity of JC-WT classification to the temporal frequency of Sea-Level Pressure

A further consideration regarding the uncertainties in the JC-WT classification associated with SLP involves the temporal resolution of the variable. The choice of temporal resolution and time frequency, such as daily-mean, instantaneous at 12 UTC (original Lamb WT configuration), or 6-hourly values, can influence both absolute frequency distributions and the transitions between weather types. Hence, this issue must be carefully considered, as it may significantly affect the outcomes of the evaluation. In this regard, it can be hypothesized whether a higher temporal resolution will increase the variability of the transitions between JC-WTs, allowing

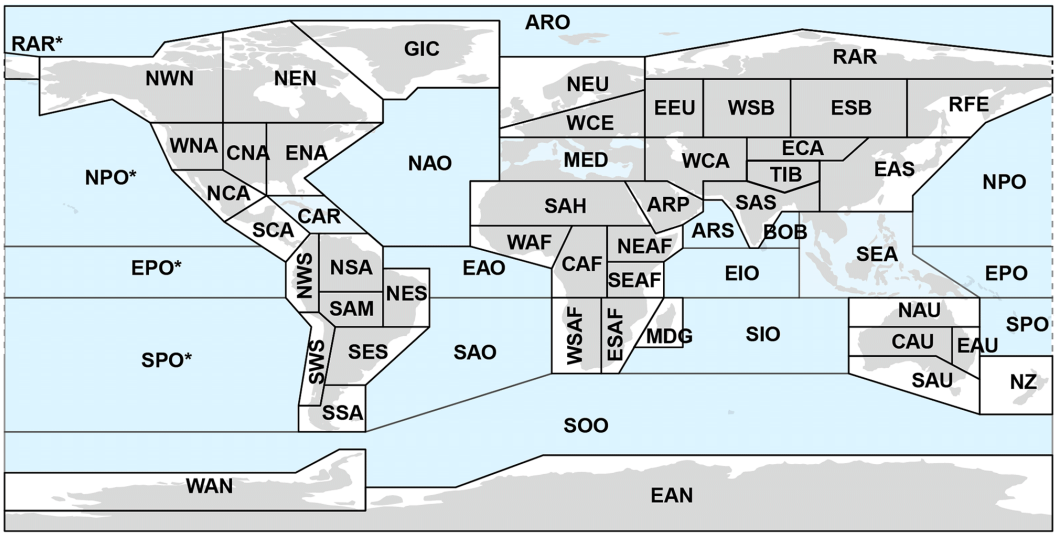

1	GIC	Greenland/Iceland
2	NWN	N.W.North-America
3	NEN	N.E.North-America
4	WNA	W.North-America
5	CNA	C.North-America
6	ENA	E.North-America
7	NCA	N.Central-America
8	SCA	S.Central-America
9-10	CAR	Caribbean
11	NWS	N.W.South-America
12	NSA	N.South-America
13	NES	N.E.South-America
14	SAM	South-American-Monsoon
15	SWS	S.W.South-America
16	SES	S.E.South-America
17	SSA	S.South-America
18	NEU	N.Europe
19	WCE	Western&Central-Europe
20	EEU	E.Europe
21-22	MED	Mediterranean

23	SAH	Sahara
24	WAF	Western-Africa
25	CAF	Central-Africa
26	NEAF	N.Eastern-Africa
27	SEAF	S.Eastern-Africa
28	WSAF	W.Southern-Africa
29	ESAF	E.Southern-Africa
30	MDG	Madagascar
31	RAR	Russian-Arctic
32	WSB	W.Siberia
33	ESB	E.Siberia
34	RFE	Russian-Far-East
35	WCA	W.C.Asia
36	ECA	E.C.Asia
37	TIB	Tibetan-Plateau
38	EAS	E.Asia
39	ARP	Arabian-Peninsula
40	SAS	S.Asia
41-42	SEA	S.E.Asia

43	NAU	N.Australia
44	CAU	C.Australia
45	EAU	E.Australia
46	SAU	S.Australia
47	NZ	New-Zealand
48	EAN	E.Antarctica
49	WAN	W.Antarctica
50	ARO	Arctic-Ocean
51	NPO	N.Pacific-Ocean
52	EPO	Equatorial.Pacific-Ocean
53	SPO	S.Pacific-Ocean
54	NAO	N.Atlantic-Ocean
55	EAO	Equatorial.Atlantic-Ocean
56	SAO	S.Atlantic-Ocean
57	ARS	Arabian-Sea
58	BOB	Bay-of-Bengal
59	EIO	Equatorial.Indic-Ocean
60	SIO	S.Indic-Ocean
61	SOO	Southern-Ocean

Figure 4.1: *Updated AR6 IPCC reference regions (top panel); land regions are in grey shading and oceanic regions in blue shading. The Caribbean (CAR), Southeast Asia (SEA) and the Mediterranean (MED) regions are considered both land and oceanic regions, so they have blue and gray shadings. Indexes, acronyms and full names of the regions are enumerated in the table in bottom panel. Source: Iturbide et al. (2020b).*

for a more accurate identification of short-time transitional types that would otherwise be misclassified in daily-mean fields; or, conversely, it will reduce variability coming at the expense of certain level of redundancy when describing the transition probabilities of more persistent types.

As an example, Fig. 4.2 illustrates the transition probability matrices (TPMs, Sec. 2.3.3) of JC-WTs derived from ERA-Interim SLP data at three different time frequencies (6-hourly, daily-mean, and instantaneous at 12 UTC, respectively), for the original Lamb WT location over the British Isles (55°N, 5°W). The number and diversity of transitions increase notably when using daily-mean or 12 UTC data, including many low-probability transitions that are not presented with 6-hourly data. Most of those transitions might be considered spurious,

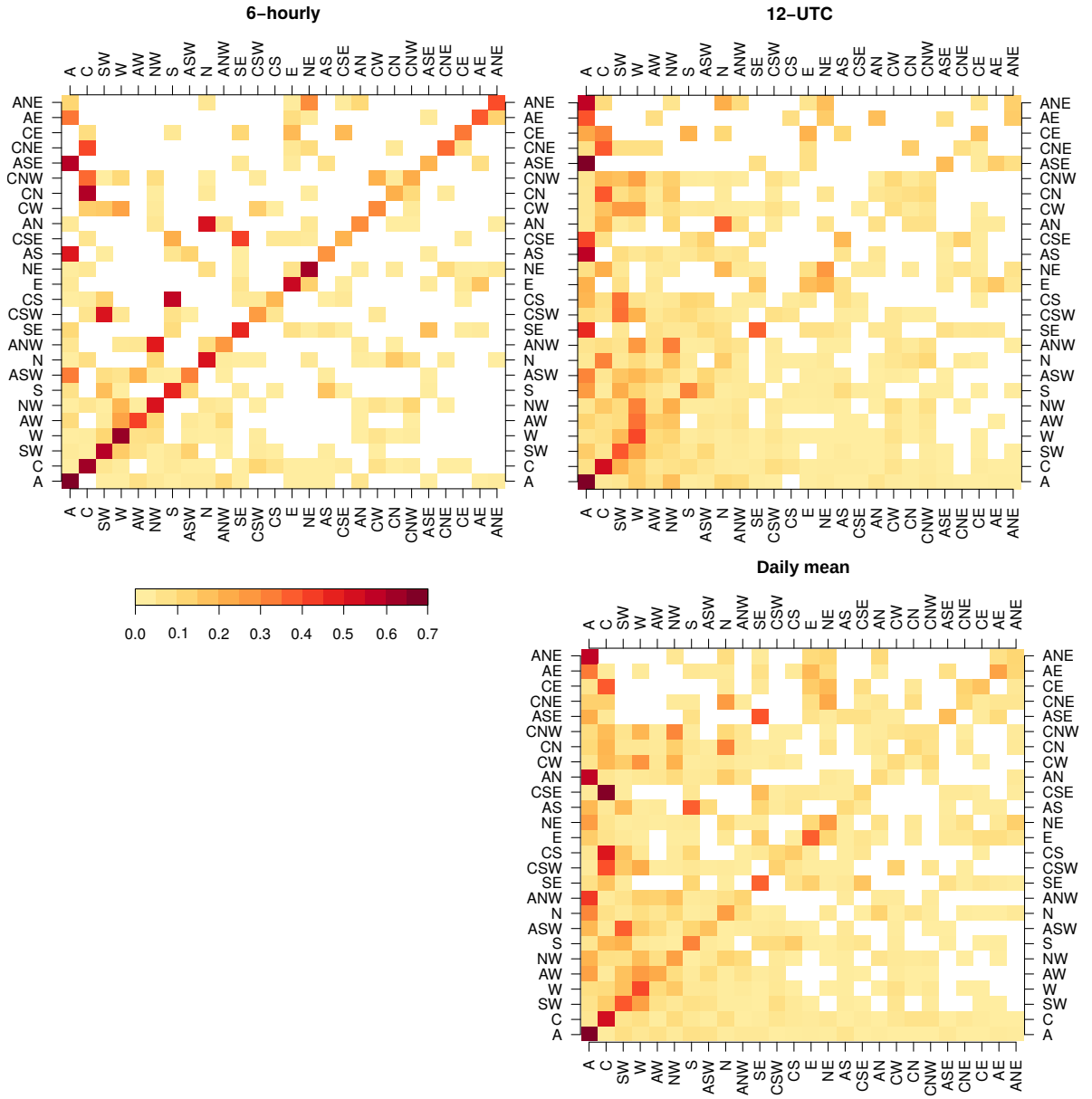

Figure 4.2: *Transition Probability Matrices (TPM, Sec. 2.3.3) derived from ERA-Interim for the JC-WTs classification at 5ºW-55ºN (i.e. center of the "cross" located over the British Isles), considering different time resolutions for the SLP (period 1981-2010). Each element of a matrix, A_{ij}, represents the probability of going from JC-WT in row i to JC-WT in column j. Therefore, the persistence probability of a JC-WT can be found by looking at the diagonal of the matrix. Non-observed transitions have been blanked to differentiate them from low-probability ones.*

arising from suboptimal temporal aggregation (daily means) or sparse sampling (single-time snapshots), and do not reflect real synoptic transitions. This effect is analogous to that found in tropical cyclone tracking, where higher temporal sampling significantly reduces positional uncertainty (i.e. Voskresenskaya et al., 2022). Therefore, where available and preferably, 6-hourly SLP data might provide a more faithful and physically consistent representation of synoptic-scale circulation variability and transitions.

4.3 Effect of observational uncertainty on JC-WT classification

Another source of uncertainty in the intercomparison of JC-WTs classifications across different datasets (reanalyses and GCMs) can arise from discrepancies in their SLP fields, derived from the different pressure reduction procedures, highly sensitive to altitude and dataset's resolution (Sec. 1.3.1). In this regard, differences in the SLP fields between reanalyses (ERA-5 is used as reference) are shown in Figures 4.3 and 4.4.

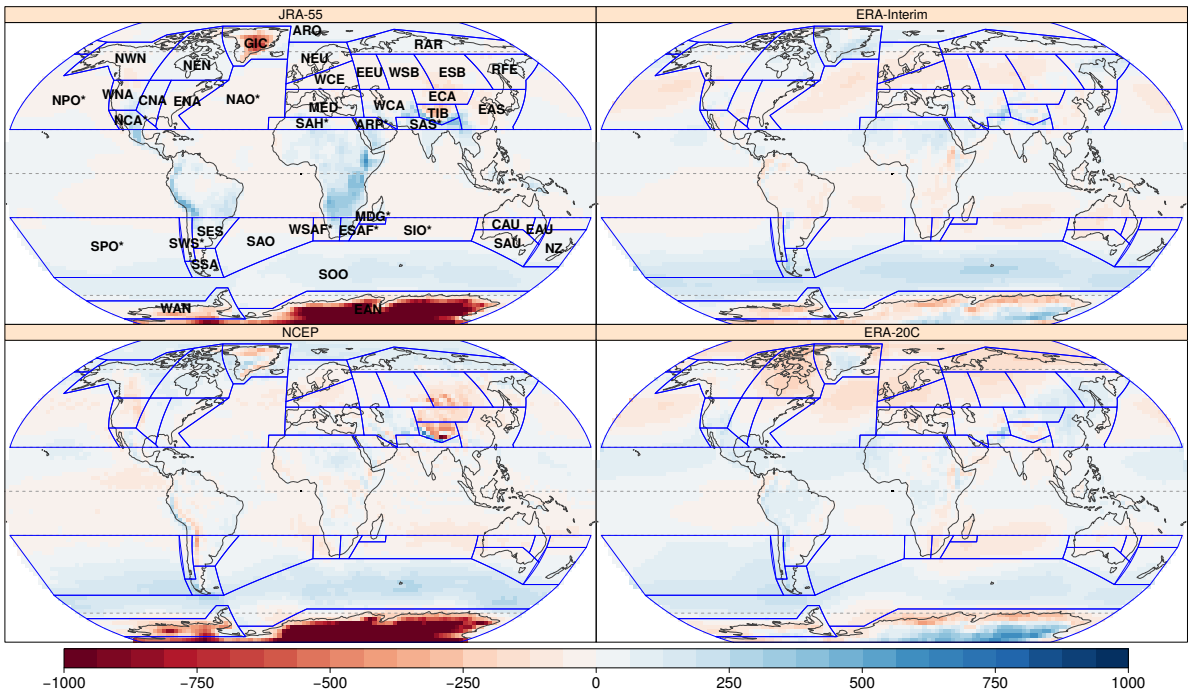

Figure 4.3: *Difference in annual mean SLP (Pa) for four reanalyses with respect to ERA-5 (1979-2005). Blue polygons depict the modified IPCC-AR6 regions (Sec. 4.1.1). The modified IPCC region polygon layer (blue lines) with the region identification codes are depicted in the top-left. Note that the original IPCC regions that have been modified to exclude the intertropical range (see Sec. 4.1.1) are marked with an asterisk.*

The problematic regions are those where the pressure reduction algorithms usually yield worse results due to the strong orographic influence. The different reanalyses apply varying pressure reduction schemes and orographic representations. These methodological differences lead to annual discrepancies of up to approximately 5 hPa in mountainous and high-elevation

regions such as the Andes, Himalayas, Greenland, Antarctica or even the Rocky Mountains (Fig. 4.3), directly affecting the robustness of SLP-based classifications. Furthermore, these discrepancies increase when looking at seasonal scales (up to 10 hPa in JJA or DJF in high-elevation regions, according to Fig. 4.4). Therefore, caution is required when interpreting circulation diagnostics in areas with complex orography, especially when comparing results across multiple datasets or model outputs.

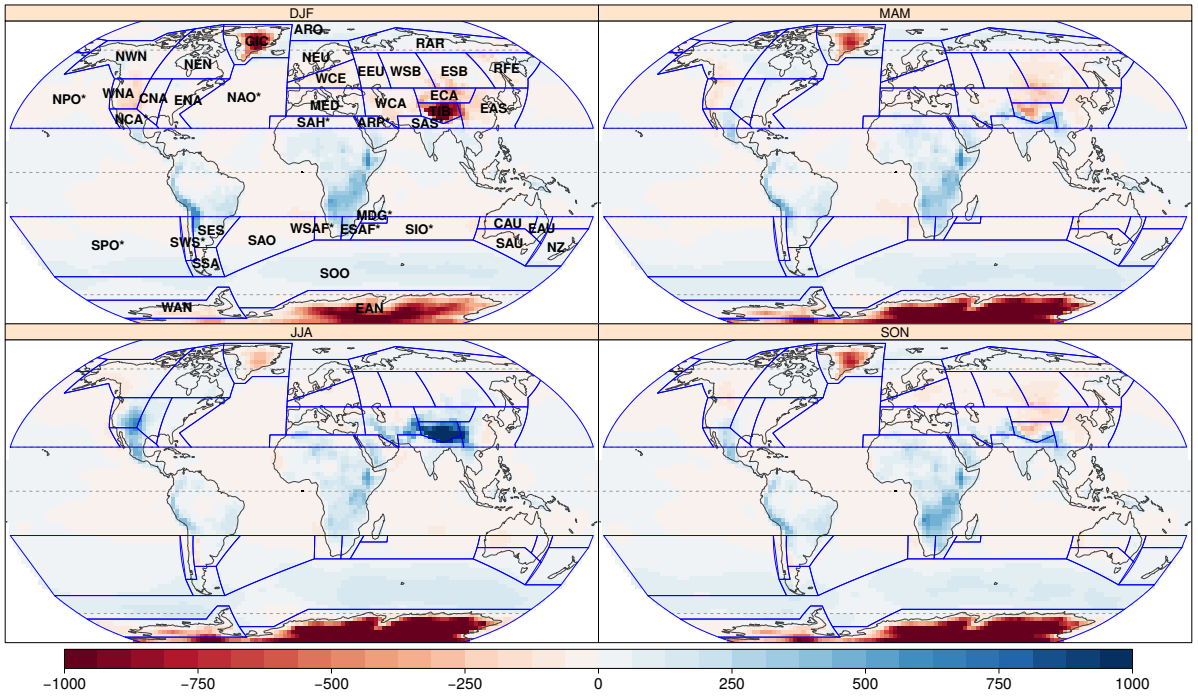

Figure 4.4: *As Fig. 4.3, but for seasonal mean SLP differences between JRA-55 and ERA-5 (1979-2005).*

As different reanalysis present differences in their SLP fields, these are expected to propagate to their JC-WT. Thus, their choice might eventually affect model evaluation experiments.

Next, reanalyses are compared in terms of their transition probability matrices (TPM). First, in order to illustrate how the TPM works (Sec. 2.3.3), a comparison of the TPM from several reanalyses is presented for the specific location over the Brithis Isles (55°N-5°W, Figs. 4.5 and 4.6). The TPM of ERA-Interim (Fig. 4.5, panel top-left) provides the reference *fingerprint* of the transitions among JC-WTs and the persistence probability of a given JC-WT (diagonal cells). As expected, the largest probabilities of remaining in the same state are associated with the most frequent JC-WTs. In particular, more than 60% (50%) of the days with type A (C) stay in the same JC-WT, followed by persistent SW, W, SE and E types (all above 30%). The most frequent transitions to a different state are from ANE, AN and ANW to A type and from CSE, CS, CSW to C type, all with probabilities above 40%. ASE to SE and AS to S type complete the picture of most common transitions. This pattern is in general very similar in

the remaining reanalyses used as alternative references, with the largest deviations occurring in ERA-20C (see Figs. 4.5 and 4.6).

In Figure 4.7, discrepancies in all weather type transitions in all grid-boxes over the globe for all reanalyses are estimated in terms of TPMS (Sec. 2.3.3) relative to ERA5. As expected, ERA-20C and ERA-Interim are more similar to ERA-5 than NCEP and JRA-55, as revealed by the TPMS (Fig. 4.7 and Fig. 4.8). For the latter two datasets, large TPMS values are obtained over Greenland (GIC), Antarctica (WAN, EAN), Northern Central-America (NCA*), West North-America (WNA), Central North-America (CNA), central Asia (WCA, ECA, EAS), Southern Asia (SAS*) and the Tibetan Plateau (TIB), where values larger than 10 are found. In the Southern Hemisphere, large discrepancies between reanalyses are found over South America (SWS* and SES regions). The above mentioned regions present complex orography, with high-altitude mountain systems such as the Himalayas, the Andes and the Rocky Mountains or thick ice sheets like Antarctica and Greenland. The discrepancies found in these regions of complex terrain are likely related to the differences in the SLP fields in the reanalyses (Fig. 4.3). They can be particularly critical for Antarctica, which is mostly ice sheet several kilometers high. Therefore, the poor representation of the SLP by the different reanalyses prevents from the application of the JC-WTs classification in these regions, as shown by their high TPMS values (Fig. 4.7). TPMS calculated for the remaining pairs of reanalyses can be found in Fig. 4.8.

The seasonal comparison between JRA-55 and ERA-5 (Fig. 4.9) generally reveals a seasonal march of the largest TPMS values towards the pole of the summer hemisphere (Northern Hemisphere in JJA and Souther Hemisphere in DJF). This is similar to the results found for type diversity and U-type frequency (Sec. 3.1), where the ITCZ (Barry and Carleton, 2013) may determine the JC-WT applicability to some point in that oscillating latitudinal band. In particular, the seasonal TPMS values for North Central-America (NCA*) and the Sahara region (SAH*) are larger than the annual ones (Fig. 4.9). In the Mediterranean (MED), Central North-America (CNA) and in West North-America (WNA), the TPMS values are the largest in JJA and lowest in DJF. Reflecting the aforementioned seasonal march, the TPMS values for South South-America (SSA), West South-Africa (WSAF*), East South-Africa (ESAF*), Madagascar (MDG*) and Central Australia (CAU) reach their maximum in DJF, with a much larger magnitude than in any other season.

According to Fig. 4.9, moderately high TPMS values are found throughout the year in the mid-latitude Indian Ocean, which extend to the eastern South Atlantic and eastern South Pacific during DJF (austral summer), particularly affecting the Southern-Ocean (SOO) region. These differences might be caused by scarce observations in that area (and the resulting increase in

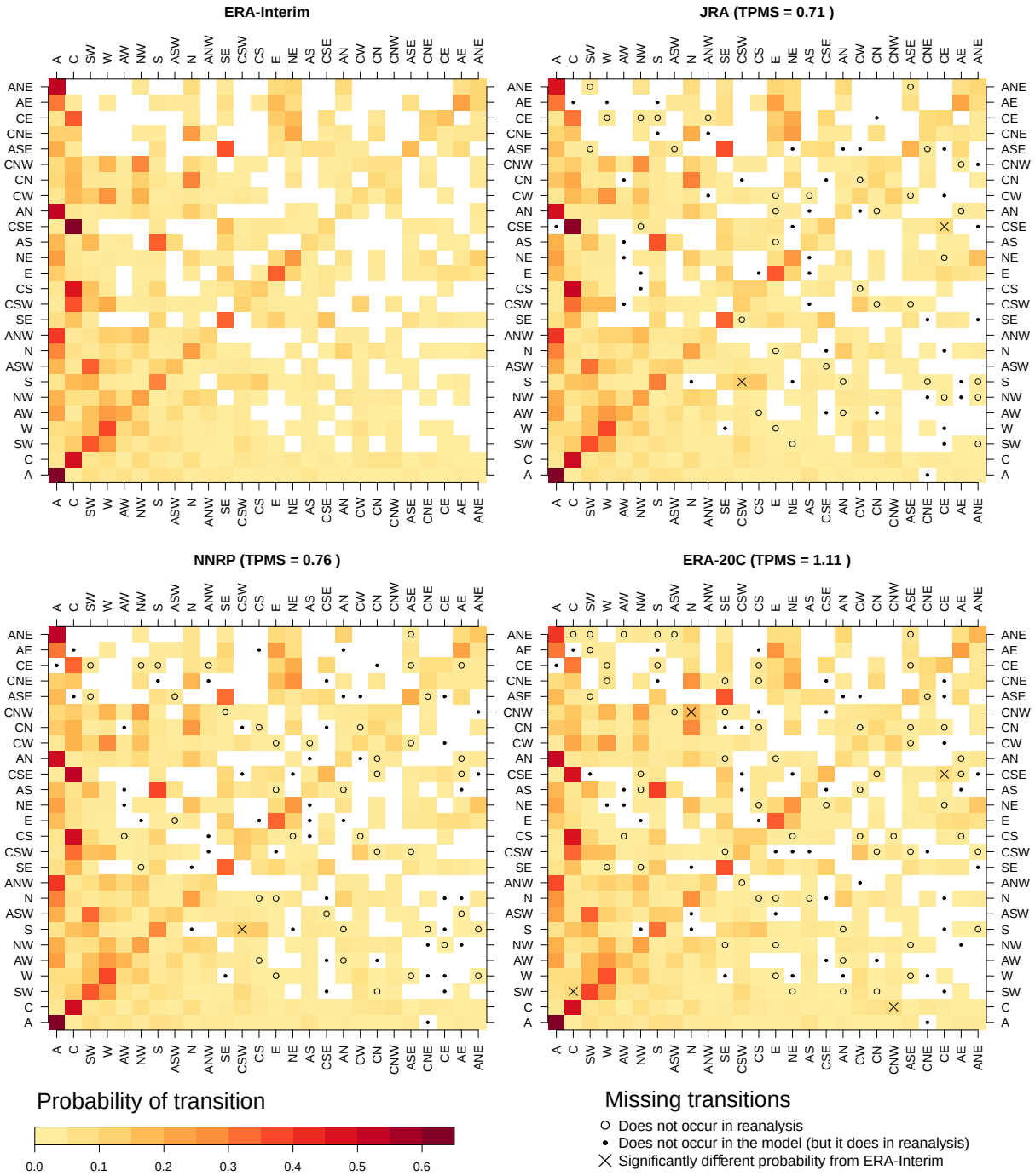

Figure 4.5: *Transition probability matrices of the reanalysis products derived from instantaneous 12-UTC JC-WT classifications. Non observed transitions have been blanked to differentiate them from low-probability ones (see also Fig. 4.6). The transition probabilities of each reanalysis are compared against ERA-Interim, used a reference to calculate the TPMS (in each panel's title). Transition probabilities significantly different from those observed in ERA-Interim are indicated by crosses. In addition, JC-WT transitions present in each reanalysis but not observed in ERA-Interim are indicated by empty circles. Likewise, solid circles indicate JC-WT transitions not present in each reanalysis, but that occur in ERA-Interim.*

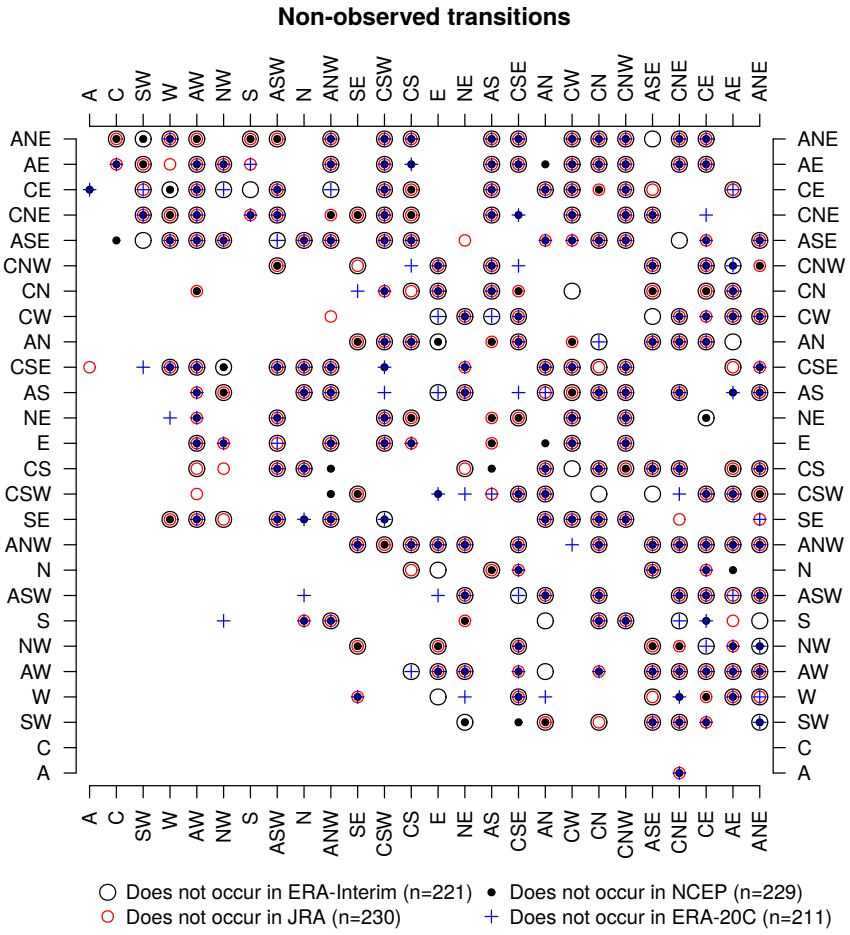

Figure 4.6: *Detail of missing transition probabilities, as captured by the different reanalysis products used in this study.*

reanalysis uncertainty) and, noteworthy, they again coincide with a relatively low type diversity, as reported in Sec. 3.1.

The large TPMS values found along the margins of the East Antarctic Ice Sheet (EAIS) are spatially aligned with an abrupt shift of the easterly katabatic winds blowing down the ice sheet to quasi-persistent westerlies at mid-latitudes, driving the Antarctic Ocean divergence zone (Davis and McNider, 1997). This singular regional modulation of the wind field might be resolved in a distinct manner by the two reanalyses, and so is the pressure reduction to mean sea-level over the ice sheet itself. Notably, the TPMS values over the West Antarctic Ice Sheet are systematically lower than those over the EAIS (compare WAN to EAN regions, respectively).

4.3.1 Regional assessments

In order to shed some light on regional TPMS, the relative biases of WTs frequencies for each IPCC region are investigated. These biases reveal misrepresentations of the synoptic conditions and their frequencies by the different reanalyses. As an illustrative example, results for the

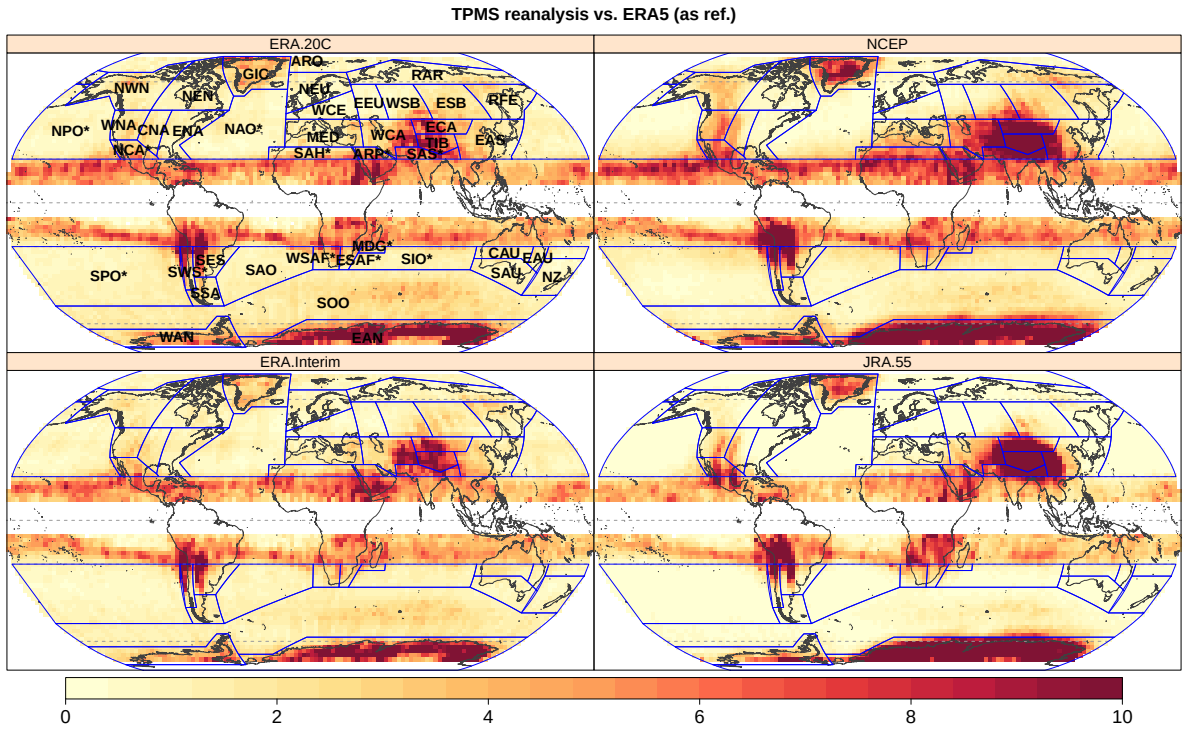

Figure 4.7: *Annual Transition Probability Matrix Scores (TPMS, Sec. 2.3.3) of NCEP, ERA-Interim, ERA-20C and JRA-55 against ERA-5 (used as reference).*

Mediterranean (MED) region are shown (Fig. 4.10). The respective results for the remaining IPCC regions can be obtained by following the working example on analysis reproducibility Notebooks (Sec. 7.3.2).

Results show biases of different magnitude and sign, depending on the reanalysis. The majority of statistically significant differences (marked with asterisks) occur for the most frequent WTs (Fig. 4.10, see WTs frequencies for ERA-5 in the right panel). The largest and most significant biases are found during summer, which coincides with high TPMS values (Fig. 4.9). For the least frequent weather types, reanalyses do not exhibit significant differences with respect to ERA-5, especially in spring, autumn and for the annual results. The unclassified type is the most frequent WT in all seasons except in winter. It exhibits significant differences among reanalyses in all seasons, especially during summer and autumn.

The consistency among reanalyses for the MED region is next analyzed in detail by comparing their respective pairwise transition probability matrices (Fig. 4.11), using the TPMS as a complementary evaluation measure of observational dissimilarity in addition to biases in WTs frequencies (Fig. 4.10). In terms of annual TPMS (not shown), a good agreement among reanalysis is found in general, similar to the results attained for winter (Fig. 4.11, lower right panels), spring and autumn. The best agreement between all reanalyses is found in winter with the

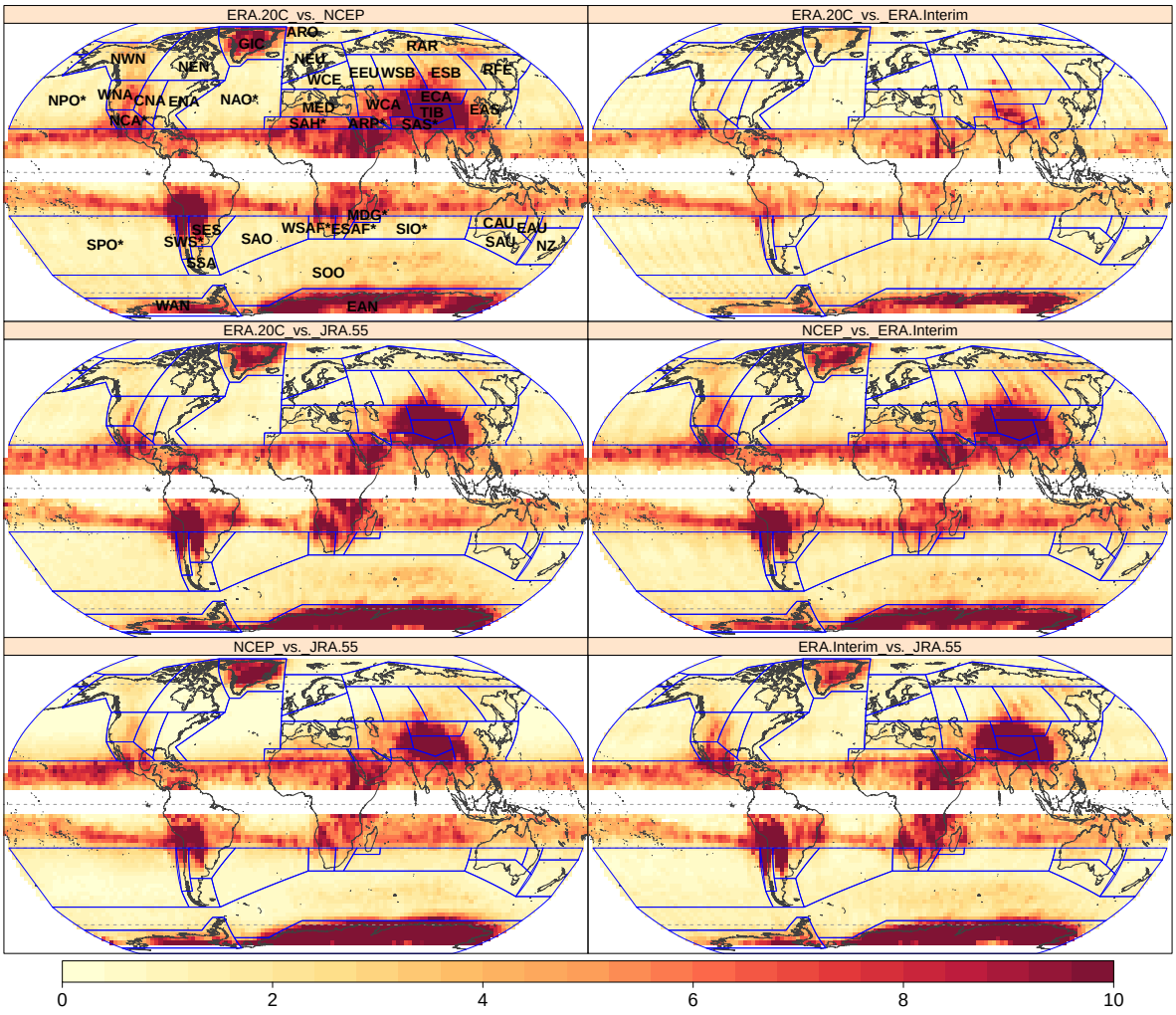

Figure 4.8: *Annual TPMS calculated between different reanalysis pairs (specific pairs are found in the sub-panels titles). Blue lines show the IPCC regions, whose abbreviations are depicted in the top-left sub-panel.*

lowest TPMS values (< 4). These results are consistent with Brands (2022b), who found similar results for this region when comparing JC-WT frequencies from JRA-55 and ERA-Interim using the mean absolute error. Higher TPMS values are found all along the Mediterranean Sea and the Iberian Peninsula in summer for all pairs of reanalyses. The high TPMS values are located mainly in the southern part of the region, showing a marked latitudinal gradient to lower TPMS values northward. This TPMS pattern aligns with the results found for type diversity and U-type frequency (Sec. 3.1).

The differences in the transitions of the weather types through the TPM are examined choosing two arbitrary grid boxes with different behaviors, one over the Balearic Islands and another over Santiago de Compostela (Fig. 4.12). For brevity, results for two distinct reanalyses

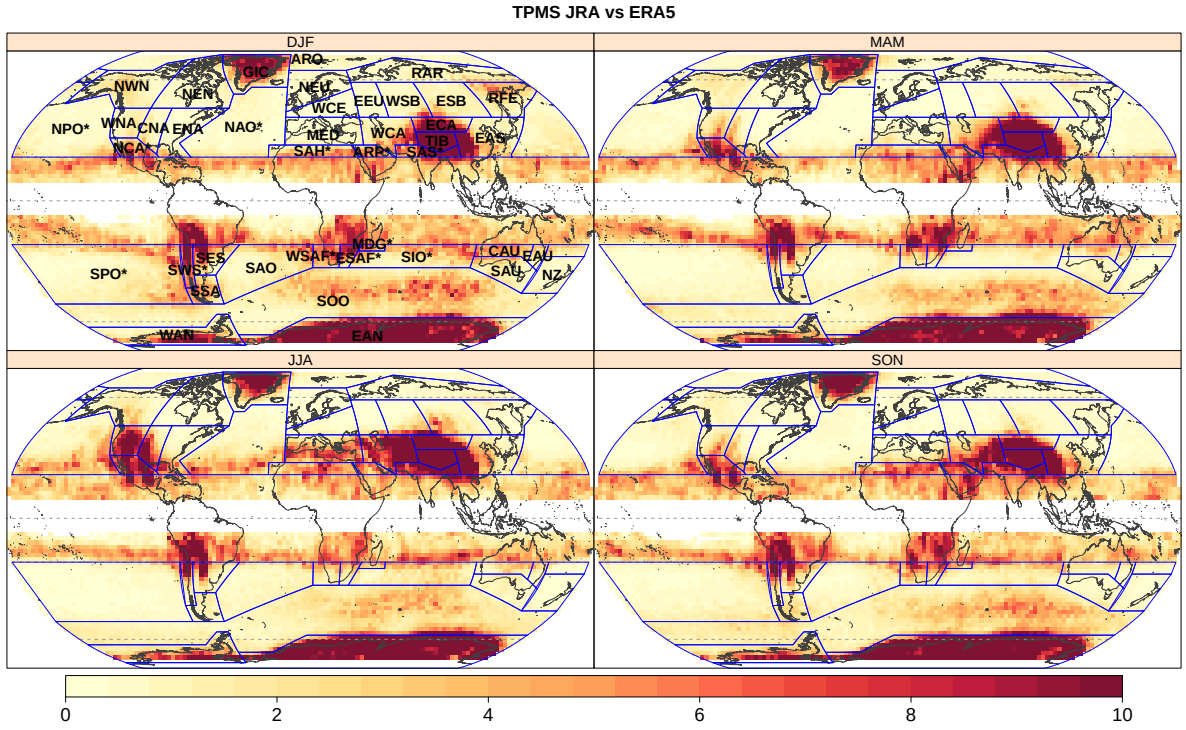

Figure 4.9: *Seasonal Transition Probability Matrix Scores (TPMS, Sec. 2.3.3) of JRA-55 reanalysis against ERA-5 (used as reference).*

are shown, namely ERA-Interim against NCEP in summer (Fig. 4.12, upper panel) and winter (Fig. 4.12, lower panel). Generally, the most likely transition for most JC-WTs is to remain in the same state. This is not the case for the Balearic Islands in summer (top-left panel), where most of the transitions occur from or to the U-type. Consequently, the U-type is found to be the most frequent type in summer (approx. 50%, Fig. 3.2). As a result, the TPMS from this TPM compared to the NCEP counterpart is 12, considerably larger than the other TPMSs displayed in Fig. 4.12.

The discrepancies between ERA-Interim and NCEP classifications in summer can be explained by the dissimilarities in the six intermediate parameters involved in the JC-WT classification (Table 2.2). As illustrated in Fig. 4.13, in summer the six parameters show a lower correlation between reanalyses in the Mediterranean Sea compared to other locations of the domain. The correlation coefficients are particularly low for the southerly flow (s) and the total flow (f, norm of southerly and westerly flow). In this example (using ERA-Interim and NCEP), the meridional component of the pressure gradient (s) emerges as the main responsible for the discrepancies between the reanalyses in terms of the resulting classifications, more than the zonal component (w) and the shear vorticities (zw, zs, z), which exhibit greater agreement. However, the degradation of parameter correlation may vary in magnitude and importance be-

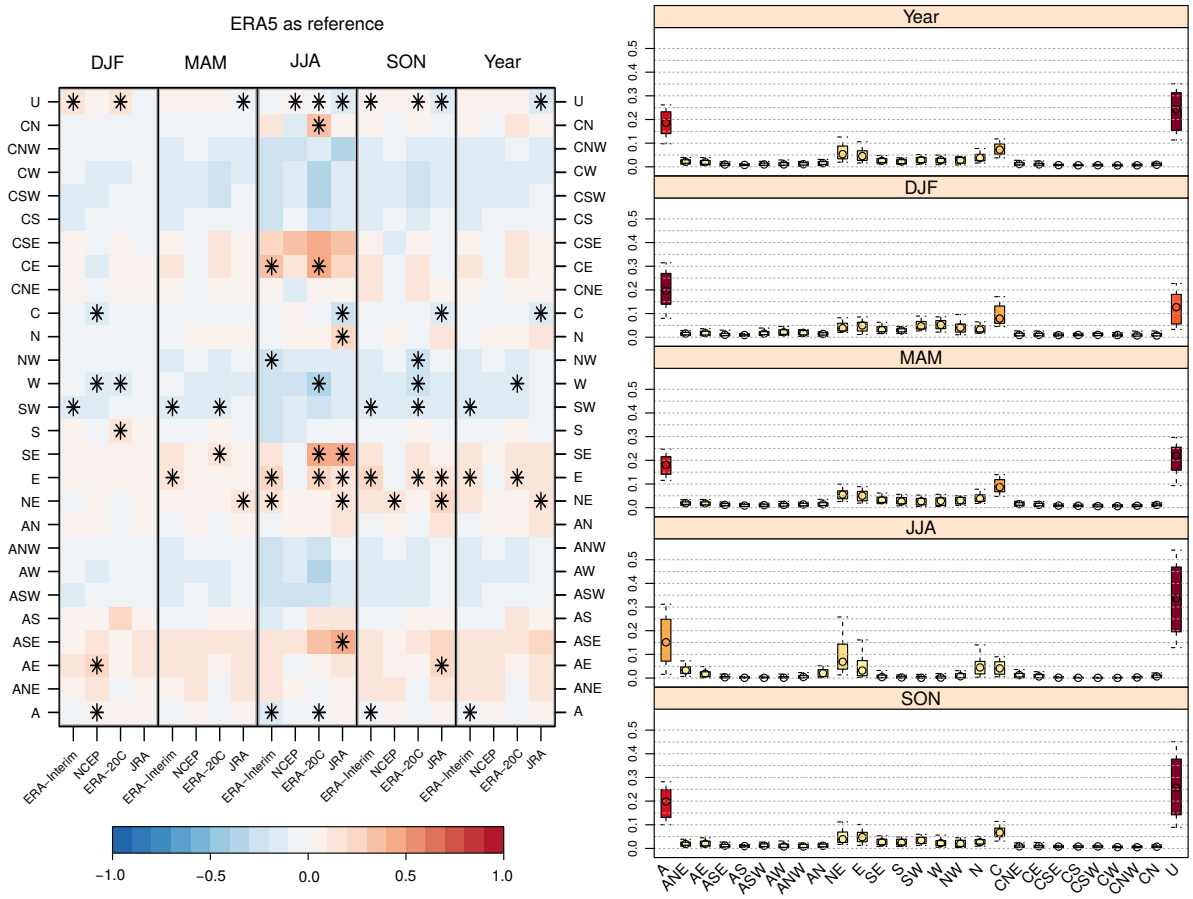

Figure 4.10: *Left: Annual and seasonal relative biases of weather type frequencies (in rows) for the different reanalyses (in columns within each season) against ERA-5 (used as reference) for MED. Asterisks indicate statistically significant biases following the two proportion Z-test (Sec. 2.3.4). Right: Annual and seasonal regional weather type frequencies as represented by ERA-5 for MED, used as reference for the relative biases on the left. Each box represents the spatial variability of each type frequency within MED, where the box upper/lower boundaries show the inter-quartile range and the lower/upper whiskers extend to the* 10^{th} *and* 90^{th} *percentiles respectively. Circles indicate the median frequency.*

tween reanalysis pairs. This finding suggests that small differences in the SLP fields can lead to significant differences in the JC-WT characteristics under situations of very weak pressure gradients, as reflected by the discrepancies of the intermediate parameters.

4.3.2 Relationships between observational uncertainty and JC-WT applicability

All things considered, a relationship between three factors is found, namely large TPMS values between reanalysis pairs (Fig. 4.7 and 4.9), a small number of WT (i.e. low WT diversity) and a high frequency of the U-type (Fig. 3.2). These three factors should be analyzed together because the large TPMS in some regions might come from the limitations in the suitability of the JC-WT classification. In regions where the classification method is suitable, the TPMS purely reflects the uncertainty among reanalyses. Figure 4.14 summarizes Figs. 3.2, 4.7 and

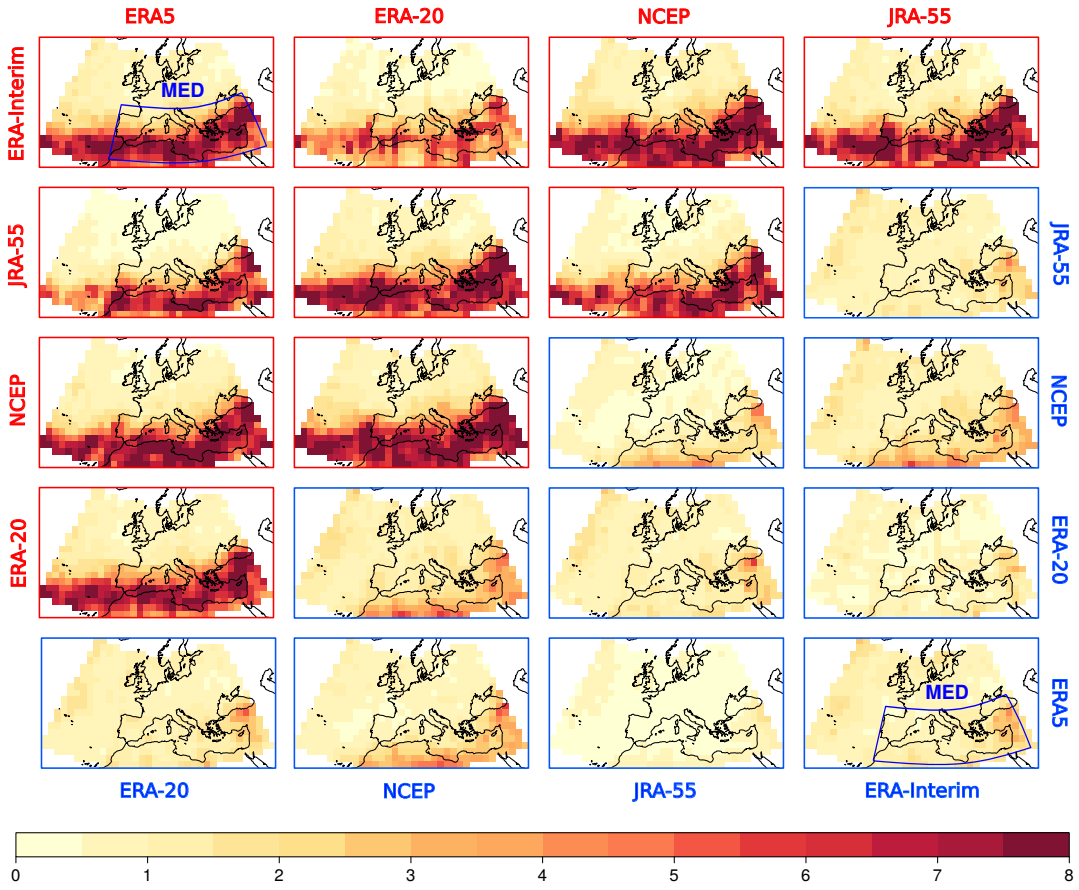

Figure 4.11: *Transition Probability Matrix Scores (TPMS, Sec. 2.3.3) for pairs of reanalyses in summer (red bordered and labeled panels) and winter (blue bordered and labeled panels), considering the all-against-all intercomparison scheme.*

4.9 for all IPCC regions and analyzes the connection between the number of distinct WTs and observational uncertainty (TPMS). The results suggest an inverse relationship between TPMS and number of JC-WTs.

Considering the criterion of JC-WT diversity, the method might be less suitable for regions like SAS* and EAN, where few distinct WTs appear (median below 16 types). Seasonally, other regions also stand out by their low number of WTs, e.g. CAU or WSAF* in boreal winter and TIB, ARP*, SAH*, NCA* and WCA in boreal summer (Fig. 4.14). There is a large spatial variability in terms of WTs diversity in some regions where the applicability of the WT classification is questionable, such as EAN, TIB, ARP*, SAH* or WSAF*. Regardless of the median number of WTs, these regions show grid cells where all WTs are registered. Additionally, there are some regions that stand out for having large TPMS (i.e. reanalysis uncertainty) despite their large number of WTs: EAN, NCA*, SWS*, ESAF*, SES, EAS, ECA and GIC; only in DJF regions TIB, SSA and WAN add to the list; and MED, WNA and CNA

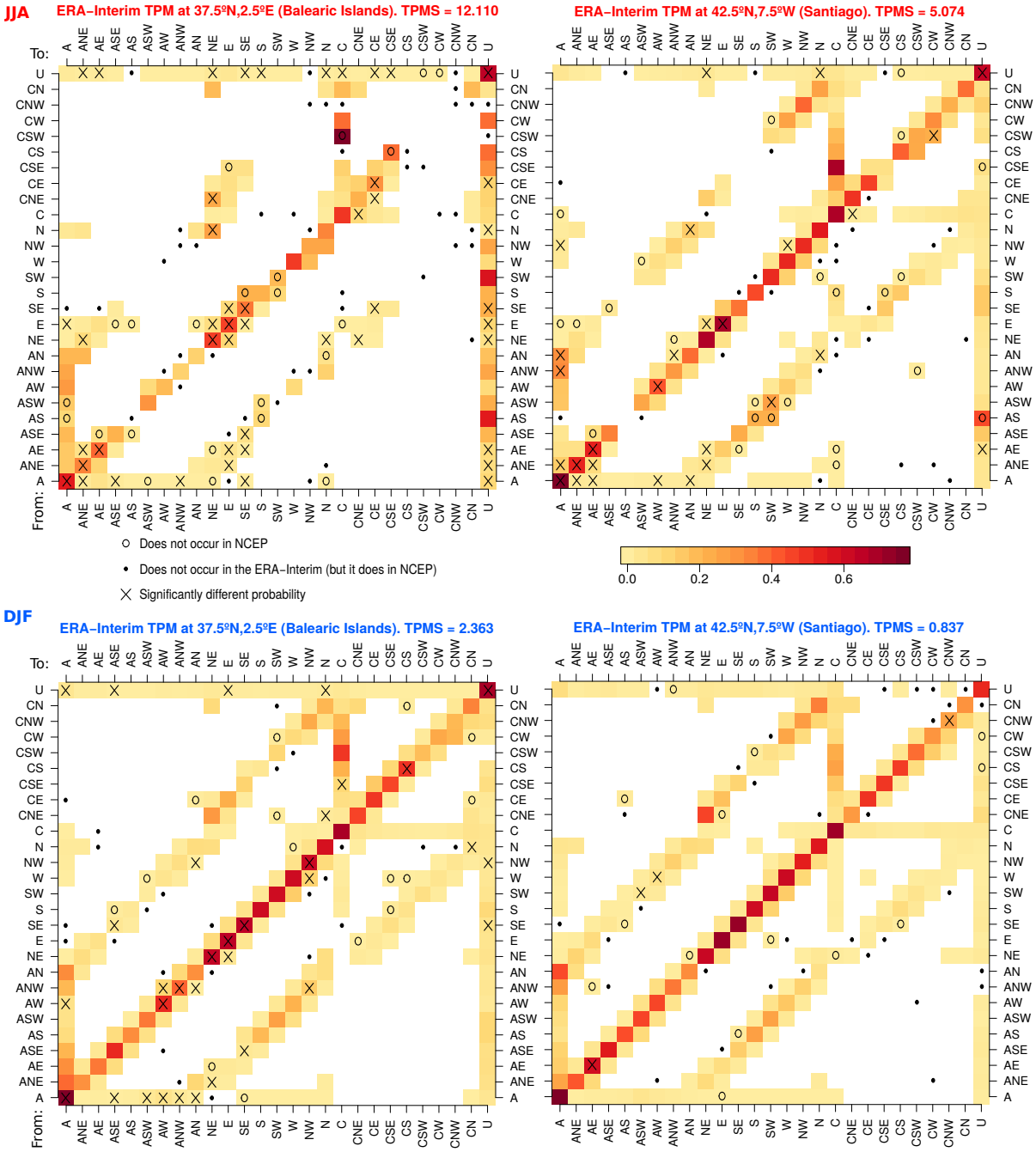

Figure 4.12: *Transition probability matrices (TPM) of JC-WTs from ERA-Interim. Two upper panels correspond to summer (JJA) and the two lower panels to winter (DJF). The two left TPMs refer to the grid box located over the Balearic Islands (large TPMS against NCEP in Fig. 4.11) and the two right TPMs refer to a grid box over Santiago de Compostela (low TPMS against NCEP in Fig. 4.11). The persistence of a WT can be found by looking at the diagonal of the matrix (Sec. 2.3.3). Non-observed transitions have been blanked to differentiate them from low-probability ones.*

in boreal summer.

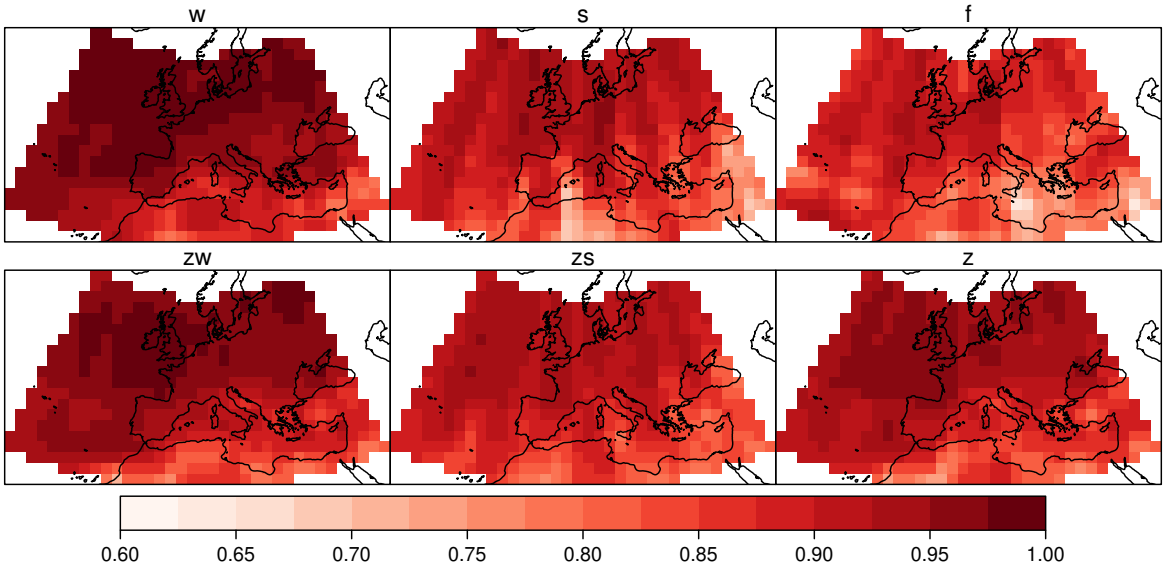

Figure 4.13: *Temporal correlation (Spearman correlation coefficient) of the six intermediate Jenkinson-Collison (JC) parameters (see equations in Table 2.2) from NCEP against ERA-Interim, in summer.*

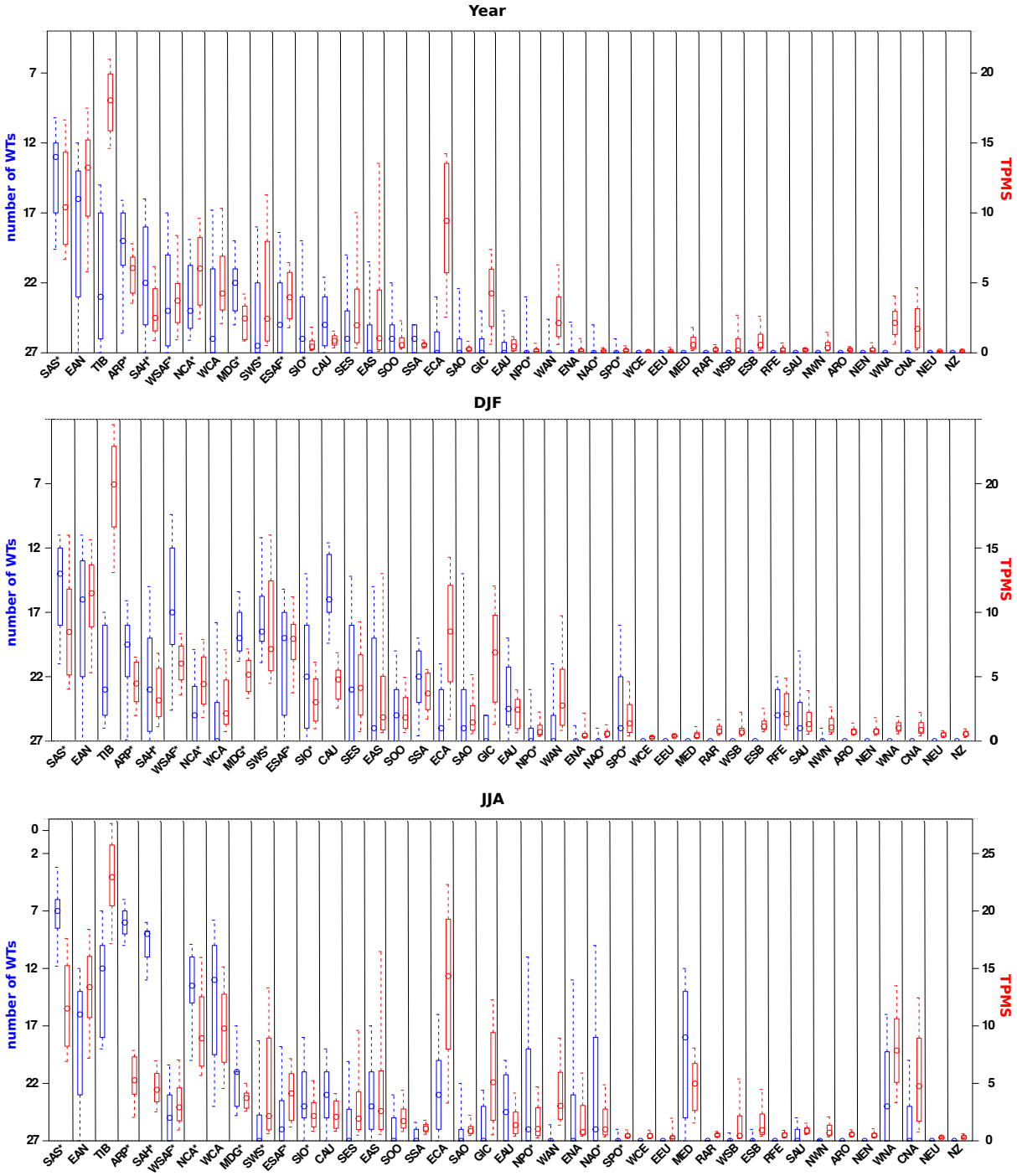

Figure 4.14: *TPMS (in red and referred to the right Y-axis) of JRA-55 against ERA-5 and the number of WTs (in blue and referred to the left Y-axis) of ERA-5 for each IPCC region (the lower the TPMS and the higher the number of WTs, the better). The three different panels correspond to annual, winter and summer results. The limits of the boxes show the spatial interquartile range and whiskers depict the 10^{th} and 90^{th} percentile. The median values are represented with a circle inside the boxes. In the three panels, regions are sorted by decreasing order of the 75^{th} percentile of the ERA-5 number of WTs at annual scale.*

5

Historical Variability in JC-WT Classification: Process-Based evaluation of GCMs

This Chapter focuses on the process-based evaluation of GCMs stemming from the two latest CMIP (CMIP5 and CMIP6). For this purpose, the JC-WT classification over the original Lamb (1972) domain is used, considering reanalysis as reference dataset for model validation. The main results of this Chapter are included in Fernandez-Granja et al. (2021).

5.1 Experiment setup

Here, the JC-WT classification is obtained in its original location (British Isles, 55°N-5°W) defined by Lamb (1972) to classify daily mean SLP patterns from CMIP historical GCM simulations and several reanalyses. Furthermore, this geographical location is crucial for assessing atmospheric circulation within the Atlantic sector of the EURO-CORDEX domain, making it particularly advantageous for ranking GCMs in the context of this downscaling initiative (Sec. 1.2.4) and for the intercomparison between model generations (Sec. 1.2.2). Regarding reanalysis data, the ERA-Interim reanalysis (Dee et al., 2011) is considered as the main quasi-observational reference to evaluate model simulations. For all datasets, the 30-year period 1981-2010 is considered, which follows the World Meteorological Organization (WMO) guidelines on the calculation of climate normals (WMO, 2017) and represents a typical historical period in future climate assessments. This period leads to a sample of ca. 11000 days per dataset.

GCM historical simulations from CMIP5 and CMIP6 experiments are used to evaluate different model generations. A set of 9 model pairs (Table 5.1) is selected to specifically account for potential model improvement. Each GCM pair was developed in a different modeling center, although this does not guarantee model independence (Boé, 2018). As CMIP5 historical experiment ends in 2005, the period 2006-2010 from the RCP8.5 scenario run was considered to fill

the common 1981-2010 analysis period. This has been done in previous studies (e.g. Casanueva et al., 2020) and there is no expected impact on the results, since the difference in the forcing across scenarios is very small for the filled period.

Following some previous studies using the JC-WTs scheme in a location near the British Isles, all days are classified in 26 classes that are assigned to a specific WT (see e.g. Trigo and DaCamara, 2000; Brands et al., 2014b; Ramos et al., 2014b; Pereira et al., 2018). The Unclassified (U) type is not considered in this configuration, as its frequency of occurrence is negligible for the target location. Therefore, U-type time steps are reassigned to other weather types by just not applying rule n° 5 from Jenkinson and Collison (1977) WT assignation rules (see Sec. 2.2). For illustrative purposes, Figure 5.1 shows composite maps of SLP for the 8 most common JC-WTs over an extended European domain, as derived from the ERA-Interim (Dee et al., 2011) reanalysis. These 8 JC-WTs gather 74% of the days and are consistent with previous studies (Trigo and DaCamara, 2000; Brands et al., 2014b; Fealy and Mills, 2018b).

CMIP5	**Grid** (°)	**CMIP6**	**Grid** (°)	**Modeling Center** (CMIP5) CMIP6
CanESM2	2.81	CanESM5	2.81	Canadian Centre for Climate Modelling and Analysis
CNRM-CM5	1.41	CNRM-CM6-1	1.41	Centre National de Recherches Météorologiques - Centre Européen de Recherche et de Formation Avancée en Calcul Scientifique
EC-EARTH	1.13	EC-EARTH3	0.70	(Irish Centre for High-end Computing) EC-EARTH Consortium
GFDL-ESM2M	2.26	GFDL-ESM4	1.00	NOAA - Geophysical Fluid Dynamics Laboratory
HadGEM2-ES	1.59	UKESM1-0-LL	1.59	Met Office Hadley Centre
IPSL-CM5-LR	2.96	IPSL-CM6A-LR	1.98	Institut Pierre-Simon Laplace
MIROC5	1.41	MIROC6	1.41	(Japan Agency for Marine-Earth Science and Technology, JAMSTEC) JAMSTEC, AORI, NIES and R-CCS
MPI-ESM-LR	1.88	MPI-ESM1-2-LR	1.88	Max Planck Institute for Meteorology
NorESM1-M	2.21	NorESM2-LM	2.21	Norwegian Climate Center - Norwegian Meteorological Institute
		Reanalysis	**Grid** (°)	**Modeling Center**
		ERA-Interim	0.75	European Center for Medium Range Weather Forecasts
		JRA-55	0.56	Japanese Meteorological Agency
		NCEP	2.5	National Centers for Environmental Prediction / National Center for Atmospheric Research
		ERA-20C	1.13	European Center for Medium Range Weather Forecasts

Table 5.1: *Set of CMIP5 and CMIP6 models used in the study, their nominal resolution at the Equator (in °) and modelling center (top). Reanalysis datasets used (bottom).*

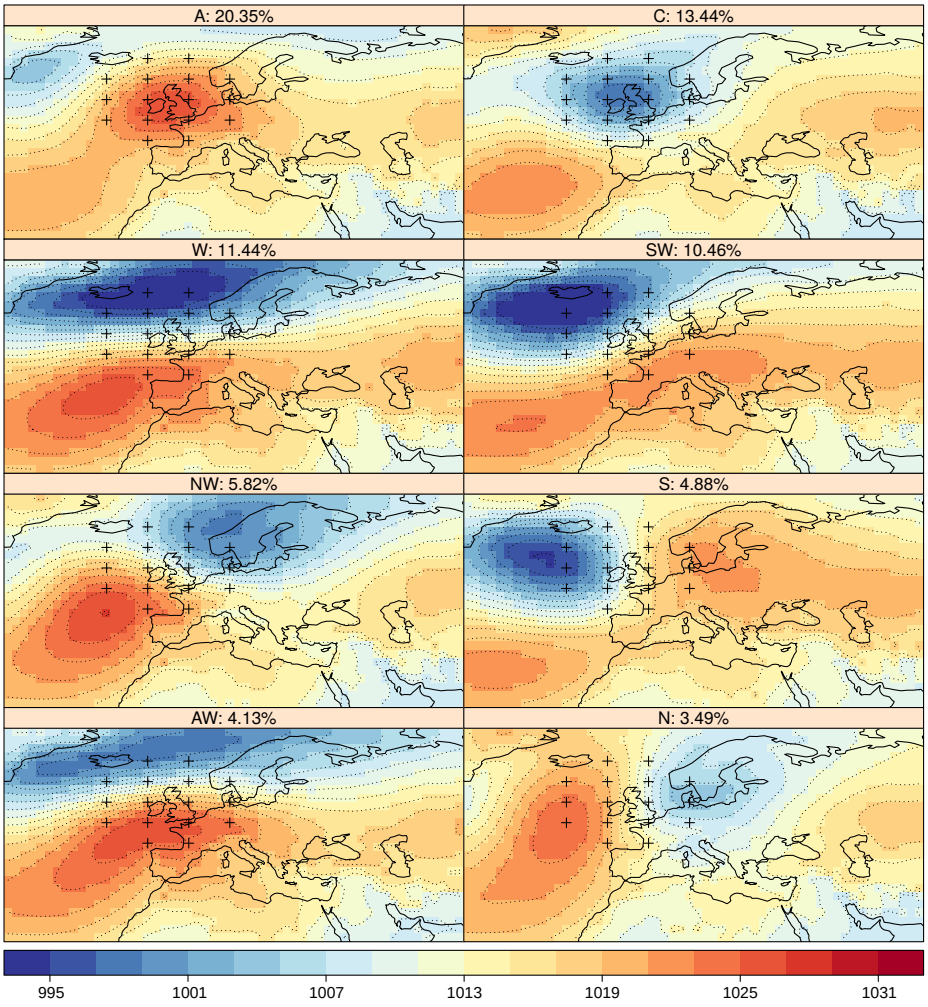

Figure 5.1: *Composite maps of daily mean SLP (hPa) for the Jenkinson-Collison Weather Types (JC-WTs) derived from ERA-Interim for the period 1981-2010. A subset of the 8 (out of 26) most frequent JC-WTs annually is displayed. Sub-panels are labelled with their JC-WT abbreviation (frequency in %) and sorted in decreasing frequency order from top to bottom and from left to right. The colorbar is centered on average sea-level atmospheric pressure (reds are highs and blues are lows). JC-WT's grid coordinates are also indicated over the British Isles domain. Similar composite maps are obtained for the GCMs and reanalyses in Table 5.1; their spatial correlations with the ERA-Interim pattern are shown in Fig. 5.2.*

5.2 Observed JC-WT frequencies

In Chapter 4, observational uncertainty in atmospheric circulation is analyzed using five different reanalyses, including ERA-Interim. Results presented there (Figs. 4.7, 4.9) show that the observational uncertainty (as evaluated with the Transition Probability Matrix Score, TPMS) in the area centered in the British Isles (55ºN, 5ºW) is, in general, relatively low compared to other regions of the world. This conclusion also holds for the SLP spatial patterns associated with the most frequent JC-WTs (Fig 5.2, left panel). Similarly, Brands (2022b) compared ERA-Interim against JRA-55 for the entire Northern Hemisphere on an annual scale, and also reported a low discrepancy between reanalyses in terms of Mean Absolute Error (MAE) of the JC-WTs in the British Isles. Despite the reduced reanalysis spread in this region, three additional reanalysis products (Table 5.1) are considered to account for observational uncertainty: JRA55 (Kobayashi et al., 2015; Harada et al., 2016), NCEP–NCAR reanalysis (hereafter NCEP, Kalnay et al., 1996), and the ECMWF ERA-20C (Poli et al., 2016), hence allowing for a quantitative measure of multimodel spread compared to reanalysis uncertainty.

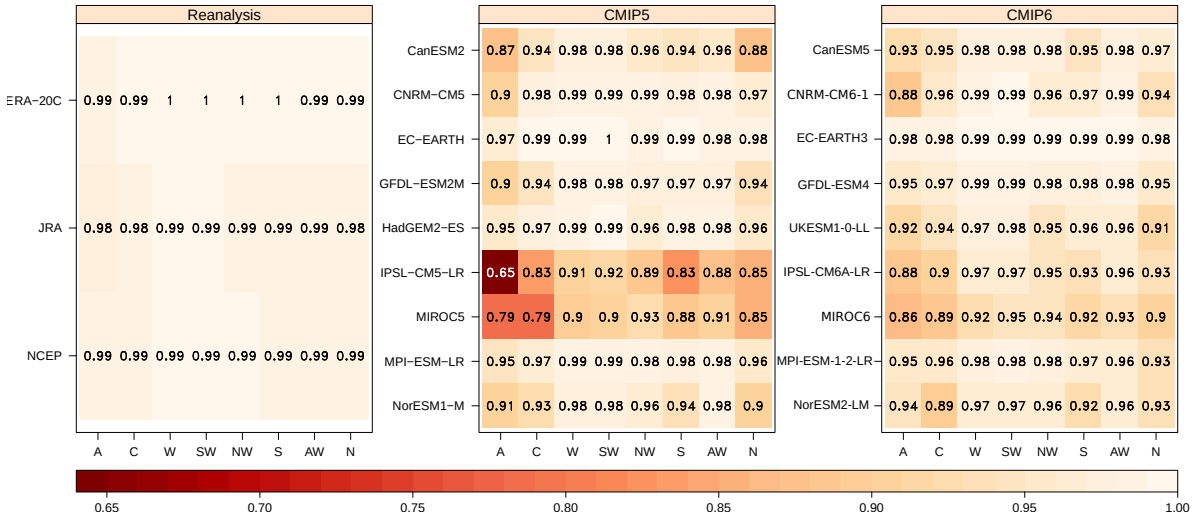

Figure 5.2: *Spatial Correlations of SLP patterns associated with the eight dominant JC-WTs of all models (right panels, CMIP5 and CMIP6) and reanalyses (left panel) included in Chapter 5 with respect to ERA-Interim (depicted in Fig.5.1), considering the spatial domain shown in Fig. 5.1.*

The resulting frequencies of the observed JC-WTs, as represented by the four reanalysis products, are analyzed first. In Fig. 5.3, JC-WT seasonal frequencies are depicted, sorted in decreasing order according to annual ERA-Interim JC-WT frequencies. In general, small differences in the frequencies are found between the reanalysis for all seasons. The common set of eight prevailing JC-WTs has, however, different seasonal frequencies. In DJF, Westerly (W) and Southwesterly (SW) flow types are more frequent than the Cyclonic (C) type, and both exceed the annual time-scale reference. Westerly flow decays in March–April–May or boreal

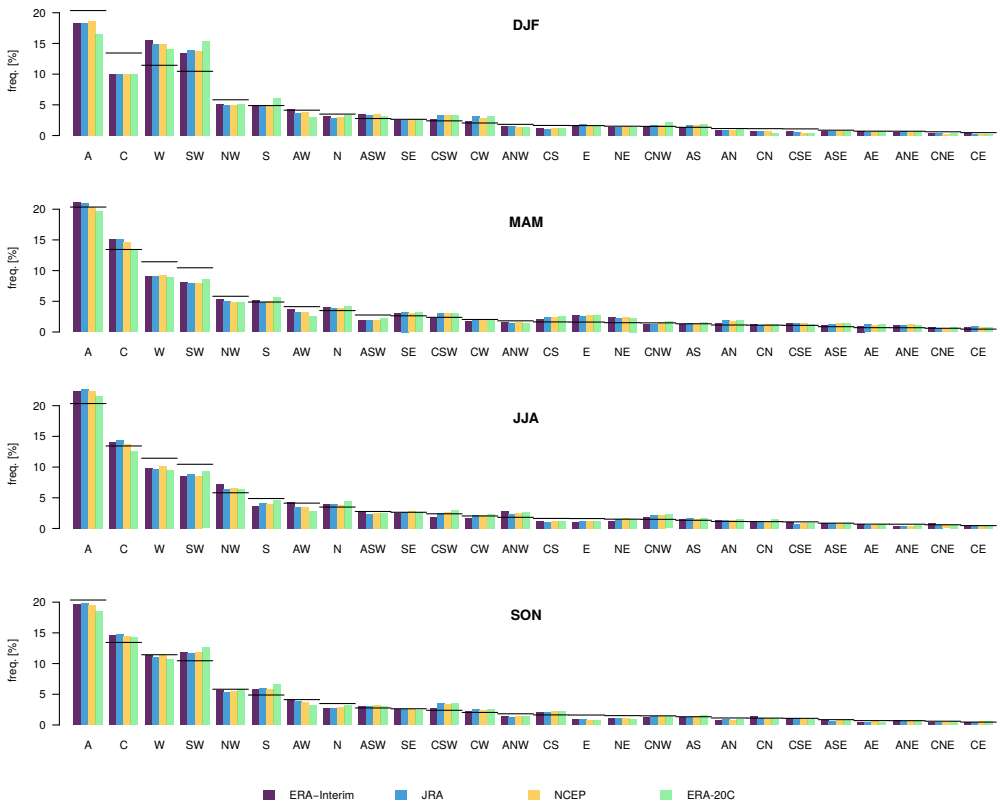

Figure 5.3: *Comparison of the seasonal relative frequencies of JC-WTs obtained from the four different reanalysis (ERA-Interim, JRA, NCEP and ERA-20C, in colors) for the JC-WT classification over the Bristish Isles. The JC-WTs are sorted in decreasing order of their annual frequencies in ERA-Interim, indicated with horizontal segments in all panels for reference.*

spring (MAM) and JJA, and the Anticyclonic (A) type becomes more prevalent in summer. Types A, C , W and SW are the four most frequent JC-WTs in all seasons. Types S (South), NW (Northwesterly) and AW (Anticyclonic Westerly) are among the eight most dominant in all seasons. Pure-directional type N (North) is also in the top-8 except in winter, when it is less frequent than type ASW (Anticyclonic Southwesterly). However, N type represents close to 5% of the days in all seasons and also appears among the first eight JC-WTs for annual ERA-Interim. In light of these results, the following JC-WT subset is used hereinafter for a more detailed analysis of model biases (Sec. 5.3): A, C, W, SW, NW, S, AW and N.

The observational uncertainty in the JC-WT relative frequencies is small, as their magnitudes are similar among the different reanalysis datasets, with the exception of ERA-20C (Fig. 5.3). This reanalysis shows lower JC-WT relative frequencies as compared to ERA-Interim, JRA and NCEP, especially in the two most frequent types (A and C), which is compensated mainly by an increased frequency in the S and SW flow types. This fact could be due to the different data sources of the ERA-20C reanalysis compared to the other available reanalyses, which, in turn, might lead to differences in the JC-WTs classification (see also Chapter 4.3). The

ERA-20C reanalysis only assimilates sea-level pressure data from surface-only observations to maintain consistency over time (Poli et al., 2016). In contrast, the rest of the reanalyses (showing a more consistent distribution of JC-WT frequencies) assimilate many surface, upper-air and satellite observations (Fujiwara et al., 2017). Our findings are in line with previous literature, which highlights the poor representation of upper atmospheric processes because data from the free atmosphere are not available in surface-only input reanalyses. For example, lower cyclones in the Northern Hemisphere (Wang et al., 2006), fewer northern high-latitude blocking frequency (Rohrer et al., 2018), and lower occurrence of westerly circulation types (Stryhal and Huth, 2017) have been detected for ERA-20C and other surface-only input reanalyses.

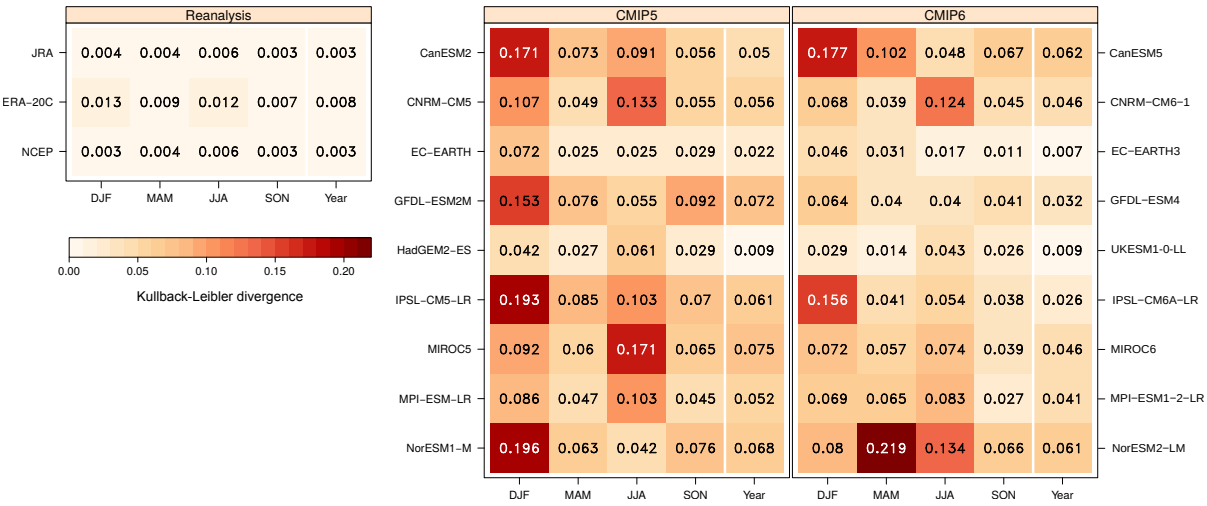

Figure 5.4: *Kullback–Leibler Divergence (KL, Sec. 2.3.2; seasonal and annual values, in columns within each panel) for the different reanalyses (left panel) and GCM experiments (right panels, CMIP5 and CMIP6). The 26 JC-WTs need to be considered as the KL formulation expects PMFs where the sum of the probabilities of the samples is equal to 1.*

Figure 5.4 (left panel) shows the similarity between the reanalyses ERA-20C, JRA and NCEP with respect to ERA-Interim by using the KL Divergence (Sec. 2.3.2). Again, among the reanalyses, ERA-20C shows the largest differences with respect to ERA-Interim ($KL = 0.008$) compared to the other reanalyses (0.003 for both the JRA and NCEP). Given the good agreement in the JC-WTs classification regardless of the use of ERA-Interim, JRA and NCEP, in the following ERA-Interim is used as reference. Further results considering the other reanalyses as reference are provided in Figs. 5.5, 5.6 and 5.7 for a more comprehensive picture of the reanalysis uncertainty. Interestingly, JRA and NCEP agree better with ERA-20C than ERA-Interim in terms of KL divergence (Fig. 5.7). This aligns well with Chang and Yau (2016), who found that major storm tracks in the Northern Hemisphere in ERA-20C and JRA are in good agreement with radiosonde observations.

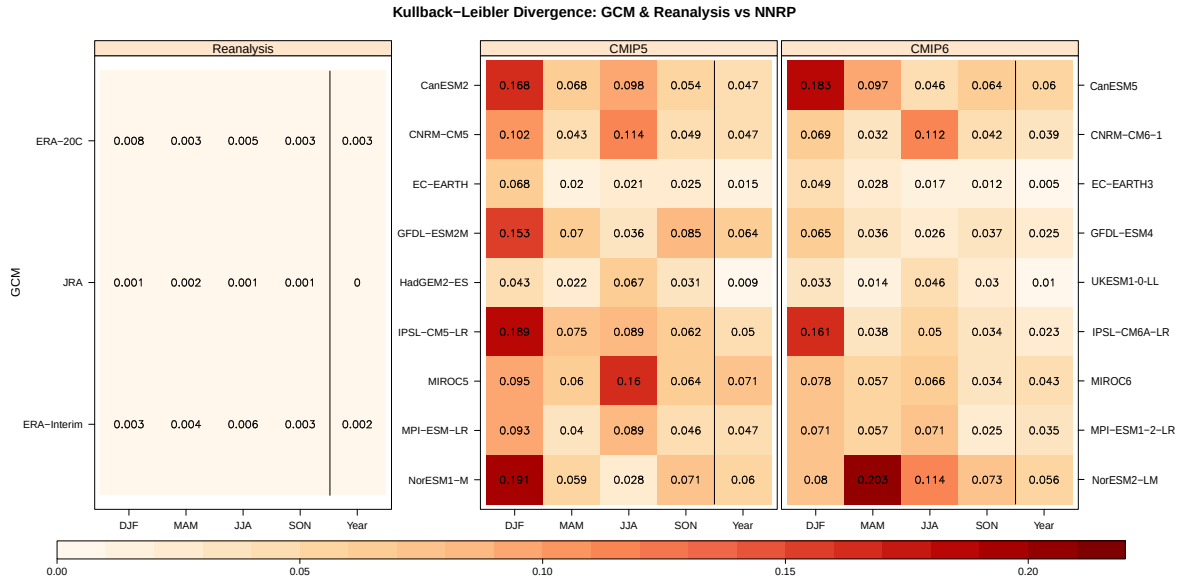

Figure 5.5: *As Fig. 5.4 but with NCEP as reference.*

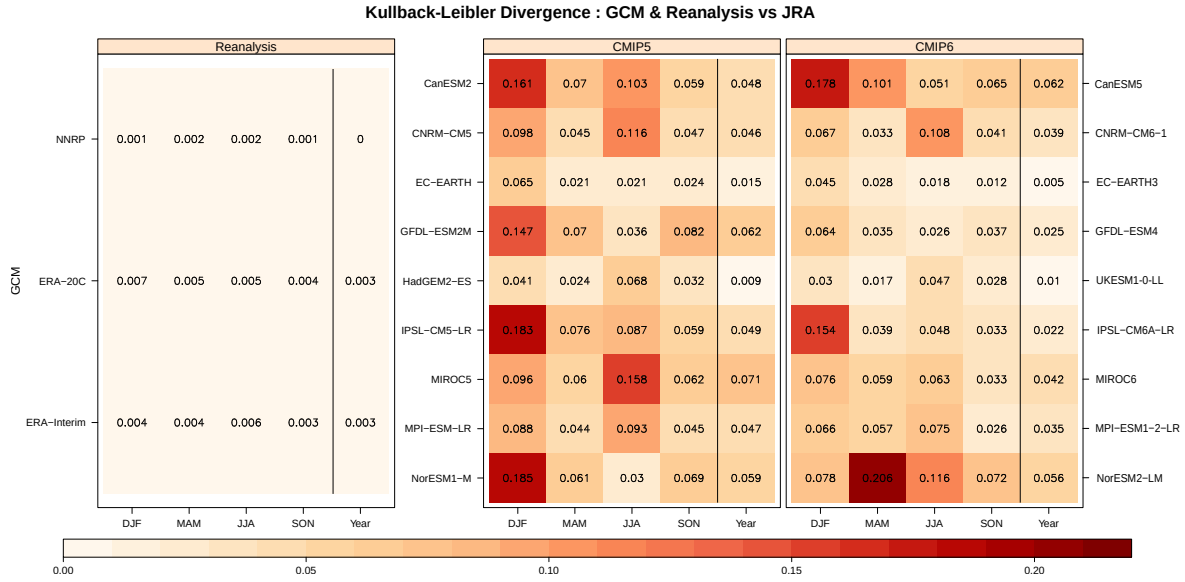

Figure 5.6: *As Fig. 5.4 but with JRA-55 as reference.*

5.3 Evaluation of modeled JC-WTs frequency

Model agreement with ERA-Interim reanalysis is analyzed first in terms of the KL divergence (Fig. 5.4, right panels). However, as annual KL divergence can hide the compensation of large biases, both annual and seasonal timescales are later considered for the analysis of relative biases. Overall, there is a clear improvement from CMIP5 to CMIP6, although large KL divergences in CMIP5 in specific seasons only slightly diminish or move to another season in CMIP6. Similar

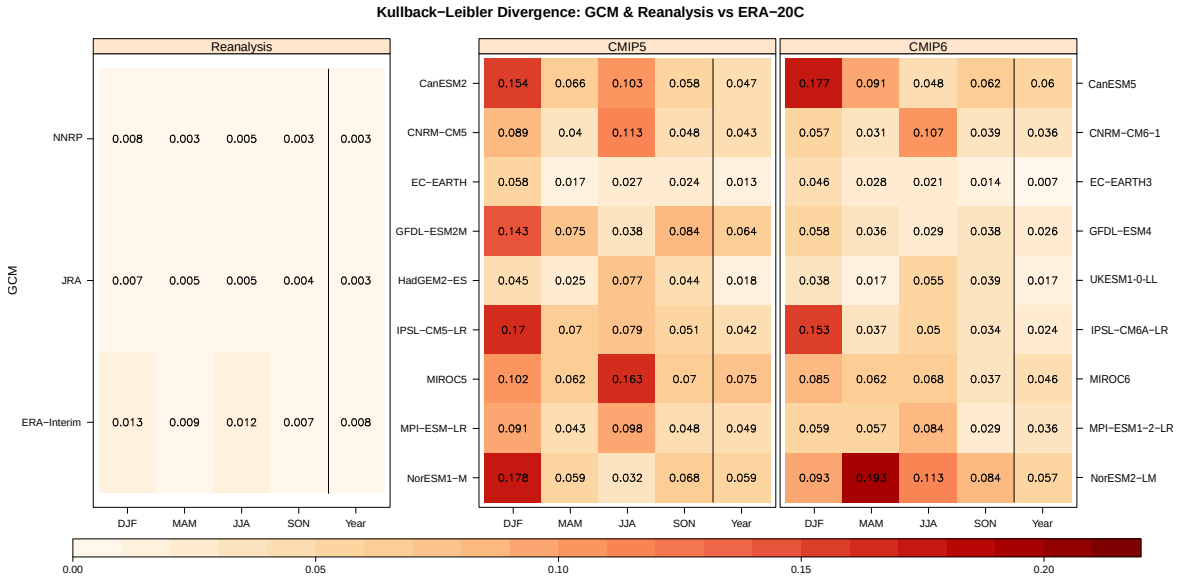

Figure 5.7: *As Fig. 5.4 but with ERA-20C as reference.*

conclusions hold when the other three reanalyses are used as reference (see Figs. 5.5, 5.6 and 5.7). At annual timescales, CMIP6 EC-EARTH3 exhibits the lowest deviation ($KL = 0.007$), followed by UKESM1-0-LL (0.009), HadGEM2 (0.009), EC-EARTH (0.022) and IPSL-CM6A-LR (0.026). EC-EARTH3 also shows slightly better performance than ERA-20C at the annual scale, which deteriorates in the seasonal analyses (e.g. $KL = 0.046$ in winter, $KL = 0.031$ in spring) probably due to biases in the timing along the year and the persistence of the weather types. The largest KL divergences occur in winter for most CMIP5 and CMIP6 models, followed by summer and spring.

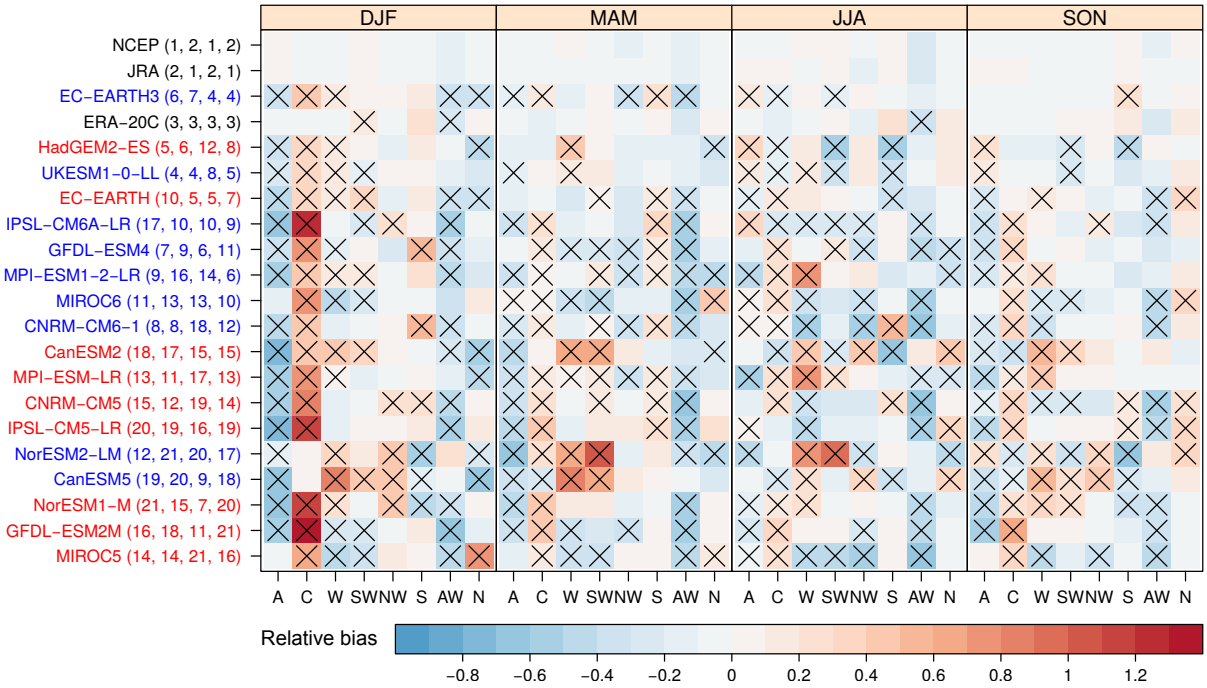

Figure 5.8: *Relative bias of JC-WT frequencies for the different reanalyses and GCM experiments with respect to ERA-Interim (in rows: reanalyses in black font, CMIP5 GCMs in red, CMIP6 GCMs in blue) for the four seasons (in columns). Rows are sorted following the ranking given by the annual KL Divergence in Fig. 5.4 (seasonal rankings are given in brackets). Crosses indicate statistically significant biases following a Z-test of proportions (Sec. 2.3.4).*

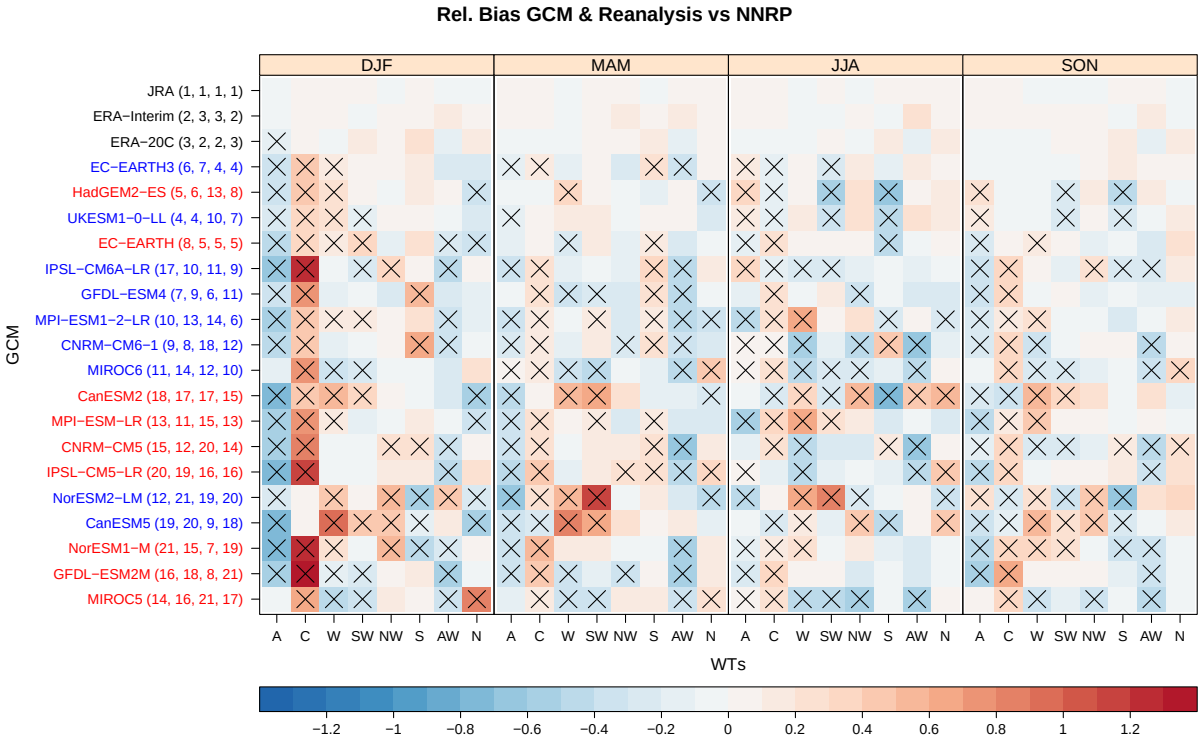

Figure 5.9: *As Fig. 5.8 but with NCEP as reference.*

To explain such differences the seasonal GCM biases for the main JC-WT frequencies are

analyzed next. The KL divergence of the CMIP5 and CMIP6 models allows to rank them according to their ability to reproduce synoptic conditions with respect to their agreement with ERA-Interim. The general improvement of CMIP6 considering the annual KL divergence (Fig. 5.4) is also evident in terms of relative biases (Fig. 5.8). Overall, smaller biases are found for CMIP6, except for IPSL-CM6A-LR in winter, NorESM2-LM and CanESM5 in spring, and NorESM2-LM in summer. All models present the worst performance for the two most frequent JC-WTs (namely anticyclonic and cyclonic) in winter (in agreement with Fig. 5.4), with opposite sign biases. Along the four seasons, most models overestimate cyclonic type frequencies whereas they simulate too few anticyclonic conditions. The latter might be associated with the general underestimation of the frequency of the European winter blocking, which is a well-known drawback of CMIP5 models (see e.g. Masato et al., 2013). Overall, CMIP6 GCMs reduce biases in the frequency of the A and C types compared to their CMIP5 counterparts, especially NorESM2-LM and GFDL-ESM4, although statistically significant differences with ERA-Interim still remain.

Results are not conclusive for the other main JC-WTs, for which different magnitude and sign of biases are found depending on the model. The frequency of W and SW types is overestimated by NorESM2-LM and CanESM5 in spring (also NorESM2-LM in summer), performing worse than their CMIP5 counterparts. AW type is underestimated by most models in spring, regardless of the CMIP experiment. Most GCMs do not exhibit significant differences with respect to ERA-Interim for the least frequent weather types, especially in MAM and September–October–November or boreal autumn (SON). The overall conclusions about the CMIP6 improvement over CMIP5 also hold for the SLP spatial patterns of the most frequent WTs (Fig. 5.2). Finally, GCM evaluation with respect to the three other reanalyses leads to similar conclusions and similar rankings (see Figs. 5.9, 5.10 and 5.11).

Despite the improvement of CMIP6 models upon their CMIP5 predecessors, some biases still remain, which might be due to the limitations in simulating the most frequent conditions (such as A and C types) and the transitions from one type into another.

5.4 JC-WT transition probabilities from GCMs

In order to shed some light on the biases found, the transition probabilities from one type to another are investigated, since they might explain the misrepresentation of the synoptic conditions and their frequencies by most GCMs already depicted in Fig. 5.8. Overall, the ability of the GCMs to reproduce qualitatively the reference TPM regardless of the CMIP generation is remarkable (see Figs. 5.12b-c and also 5.13-5.20).

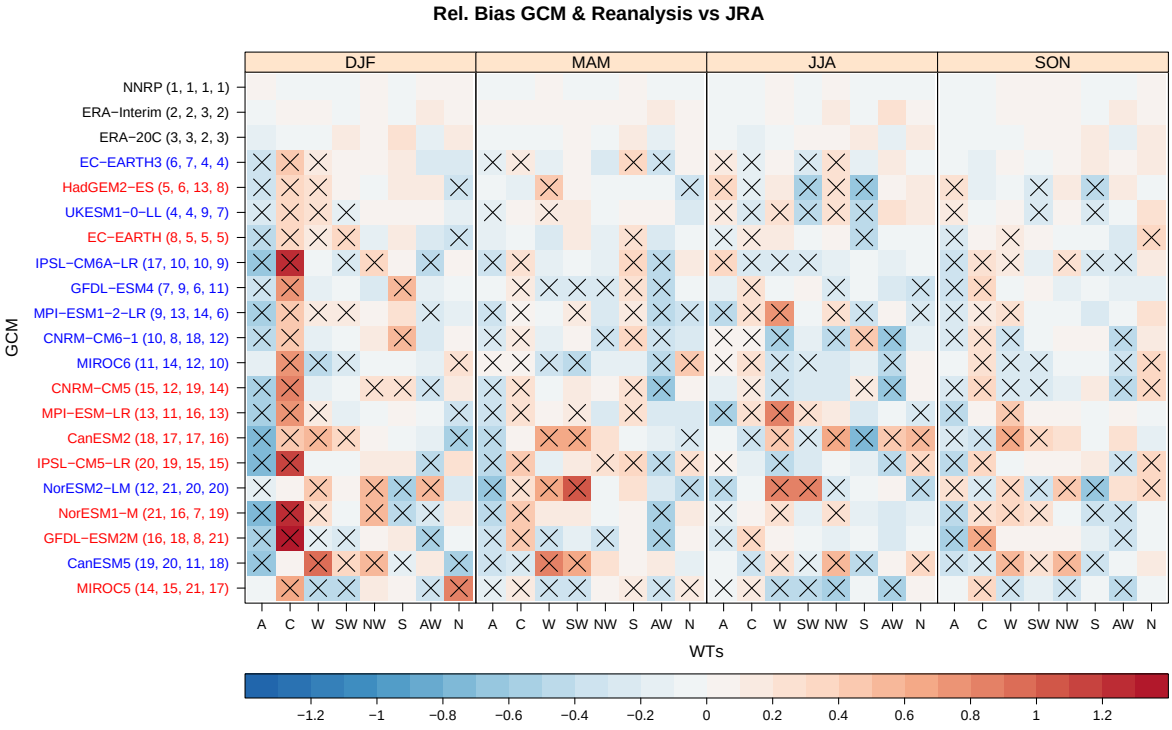

Figure 5.10: *As Fig. 5.8 but with JRA-55 as reference.*

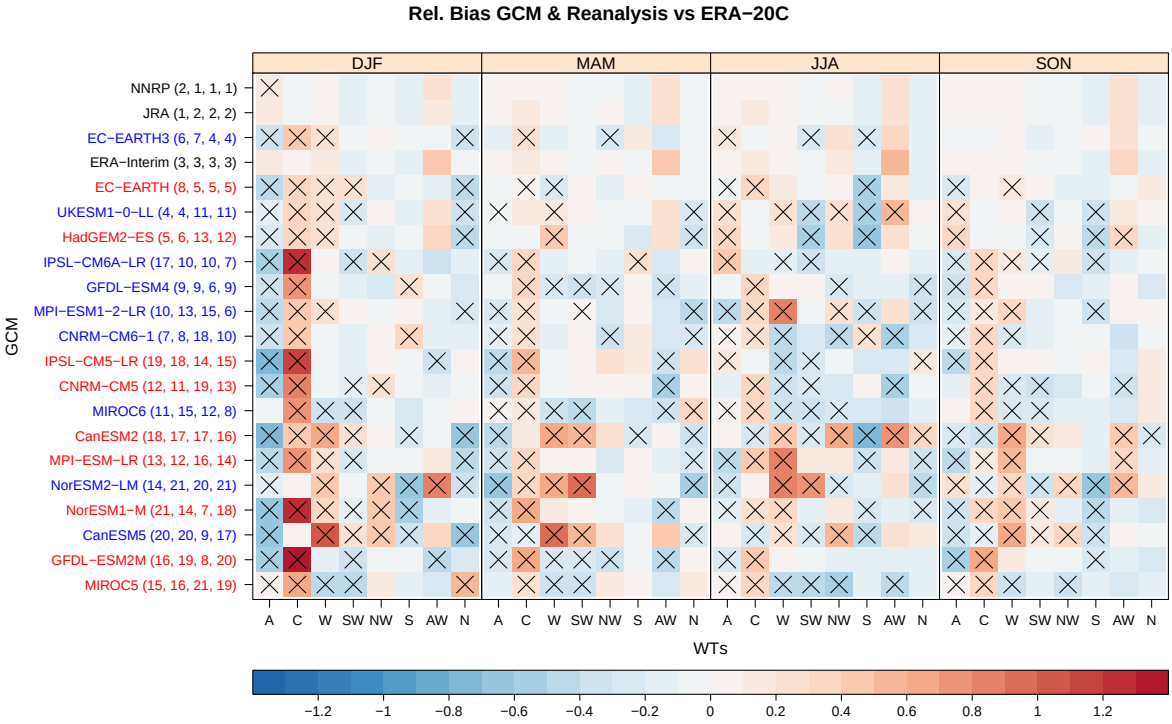

Figure 5.11: *As Fig. 5.8 but with ERA-20C as reference.*

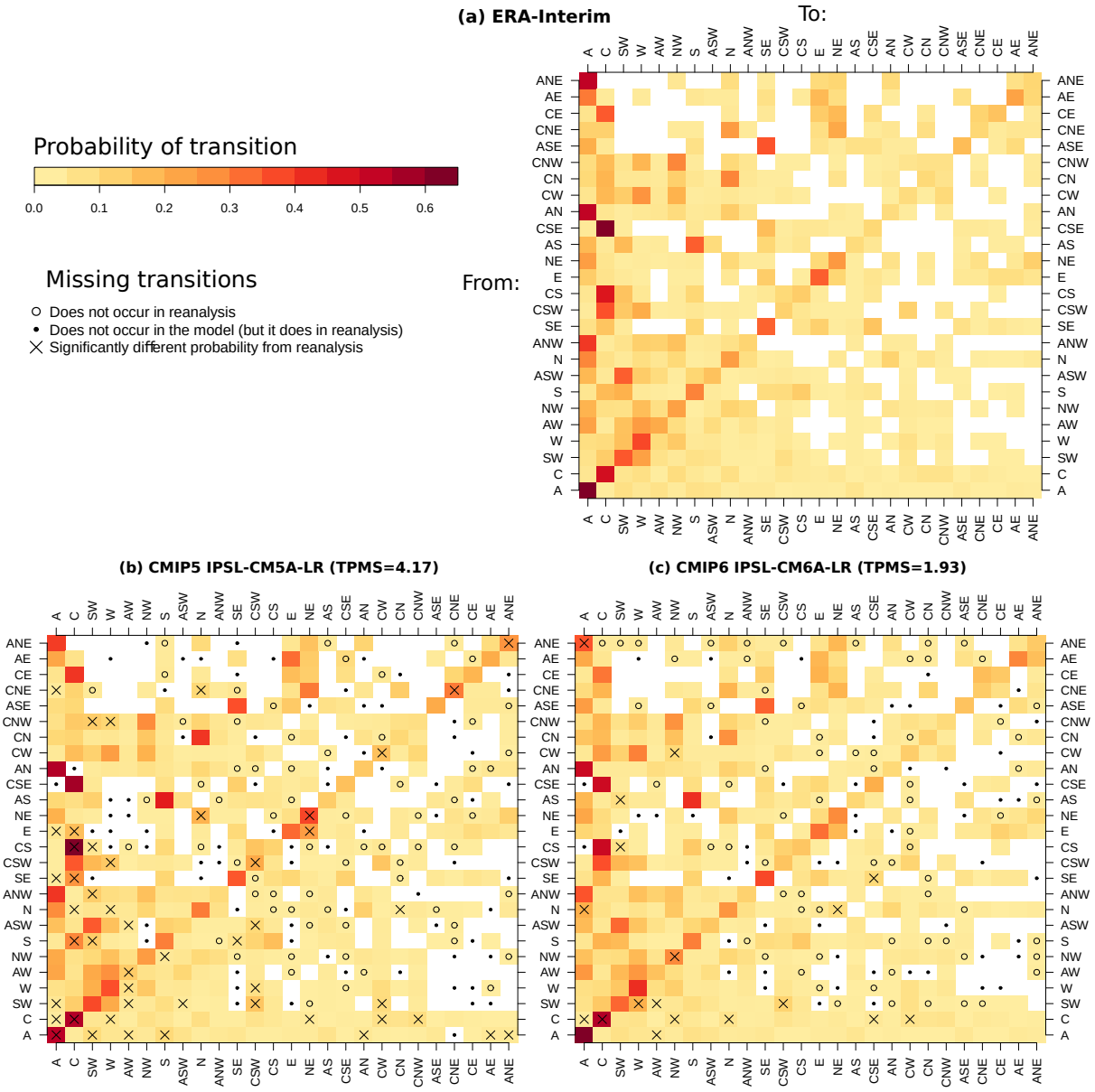

Figure 5.12: *Transition probability matrix (A) of JC-WTs for ERA-Interim (**a**), the CMIP5 model IPSL-CM5A-LR (**b**) and its new version CMIP6 IPSL-CM6A-LR (**c**) for the historical period 1981-2010 for the JC-WT classification over the British Isles. $A_{ij} = p(X_t = j|X_{t-1} = i)$ represents the probability of going from JC-WT in row i to JC-WT in column j. Therefore, the persistence probability of a JC-WT can be found by looking at the diagonal of the matrix. Non observed transitions have been blanked to differentiate them from low-probability ones. Transition probabilities significantly different from those in ERA-Interim, obtained from a two-proportions Z-Test (Sec. 2.3.4), are indicated by crosses. In addition, JC-WT transitions simulated by the model but not observed in ERA-Interim are indicated by empty circles. Likewise, solid circles indicate JC-WT transitions not simulated by the model, but that occur in ERA-Interim. The corresponding TPMS values attained against ERA-Interim are indicated in parenthesis in the titles of panels (**b**) and (**c**).*

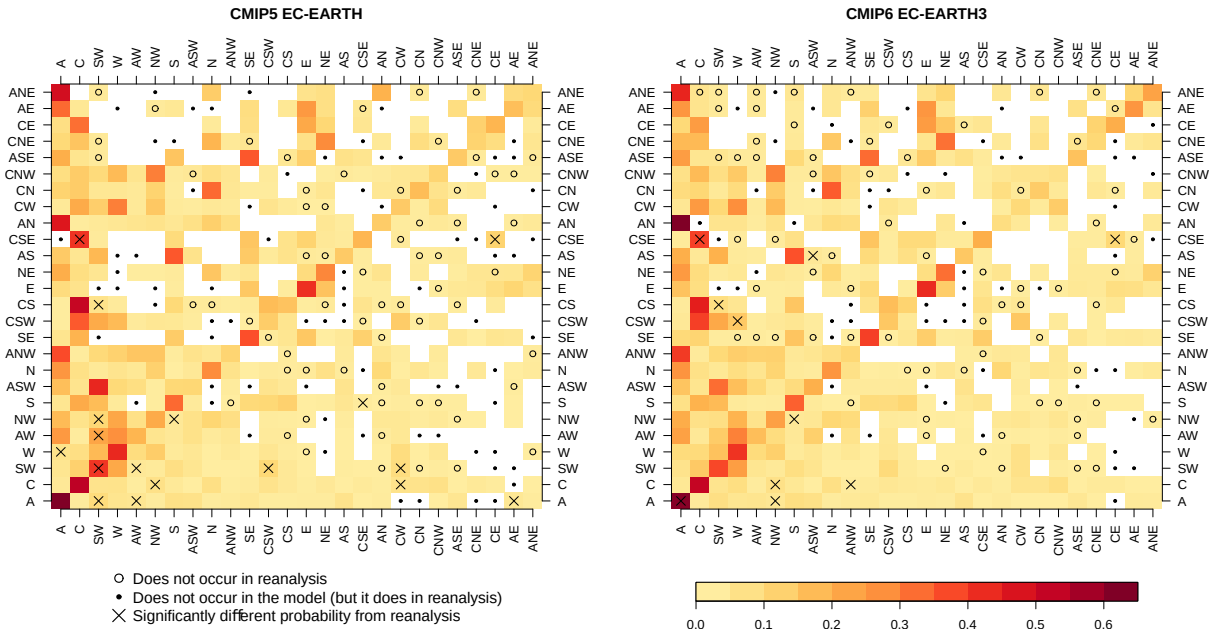

Figure 5.13: *Transition probability matrices of CMIP5 EC-EARTH and CMIP6 EC-EARTH3.*

All GCMs TPM *fingerprints* capture fairly well the pattern of ERA-Interim (used as reference), although there are important deviations in the magnitude of their probabilities in some cases. As a result, most GCMs fail to achieve the high persistence probabilities of the most frequent cyclonic and anticyclonic JC-WTs. In particular, considering the statistical significance of their probabilities, the high-persistence probability of the anticyclonic JC-WT is only adequately reproduced by a few models, namely CMIP5 EC-EARTH and HadGEM2-ES (Figs. 5.13 and 5.15), and the CMIP6 models IPSL-CM6A-LR (Fig. 5.12c) and UKESM1-0-LL (Fig. 5.15). The probability of persistence of the purely cyclonic JC-WT (the second most frequent in the historical record) is significantly well reproduced by the CMIP5 models EC-EARTH, HadGEM2-ES, MPI-ESM-LR, as well as their CMIP6 counterparts (Figs. 5.13, 5.15 and 5.18, respectively), CMIP5 CanESM2 (Fig. 5.20, left panel) and CMIP6 NorESM2-LM (Fig. 5.19, right panel).

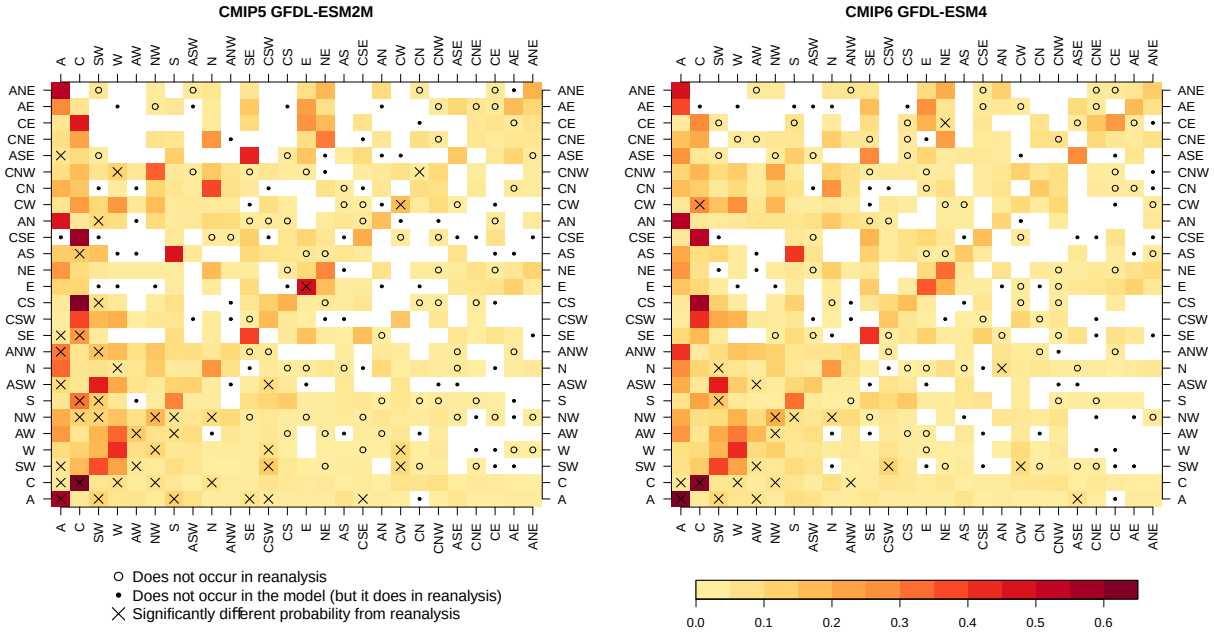

Figure 5.14: *Transition probability matrices of CMIP5 GFDL-ESM2M and CMIP6 GFDL-ESM4.*

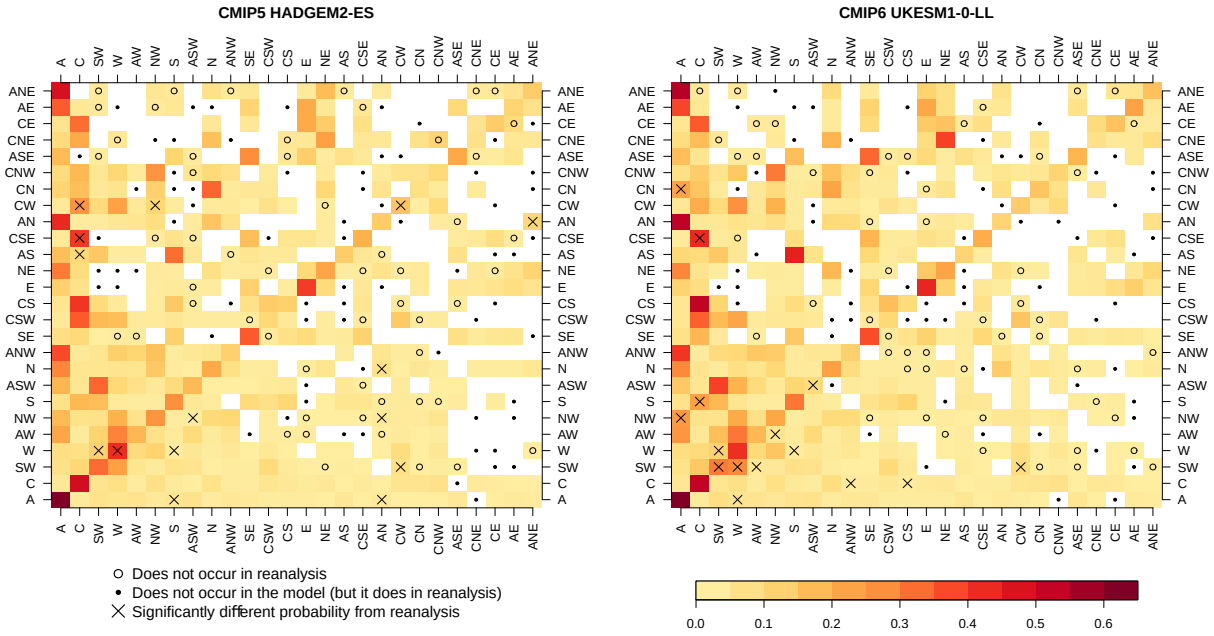

Figure 5.15: *Transition probability matrices of CMIP5 HadGEM2-ES and CMIP6 UKESM1-0-LL.*

The TPM information of all GCMs (and reanalyses) is quantitatively summarized with the TPMS in Figure 5.21. The improvement of CMIP6 over CMIP5 is especially remarkable for IPSL-CM6A-LR and GFDL-ESM4 models. Both GCMs are able to capture more correctly the transition probabilities between the principal JC-WTs (such as A, C, SW or W types) than their CMIP5 counterparts, but not yet the persistence probabilities of A and C types (Fig. 5.12 and 5.14, respectively). Interestingly, the TPMS spread associated with the observational uncertainty is much reduced in the case of the CMIP6 ensemble, pointing to a better

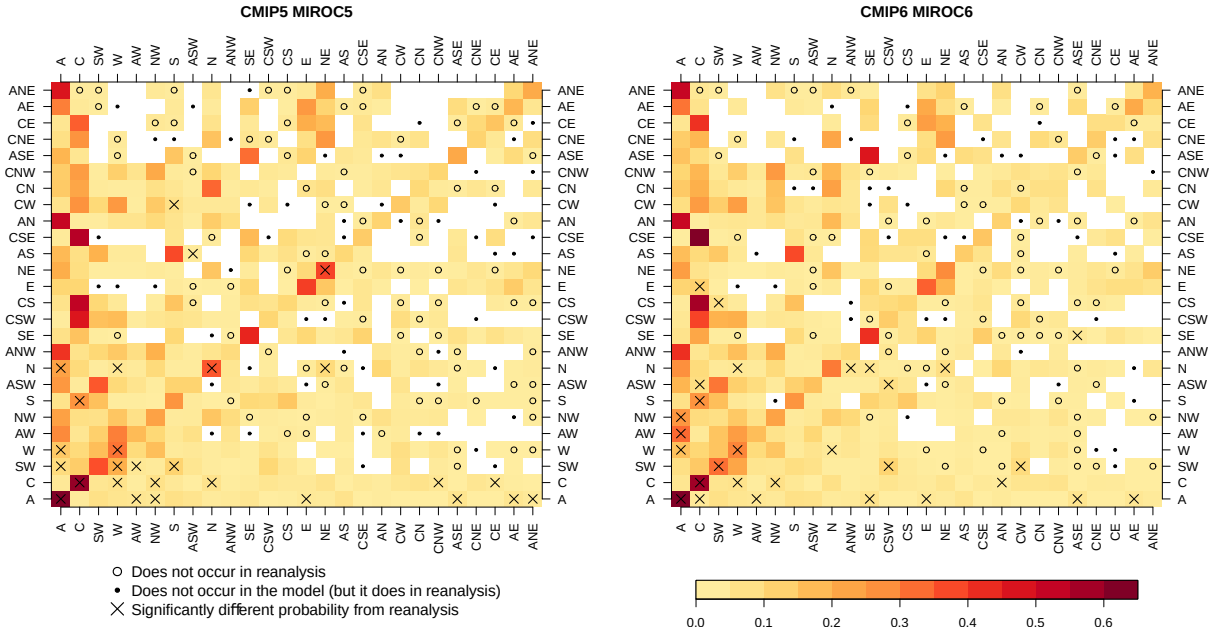

Figure 5.16: *Transition probability matrices of CMIP5 MIROC5 and CMIP6 MIROC6.*

general agreement in their representation of atmospheric circulation, with the exception of two out-lying, poor-performing models, namely NorESM2-LM and CanESM5, which deteriorate in CMIP6 (Fig. 5.21). Although NorESM2-LM improves on the persistence probability of the cyclonic type, the transitions from CNE to C and from ASW to SW get worse in CMIP6 (Fig. 5.19), in line with the reduced bias of C type in winter and the large biases found for SW type in spring and summer (Fig. 5.8). Similarly, CanESM5 presents too persistent C type and too high transition probabilities from AW and SW to W (Fig. 5.20), which might be related to the overestimation of the frequencies of W type in winter and spring (Fig. 5.8).

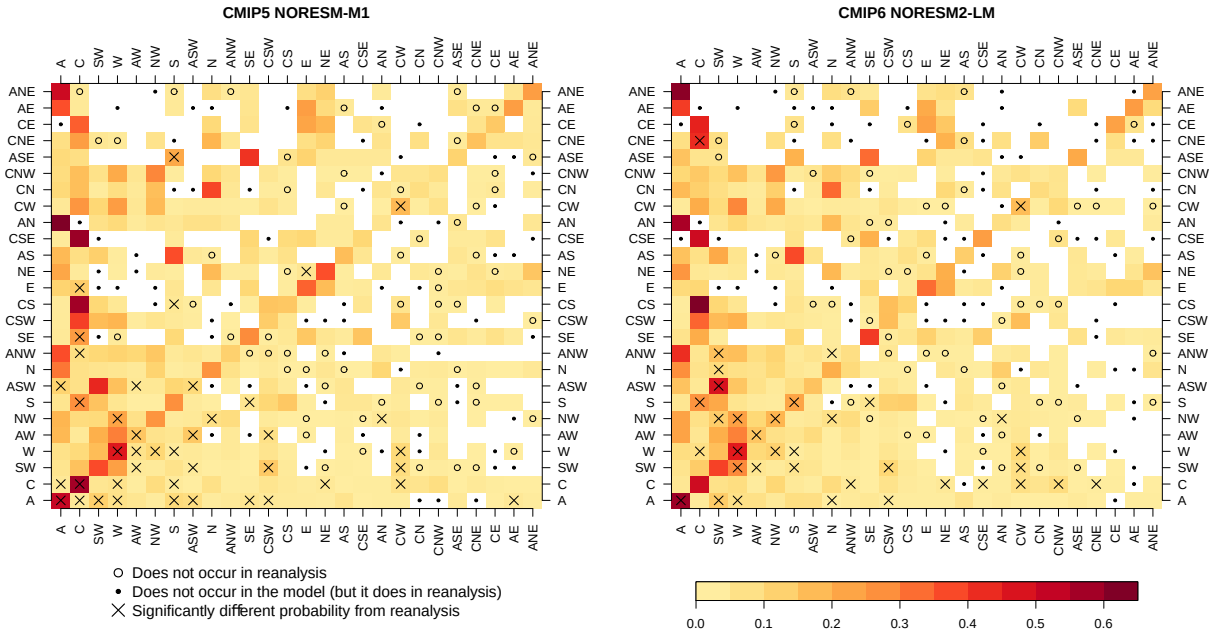

Figure 5.19: *Transition probability matrices of CMIP5 NorESM-M1 and CMIP6 NorESM2-LM*

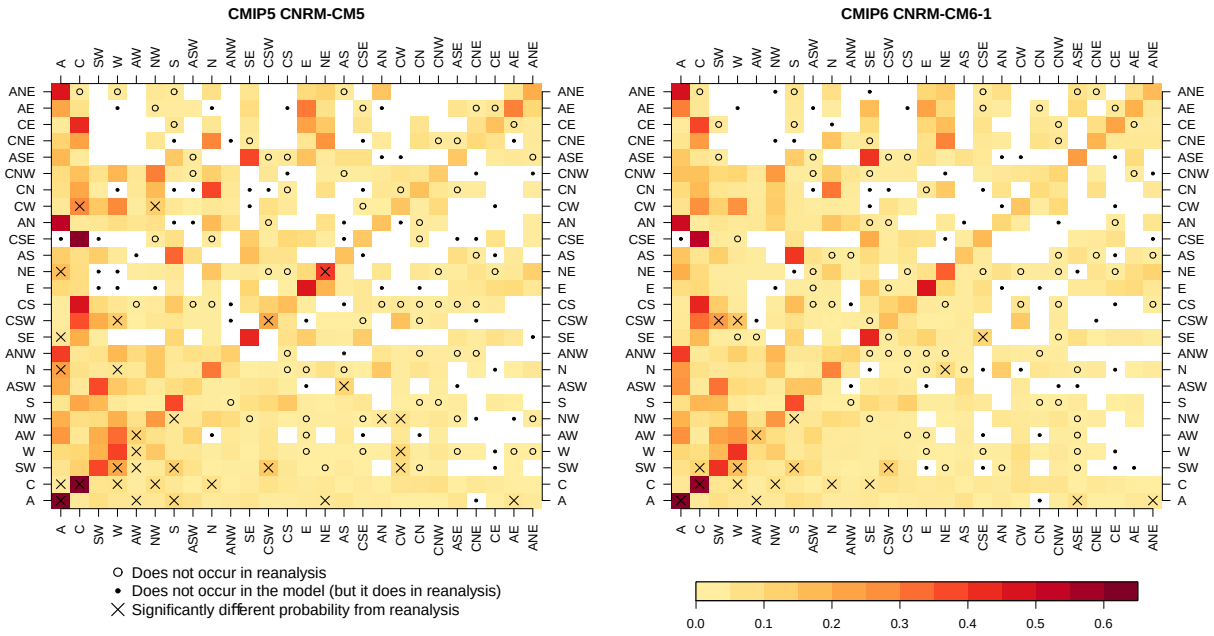

Figure 5.17: *Transition probability matrices of CMIP5 CNRM-CM5 and CMIP6 CNRM-CM6-1.*

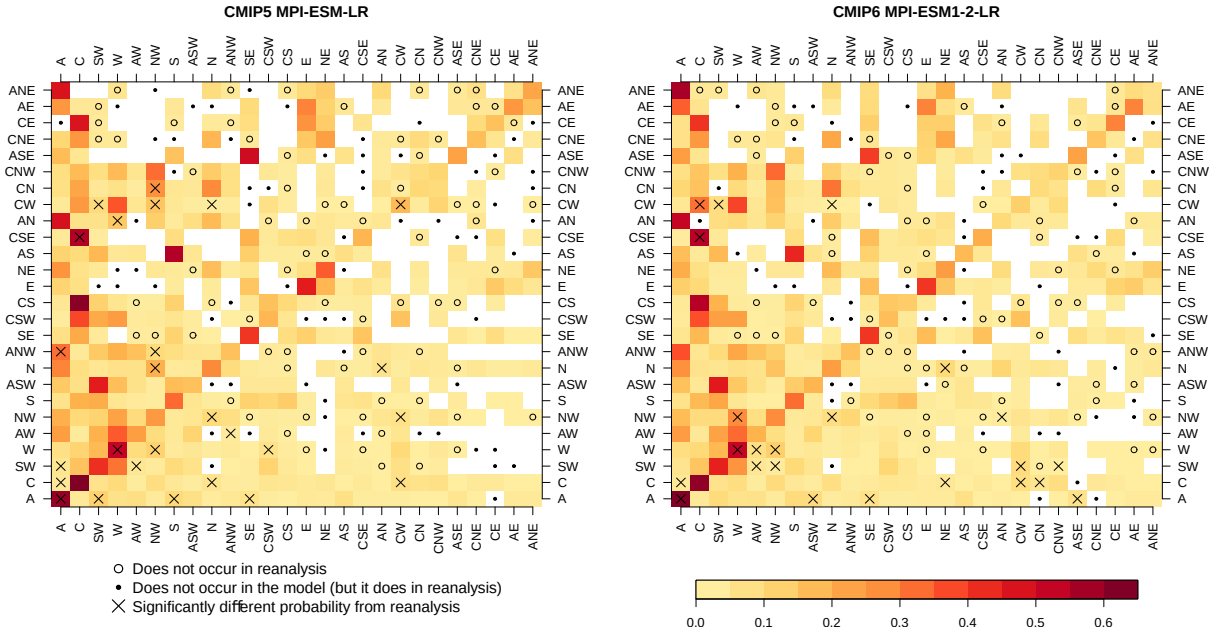

Figure 5.18: *Transition probability matrices of CMIP5 MPI-ESM-LR and CMIP6 MPI-ESM1-2-LR.*

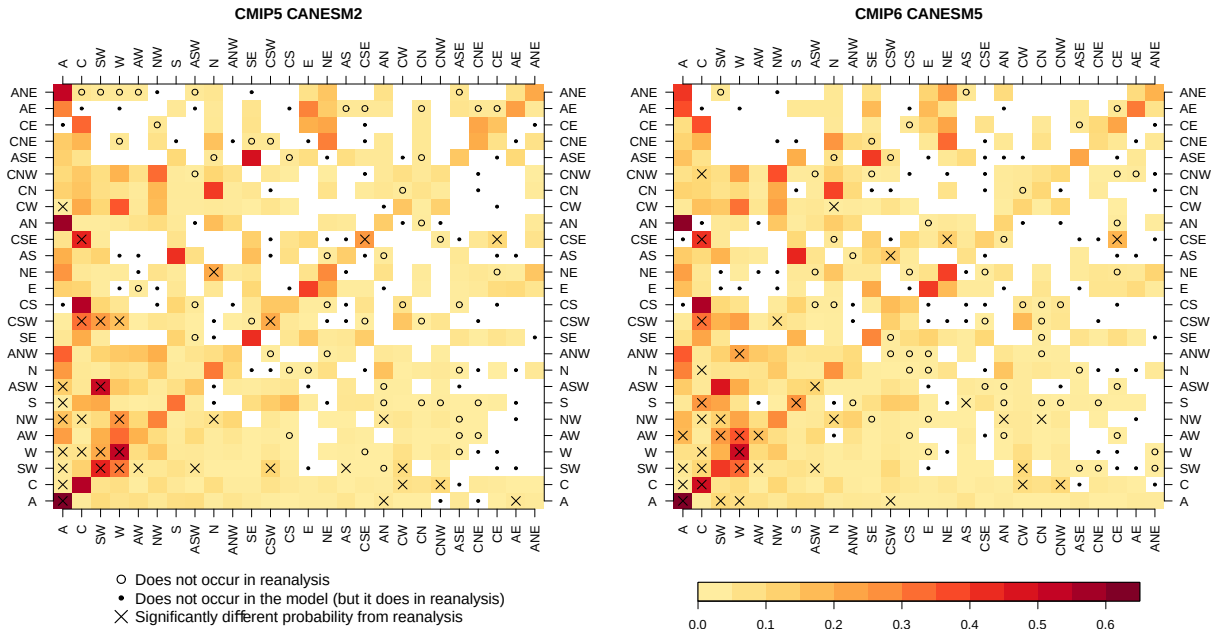

Figure 5.20: *Transition probability matrices of CMIP5 CanESM2 and CMIP6 CanESM5*

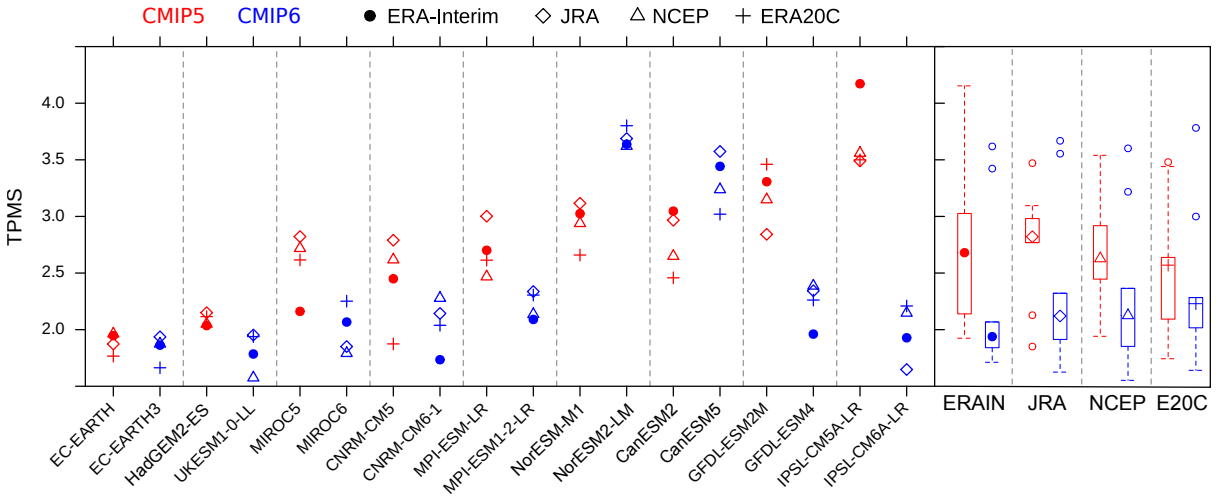

Figure 5.21: *Transition probability matrix scores (TPMS) for CMIP5/CMIP6 models (red/blue symbols), considering as reference different reanalysis products (different markers). The results are presented as CMIP5-CMIP6 GCM pairs, in ascending order of TPMS from left to right, attained by CMIP5 models and ERA-Interim as reference (solid circles). Boxplots on the right summarize the results for each individual observational reference (each marker indicating the median) and CMIP project (color).*

As for the JC-WTs frequencies (Fig. 5.3), very similar TPMs are found for JRA ($TPMS = 0.71$) and NCEP ($TPMS = 0.76$) compared to ERA-Interim and a larger TPMS for ERA-20C ($TPMS = 1.11$, see also Fig. 4.5). The improved performance of CMIP6 compared to CMIP5 is independent of the reanalysis used as reference (Fig. 5.21), in line with the results of Cannon (2020). Overall, the differences due to the choice of the reference dataset are smaller than model and experiment uncertainties.

5.5 Discussion of process-based evaluation outcomes

While there is a general increase in spatial resolution and an integration of more complex components in CMIP6, these developments take place unevenly for each GCM. For instance, EC-EARTH which is a skillful CMIP5 model improves upon most CMIP6 GCMs, partly due to its rather high resolution (Table 5.1). A substantial improvement is found for GFDL and IPSL in CMIP6, which have been developed at higher resolutions than their CMIP5 predecessors. Conversely, CanESM and NorESM, which keep a coarse resolution in CMIP6 (the only ones above 2°), deteriorate their TPMS in CMIP6. All the above suggests that the increase of spatial resolution is a factor of improvement in the representation of the atmospheric circulation in the GCMs.

Previous studies also find that increasing horizontal resolution of the GCMs leads to a large improvement in the models' simulation of the main Euro-Atlantic wintertime weather regimes (Dawson et al., 2012; Strommen et al., 2019) and, particularly, Northern Hemisphere (D'Andrea et al., 1998) and European winter blocking (Matsueda et al., 2009; Berckmans et al., 2013; Davini et al., 2017). The better performance of higher-resolution simulations can be attributed to the more realistic orography (Jung et al., 2012) and more realistic representation of Rossby wave breaking processes, which are known to be important in maintaining persistent anomalies (Woollings et al., 2008; Masato et al., 2012). A recent work based on results of the PRIMAVERA project (Fabiano et al., 2020) shows that the weather regimes tend to be more tightly clustered in the increased resolution simulations, thus resembling the observed ones more closely. However, increased resolution does not improve all aspects in the same way. For instance, Fabiano et al. (2020) find an improvement of the spatial pattern, but limited impact on the frequency of occurrence and persistence of the weather regimes. While resolution stands as a relevant factor, it is not decisive, since some models (here CNRM, HadGEM, MIROC and MPI) improve on TPMS in CMIP6 even though they keep the same resolution. According to Dawson and Palmer (2015) the simulation of spatial and temporal aspects of weather regimes at low resolution can be significantly improved by the introduction of a stochastic physics scheme, highlighting the importance of small-scale processes on large-scale climate variability. Indeed further improvements are needed to alleviate remaining biases, for instance, better location of the winter blocking is associated with realistic Gulf Stream sea surface temperature (O'Reilly et al., 2016).

Another outcome of this Thesis is that the use of different observational references stands as a minor source of uncertainty compared to model and experiment uncertainties, as expected following results from Chapter 4, which show small observational uncertainty in the studied

region here. With this regard, results are robust to the selected reference reanalysis and the improvement of CMIP6 over CMIP5 is independent of this choice (in agreement with Cannon, 2020).

Note that model internal variability is not considered in this study and observational uncertainty is used as reference for substantive changes in the ability of the models to represent the circulation types. Other sources of uncertainty related to the WT classification method remain. Results might be sensitive to the circulation classification algorithm used and, therefore, rankings, model performance and even CMIP6 quantitative improvements are particular for the JC-WT classification. Cannon (2020) also found an overall improvement in CMIP6 models when using two objective classification algorithms. Thus, a qualitative improvement of CMIP6 is noteworthy regardless of the classification algorithm and evaluation metrics. However, this remains as another source of uncertainty and is a very interesting aspect to tackle in future work.

The results obtained in this Chapter have important implications for downscaling applications. Any systematic bias in the simulation of WTs (whether in their frequency, seasonal distribution, or prevailing circulation regimes) can significantly affect the realism and reliability of regional climate projections derived through downscaling (Sec. 1.2.4). The process-based evaluation results shown in this Chapter can inform the selection or weighting of global climate models (GCMs) prior to downscaling. For example, models that accurately reproduce the observed WT distributions and their seasonal variability are expected to produce more credible regional projections when used as input for downscaling experiments. However, GCMs exhibiting large discrepancies can propagate errors related to atmospheric circulation into local-scale projections.

Interestingly, the models exhibiting in this Chapter the best performance in reproducing the features of reanalysis-based JC-WTs, namely EC-Earth3, UKESM1-0-LL, MIROC6, IPSL-CM6A-LR, and MPI-ESM1-2-LR, largely overlap with those identified as highly plausible in the recent EURO-CORDEX model selection framework (Sobolowski et al., 2023). Despite minor differences in model configurations (e.g., the use of EC-Earth3 instead of the *veg* variant, or the lower-resolution version of MPI-ESM1-2), this convergence reinforces the robustness of the plausibility criterion applied in this Thesis. Specifically, the consistency between large-scale circulation realism, quantified here via JC-WT frequencies, and the broader plausibility metrics used in the CORDEX framework (which include regional circulation patterns, blocking frequency, and storm-track behavior) support the use of process-based evaluation approaches as a complementary tool for model selection in downscaling workflows.

6

Projected Global Changes in Atmospheric Circulation

In this Chapter, an analysis of JC-WT trends and the emergence of climate change signals in the future projections from GCMs is conducted. The main results are included in Fernández-Granja et al. (2025).

6.1 Experiment setup

In this experiment, the JC-WT methodology is applied to classify instantaneous 6-hourly SLP patterns from a multi-model ensemble of 41 Global Climate Models (GCMs) from both CMIP5 and CMIP6 (Table 6.1). The GCMs were previously interpolated into a common regular grid of 2.5° (Sec. 2.1.2). Their future simulations for the most extreme forcing experiments are considered, i.e. Representative Concentration Pathway (RCP) 8.5 for CMIP5 (Moss et al., 2010) and Shared Socioeconomic Pathway (SSP) 5-8.5 for CMIP6 (Riahi et al., 2017), using the projected SLP fields for the entire simulation period (2006-2100 for CMIP5 and 2015-2100 for CMIP6). Here, the same JC-WTs aggregation approach as in Trigo and DaCamara (2000) and Herrera-Lormendez et al. (2023) is applied, reducing the 27 original types to 11 (Sec. 2.2). This strategy eases (1) a simpler interpretation and comparability of the results; (2) a clearer depiction of emerging trends and patterns; and (3) a larger sample size for each weather type, thereby improving the consistency and robustness of the results across regions and models. The JC-WT classification is obtained for all the grid-points in a band from 30° to 70° north and south (Jones et al., 2013), resulting in a 6-hourly database of the JC-WT classification for the ensemble of GCMs (Sec. 7.3.2).

The corresponding JC-WT classification for the historical simulations are obtained from the existing JC-WT historical catalogs from Brands (2022a) and Brands et al. (2023c) for the periods 1979-2005 for CMIP5 and 1979-2014 for CMIP6. This yields a complete and methodologically consistent database of continuous 6-hourly series spanning the period 1979-2100 for the 41 GCM ensemble. Furthermore, GSAT is analyzed for each GCM from the pre-industrial baseline period

(1850–1900) as well as until the end of the 21st century (1979-2100) for the global warming levels calculation (GWL, Seneviratne et al., 2021; Iturbide et al., 2022, see Sec. 2.4.1). As for SLP, data for the strong emission scenarios (RCP8.5 for CMIP5 and SSP5-8.5 for CMIP6) were considered for GSAT, allowing to find GWLs well beyond the observed range.

Following Diez-Sierra et al. (2023), here GWL plots (Sec. 2.4.1) are used to examine how changes in one variable (with respect to a baseline) relate to a given GWL for a specific time period (e.g., 10 years) in the 21st century. Typically, GWLs are calculated using the pre-industrial baseline period of 1850–1900. However, since the SLP of the historical GCM simulations does not always cover the entire baseline period, a more recent climate baseline is sometimes used to calculate the changes of the target variable (JC-WT frequencies in this Thesis). Thus, 1979–2005 is used as the reference period to assess changes in JC-WT frequencies, while the pre-industrial baseline (1850–1900) is used to determine the increase in GSAT.

As an example, Fig. 6.1 represents a GWL scaling plot for the Anticyclonic type (A) based on CMIP5 and CMIP6 data at a specific location near the British Isles ($50°N, 15°W$). The X-axis shows global warming levels, indicated as the change from the specific decade of the GSAT in the 21st century relative to the pre-industrial baseline period of 1850–1900, ranging from +0° to +7°C. The Y-axis displays changes in the A-type frequency for each decade compared to the 1979–2005 period. These results are derived from a total of 41 CMIP5 and CMIP6 models (dots colored by decade, adding up to 410 points).

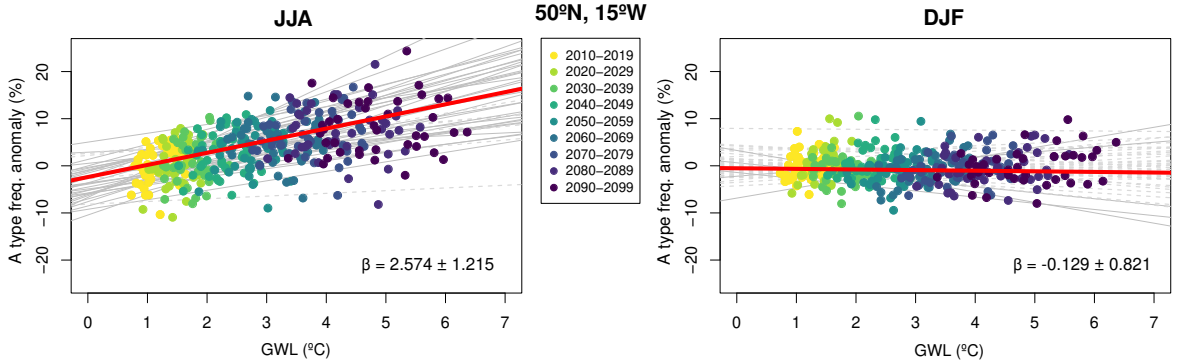

Figure 6.1: *Seasonal trends of the Anticyclonic type (A) from the 41 GCMs in boreal summer (JJA, left panel) and winter (DJF, right panel) at a grid-box location near to British Isles ($50°N, 15°W$). Each point represents the projected future change in the A-type frequency for each GCM and decade (the latter depicted with different colors) as a function of global warming. Individual model slopes (β parameter) are represented in grey (dashed lines represent slopes that are not statistically significant at the 90% confidence level). The 41 GCM ensemble mean slope is indicated at the bottom right (mean ± standard deviation) and displayed in red in the graph. See Sec. 6.1 for more details.*

Following this GWL scaling approach, a potentially significant linear response between a certain JC-WT frequency and the GWL is explored. For this purpose, a simple linear regression

GCM (res. gb)	Identifier	Modeling Center
CMIP5		
ACCESS1-0 (192 x 144)	https://hdl.handle.net/21.14106/b7ea1cf25565c7ac36b826ad5c43eb588b30cbb3	Commonwealth Scientific & Industrial Research Organisation (CSIRO); Bureau of Meteorology (BoM)
ACCESS1-3 (192 x 144)	https://hdl.handle.net/21.14106/18192275afea195193c9c8b4245d06bc708b7a38	Commonwealth Scientific & Industrial Research Organisation (CSIRO); Bureau of Meteorology (BoM)
bcc-csm1-1 (128 x 64)	https://hdl.handle.net/21.14106/2823d590c8bdf3761b6ff768f2e52902526921d3	Beijing Climate Center (BCC)
CanESM2 (128 x 64)	https://hdl.handle.net/21.14106/690bf891d54d83646e500832582c2fc81d2152d6	Canadian Centre for Climate Modelling and Analysis (CCCma)
CCSM4 (288 x 192)	https://hdl.handle.net/21.14106/caa97cfc28635a781d6f755a062a99346a99f39b	National Center for Atmospheric Research (NCAR)
CMCC-CM (480 x 240)	https://hdl.handle.net/21.14106/a82b1965d08222fbdc1f56625e0421dab1f57a62	Centro Euro-Mediterraneo sui Cambiamenti Climatici (CMCC)
CNRM-CM5 (256 x 128)	https://hdl.handle.net/21.14106/070ace82a225a0711f1b34229324b1e009c18e2e	Centre National de Recherches Météorologiques (Meteo-France/CNRM); Centre Européen de Recherche et de Formation Avancée en Calcul Scientifique (CERFACS)
CSIRO-Mk3-6-0 (192 x 96)	https://hdl.handle.net/21.14106/590d1c7fa6b38c31e087d5a245671c89b02888d2	Commonwealth Scientific & Industrial Research Organisation (CSIRO); Queensland Climate Change Centre of Excellence (QCCCE)
EC-EARTH (320 x 160)	https://hdl.handle.net/21.14106/4008a720db188e0c395097b1e1dc007f20e82872	EC-EARTH Consortium
GFDL-CM3 (144 x 90)	https://hdl.handle.net/21.14106/a4c2dbb73867d154aafcb9f07b9b328de301060c	Geophysical Fluid Dynamics Laboratory/NOAA (GFDL)
HadGEM2-CC (192 x 144)	https://hdl.handle.net/21.14106/2b2d36ad24aad406396b406439ee2f4911f99903	Met Office Hadley Centre (MOHC)
HadGEM2-ES (192 x 144)	https://hdl.handle.net/21.14106/4f619df8f27c18626c7b81c0e234a8bd152b28b2	Met Office Hadley Centre (MOHC)
inmcm4 (180 x 120)	https://hdl.handle.net/21.14106/0b59f7a1c3beb6d39af494d11e06eb6abfe313ee	Institute of Numerical Mathematics (INM)
IPSL-CM5A-LR (96 x 96)	https://hdl.handle.net/21.14106/fbabf3ddc00dbe7a90153c40afbb72633ce762c9	Institut Pierre-Simon Laplace (IPSL)
IPSL-CM5A-MR (96 x 96)	https://hdl.handle.net/21.14106/3d7f84c87248914f02e646a109dc79702978d366	Institut Pierre-Simon Laplace (IPSL)
MIROC5 (256 x 128)	https://hdl.handle.net/21.14106/e1bc91c12e24571ef9e03cc0109345868c06d4e3	Atmosphere and Ocean Research Institute, the University of Tokyo (AORI); National Institute for Environmental Studies (NIES); Japan Agency for Marine-Earth Science and Technology (JAMSTEC)
MIROC-ESM (128 x 64)	https://hdl.handle.net/21.14106/53a5e7159b12b806c4aa008d0489f218f3134ad7	Atmosphere and Ocean Research Institute, the University of Tokyo (AORI); National Institute for Environmental Studies (NIES); Japan Agency for Marine-Earth Science and Technology (JAMSTEC)
MPI-ESM-LR (192 x 96)	https://hdl.handle.net/21.14106/629557221f1d1394ecaa7661d3577d9d8dca2626	Max Planck Institute for Meteorology (MPI-M)
MPI-ESM-MR (192 x 96)	https://hdl.handle.net/21.14106/598a93901a5e7a563d38ff019e53f56909853935	Max Planck Institute for Meteorology (MPI-M)
NorESM1-M (144 x 96)	https://hdl.handle.net/21.14106/c8e0b84a1444a87a40cd36a29ed41e186a0f6bc1	NORCE Norwegian Research Centre (NORCE); Norwegian Meteorological Institute (MET Norway)
CMIP6		
ACCESS-CM2 (192 x 144)	https://doi.org/10.22033/ESGF/CMIP6.2281	CSIRO-ARCCSS
ACCESS-ESM1-5 (192 x 144)	https://doi.org/10.22033/ESGF/CMIP6.2288	Commonwealth Scientific & Industrial Research Organisation (CSIRO)
BCC-CSM2-MR (320 x 160)	https://doi.org/10.22033/ESGF/CMIP6.1725	BCC
CMCC-CM2-SR5 (288 x 192)	https://doi.org/10.22033/ESGF/CMIP6.1362	CMCC
CNRM-CM6-1 (256 x 128)	https://doi.org/10.22033/ESGF/CMIP6.1375	Centre National de Recherches Météorologiques (Meteo-France/CNRM); Centre Européen de Recherche et de Formation Avancée en Calcul Scientifique (CERFACS)
CNRM-CM6-1-HR (720 x 360)	https://doi.org/10.22033/ESGF/CMIP6.1385	Centre National de Recherches Météorologiques (Meteo-France/CNRM); Centre Européen de Recherche et de Formation Avancée en Calcul Scientifique (CERFACS)
CNRM-ESM2-1 (720 x 360)	https://doi.org/10.22033/ESGF/CMIP6.4226	Centre National de Recherches Météorologiques (Meteo-France/CNRM); Centre Européen de Recherche et de Formation Avancée en Calcul Scientifique (CERFACS)
EC-EARTH3 (512 x 256)	https://doi.org/10.22033/ESGF/CMIP6.181	EC-EARTH Consortium
FGOALS-g3 (180 x 80)	https://doi.org/10.22033/ESGF/CMIP6.1783	CAS
HadGEM3-GC31-MM (432 x 324)	https://doi.org/10.22033/ESGF/CMIP6.10846	Met Office Hadley Centre (MOHC)
IPSL-CM6A-LR (144 x 144)	https://doi.org/10.22033/ESGF/CMIP6.1534	Institut Pierre-Simon Laplace
KIOST-ESM (192 x 96)	https://doi.org/10.22033/ESGF/CMIP6.1922	KIOST
MIROC-ES2L (128 x 64)	https://doi.org/10.22033/ESGF/CMIP6.902	Japan Agency for Marine-Earth Science and Technology (JAMSTEC); National Institute for Environmental Studies (NIES); Institute of Industrial Science, the University of Tokyo (IIS)
MIROC6 (256 x 128)	https://doi.org/10.22033/ESGF/CMIP6.881	Japan Agency for Marine-Earth Science and Technology (JAMSTEC); National Institute for Environmental Studies (NIES); Institute of Industrial Science, the University of Tokyo (IIS)
MPI-ESM1-2-HR (384 x 192)	https://doi.org/10.22033/ESGF/CMIP6.741	MPI-M DWD DKRZ
MPI-ESM1-2-LR (192 x 96)	https://doi.org/10.22033/ESGF/CMIP6.742	MPI-M AWI DKRZ DWD
MRI-ESM2-0 (320 x 160)	https://doi.org/10.22033/ESGF/CMIP6.621	MRI
NESM3 (192 x 144)	https://doi.org/10.22033/ESGF/CMIP6.2021	NUIST
NorESM2-LM (144 x 96)	https://doi.org/10.22033/ESGF/CMIP6.502	Norwegian Climate Center
NorESM2-MM (288 x 192)	https://doi.org/10.22033/ESGF/CMIP6.506	Norwegian Climate Center
TaiESM1 (288 x 192)	https://doi.org/10.22033/ESGF/CMIP6.9684	AS-RCEC

Table 6.1: *Details on the General Circulation Models (GCMs) used in this Chapter, along with their persistent identifiers (PIDs). The table includes their resolution expressed as number of longitudinal × latitudinal grid-boxes (gb) worldwide, and the respective modeling centers. The provided URLs correspond to the primary PIDs for model outputs prepared for the CMIP5 and CMIP6 projects. Specific sub-PIDs for historical and RCP8.5/SSP5-8.5 experiments are accessible through these primary PIDs, along with further metadata.*

is fitted between decadal changes of JC-WT frequency and GWLs, for each GCM independently. The results presented are based on two key parameters, namely 1) the slope (coefficient β), representing the linear trend of the WT frequency projected by the GCM as the global warming increases; and 2) the *p-value*, that indicates the probability that the relationship between the independent (GWLs) and dependent (JC-WT frequency changes) variables occurred by chance, using a significance t-test against the null hypothesis, at 90% confidence level, that the linear slope of the corresponding regression model is zero. Multi-model mean slope is considered to assess the overall ensemble trend. Additionally, in order to address multi-model ensemble uncertainty, a robustness test is applied following the IPCC simple approach (IPCC, 2021). This test ensures that at least the 80% of the GCMs show a statistically significant slope. This analysis is performed for each grid-box covering the entire area of study.

The spatial location and the time when robust JC-WTs frequencies signals emerge (Sec. 2.4.2) at grid-box level are estimated here applying the advanced method for ToE detection from IPCC-WGI AR6 (Gutiérrez et al., 2021, Cross-Chapter Box Atlas.1), in decade-long intervals. This approach was used in previous studies to analyze climate change as a function of global warming by estimating the threshold above which the signal of change emerges consistently from natural variability (Seneviratne et al., 2016; Kirchmeier-Young et al., 2019). This method categorizes the multi-model ensemble signal into three types: (1) robust signal, (2) conflicting signal, and (3) no change or not robust signal. Categories 1 and 2 represent cases where more than two-thirds of the models show a change greater than their model-specific natural variability threshold (γ). Then, if more than 80% of the models agree on the direction of change, the signal is classified as robust (category 1); if not, it is classified as conflicting (category 2). In this Thesis, category 1 is further subdivided into 1a (positive change) or 1b (negative change) which allows to analyze not only the emerging signals in different circulation patterns but also their respective signs. Category 3 indicates either no significant change or a lack of robust change, with less than two-thirds of the models showing a robust signal. The threshold used to detect robustness of a GCM signal (understood as decadal signals that stand out from historical natural variability) is $\gamma = 1.645\sqrt{2/10} * \sigma_{hist}$, corresponding to a 90% confidence interval for decadal variability, where σ_{hist} represents the model-specific interannual standard deviation from the detrended baseline period 1979–2005. The *decade of emergence* is estimated for each grid-box as the first decade when the signals in the WTs frequencies are categorized as robust (category 1, i.e. at least two-thirds of the GCMs show a change greater than their respective γ and more than 80% of the GCMs agree on the direction of change).

6.2 Major trends in circulation patterns

In this section, global seasonal trends in the frequencies of JC-WTs are analyzed. Firstly, a climatological historical picture of multi-model ensemble JC-WTs frequencies is provided (Fig. 6.2 and Fig. 6.3) serving as a reference for the depicted trends (Fig. 6.4).

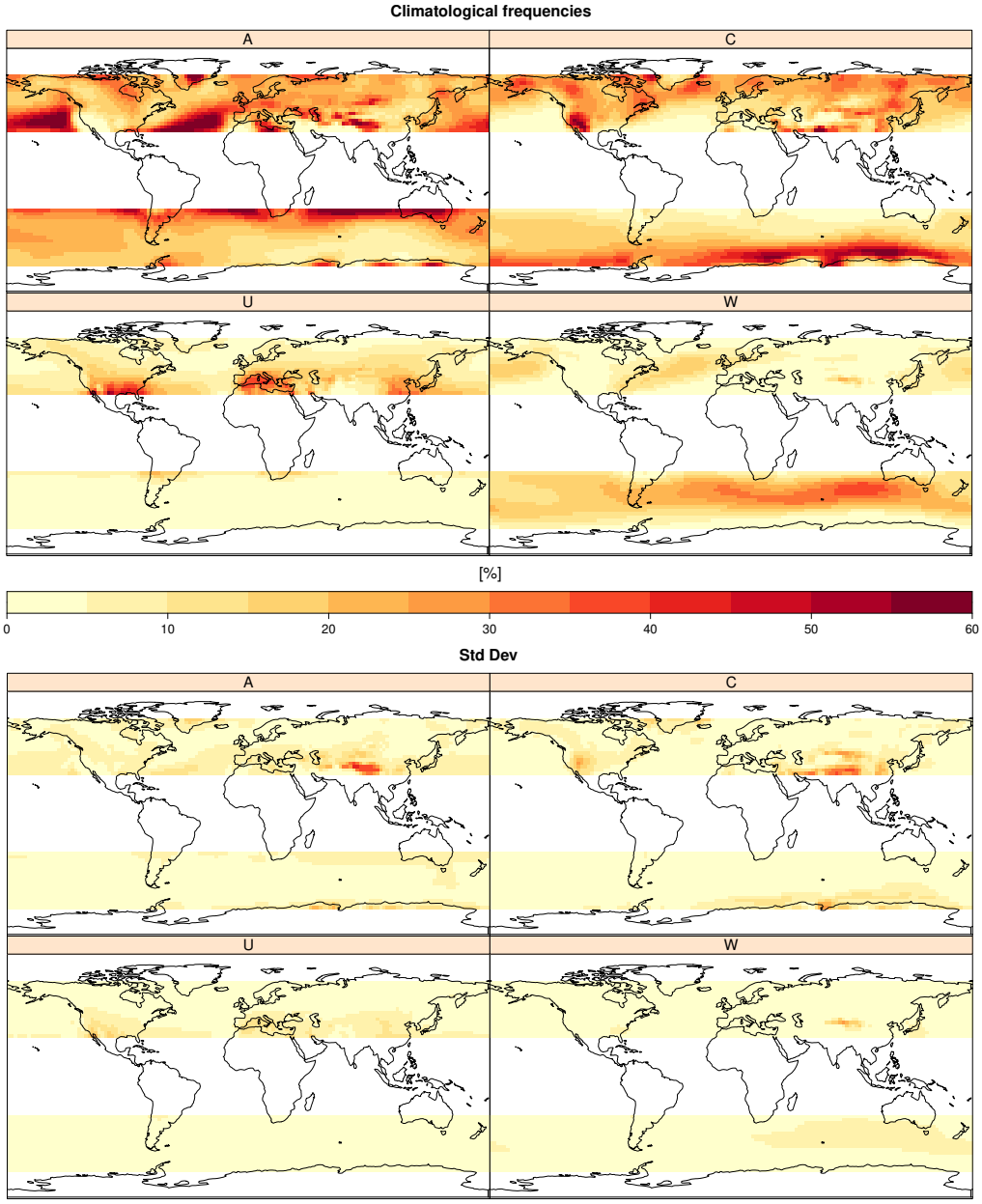

Figure 6.2: *Global JC-WTs frequency of Anticyclonic (A), Cyclonic (C), Unclassified (U), and Westerly (W) types for the multi-model ensemble mean and their standard deviation for the historical period 1979-2005 in JJA.*

In order to illustrate the GWL approach, trends are examined from a single grid-box, represented by a GWL plot (Fig. 6.1). For this particular point near the British Isles ($50°N, 15°W$), the resulting multi-model mean linear scaling is $\beta = 2.574$ in boreal summer, with a standard deviation of 1.215. This means that every 1°C increase in global warming, the frequency of the A type increases by 2.574% relative to the historical baseline. As expected, the GSAT signals corresponding to the first decade (yellow dots) show the lowest GWLs and the lowest changes in JC-WT frequency. It is also noticeable that the models exhibit greater agreement in the first decades, with the multi-model spread progressively increasing throughout the 21st century. These changes exhibit a strong seasonal dependency, as for the same location and weather type, the JC-WT frequency shows minimal variations with global warming in winter.

The application of this approach to all gridboxes in the domain of study allows to analyze the evolution of the different seasonal JC-WT frequencies along the 21st century worldwide (Fig. 6.4 for summer –JJA– and winter –DJF–, and Fig. 6.5 for autumn –SON– and spring –MAM–). For the sake of brevity, results for the Anticyclonic (A), Cyclonic (C), Unclassified (U), and Westerly (W) types are presented first (Fig. 6.4), as they have the most robust trends. Results for the remaining types (NW, N, NE, E, SW, S and SE) can be found in Figs. 6.6 for JJA, 6.7 for DJF, 6.8 for SON and 6.9 for MAM.

The projected JC-WT frequencies depicted in Fig. 6.4 unveil robust trends along the 21st century in JJA and DJF over sizeable extratropical global areas. During JJA, a significant increase in the frequency of A-type occurrences is detected, with certain trends reaching up to 3.0% per degree of global warming, within the subtropical high-pressure belt of the Southern Hemisphere. This region, where A-type is a dominant circulation type (Liljequist, 1970; Barry and Carleton, 2013), is highlighted by the main high-pressure centers along this belt (Figs. 6.2 and 6.3). Conversely, during DJF, significant negative trends are found for the A type in the same Southern Hemisphere high-pressure centers, ranging from -2.0% to -2.5% per degree of global warming.

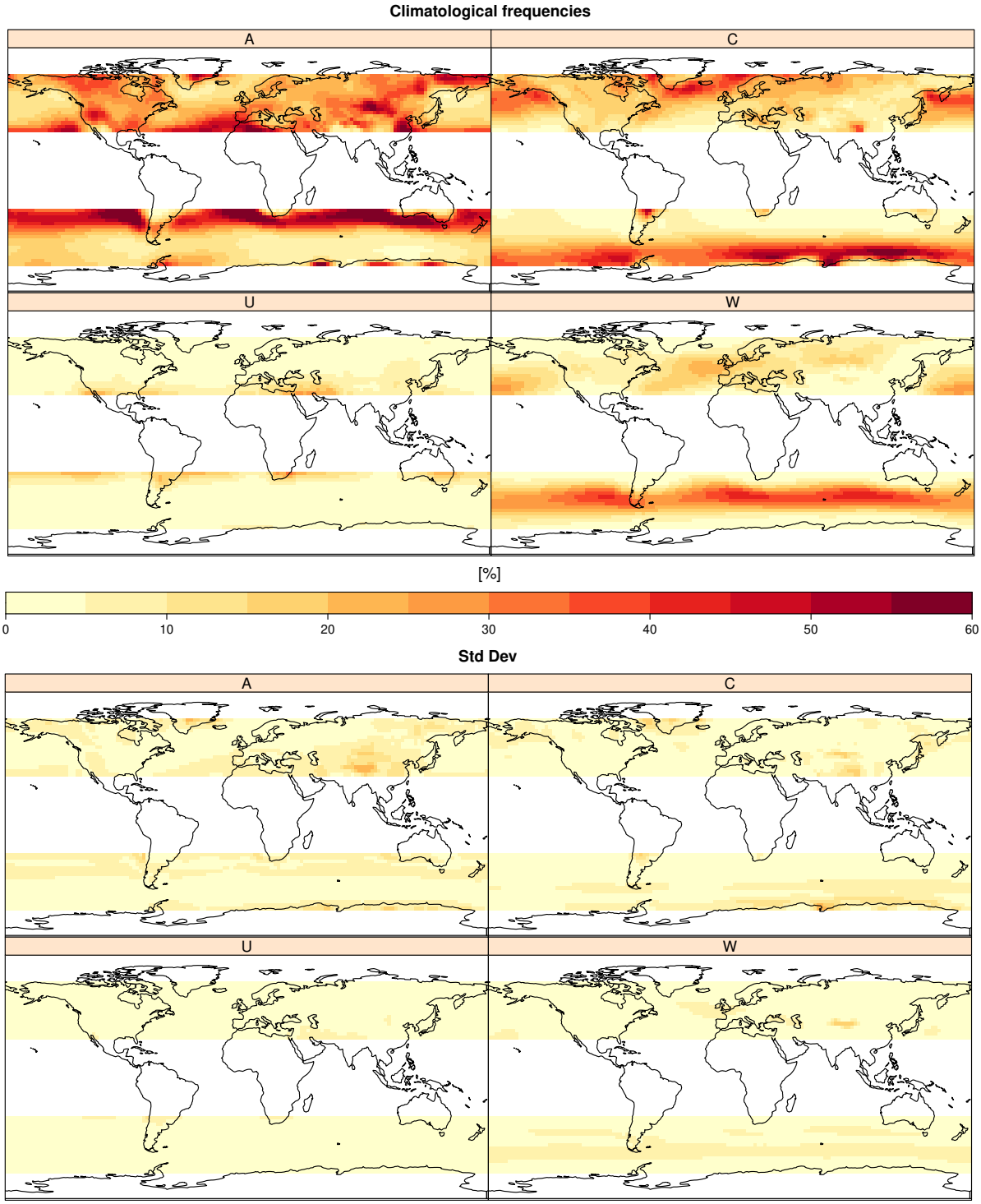

Figure 6.3: *As in Figure 6.2, but for DJF.*

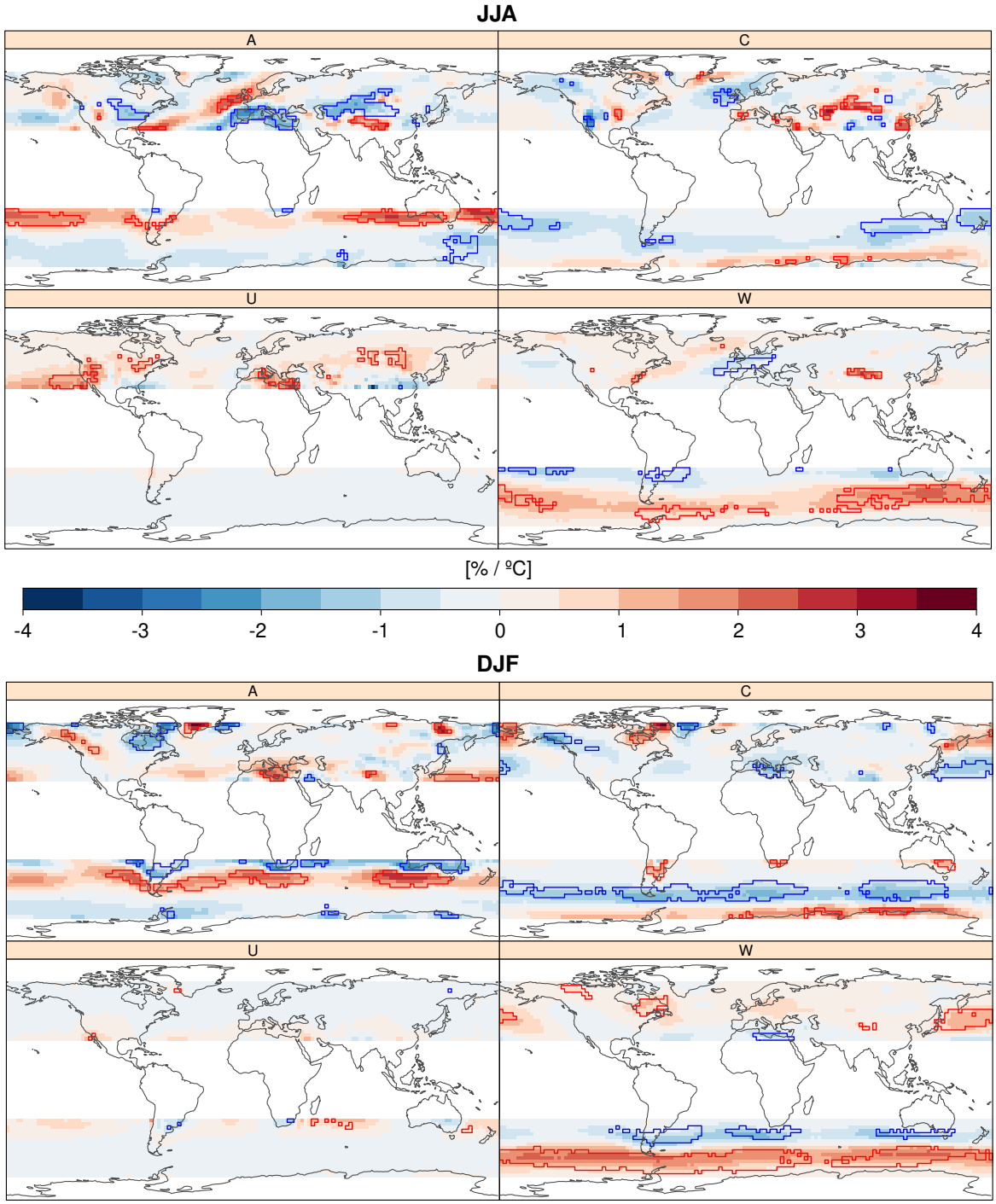

Figure 6.4: *Maps depicting the multi-model mean trend (slope, β) of the 41 GCM ensemble ($30° - 70°$ North and South) for the frequencies of Anticyclonic (A), Cyclonic (C), Unclassified (U), and Westerly (W) JC-WTs, for JJA (upper panels) and DJF (lower panels). Blue (negative trend) and red (positive) polygons depict grid-boxes where the ensemble provides robust results (i.e., at least 80% of models have a significant trend at a 90% confidence level, see Sec. 6.1).*

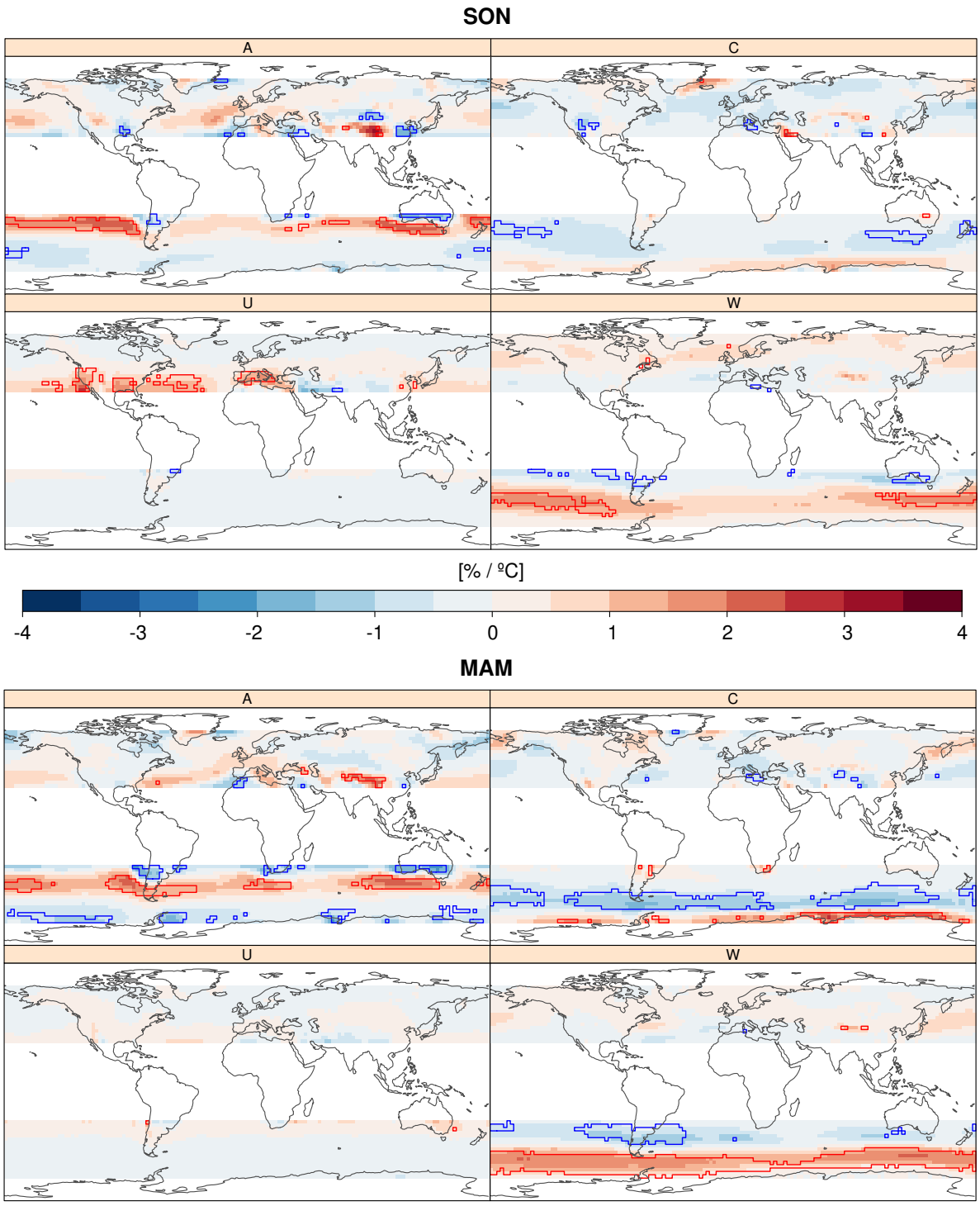

Figure 6.5: *As in Figure 6.1 but for autumn (SON) and spring (MAM).*

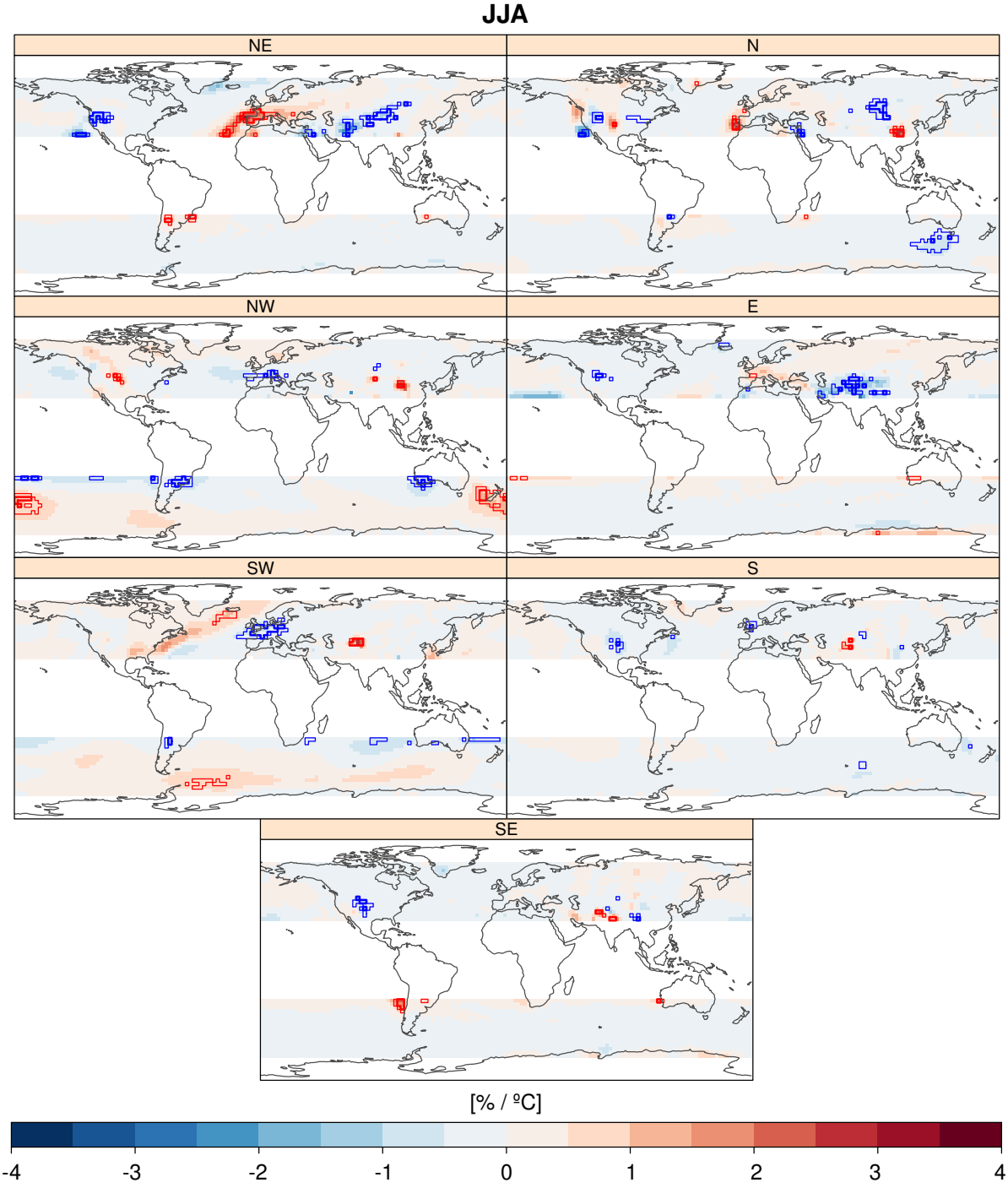

Figure 6.6: *As in Figure 6.4, but for JJA only and WTs: Northeasterly (NE), Northerly (N), Northwesterly (NW), Eeasterly (E), Southwesterly (SW), Southerly (S) and Southeasterly (SE).*

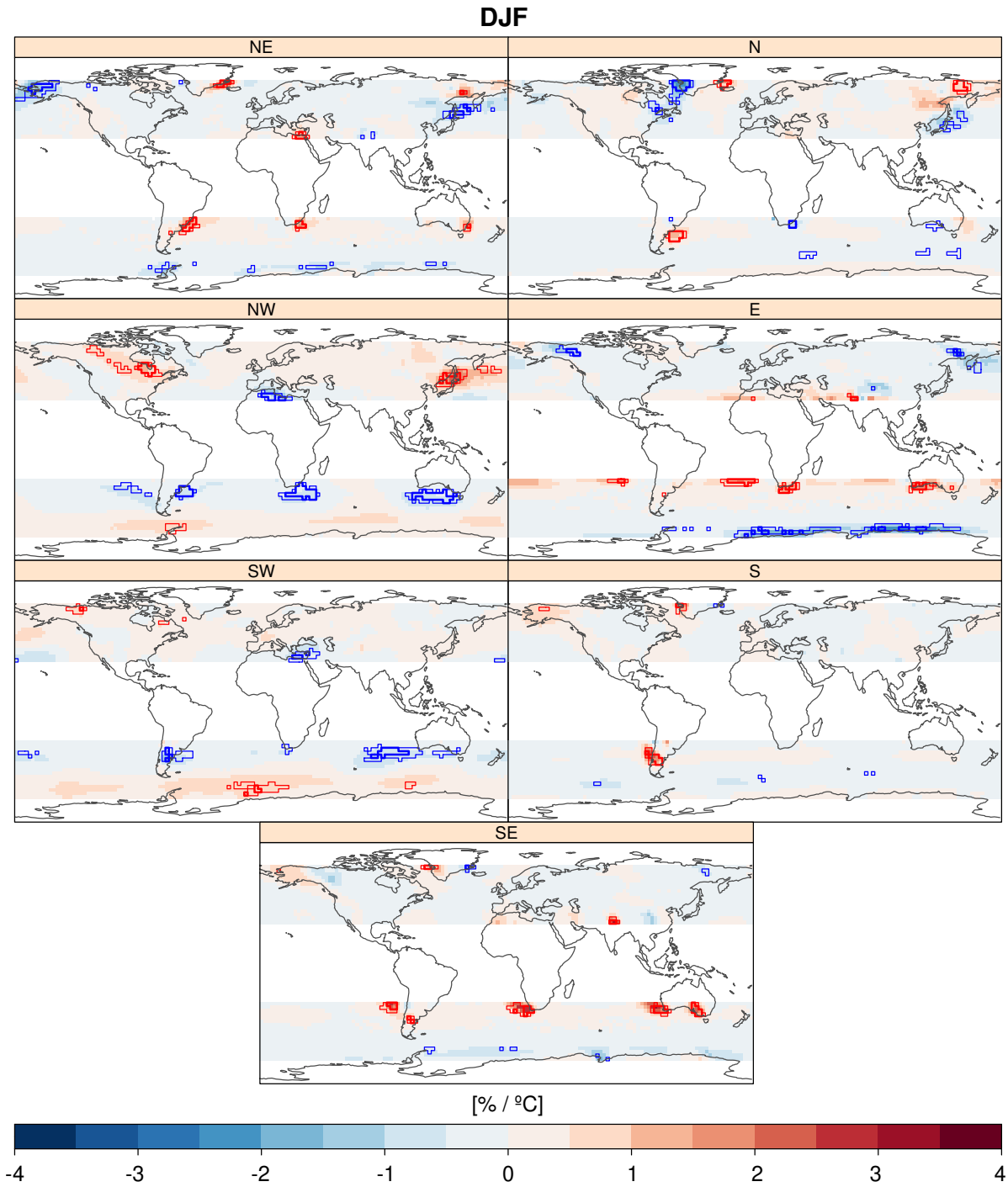

Figure 6.7: *As in Figure 6.6, but for DJF.*

Simultaneously, there is a robust increase in the C type, along with a notable rise in the frequency of the A-type at latitudes just south of these centers. Results indicate that, for both seasons, there is a robust increase of up to 3.0% per degree of global warming in the frequency of the W-type in the Subantarctic Belt, accompanied by a simultaneous robust decrease in the frequency of the W-type in the latitudes immediately above it. All this suggests a southward displacement of the whole zonal circulation that contracts towards Antarctica. The projected

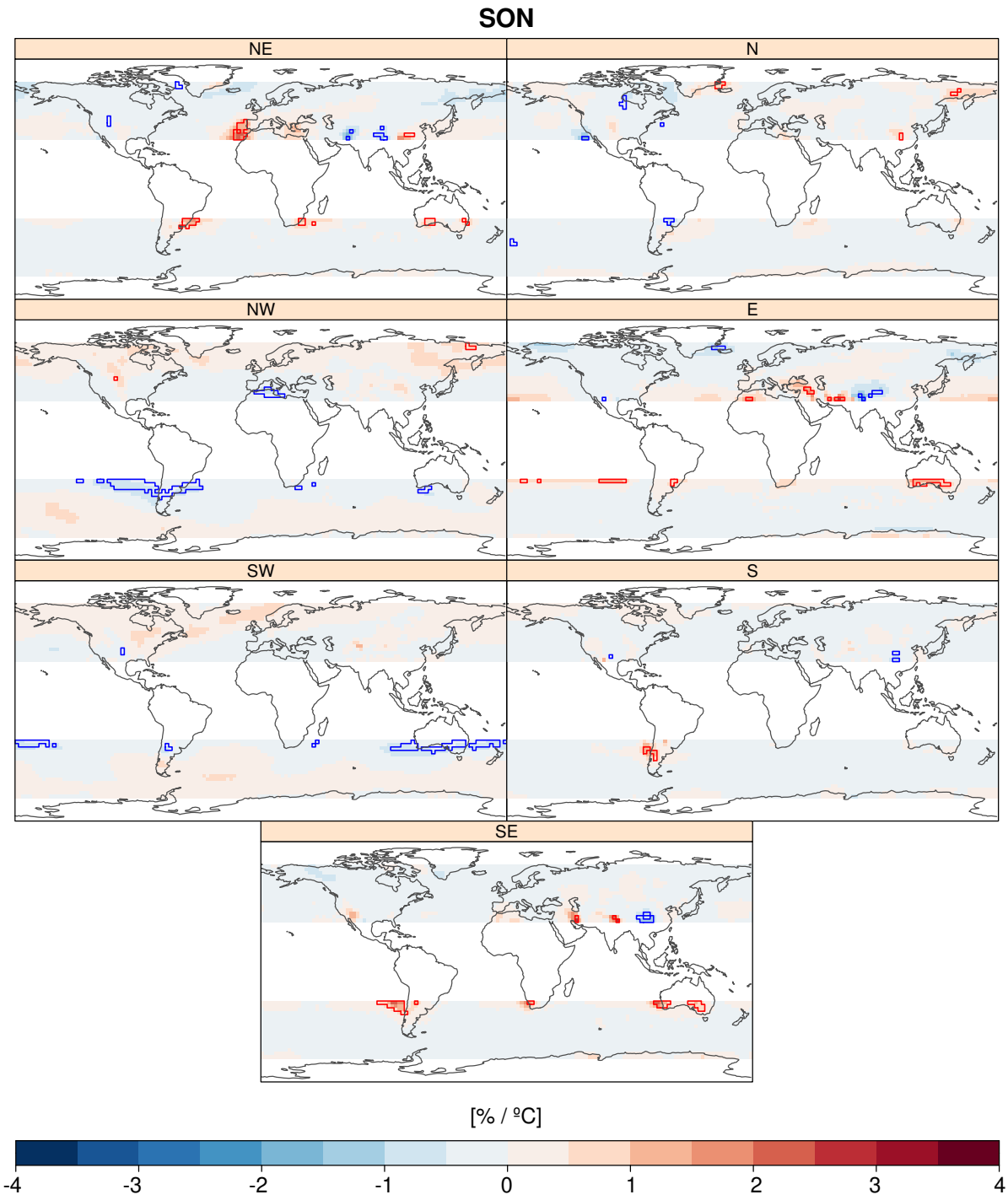

Figure 6.8: *As in Figure 6.6, but for SON.*

positive trends of W-type in lower Southern Hemisphere latitudes are consistent with observed trends towards the positive phase of the Southern Annular Mode (SAM, Marshall, 2003), with the maximum increment occurring in austral summer (DJF), as well as projected circulation responses of SAM under global warming scenarios (Kushner et al., 2001). The positive SAM phase is characterized by lower anomalous air pressure over Antarctica and higher anomalous

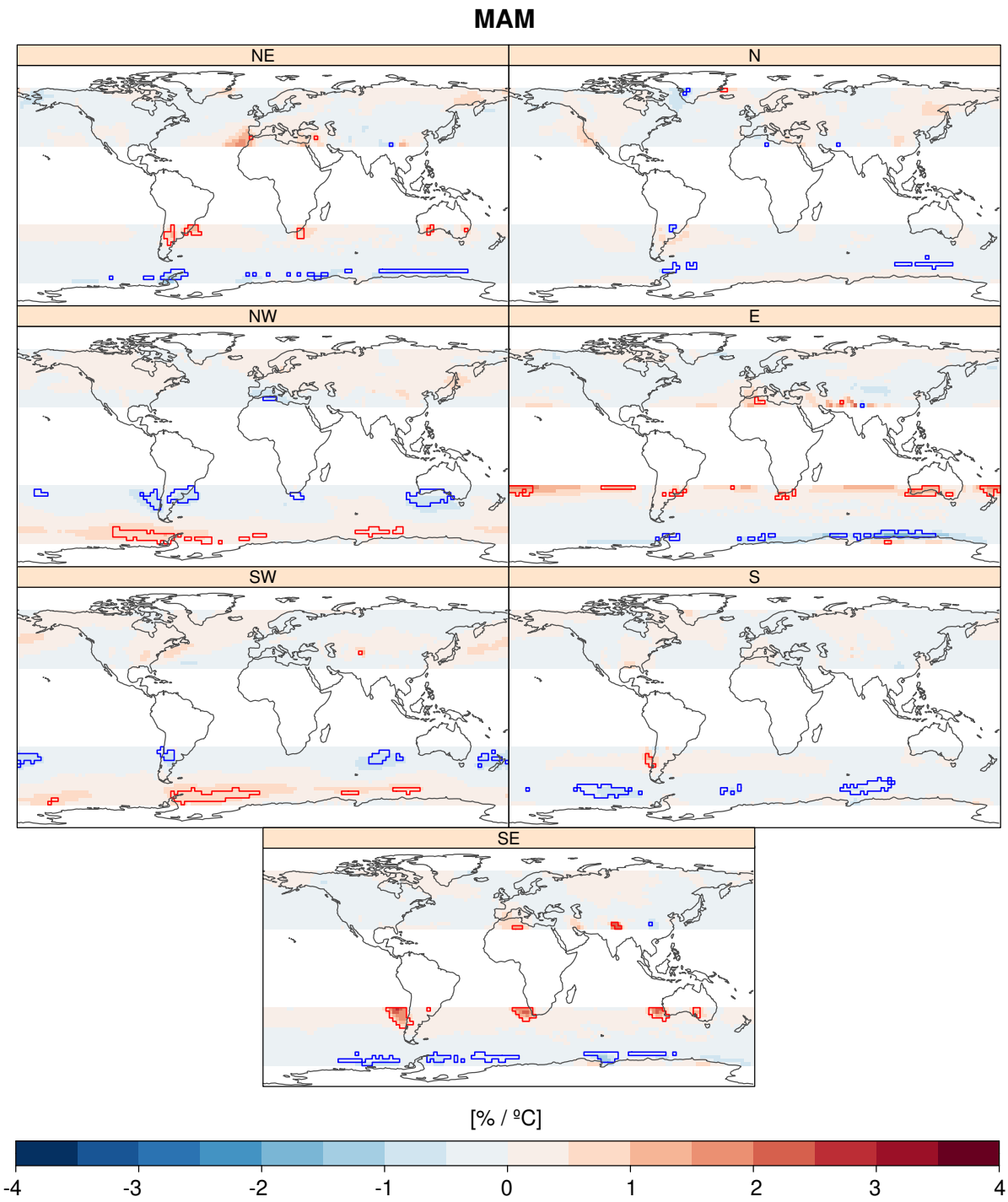

Figure 6.9: *As in Figure 6.6, but for MAM.*

air pressure over the mid-latitudes (Lee et al., 2019), with strong effects on the atmospheric and oceanic circulation system, including warming and drying over Patagonia, increased upwelling of warm Circumpolar Deep Water, and glacier recession in western Antarctica and the Antarctic Peninsula (Thompson and Solomon, 2002), among other impacts. On the other hand, mostly non-robust trends are projected for the U-type (containing the samples with lowest pressure

gradient) over most regions, except in a few regions from the Northern Hemisphere like the Mediterranean basin, Eastern Siberia and Eastern and Western America, restricted to JJA.

The detected changes for the A, W and U types point to a redistribution or displacement of A, W and U flows moving poleward. The high pressure centers with positive trends in the subtropical belt are receiving U-type flow from the intertropical band, where it is most prevalent (see Fig. 6.2 and Sec. 3.1), and constraining the A-type flow poleward. This could explain the positive trends of the A-type in the Southern Hemisphere, in regions where Westerly flows would typically dominate (Barry and Carleton, 2013; Fernández-Granja et al., 2023, Figs. 6.2 and 6.3). A similar situation might be occurring with the W-type, which becomes more frequent near the Antarctic Circle and less frequent at immediate higher latitudes, where the A-type is increasing. These results are coherent with a poleward expansion of the Hadley cell (Grise et al., 2019) and a poleward shift of the jet stream position (Woollings et al., 2023) in both hemispheres and seasons, and suggest a projected positive trend of the positive AMO phase consistent with current observations.

Additionally, Fig. 6.4 illustrates that, in general for JJA and DJF, trends of the A-type are opposite to those of the C-type. These two types might change in opposing ways throughout the century. An example of this behavior can be found in the northern Pacific Ocean, where dipoles of increasing-decreasing frequency for the A-type are identified, as well as dipoles of decreasing-increasing frequency for the C-type. This area is influenced by the Pacific/North American (PNA) teleconnection pattern (Barnston and Livezey, 1987, PNA), which describes the flow pattern over the Northeast Pacific sector. In Fig. 3.9 (Sec. 3.2.3), JC-WTs with strong correlations with the PNA are explored, depicting a pressure dipole of high and low systems shown by this A-C types dipole. In Fig. 6.4, the trends in both A and C types are consistent with the location of PNA pressure anomalies over western Canada and the Aleutians (van den Dool et al., 2000). During JJA, when the positive phase of the PNA is weaker (van den Dool et al., 2000; Chen and den Dool, 2003), the occurrence of the cyclone-anticyclone dipole decreases. In contrast, during DJF, when the PNA positive phase is stronger, the frequency of this dipole is projected to increase robustly throughout the 21st century. Additionally, the frequency of W-type might also increase robustly in the North Pacific in DJF, likely due to the flow produced by the convergence of an increasingly frequent A-C dipole.

In the Atlantic, the North Atlantic Oscillation (NAO) teleconnection pattern is represented by the JC-WT dominant frequencies with a characteristic surface pressure anomaly pattern of high/low (types A/C) pressure centers over the Azores/Iceland (see Fig. 3.8 in Sec. 3.2.3). Results for future trends unveil a robust increase in the frequency of the A-type (Fig. 6.4),

reflecting the high-pressure anomaly associated with the positive phase of the NAO, especially in boreal summer. This positive trend in the NAO region represents the strongest trend of the A-type during summer in the northern hemisphere, pointing to a robust increase of the frequency of positive summer NAO phase. Although the summer NAO is weaker and confined to northern latitudes compared to its winter counterpart, with a southern lobe located over the British Isles (Folland et al., 2009), it has a significant association with precipitation in the Mediterranean, among other regional climate impacts (Bladé et al., 2011). In the same vein, a significant summer reduction in the frequency of the A-type is found in the Mediterranean Basin and the Iberian Peninsula (Fig. 6.4). This change may be associated with the projected reduction in climatological SLP values in the Mediterranean, as previously identified in CMIP5 models (Giorgi and Lionello, 2008). Furthermore, it could be connected to the projected poleward expansion of the Hadley cell, as found in both CMIP5 and CMIP6 models (Grise et al., 2019), especially when considering the substantial increase in the frequency of the U-type in the Mediterranean during summer. Moreover, in boreal winter, A-type shows a robust positive trend in the central-eastern Mediterranean. This robust circulation change is likely related to a projected increase of SLP in DJF for that region (Giorgi and Lionello, 2008), connected to a relative cooling phenomenon of the Mediterranean Sea compared to its surrounding land areas and associated with a decrease in precipitation (Tuel and Eltahir, 2020).

From a regional perspective, our findings over Europe align with recent related studies. For example, Herrera-Lormendez et al. (2023) report a notable summer increase in the frequency of U, NE, and E types over Europe using an ensemble of eight CMIP6 models, alongside a reduction in west-dominated patterns. Moreover, a negative trend in cyclonic circulations during winter is found, which is consistent with the results presented in Figs. 6.4 and 6.7 (here based on a larger ensemble).

We highlight additional robust trends displayed in Fig. 6.5, related to projected JC-WT frequency changes throughout the 21st century in MAM and SON across the extratropical regions. Particularly noteworthy are the trends associated with type U in SON over the Mediterranean and the southern part of North America (at the boundary with the subtropical zone of the Northern Hemisphere). According to Fig. 6.2, type U is the most representative pattern in both the Mediterranean and southern North America during JJA, which suggests a shift in the prevailing synoptic regimes from the boreal summer to autumn. Similar situations can be observed for other JC-WTs in Fig. 6.5 during both MAM and SON, especially in the Southern Hemisphere, where types A, C, and W are projected to exhibit significant trends that are spatially comparable to those occurring in JJA, albeit generally weaker in intensity. Several

studies have highlighted that climate change may not only shift the frequency of specific synoptic patterns but also alter the timing and duration of seasons themselves, resulting in earlier springs, delayed autumns, and prolonged summer-like circulation conditions (**????**) Synoptic regimes are evolving throughout the year, especially in regions where seasonal boundaries are shifting.

6.3 Emergence of climate change signals

Here the Time of Emergence (ToE) of changes in the seasonal frequencies of JC-WTs is analyzed worldwide, indicating the time at which the robust trends detected in Sec. 6.2 stand out from the internal variability. JJA and DJF ToE is represented in (Fig. 6.10), and SON and MAM ToE is depicted in Fig. 6.11. The decade of emergence is identified as the first decade in which the WT frequency anomaly (with respect to a historical baseline) exceeds a model-specific threshold, based on the standard deviation of historical WT frequencies. The emergence is considered robust when it is fulfilled by at least two-thirds of the models and at least 80% of the models agree on the direction –either positive or negative– of the change in WT frequency (Sec. 6.1).

A progressive emergence of significant frequency changes is identified in the course of the 21st century (Fig. 6.10). Furthermore, the emergence is spatially consistent with the extent of the robust trends found before (Fig. 6.4). Note that here, the ToE estimation relies on the IPCC's *advanced* method for robustness and agreement, which includes additional filtering for uncertainty due to internal variability, making it more restrictive than the simple method for assessing trend significance.

Emergent signals are notably present in most weather types during the summer season (JJA in the Northern Hemisphere and DJF in the Southern Hemisphere). While climate change signals typically emerge in the far future in most grid boxes (2070–2100), some examples of earlier emergence also occur. For example, A-type exhibits early emergence during the initial decades of the 21st century in the Mediterranean (negative signal, i.e. less frequent A-type), the Pacific coast of North America (negative and positive) and Central Asia (negative) during JJA, as well as the Southern Hemisphere subtropical high-pressure belt (both positive and negative) and the Mediterranean (positive) during DJF. Similarly, early positive emergence is observed for U-type in the Mediterranean during JJA, and for C-type in DJF around the Polar Circle over Greenland (negative) and the NE Arctic region of Canada (positive).

Remarkably, C and W types show extensive emergence across the Southern Hemisphere during the late 21st century in austral summer (DJF). These regions already showed robust

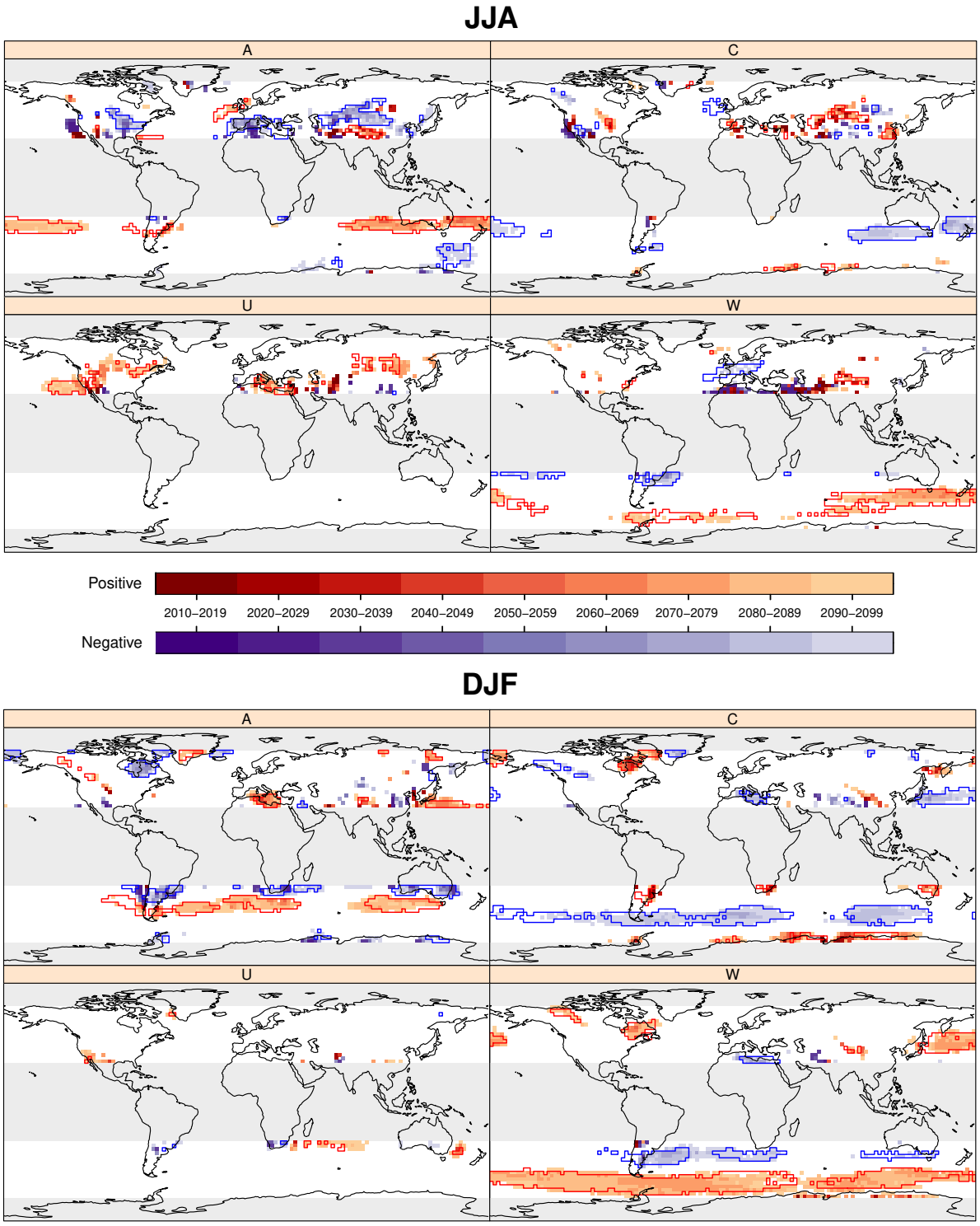

Figure 6.10: *Time of Emergence (ToE, Sec. 2.4.2), represented as decade intervals, of the multi-model ensemble over the area of study (30° − 70° North and South, grey gridboxes depict areas out of the domain of analysis) for the frequencies of Anticyclonic (A), Cyclonic (C), Unclassified (U), and Westerly (W) JC-WTs, in JJA (upper panels) and DJF (lower panels). Polygons from Fig. 6.4 enclose robust trend areas throughout the 21st century –blue (negative trends) and red (positive trends)–. White grid-boxes indicate locations where no significant signal emerges along the 21st century.*

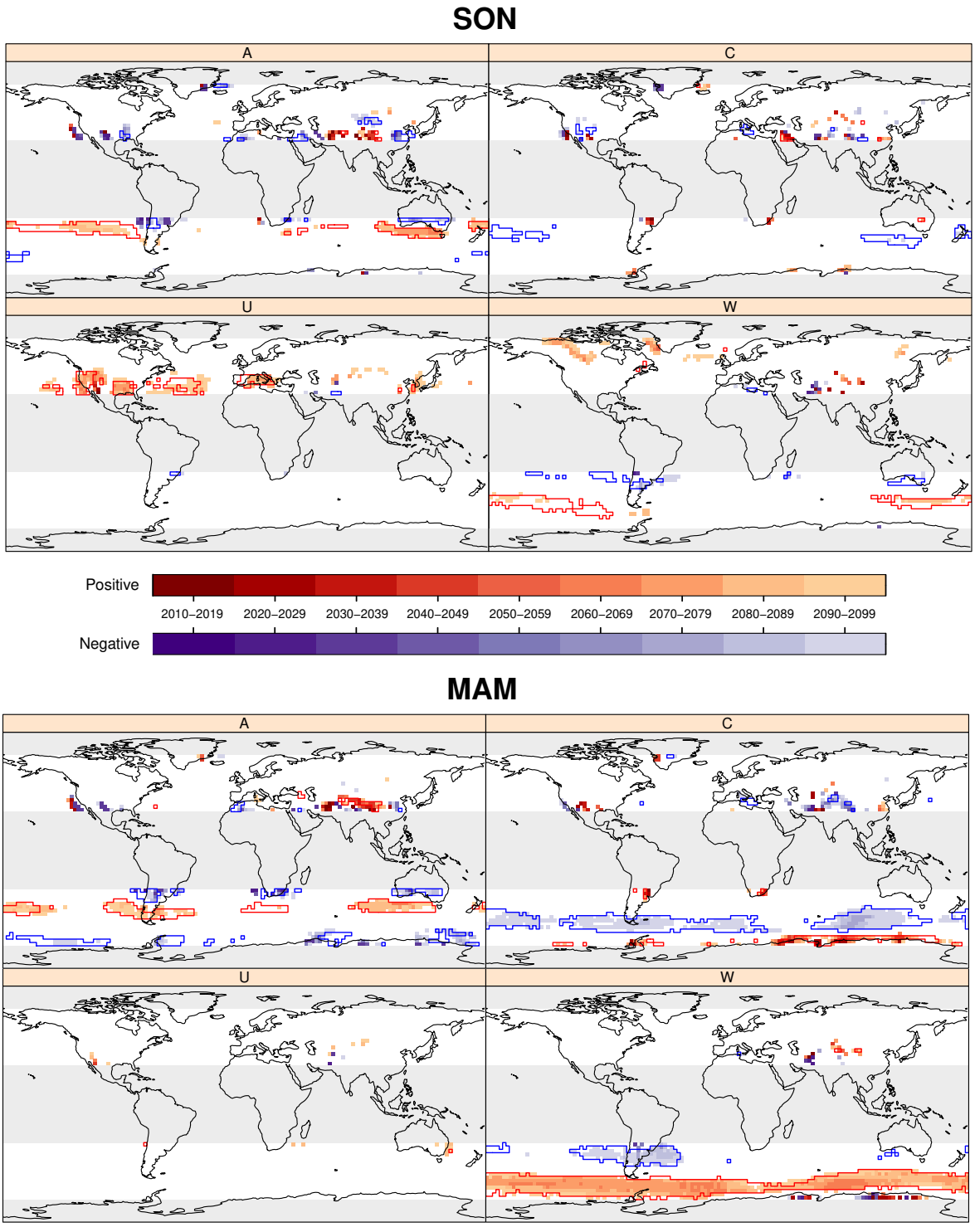

Figure 6.11: *As in Figure 3 from the Manuscript, but for SON and MAM.*

trends in Fig. 6.4, reinforcing the findings of an on-going increase of the SAM positive phase and its associated impacts (Sec. 6.2). Examining JC-WT trends and emergence of their projected signals together reveals that robust trends (Fig. 6.4) do not always correspond to the earliest emergence (see the overlaid polygons in Fig. 6.10 showing robust trends from Fig. 6.4). This holds true for W and C types in DJF in the Southern Hemisphere, where robust trends are detected but signals do not emerge until the last decades of the 21st century. It similarly occurs with A type in the NAO region (JJA) and just below the subtropical high-pressure belt (JJA and DJF), as well as in the North Pacific for A and C types during DJF. An exception to this can be found in the Mediterranean, where changes in A (DJF and JJA) and U (JJA) types emerge in the first decades.

As shown in Fig. 6.1, the variability in the changes of WT frequencies among models increases throughout the 21st century. The continued emergence of WT signals into the last decades of the 21st century suggests that such WT frequency changes, relative to the historical baseline, are projected to accelerate faster than the internal variability of the ensemble. This supports the consistency and robustness of these emergent signals, as they do not only persist, but they also intensify over time.

Part III

Concluding remarks

7

Conclusions, Contributions and Future Perspectives

7.1 Key findings

Here, the key findings of the Thesis are outlined, for each of the goals listed in Section 1.6 (in *italic*), for clarity.

1. *Assess the potential and limits of the JC-WT methodology as a process-based diagnostic tool to evaluate the atmospheric circulation of GCMs*

   - *Examine the global extratropical applicability of the JC-WT classification method (including the Southern Hemisphere)*

     This Thesis is the first research work addressing the global application of the JC-WTs. Its spatial limits of applicability are defined in Chapter 3 (Sec. 3.1), providing an extension of this popular classification method that can serve as a potential tool for process-based climate model evaluation. It is shown that the JC-WT approach can be reliably applied over most of the regions within 23.5° and 80° latitude in both hemispheres. Over most of this area of applicability, a large diversity of WTs is found, while the U-type (representing situations with weak pressure gradients) occurs with low frequency. The loss of applicability of the method is identified with the transition zone where the diversity of WTs decreases sharply at the same time that the U-type becomes the dominant type. This transition marks an empirical applicability threshold of 16 distinct WTs.

   - *Connect the JC-WTs to the main modes of climate variability (such as predominant teleconnection indices and atmospheric blockings), as a way to evaluate the physical consistency, meaningfulness and diagnostic capability of the classification scheme.*

     The JC-WTs method, based on near-surface circulation, is able to produce WTs that significantly correlate with the main modes of low-frequency variability, including

atmospheric blockings (Chapter 3, Sec. 3.2). This regional evaluation is physically consistent with the imprint these variability modes have on the geopotential in the mid-troposphere, operating on larger-scales.

The methodology reproduces well-known teleconnections and blockings, with physically interpretable circulation types in terms of spatial pattern and seasonal cycle. Moreover, to the author's knowledge, it also reveals some previously undocumented relationships, such as the association between cyclonic circulation types in the western Sahara desert and Anatolia with the SCAND index (active in DJF and JJA). In the same vein, for the North Atlantic (ATL) and continental (RUS) blocking events affecting European climate, the predominance of the purely anticyclonic type is not confined to the source region of detection of the blocking. It also reigns over a substantial fraction of the subtropical North Atlantic, depicting a zonal circumpolar bridge that allows to objectively delimit the area of influence of these events in terms of near-surface circulation.

In conclusion, these findings demonstrate the links between near-surface and large-scale atmospheric circulation by underlining the potential of the JC-WT classification approach to detect the imprint of the main modes of atmospheric low-frequency variability on the regional near-surface circulation. These results provide a more detailed and nuanced understanding of the underlying atmospheric mechanisms that give rise to the different JC-WT configurations. They further support the consistency and usefulness of the JC-WT classification, remaining as a valuable tool for process-based model evaluation purposes and climate impact research. These results may provide an opportunity to perform the same analyses in other regions of the world where there are known teleconnections or other blocking events, thereby extending the results presented here about their links with near-surface circulation.

2. *Evaluate the ability of the new generation of GCMs from CMIP5/6, developed for the IPCC Fifth and Sixth Assessment Reports (AR5 and AR6, respectively), on their ability to represent observed large-scale atmospheric circulation patterns. This process-based evaluation involves:*

   - *Analyze the observational uncertainty in the JC-WT classification.*

     The TPMS (Chapter 4), which provide a measure of WTs transition probability agreement, unveils a general consistency between reanalyses within the applicability range described in Sec. 3.1. On the one hand, there are regions where the JC-WT

approach is in principle applicable but its practical use is hampered by a large reanalysis uncertainty. These are the Mediterranean (MED) in JJA, and Madagascar (MDG*) and East Southern-Africa (ESAF*) in DJF. On the other hand, there are regions where JC-WT is less suitable irrespective of the reanalysis uncertainty. These are Arabian-Peninsula (ARP*) and SAHara (SAH*) in JJA, and West Southern-Africa (WSAF*) and Central Australia (CAU) in DJF. Likewise, there are regions with complex orography where the JC-WT classification should be taken with caution as the SLP is estimated through pressure reduction algorithms, differently for each dataset. This analyses confirm the expected large discrepancies among reanalyses there: Greenland (GIC), Antarctica (WAN, EAN), Northern Central-America (NCA*), West North-America (WNA), Central North-America (CNA), central Asia (WCA, ECA, EAS), Southern Asia (SAS*) and the Tibetan Plateau (TIB). Both the 16-type diversity threshold (found in Chapter 3, Sec. 3.1) and large TPMS areas exhibit a seasonal march towards the pole of the respective summer hemisphere. This excursion is particularly strong for the TPMS during JJA (boreal summer).

- *Quantify the ability of CMIP5/6 models to reproduce historical JC-WTs classifications in the extratropics, focusing on a diversity of WTs features and evaluation metrics.*

  Results from Chapter 5 show a general improvement of CMIP6 over CMIP5 in terms of several statistics related to the simulated frequencies of the JC-WTs and to their temporal sequences (persistence probability and transition probability from one type to another). Well-performing GCMs in CMIP5 (e.g. EC-EARTH and HadGEM2-ES) also exhibit a good performance in CMIP6. Large improvements are found for IPSL-CM5A-LR and GFDL-ESM4, whereas important biases remain or move along the year in other CMIP6 GCMs (e.g. NorESM2-LM). Such remaining biases relate to their inaccuracies in representing observed transition probabilities, that in general tend to occur for specific seasons.

  Overall, GCMs show a remarkable ability to represent transition probabilities between JC-WTs. Despite some significant differences for particular transitions, the GCM TPM *fingerprints* are generally able to faithfully represent the pattern of most likely transitions as represented by the reanalysis, even for the worse performing models. Furthermore, these results are consistent across reanalysis products.

  A general recommendation about the use of specific GCMs is difficult to make, since it depends on the applications of interest, which are usually focused on a given sea-

son or might be more sensitive to some weather types (e.g. those leading to extreme events in a particular area). In this sense, based on these results, a climate data user could identify specific seasons and JC-WTs which particular GCMs fail to reproduce plausibly. This application-dependent selection can be feasible for statistical downscaling. However, for dynamical downscaling a general performance (all JC-WTs, all seasons) should be sought.

3. *Estimate projected future changes in the atmospheric circulation patterns on the smaller synoptic scale (by means of the JC-WTs classification) globally, thus considering a closer link to local-scale climate variability relevant for impact studies.*

   - *Identify emerging changes of JC-WT from model ensemble internal variability.*

     By applying the JC-WT classification globally, Chapter 6 provides a comprehensive framework for understanding the impacts of climate change on global large-scale circulation. A more detailed understanding of the temporal and spatial dynamics of these changes is possible thanks to a methodology based on the scaling by means of Global Warming Levels (GWL). This way, linear relationships between regional responses and global warming are analyzed, along with the estimation of the emergence (ToE) of robust signals. These results have practical connections with climate impact researchers, particularly in areas where shifts in atmospheric circulation are likely to play a fundamental role.

     The analysis in Chapter 6 reveals significant trends in JC-WTs across key climatic regions, with statistically significant trends which might be connected to substantial changes of well-known circulation patterns (Chapter 3, Sec. 3.2) closely related to the JC-WTs across the extra-tropics. For instance, significant trends are identified in regions influenced by recurrent teleconnection patterns such as the NAO and PNA. The Cyclonic type also exhibits robust trends of both signs over Greenland and the Arctic region of Canada. Additionally, the Anticyclonic type shows significant negative changes in the Mediterranean in JJA and positive in DJF; and significant positive trends across an extensive area in the Southern Hemisphere encompassing the subtropical high-pressure belt. The Westerly type shows significant positive changes in the subantarctic regions, meanwhile the Unclassified type exhibits notable positive variations in the Mediterranean or near the intertropics. Our results may also support findings from state-of-the-art studies suggesting shifts in weather regimes and seasonal synoptic patterns.

The emergence of climate change signals is closely related to the robustness of these trends. While most signals emerge prominently by the 2070s, some regions show earlier emergence, such as the Mediterranean, where anticyclonic and unclassified types display emergent signals as early as in the present decades (2020's). This variability in the timing of emergence reflects the interplay between natural variability and the growing influence of anthropogenic forcing in the atmospheric circulation of models.

The intensification of emergent signals toward the late 21st century highlights the importance of these trends when understanding future climate scenarios. Such JC-WT changes are projected to grow faster than the historical internal variability in each GCM independently, reinforcing the robustness and relevance of these changes. This Chapter focuses on the critical role of large-scale circulation patterns in shaping regional climate responses, offering valuable insights for policymakers and researchers addressing the challenges of a changing climate.

- *Generate a catalog of global JC-WT from more than 50 GCMs for both their historical simulations and future CMIP5 and CMIP6 projections.*

  Derived from the different objectives of this Thesis, and in order to support future studies that may benefit from the JC-WT classifications, several open-access online data repositories were generated. These repositories contain JC-WT catalogs derived from multiple GCMs and reanalysis datasets. They are described in detail in Sections 7.3.2 and 7.4 and include JC-WT classifications at 6-hourly resolution for 41 models under future scenarios (2005–2100) and 5 reanalyses covering the period 1979–2005. These datasets collectively take up a total of 11.5 GB. In this way, it was possible to substantially reduce and summarize the 1500 GB of SLP data from reanalyses and GCMs (Sec. 2.1.2) into weather types, with the application of the JC-WT classification method.

7.2 Related publications and contributions

The main contributions of this Thesis (Part III) have resulted from a number of publications in international journals and conference proceedings that are relevant to the fields of atmospheric sciences and meteorology. More specifically, three papers were published in peer-reviewed journals, another one is currently in review process, and an additional publication can be found in the proceedings of the *12th Congreso de la Asociación Española de Climatología (AEC)*:

- Section 3.1 in Chapter 3 and the entire Chapter 4 are based on **Fernández-Granja, J. A.**, S. Brands, J. Bedia, A. Casanueva and J. Fernández: "Exploring the limits of the Jenkinson–Collison weather types classification scheme: a global assessment based on various reanalyses". *Climate Dynamics*, 2023, doi:10.1007/s00382-022-06658-7 (1^{st} quartile in JCR[1]).

- Section 3.2 in Chapter 3 is based on **Fernández-Granja, J. A.**, J. Bedia, A. Casanueva, S. Brands and J. Fernández: "The signature of the main modes of climatic variability as revealed by the Jenkinson-Collison classification over Europe". *International Journal of Climatology*, 2024, doi:10.1002/joc.8569 (2^{nd} quartile in JCR).

- Section 4.3 in Chapter 4 is also based on **Fernández-Granja, J. A.**, S. Brands, J. Bedia, A. Casanueva and J. Fernández: "Regional assessment of the Jenkinson-Collison Weather Types classification and Observational Uncertainty based on different reanalyses over the Mediterranean region". *Retos del cambio climático: impactos, mitigación y adaptación.* [Madrid]: Asociación Española de Climatología; Agencia Estatal de Meteorología, pp. 55-66, 2022, ISBN: 978-84-125772-1-1.

- The entire Chapter 5 is based on **Fernández-Granja, J. A.**, A. Casanueva, J. Bedia and J. Fernández: "Improved atmospheric circulation over europe by the new generation of cmip6 earth system models". *Climate Dynamics*, 2021, doi:10.1007/s00382-021-05652-9 (1^{st} quartile in JCR).

- The entire Chapter 6 is based on **Fernández-Granja, J. A.**, J. Bedia, A. Casanueva, S. Brands and J. Fernández: "Emerging near-surface extratropical circulation changes due to climate change: A weather typing based global analysis". *Under review in npj — Climate and Atmospheric Science*, 2025, (1^{st} quartile in JCR).

Furthermore, the previous contributions were presented in these national and international conferences, as presenter and first author:

- **European Geosciences Union, EGU 2021** (Vienna, Austria. April 19–31, 2021): oral presentation. *Transition probabilities between synoptic weather types as a fingerprint for climate model evaluation.* J. A. Fernández-Granja, A. Casanueva, J. Bedia, J. Fernández.

- **European Geosciences Union, EGU 2022** (Vienna, Austria. May 23–27, 2022): oral presentation. *A worldwide assessment of the Jenkinson-Collison atmospheric circulation*

[1]Journal Citation Reports (JCR) is an online tool hosted by Web of Science that allows the measurement of the relative importance of a journal within its corresponding thematic based on the number of citations its papers receive annually.

classification and observational uncertainty based on different reanalysis. J. A. Fernández-Granja, S. Brands, J. Bedia, A. Casanueva, J. Fernández.

- **12º Congreso de la Asociación Española de Climatología (AEC)** (Santiago de Compostela. October 18–21, 2022): oral presentation. *Regional assessment of the Jenkinson-Collison weather types classification and observational uncertainty based on different reanalyses over the Mediterranean region.* J. A. Fernández-Granja, S. Brands, J. Bedia, A. Casanueva, J. Fernández.

- **Congreso CLIVAR 2023** (Madrid. January 24–26, 2023): oral presentation. *Assessment of the Jenkinson-Collison weather type classification in the Mediterranean: suitability of the method and reanalysis uncertainty.* J. A. Fernández-Granja, S. Brands, J. Bedia, A. Casanueva, J. Fernández.

- **European Geosciences Union, EGU 2023** (Vienna, Austria. April 24–28, 2023): poster presentation. *Characterization of Mediterranean large-scale atmospheric circulation based on Jenkinson-Collison weather type classification.* J. A. Fernández-Granja, A. Casanueva, J. Bedia, S. Brands, J. Fernández.

- **International Conference on Regional Climate ICRC-CORDEX 2023** (Trieste, Italy. September 25–29, 2023): oral presentation. *Performance, dependencies and spread of the CMIP global climate models for selected CORDEX domains as described by the low-level circulation.* J. A. Fernández-Granja, S. Brands, A. Casanueva, J. Bedia, J. Fernández.

- **World Climate Research Program (WCRP) Open Science Conference** (Kigali, Rwanda. October 23–27, 2023): poster presentation. *Global assessment of future changes in low-level circulation based on the Jenkinson–Collison weather type classification.* J. A. Fernández-Granja, A. Casanueva, J. Bedia, S. Brands, J. Fernández.

- **European Geosciences Union, EGU 2024** (Vienna, Austria. April 14–19, 2024): oral presentation. *Global changes in low-level circulation types under future anthropogenic forcing.* J. A. Fernández-Granja, A. Casanueva, J. Bedia, S. Brands, J. Fernández.

- **15th International Meeting on Statistical Climatology (IMSC 2024)** (Toulouse, France. June 24–28, 2024): oral presentation. *Global-scale evaluation of classifications methods for atmospheric circulation.* J. A. Fernández-Granja, J. Stryhal, R. Huth.

- **13º Congreso de la Asociación Española de Climatología (AEC)** (San Lorenzo del Escorial (Madrid). January 22–24, 2025): oral presentation. *Global analysis of emerging changes in atmospheric circulation patterns under climate change: Insights from the Jenkinson-Collison classification.* J. A. Fernández-Granja, A. Casanueva, J. Bedia, S. Brands, J. Fernández.

7.3 Open Software implementations and research reproducibility

7.3.1 Contributions to open source climate Software

Within this Thesis, most software contributions were carried out in the `climate4R` framework (Sec. 2.5), more precisely in the `transformeR` package. Several functions were implemented to introduce and extend the library's functionalities in clustering analysis. In particular, I included the implementation of `clusterGrid`[2], as a wrapper of several clustering methods such as K-means or self-organizing maps, among others; and `lambWT`[3], for the JC-WT classification method. My contribution also involved pre-processing and post-processing of the input/output for these functions and the adaptation of other functions to allow dealing with classes (WTs). Beyond the implementation of different weather-typing methods, the contributions of this Thesis to the `climate4R` framework have facilitated their integration in specific downscaling and bias adjustment methods, thus contributing to other research lines of the group, such as the development of weather-type conditioned calibration methods of satellite products in tropical regions (Mirones et al., 2023). Furthermore, other auxiliary functions were implemented to develop some of the methodologies involved in the Thesis (such as GWLs, ToE or evaluation metrics in Chapter 2).

7.3.2 Reproducibility and data availability

Reproducibility and transparency are essential components of high-quality scientific development. FAIR principles (Findability, Accessibility, Interoperability and Reuseability) are nowadays well established in the scientific community, offering users guidelines to encourage the re-use of their data and code (Wilkinson et al., 2016).

In accordance with these guidelines, a set of notebooks were developed in R programming language. They contain the software code implementations for the methodological aspects of this Thesis and allow users to reproduce the main outcomes. They are available in a dedicated GitHub repository: https://github.com/SantanderMetGroup/notebooks/tree/devel.

[2]https://github.com/SantanderMetGroup/transformeR/blob/devel/R/clusterGrid.R
[3]https://github.com/SantanderMetGroup/transformeR/blob/devel/R/lambWT.R

Each notebook is linked to the related published paper (see Table 7.1). An environment with R version 4.2.3 (2023-03-16) and the latest version of the *climate4R* framework (v2.5.4) are required to run these notebooks. Besides, *climate4R* can be conveniently installed using a dedicated `conda` image, which eases the installation of all needed dependencies (for installation instructions, see https://github.com/SantanderMetGroup/climate4R).

Section	Manuscript	Notebook
Chapter 3, Sec. 3.1 and Chapter 4, Sec. 4.3	Fernández-Granja et al. (2023): *Exploring the limits of the Jenkinson–Collison weather types classification scheme: a global assessment based on various reanalyses*	`2021_JC_Worldwide_-suitability.Rmd`
Chapter 5	Fernandez-Granja et al. (2021): *Improved atmospheric circulation over Europe by the new generation of CMIP6 Earth system models*	`2020_Lamb_ClimDyn.Rmd`
Chapter 6	Fernández-Granja et al. (2025): *Emerging near-surface extratropical circulation changes due to climate change: A weather typing based global analysis*	`2024_JCWT_trends.Rmd`

Table 7.1: *References to the reproducible Jupyter notebooks, along with citations to the corresponding papers and the related results sections of this Thesis.*

Additionally, datasets with the generated JC-WT catalogs (from GCMs and reanalysis datasets) are provided via Zenodo[4]. Two datasets were created within this Thesis: one with the JC-WT catalogs from the 5 reanalyses and the modified layer of IPCC regions (Sec. 4.1.1), and another one with the JC-WT catalogues derived from the 41 GCM future simulations used in Chapter 6:

- **Fernández-Granja, J. A.**, Bedia, J., Brands, S., Casanueva, A., and Fernández, J.: "Global Extra-tropical Circulation Database based on the Jenkinson-Collison Classification calculated with 6-hourly mean sea-level pressure fields from various reanalysis datasets", (1.1.0-alpha) [Data set]. Zenodo, 2022, https://doi.org/10.5281/zenodo.15847558

- **Fernández-Granja, J. A.**, Bedia, J., Brands, S., Casanueva, A., and Fernández, J.: "Global Jenkinson-Collison Weather Type (JC-WT) classifications until 2100 from

[4]Zenodo is a free, open-access repository developed by CERN under the European OpenAIRE programme, that enables to share, preserve, and cite a wide range of research outputs (publications, datasets, and software) by assigning persistent Digital Object Identifiers (DOIs) to each submission.

CMIP5/6 GCMs under anthropogenic forcing experiments (RCP 8.5 and SSP5-8.5)", (Beta) [Data set]. Zenodo, 2024, https://doi.org/10.5281/zenodo.14282539

7.3.3 Computing requirements and scalability considerations

In order to reproduce the results shown in this Thesis, a virtual machine with the following specifications was used:

- **Operating system:** Ubuntu 22.04.6 LTS (64-bit)
- **Memory:** 64 GB
- **Processor:** 2× Intel(R) Xeon(R) CPU E5-2670 @ 2.60GHz (16 cores, 32 threads)

Note that some of the notebooks shown in Sec. 7.3.2 can run on computers with less RAM. In order to provide a quantitative reference of the computational requirements associated with the JC-WT classification, a benchmarking test was performed using the `microbenchmark` function in R. The test consisted of executing ten times, in a single core, the classification of the 94-year-long SLP time series (2006-2100) corresponding to the EC-Earth model under the RCP8.5 scenario for a single grid-box. Results yielded a minimum execution time of 29.7 seconds, a mean of 30.5 seconds, and a maximum of 31.4 seconds. This setup assumes that SLP data are already interpolated to a common 2.5°×2.5° grid and spatially subsetted to the 16-point cross required by the method (see Fig. 2.1). Considering that the JC-WT classification is applied over 34 latitudinal rows (covering 30°–70°, North and South) and 144 longitudes columns (180°W to 180°E), the total number of grid-boxes per model is 4896. Under the described hardware conditions, the full global JC-WT computation for a single model and scenario requires approximately 41 hours. Importantly, all years are processed at once, as empirical testing confirmed a linear scaling with the size of the temporal dimension in the WTs calculations; thus, avoiding temporal subsetting may improve computational efficiency. When the WT calculations is scaled to large ensembles (e.g., CMIP5/6), the software implementation can benefit from parallel executions in different cores over grid-boxes or model members, for instance. Output storage requirements are moderate, with the JC-WT classifications for 94 years occupying approximately 450 MB per model and scenario.

7.4 External collaborations and partnerships

Within the framework of this Thesis, synergies have been developed leading to collaborations with researchers from the Instituto de Física de Cantabria (IFCA) and the University

of Cantabria, as well as with external and international institutions. This is evidenced by the co-authorship of papers and conference proceedings (Sec. 7.2) of external and international researchers (Dr. Swen Brands, Dr. Jan Stryhal and Prof. Radan Huth). This Thesis also gave me the chance to contribute to their work as well, and such collaborations are consolidated in four more publications, two Zenodo repositories, a 3-month research stay in the Czech Academy of Sciences and contributions to the selection of driving CMIP6 GCMs for the most recent EURO-CORDEX experiment:

- Brands, S., **Fernández-Granja, J. A.**, Bedia, J., Casanueva, A. and Fernández, J.: "A global climate model performance atlas for the southern hemisphere extratropics based on regional atmospheric circulation patterns". *Geophysical Research Letters*, 50, 2023, doi: 10.1029/2023GL103531 (1^{st} quartile in JCR).

- Mirones, Ó., Bedia, J., **Fernández-Granja, J. A.**, Herrera, S., Van Vloten, S. O., Pozo, A., Cagigal, L., and Méndez, F. J.: "Weather-type-conditioned calibration of Tropical Rainfall Measuring Mission precipitation over the South Pacific Convergence Zone". *International Journal of Climatology*, 43(2), 1193–1210, 2023, doi: 10.1002/joc.7905

- Brands, S., **Fernández-Granja, J. A.**, Fernández, J., Bedia, J., Casanueva A. and J. J. Taboada: "Performance of the CMIP6 global climate models over the Iberian Peninsula and relationships with the simulated climate system complexity". *Retos del cambio climático: impactos, mitigación y adaptación.* [Madrid]: Asociación Española de Climatología; Agencia Estatal de Meteorología, pp. 67-79, 2022, ISBN: 978-84-125772-1-1.

- Brands, S., **Fernández-Granja, J. A.**, Bedia, J., Casanueva, A. and Fernández, J.: "Southern Hemisphere Lamb Weather Types from historical GCM experiments and various reanalyses (2.0) [Data set]". Zenodo, 2023, doi: 10.5281/zenodo.7872012.

- Brands, S., Fernández, J., Hidalgo, H., Barimalala, R., Ashfaq, M., Bettolli, M. L., Hadjinicolaou, P., Solman, S., Maraun, D., Cavazos, T., **Fernandez-Granja, J. A.**, González-Abad, J., Mindlin, J., Soto-Navarro, J., Somot, S., Paquin, D., Kawase, H., Driouech, F., Orr, A., ... Gutiérrez, J. M.: "CORDEX Collection of Regional-Scale Climate Processes and Metrics for Climate Model Evaluation". Zenodo, 2025, doi: 10.5281/zenodo.15348836

- **Reseach Stay:** From 23 March 2023 to 27 June 2023 (3 months and 4 days) at the Institute of Atmospheric Physics of the Czech Academy of Sciences (Prague, Czech Republic) under the supervision of Prof. Radan Huth. This research stay, undertaken at an

international R+D[5] centre, is closely related to a publication *in progress* and the future work of this Thesis (see Sec. 7.5).

- Stryhal, J., **Fernández-Granja, J. A.**, and Huth, R.: "Unveiling seasonal synoptic-scale links: A global evaluation of atmospheric circulation and climate connections". *In preparation.*

7.5 Prospective directions for future research

Throughout this Thesis, multiple sources of uncertainty have been assessed in the various analyses conducted (e.g., observational uncertainty), and necessary sensitivity tests of the different results presented (such as sensitivity to the temporal resolution of the data, among other tests). However, conclusions rely on a single alternative regarding the clustering or synoptic classification algorithms, the JC-WTs classification method. This implies that a comprehensive methodological uncertainty analysis remains pending; that is, an examination of how the results of this Thesis might vary if alternative and well-known synoptic classification methods, such as K-means (Hastie et al., 2001), Self-Organizing Maps (SOM; Kohonen, 1982), or Principal Component Analysis (PCA; Preisendorfer and Mobley, 1988), among others, are employed instead of the JC-WT classification.

The choice of the JC-WTs methodology for this Thesis was strongly motivated by the various advantages already documented in the literature (Sec. 2.2). Thus, this algorithm was considered, a priori, a better candidate than other existing methods for conducting a process-based evaluation of climate models. Although methodological studies exploring different clustering algorithms for various applications have been conducted (see Sec. 1.5.1 for more information), the current literature lacks studies specifically addressing methodological uncertainty in process-based model evaluations.

Huth et al. (1993, 2008) conducted reviews and comparisons of different synoptic classification methods, including objective, automated, and multi-variable techniques. These two articles are highlighted references in this field. In fact, Prof. R. Huth and other researchers from his institution, the Institute of Atmospheric Physics (IAP) of the Czech Academy of Sciences (CAS) in Prague (Czech Republic), were actively involved in the COST733 Action on this topic (Philipp et al., 2010). Furthermore, Stryhal and Huth (2017), both from IAP (CAS), performed a comparison of winter circulation patterns from reanalyses throughout Europe using different classification methods. They found significant discrepancies in the classification outcomes when applying different WT methods to the same pair of reanalyses, highlighting the

[5]R+D: Research and Development

strong methodological dependence and the lack of direct correspondence between the resulting WTs from different methods.

The aforementioned international research centre (IAP, CAS) was selected for the research stay undertaken as part of this Thesis (Sec. 7.4), given their strong expertise in synoptic classification methodologies. The objective of the stay was to analyze the methodological uncertainty associated with process-based evaluations of large-scale climate models. The outcomes derived from this stay are work in progress and expect to be submitted to a scientific journal in the coming months. That work aims to present a global-scale evaluation of up to five different WTs methods (Jenkinson-Collison, Grosswettertypes (Hess and Brezowsky, 1969), Lund method (Lund, 1963), Principal Components and K-means), taking into account different method-specific configurations, by assessing the impact of atmospheric circulation on multiple surface climate variables (2-meter mean, maximum, and minimum temperature, total precipitation, 10-meter wind gust, and total cloud cover). Results reveal the WT method with the strongest links to the surface variables, region by region, covering the entire globe. The seasonal variability of these links is further examined as well as the influence of the configuration of the WT method. These results aim to assist researchers with the methodological choices in the development of future studies related to WTs, enrich the overall comprehension of atmospheric circulation, improving our capacity to identify and study regions with significant climatic interactions, and ultimately refine the sensitivity assessments of this Thesis. The classification methods employed in this work rely exclusively on SLP fields. However, recent studies have addressed the potential of incorporating additional atmospheric levels, such as mid-tropospheric geopotential height (Z500), to better capture circulation patterns. For instance, Miró et al. (2020) propose a modified version of the JC-WT method that integrates Z500 information in a regional application over Catalonia, demonstrating an added value of such vertical extension when correlating the WTs with daily precipitation. It might be worth opening the door to new methods incorporating Z500 in order to perform global process-based evaluations of GCMs.

In other aspects, Brands et al. (2025) address the results of ongoing WCRP-CORDEX (Sec. 1.2.4) activities to identify regional-scale climatic phenomena, relevant for global climate model evaluation against observational datasets. The identified climate phenomena, also known as “processes” or “diagnostics”, have distinct aspects (or features), each of which can be described by one or several metrics for evaluation. Brands et al. (2025) complements the work of the WCRP-CMIP Model Benchmarking Task Team (MB-TT Team, 2024), which currently focuses on global or continental-scale diagnostics. In contrast, the CORDEX approach operates at a finer scale, employing high-resolution diagnostics at the synoptic scale that require daily

or sub-daily data. The results presented in this Thesis are being shared with the MB-TT to foster synergies and support further decision-making. In particular, the JC-WTs (as climate "process") and the TPMS (as "diagnostics"), both important tools in this Thesis, have been included in this benchmark to evaluate CMIP7, the future GCMs generation. This paves the way for continued support to process-based evaluation within the CORDEX framework, in view of the forthcoming new generation of climate models, as part of future work.

Bibliography

Addor, N., M. Rohrer, R. Furrer, and J. Seibert, 2016: Propagation of biases in climate models from the synoptic to the regional scale: Implications for bias adjustment. *Journal of Geophysical Research: Atmospheres*, **121**, 2075–2089, doi:10.1002/2015JD024040.

Anderberg, M. R., 1973: *Cluster Analysis for Applications*. Academic Press, New York.

Anstey, J. A., P. Davini, L. J. Gray, T. J. Woollings, N. Butchart, C. Cagnazzo, B. Christiansen, S. C. Hardiman, S. M. Osprey, and S. Yang, 2013: Multi-model analysis of northern hemisphere winter blocking: Model biases and the role of resolution. *Journal of Geophysical Research: Atmospheres*, **118**, 3956–3971, doi:10.1002/jgrd.50231.

Banerjee, A., J. Fyfe, L. Polvani, D. Waugh, and K.-L. Chang, 2020: A pause in southern hemisphere circulation trends due to the montreal protocol. *Nature*, **579**, 544–548, doi:10.1038/s41586-020-2120-4.

Barnes, E. A. and J. A. Screen, 2015: The impact of arctic warming on the midlatitude jet-stream: Can it? has it? will it? *WIREs Climate Change*, **6**, 277–286, doi:https://doi.org/10.1002/wcc.337.

Barnston, A. G. and R. E. Livezey, 1987: Classification, seasonality and persistence of low-frequency atmospheric circulation patterns. *Monthly weather review*, **115**, 1083–1126, doi:https://doi.org/10.1175/1520-0493(1987)115¡1083:CSAPOL¿2.0.CO;2.

Barriopedro, D., E. M. Fischer, J. Luterbacher, R. M. Trigo, and R. Garcia-Herrera, 2011: The Hot Summer of 2010: Redrawing the Temperature Record Map of Europe. *Science*, **332**, 220–224, doi:10.1126/science.1201224.

Barriopedro, D., R. García-Herrera, A. R. Lupo, and E. Hernández, 2006: A climatology of Northern Hemisphere blocking. *Journal of Climate*, **19**, 1042–1063, doi:10.1175/JCLI3678.1.

Barry, R. G. and A. M. Carleton, 2013: Synoptic and dynamic climatology. Routledge.

Bedia, J., J. Baño-Medina, M. N. Legasa, M. Iturbide, R. Manzanas, S. Herrera, A. Casanueva, D. San-Martín, A. S. Cofiño, and J. M. Gutiérrez, 2020: Statistical downscaling with

the downscaler package (v3.1.0): contribution to the VALUE intercomparison experiment. *Geoscientific Model Development*, **13**, 1711–1735, doi:https://doi.org/10.5194/gmd-13-1711-2020, publisher: Copernicus GmbH.
URL https://gmd.copernicus.org/articles/13/1711/2020/

Bedia, J., N. Golding, A. Casanueva, M. Iturbide, C. Buontempo, and J. M. Gutiérrez, 2018: Seasonal predictions of Fire Weather Index: Paving the way for their operational applicability in Mediterranean Europe. *Climate Services*, **9**, 101–110, doi:10.1016/j.cliser.2017.04.001.

Bedia, J., S. Herrera, J. M. Gutiérrez, G. Zavala, I. R. Urbieta, and J. M. Moreno, 2012: Sensitivity of fire weather index to different reanalysis products in the Iberian Peninsula. *Natural Hazards and Earth System Sciences*, **12**, 699–708, doi:10.5194/nhess-12-699-2012.

Bedia, J., D. San-Martín, M. Iturbide, S. Herrera, R. Manzanas, and J. M. Gutiérrez, 2019: The METACLIP semantic provenance framework for climate products. *Environmental Modelling & Software*, doi:10.1016/j.envsoft.2019.07.005.

Benestad, R. E., I. Hanssen-Bauer, and D. Chen, 2008: *Empirical-Statistical Downscaling*. World Scientific Publishing, Singapore, 1st edition.

Berckmans, J., T. Woollings, M.-E. Demory, P.-L. Vidale, and M. Roberts, 2013: Atmospheric blocking in a high resolution climate model: influences of mean state, orography and eddy forcing. *Atmospheric Science Letters*, **14**, 34–40, doi:10.1002/asl2.412.

Bhend, J. and P. Whetton, 2013: Consistency of simulated and observed regional changes in temperature, sea level pressure and precipitation. *Climatic Change*, **118**, 799–810, doi:10.1007/s10584-012-0691-2.

Blackport, R. and J. C. Fyfe, 2022: Climate models fail to capture strengthening wintertime north atlantic jet and impacts on europe. *Science Advances*, **8**, eabn3112, doi:10.1126/sciadv.abn3112.

Bladé, I., B. Liebmann, D. Fortuny, and G. J. v. Oldenborgh, 2011: Observed and simulated impacts of the summer NAO in Europe: implications for projected drying in the Mediterranean region. *Climate Dynamics*, **39**, 709–727, doi:10.1007/s00382-011-1195-x.

Boé, J., 2018: Interdependency in multimodel climate projections: Component replication and result similarity. *Geophysical Research Letters*, **45**, 2771–2779, doi:10.1002/2017GL076829.

Brands, S., 2022a: A circulation-based performance atlas of the CMIP5 and 6 models for regional climate studies in the northern hemisphere [data set]. *Zenodo*, doi:https://doi.org/10.5281/zenodo.4452080.

— 2022b: A circulation-based performance atlas of the cmip5 and 6 models for regional climate studies in the northern hemisphere mid-to-high latitudes. *Geoscientific Model Development*, **15**, 1375–1411, doi:10.5194/gmd-15-1375-2022.

— 2022c: Common error patterns in the regional atmospheric circulation simulated by the cmip multi-model ensemble. *Geophysical Research Letters*, **49**, e2022GL101446, doi:https://doi.org/10.1029/2022GL101446.

Brands, S., J. Fernández, H. Hidalgo, R. Barimalala, M. Ashfaq, M. L. Bettolli, P. Hadjinicolaou, S. Solman, D. Maraun, T. Cavazos, J. A. Fernandez-Granja, J. González-Abad, J. Mindlin, J. Soto-Navarro, S. Somot, D. Paquin, H. Kawase, F. Driouech, A. Orr, L. Das, S. Sobolowski, R. E. Benestad, T. Ngo-Duc, P. Mooney, J. Evans, E. Coppola, and J. M. Gutiérrez, 2025: CORDEX collection of regional-scale climate processes and metrics for climate model evaluation. *Zenodo*, doi:10.5281/zenodo.15348836.

Brands, S., J. A. Fernández-Granja, J. Bedia, A. Casanueva, and J. Fernández, 2023a: A global climate model performance atlas for the southern hemisphere extratropics based on regional atmospheric circulation patterns. *Geophysical Research Letters*, **50**, doi:https://doi.org/10.1029/2023GL103531.

— 2023b: A global climate model performance atlas for the southern hemisphere extratropics based on regional atmospheric circulation patterns. *Geophysical Research Letters*, **50**, doi:https://doi.org/10.1029/2023GL103531.

— 2023c: Southern hemisphere lamb weather types from historical gcm experiments and various reanalyses [data set]. *Zenodo*, doi:10.5281/zenodo.7872012.

Brands, S., J. Gutiérrez, S. Herrera García, and A. Cofiño, 2012a: On the use of reanalysis data for downscaling. *Journal of Climate*, **25**, 2517–2526, doi:10.1175/JCLI-D-11-00251.1.

Brands, S., S. Herrera, J. Fernández, and J. M. Gutiérrez, 2013: How well do CMIP5 Earth System Models simulate present climate conditions in Europe and Africa? *Climate Dynamics*, **41**, 803–817, doi:10.1007/s00382-013-1742-8.

Brands, S., S. Herrera, and J. Gutiérrez, 2014a: Is eurasian snow cover in october a reliable statistical predictor for the wintertime climate on the iberian peninsula? *International Journal of Climatology*, **34**, 1615–1627, doi:https://doi.org/10.1002/joc.3788.

— 2014b: Is eurasian snow cover in october a reliable statistical predictor for the wintertime climate on the iberian peninsula? *International Journal of Climatology*, **34**, 1615–1627, doi:https://doi.org/10.1002/joc.3788.

Brands, S., R. Manzanas, J. M. Gutiérrez, and J. Cohen, 2012b: Seasonal predictability of wintertime precipitation in Europe using the snow advance index. *Journal of Climate*, **25**, 4023–4028, doi:https://doi.org/10.1175/JCLI-D-12-00083.1.

Brunner, L., A. G. Pendergrass, F. Lehner, A. L. Merrifield, R. Lorenz, and R. Knutti, 2020: Reduced global warming from cmip6 projections when weighting models by performance and independence. *Earth System Dynamics*, **11**, 995–1012, doi:10.5194/esd-11-995-2020.

Bueh, C. and H. Nakamura, 2007: Scandinavian pattern and its climatic impact. *Quarterly Journal of the Royal Meteorological Society: A journal of the atmospheric sciences, applied meteorology and physical oceanography*, **133**, 2117–2131, doi:https://doi.org/10.1002/qj.173.

Buehler, T., C. C. Raible, and T. F. Stocker, 2011: The relationship of winter season North Atlantic blocking frequencies to extreme cold or dry spells in the ERA-40. *Tellus A: Dynamic Meteorology and Oceanography*, **63**, 174–187, doi:10.1111/j.1600-0870.2010.00492.x.

Busuioc, A., D. Chen, and C. Hellström, 2001: Performance of statistical downscaling models in GCM validation and regional climate change estimates: application for Swedish precipitation: STATISTICAL DOWNSCALING FOR SWEDISH PRECIPITATION. *International Journal of Climatology*, **21**, 557–578, doi:10.1002/joc.624.

Cannon, A., 2020: Reductions in daily continental-scale atmospheric circulation biases between generations of Global Climate Models: CMIP5 to CMIP6. *Environmental Research Letters*, doi:10.1088/1748-9326/ab7e4f.

Casanueva, A., S. Kotlarski, A. Fischer, A. Flouris, T. Kjellstrom, B. Lemke, L. Nybo, C. Schwierz, and M. Liniger, 2020: Escalating environmental summer heat exposure—a future threat for the European workforce. *Regional Environmental Change*, **20**, doi:10.1007/s10113-020-01625-6.

Casanueva, A., C. Rodríguez-Puebla, M. D. Frías, and N. González-Reviriego, 2014: Variability of extreme precipitation over Europe and its relationships with teleconnection patterns.

Hydrology and Earth System Sciences, **18**, 709–725, doi:10.5194/hess-18-709-2014, publisher: Copernicus GmbH.

Chang, E. and A. Yau, 2016: Northern hemisphere winter storm track trends since 1959 derived from multiple reanalysis datasets. *Climate Dynamics*, **47**, doi:10.1007/s00382-015-2911-8.

Chang, E. K. M., Y. Guo, and X. Xia, 2012a: Cmip5 multimodel ensemble projection of storm track change under global warming. *Journal of Geophysical Research: Atmospheres*, **117**, doi:10.1029/2012JD018578.

— 2012b: CMIP5 multimodel ensemble projection of storm track change under global warming. *Journal of Geophysical Research: Atmospheres*, **117**, doi:10.1029/2012JD018578.

Chang, E. K. M., C.-G. Ma, C. Zheng, and A. M. W. Yau, 2016: Observed and projected decrease in northern hemisphere extratropical cyclone activity in summer and its impacts on maximum temperature. *Geophysical Research Letters*, **43**, 2200–2208, doi:https://doi.org/10.1002/2016GL068172.

Chemke, R. and J. Yuval, 2023: Human-induced weakening of the northern hemisphere tropical circulation. *Nature*, 529–532, doi:10.1038/s41586-023-05903-1.

Chen, D., 2000: A monthly circulation climatology for sweden and its application to a winter temperature case study. *International Journal of Climatology.*, **20**, 1067–1076, doi:10.1002/1097-0088(200008)20:103.0.CO;2-Q.

Chen, W. Y. and H. V. den Dool, 2003: Sensitivity of teleconnection patterns to the sign of their primary action center. *Monthly Weather Review*, **131**, 2885 – 2899, doi:10.1175/1520-0493(2003)131¡2885:SOTPTT¿2.0.CO;2.

Cherkassky, V. S. and F. Mulier, 1998: *Learning from Data: Concepts, Theory, and Methods*. Wiley, New York.

Christensen, J., F. Boberg, O. Christensen, and P. Lucas-Picher, 2008: On the need for bias correction of regional climate change projections of temperature and precipitation. **35**, L20709, doi:10.1029/2008GL035694.

Cinquini, L., D. Crichton, C. Mattmann, J. Harney, G. Shipman, F. Wang, R. Ananthakrishnan, N. Miller, S. Denvil, M. Morgan, Z. Pobre, G. M. Bell, B. Drach, D. Williams, P. Kershaw, S. Pascoe, E. Gonzalez, S. Fiore, and R. Schweitzer, 2012: The Earth System Grid Federation: An open infrastructure for access to distributed geospatial data. *2012 IEEE 8th International*

Conference on E-Science, IEEE, Chicago, IL, USA, 1–10.
URL http://ieeexplore.ieee.org/document/6404471/

Cofiño, A., J. Bedia, M. Iturbide, M. Vega, S. Herrera, J. Fernández, M. Frías, R. Manzanas, and J. Gutiérrez, 2018: The ECOMS User Data Gateway: Towards seasonal forecast data provision and research reproducibility in the era of Climate Services. *Climate Services*, **9**, 33–43, doi:10.1016/j.cliser.2017.07.001.

Colle, B. A., Z. Zhang, K. A. Lombardo, E. Chang, P. Liu, and M. Zhang, 2013: Historical Evaluation and Future Prediction of Eastern North American and Western Atlantic Extratropical Cyclones in the CMIP5 Models during the Cool Season. *Journal of Climate*, **26**, 6882–6903, doi:10.1175/JCLI-D-12-00498.1.

Comas-Bru, L. and A. Hernández, 2018: Reconciling North Atlantic climate modes: revised monthly indices for the East Atlantic and the Scandinavian patterns beyond the 20th century. *Earth System Science Data*, **10**, 2329–2344, doi:10.5194/essd-10-2329-2018, publisher: Copernicus GmbH.

Conway, D. and P. Jones, 1998: The use of weather types and air flow indices for gcm downscaling. *Journal of Hydrology*, **212**, 348–361.

Coumou, D., G. Di Capua, S. Vavrus, L. Wang, and S.-Y. Wang, 2018: The influence of arctic amplification on mid-latitude summer circulation. *Nature Communications*, **9**, doi:10.1038/s41467-018-05256-8.

Coumou, D., J. Lehmann, and J. Beckmann, 2015: The weakening summer circulation in the northern hemisphere mid-latitudes. *Science*, **348**, 324–327, doi:10.1126/science.1261768.

Cover, T. M. and J. A. Thomas, 2006: *Elements of Information Theory*. John Wiley & Sons.

Cox, T., A. Donohoe, K. C. Armour, D. M. W. Frierson, and G. H. Roe, 2024: Trends in atmospheric heat transport since 1980. *Journal of Climate*, **37**, 1539 – 1550, doi:10.1175/JCLI-D-23-0385.1.

Croci-Maspoli, M., C. Schwierz, and H. C. Davies, 2007: A Multifaceted Climatology of Atmospheric Blocking and Its Recent Linear Trend. *Journal of Climate*, **20**, 633–649, doi:10.1175/JCLI4029.1, publisher: American Meteorological Society Section: Journal of Climate.

D'Andrea, F., S. Tibaldi, M. Blackburn, G. Boer, M. Déqué, M. R. Dix, B. Dugas, L. Ferranti, T. Iwasaki, A. Kitoh, V. Pope, D. Randall, E. Roeckner, D. Strauss, W. Stern, H. Van den

Dool, and D. Williamson, 1998: Northern Hemisphere atmospheric blocking as simulated by 15 atmospheric general circulation models in the period 1979-1988. *Climate Dynamics*, **14**, 385–407, doi:10.1007/s003820050230.

Davini, P., S. Corti, F. D'Andrea, G. Rivière, and J. von Hardenberg, 2017: Improved winter european atmospheric blocking frequencies in high-resolution global climate simulations. *Journal of Advances in Modeling Earth Systems*, **9**, 2615–2634, doi:10.1002/2017MS001082.

Davis, A. and R. McNider, 1997: The development of antarctic katabatic winds and implications for the coastal ocean. *Journal of the atmospheric sciences*, **54**, 1248–1261.

Dawson, A. and T. N. Palmer, 2015: Simulating weather regimes: impact of model resolution and stochastic parameterization. *Climate Dynamics*, **44**, 2177–2193, doi:10.1007/s00382-014-2238-x.

Dawson, A., T. N. Palmer, and S. Corti, 2012: Simulating regime structures in weather and climate prediction models: REGIMES IN WEATHER AND CLIMATE MODELS. *Geophysical Research Letters*, **39**, doi:10.1029/2012GL053284.

Dee, D. P., S. M. Uppala, A. J. Simmons, P. Berrisford, P. Poli, S. Kobayashi, U. Andrae, M. A. Balmaseda, G. Balsamo, P. Bauer, P. Bechtold, A. C. M. Beljaars, L. van de Berg, J. Bidlot, N. Bormann, C. Delsol, R. Dragani, M. Fuentes, A. J. Geer, L. Haimberger, S. B. Healy, H. Hersbach, E. V. Hólm, L. Isaksen, P. Kaallberg, M. Kohler, M. Matricardi, A. P. McNally, B. M. Monge-Sanz, J. Morcrette, B. Park, C. Peubey, P. de Rosnay, C. Tavolato, J.-N. Thépaut, and F. Vitart, 2011: The ERA-Interim reanalysis: configuration and performance of the data assimilation system. *Q J R Meteorol Soc*, **137**, 553–597, doi:10.1002/qj.828.

Deser, C., J. Hurrell, and A. Phillips, 2017: The role of the north atlantic oscillation in european climate projections. *Climate Dynamics*, **49**, 3141–3157, doi:10.1007/s00382-016-3502-z.

Deser, C., F. Lehner, K. Rodgers, T. Ault, T. Delworth, P. DiNezio, A. Fiore, C. Frankignoul, J. Fyfe, D. Horton, J. Kay, R. Knutti, N. Lovenduski, J. Marotzke, K. McKinnon, S. Minobe, J. Randerson, J. Screen, I. Simpson, and M. Ting, 2020: Insights from earth system model initial-condition large ensembles and future prospects. *Nature Climate Change*, **10**, 277–286, doi:10.1038/s41558-020-0731-2.

Deser, C., A. Phillips, V. Bourdette, and H. Teng, 2012: Uncertainty in climate change projections: The role of internal variability. *Climate Dynamics*, **38**, 527–546, doi:10.1007/s00382-010-0977-x.

Diaconescu, E. P. and R. Laprise, 2013: Can added value be expected in RCM-simulated large scales? *Climate Dynamics*, **41**, 1769–1800, doi:10.1007/s00382-012-1649-9.

Diez-Sierra, J., M. Iturbide, J. Fernández, J. Gutiérrez, J. Milovac, and A. Cofiño, 2023: Consistency of the regional response to global warming levels from cmip5 and cordex projections. *Climate Dynamics*, 4047–4060, doi:10.1007/s00382-023-06790-y.

Donat, M. G., G. C. Leckebusch, J. G. Pinto, and U. Ulbrich, 2010: Examination of wind storms over central europe with respect to circulation weather types and nao phases. *International Journal of Climatology*, **30**, 1289–1300, doi:https://doi.org/10.1002/joc.1982.

Dong, B., R. Sutton, L. Shaffrey, and B. Harvey, 2022: Recent decadal weakening of the summer eurasian westerly jet attributable to anthropogenic aerosol emissions. *Nature Communications*, **13**, 1148, doi:10.1038/s41467-022-28816-5.

Dosio, A., 2016: Projections of climate change indices of temperature and precipitation from an ensemble of bias-adjusted high-resolution EURO-CORDEX regional climate models: BIAS-ADJUSTED CLIMATE CHANGE INDICES. *Journal of Geophysical Research: Atmospheres*, **121**, 5488–5511, doi:10.1002/2015JD024411.

Edwards, P. N., 2011: History of climate modeling. *WIREs Climate Change*, **2**, 128–139, doi:https://doi.org/10.1002/wcc.95.

Elbaum, E., C. I. Garfinkel, O. Adam, E. Morin, D. Rostkier-Edelstein, and U. Dayan, 2022: Uncertainty in projected changes in precipitation minus evaporation: Dominant role of dynamic circulation changes and weak role for thermodynamic changes. *Geophysical Research Letters*, **49**, e2022GL097725, doi:https://doi.org/10.1029/2022GL097725.

Everitt, B., S. Landau, M. Leese, and D. Stahl, 2011: *Cluster Analysis*. Wiley Series in Probability and Statistics, Wiley, New York, 5 edition.

Evin, G., S. Somot, and B. Hingray, 2021: Balanced estimate and uncertainty assessment of european climate change using the large euro-cordex regional climate model ensemble. *Earth System Dynamics*, **12**, 1543–1569, doi:10.5194/esd-12-1543-2021.
URL https://esd.copernicus.org/articles/12/1543/2021/

Eyring, V., S. Bony, G. A. Meehl, C. A. Senior, B. Stevens, R. J. Stouffer, and K. E. Taylor, 2016: Overview of the coupled model intercomparison project phase 6 (cmip6) experimental design and organization. *Geoscientific Model Development*, **9**, 1937–1958, doi:10.5194/gmd-9-1937-2016.

Eyring, V., P. M. Cox, G. M. Flato, P. J. Gleckler, G. Abramowitz, P. Caldwell, W. D. Collins, B. K. Gier, A. D. Hall, F. M. Hoffman, G. C. Hurtt, A. Jahn, C. D. Jones, S. A. Klein, J. P. Krasting, L. Kwiatkowski, R. Lorenz, E. Maloney, G. A. Meehl, A. G. Pendergrass, R. Pincus, A. C. Ruane, J. L. Russell, B. M. Sanderson, B. D. Santer, S. C. Sherwood, I. R. Simpson, R. J. Stouffer, and M. S. Williamson, 2019: Taking climate model evaluation to the next level. *Nature Climate Change*, **9**, 102–110, doi:10.1038/s41558-018-0355-y.

Eyring, V., N. Gillett, K. Achuta Rao, R. Barimalala, M. Barreiro Parrillo, N. Bellouin, C. Cassou, P. Durack, Y. Kosaka, S. McGregor, S. Min, O. Morgenstern, and Y. Sun, 2021: *Human Influence on the Climate System*, Cambridge University Press, Cambridge, United Kingdom and New York, NY, USA. 423–552.

Fabiano, F., H. M. Christensen, K. Strommen, P. Athanasiadis, A. Baker, R. Schiemann, and S. Corti, 2020: Euro-atlantic weather regimes in the primavera coupled climate simulations: impact of resolution and mean state biases on model performance. *Climate Dynamics*, **54**, 5031–5048, doi:10.1007/s00382-020-05271-w.
URL https://doi.org/10.1007/s00382-020-05271-w

Favà, V., J. J. Curto, and M. C. Llasat, 2015: Relationship between the summer NAO and maximum temperatures for the Iberian Peninsula. *Theoretical and Applied Climatology*, 1–15, doi:10.1007/s00704-015-1547-2.

Fealy, R. and G. Mills, 2018a: Deriving lamb weather types suited to regional climate studies: A case study on the synoptic origins of precipitation over ireland. *International Journal of Climatology*, doi:10.1002/joc.5495.

— 2018b: Deriving Lamb weather types suited to regional climate studies: A case study on the synoptic origins of precipitation over Ireland. *International Journal of Climatology*, **38**, 3439–3448, doi:10.1002/joc.5495, 00000.

Fernandez-Granja, J. A., S. Brands, J. Bedia, A. Casanueva, and J. Fernández, 2022: *Regional assessment of the Jenkinson-Collison Weather Types classification and Observational Uncertainty based on different reanalyses over the Mediterranean region*. 75–86.

Fernandez-Granja, J. A., A. Casanueva, J. Bedia, and J. Fernández, 2021: Improved atmospheric circulation over europe by the new generation of cmip6 earth system models. *Climate Dynamics*, **56**, doi:10.1007/s00382-021-05652-9.

Fernández-Granja, J. A., J. Bedia, A. Casanueva, S. Brands, and J. Fernández, 2024: The signature of the main modes of climatic variability as revealed by the jenkinson-collison classification over europe. *International Journal of Climatology*, doi:https://doi.org/10.1002/joc.8569.

— 2025: Emerging near-surface extratropical circulation changes due to climate change: A weather typing based global analysis. *Submitted to npj — Climate and Atmospheric Science*.

Fernández-Granja, J. A., S. Brands, J. Bedia, A. Casanueva, and J. Fernández, 2023: Exploring the limits of the Jenkinson–Collison weather types classification scheme: a global assessment based on various reanalyses. *Climate Dynamics*, doi:10.1007/s00382-022-06658-7.

Feser, F., B. Rockel, H. von Storch, J. Winterfeldt, and M. Zahn, 2011: Regional Climate Models Add Value to Global Model Data: A Review and Selected Examples: . *Bulletin of the American Meteorological Society*, **92**, 1181–1192, doi:10.1175/2011BAMS3061.1.

Fita, L., R. Romero, A. Luque, K. Emanuel, and C. Ramis, 2007: Analysis of the environments of seven mediterranean tropical-like storms using an axisymmetric, nonhydrostatic, cloud resolving model. *Natural Hazards and Earth System Sciences*, **7**, 41–56, doi:10.5194/nhess-7-41-2007.

Folland, C. K., J. Knight, H. W. Linderholm, D. Fereday, S. Ineson, and J. W. Hurrell, 2009: The Summer North Atlantic Oscillation: Past, Present, and Future. *Journal of Climate*, **22**, 1082–1103, doi:10.1175/2008JCLI2459.1.

Franzke, C. L. E. and N. Harnik, 2023: Long-term trends of the atmospheric circulation and moist static energy budget in the jra-55 reanalysis. *Journal of Climate*, **36**, 2959–2984, doi:10.1175/JCLI-D-21-0724.1.

Frías, M., M. Iturbide, R. Manzanas, J. Bedia, J. Fernández, S. Herrera, A. Cofiño, and J. Gutiérrez, 2018: An r package to visualize and communicate uncertainty in seasonal climate prediction. *Environmental Modelling Software*, **99**, 101 – 110, doi:https://doi.org/10.1016/j.envsoft.2017.09.008.

Fujiwara, M., J. S. Wright, G. L. Manney, L. J. Gray, J. Anstey, T. Birner, S. Davis, E. P. Gerber, V. L. Harvey, M. I. Hegglin, C. R. Homeyer, J. A. Knox, K. Krüger, A. Lambert, C. S. Long, P. Martineau, A. Molod, B. M. Monge-Sanz, M. L. Santee, S. Tegtmeier, S. Chabrillat, D. G. H. Tan, D. R. Jackson, S. Polavarapu, G. P. Compo, R. Dragani, W. Ebisuzaki, Y. Harada, C. Kobayashi, W. McCarty, K. Onogi, S. Pawson, A. Simmons, K. Wargan, J. S. Whitaker, and C.-Z. Zou, 2017: Introduction to the sparc reanalysis intercomparison

project (s-rip) and overview of the reanalysis systems. *Atmospheric Chemistry and Physics*, **17**, 1417–1452, doi:10.5194/acp-17-1417-2017.

Gertler, C. G. and P. A. O'Gorman, 2019: Changing available energy for extratropical cyclones and associated convection in northern hemisphere summer. *Proceedings of the National Academy of Sciences*, **116**, 4105–4110, doi:10.1073/pnas.1812312116.

Gibson, P. B., P. Uotila, S. E. Perkins-Kirkpatrick, L. V. Alexander, and A. J. Pitman, 2016: Evaluating synoptic systems in the cmip5 climate models over the australian region. *Climate Dynamics*, **47**, 2235–2251.

Giorgi, F., 2006: Regional climate modeling: Status and perspectives. *Journal de Physique IV (Proceedings)*, **139**, 101–118, doi:10.1051/jp4:2006139008.

Giorgi, F., C. Jones, and G. Asrar, 2009: Addressing climate information needs at the regional level: the CORDEX framework. *WMO Bulletin*, **58**, 175–183.

Giorgi, F. and P. Lionello, 2008: Climate change projections for the mediterranean region. *Global and Planetary Change*, **63**, 90–104, doi:https://doi.org/10.1016/j.gloplacha.2007.09.005, mediterranean climate: trends, variability and change.

Gong, D. and S. Wang, 1999: Definition of antarctic oscillation index. *Geophysical research letters*, **26**, 459–462.

Goyal, R., A. Sen Gupta, M. Jucker, and M. H. England, 2021: Historical and projected changes in the southern hemisphere surface westerlies. *Geophysical Research Letters*, **48**, e2020GL090849, doi:https://doi.org/10.1029/2020GL090849.

Grimalt-Gelabert, M., M. Tomas-Burguera, G. Alomar-Garau, J. Martin-Vide, and M. García, 2013: Determination of the jenkinson and collison's weather types for the western mediterranean basin over the 1948-2009 period: Temporal analysis. *Atmosfera*, **26**, 75–94, doi:10.1016/S0187-6236(13)71063-4.

Grise, K. M., S. M. Davis, I. R. Simpson, D. W. Waugh, Q. Fu, R. J. Allen, K. H. Rosenlof, C. C. Ummenhofer, K. B. Karnauskas, A. C. Maycock, X.-W. Quan, T. Birner, and P. W. Staten, 2019: Recent tropical expansion: Natural variability or forced response? *Journal of Climate*, **32**, 1551 – 1571, doi:10.1175/JCLI-D-18-0444.1.

Grumm, R. H., 2011: The central European and Russian heat event of July–August 2010. *Bulletin of the American Meteorological Society*, **92**, 1285–1296, doi:10.1175/2011BAMS3174.1,

publisher: American Meteorological Society Section: Bulletin of the American Meteorological Society.

Gutiérrez, J., R. Jones, G. Narisma, L. Alves, M. Amjad, I. Gorodet-skaya, M. Grose, N. Klutse, S. Krakovska, J. Li, D. Martínez-Castro, L. Mearns, S. Mernild, T. Ngo-Duc, V. den Hurkm B, Y. J-H, V. Masson-Delmotte, P. Zhai, A. Pirani, S. Connors, C. Péan, S. Berger, N. Caud, Y. Chen, L. Goldfarb, M. Gomis, M. Huang, K. Leitzell, E. Lonnoy, J. Matthews, T. Maycock, T. Waterfield, O. Yelekçi, R. Yu, and B. e. Zhou, 2021: *Climate Change 2021: The physical science basis contribution of Working Group I to the Sixth Assessment Report of the Intergovernmental Panel on Climate Change*, Cambridge University Press. 1927–2058.

Hanna, E., X. Fettweis, and R. J. Hall, 2018: Brief communication: Recent changes in summer greenland blocking captured by none of the cmip5 models. *The Cryosphere*, **12**, 3287–3292, doi:10.5194/tc-12-3287-2018.

Harada, Y., H. Kamahori, C. Kobayashi, H. Endo, S. Kobayashi, Y. Ota, H. Onoda, K. Onogi, K. Miyaoka, and K. Takahashi, 2016: The jra-55 reanalysis: Representation of atmospheric circulation and climate variability. *Journal of the Meteorological Society of Japan. Ser. II*, **94**, 269–302, doi:10.2151/jmsj.2016-015.

Hartigan, J. A., 1975: *Clustering Algorithms*. Wiley Series in Probability and Statistics, Wiley, New York.

Hastie, T., R. Tibshirani, and J. Friedman, 2001: *The Elements of Statistical Learning*. Springer Series in Statistics, Springer, New York.

Hawkes, J., N. Manubens, E. Danovaro, J. Hanley, S. Siemen, B. Raoult, and T. Quintino, 2020: Polytope: Serving ECMWFs Big Weather Data. *EGU General Assembly 2020, Online, 4–8 May 2020*, EGU2020–15048, doi:10.5194/egusphere-egu2020-15048.

Hawkins, E. and R. Sutton, 2012: Time of emergence of climate signals. *Geophys. Res. Lett.*, **39**, L01702, doi:10.1029/2011GL050087.

Herrera-Lormendez, P., A. John, H. Douville, and J. Matschullat, 2023: Projected changes in synoptic circulations over Europe and their implications for summer precipitation: A CMIP6 perspective. *International Journal of Climatology*, **n/a**, doi:10.1002/joc.8033.

Hersbach, H., B. Bell, P. Berrisford, S. Hirahara, A. Horányi, J. Muñoz-Sabater, J. Nicolas, C. Peubey, R. Radu, D. Schepers, et al., 2020: The era5 global reanalysis. *Quarterly Journal of the Royal Meteorological Society*, **146**, 1999–2049.

Hess, P. and H. Brezowsky, 1969: Katalog der grosswetterlagen europas. *Neubearbeitete und Ergänzte Aufl. Bericht des Deutschen Wetterdienstes*.

Hochman, A., P. Alpert, T. Harpaz, H. Saaroni, and G. Messori, 2019: A new dynamical systems perspective on atmospheric predictability: Eastern mediterranean weather regimes as a case study. *Science Advances*, **5**, eaau0936, doi:10.1126/sciadv.aau0936.

Hodges, K. I., 1994: A General Method for Tracking Analysis and Its Application to Meteorological Data. *Monthly Weather Review*, **122**, 2573–2586, doi:10.1175/1520-0493(1994)122¡2573:AGMFTA¿2.0.CO;2.

Houghton, J. T., Y. Ding, D. J. Griggs, M. Noguer, P. J. van der Linden, X. Dai, K. Maskell, and C. A. Johnson, eds., 2001: *Climate Change 2001: The Scientific Basis. Contribution of Working Group I to the Third Assessment Report of the Intergovernmental Panel on Climate Change*. Cambridge University Press, Cambridge, United Kingdom and New York, NY, USA, third Assessment Report (TAR).

Houghton, J. T., L. G. M. Filho, B. A. Callander, N. Harris, A. Kattenberg, and K. Maskell, eds., 1996: *Climate Change 1995: The Science of Climate Change. Contribution of Working Group I to the Second Assessment Report of the Intergovernmental Panel on Climate Change*. Cambridge University Press, Cambridge, United Kingdom and New York, NY, USA, second Assessment Report (SAR).

Houghton, J. T., G. J. Jenkins, and J. J. Ephraums, eds., 1990: *Climate Change: The IPCC Scientific Assessment*. Cambridge University Press, Cambridge, United Kingdom, first Assessment Report (FAR).

Hulme, M., K. Briffal, P. Jones, and C. Senior, 1993: Validation of gcm control simulations using indices of daily airflow types over the british isles. *Climate Dynamics*, **9**, 95–105, doi:https://doi.org/10.1007/BF00210012.

Hurrell, J. W., 1995: Decadal trends in the North Atlantic Oscillation: Regional temperatures and precipitation. *Science*, **269**, 676–679, doi:https://doi.org/10.1126/science.269.5224.676.

Hurrell, J. W., Y. Kushnir, G. Ottersen, and M. Visbeck, 2003: An overview of the North Atlantic Oscillation. *Geophysical Monograph Series*, American Geophysical Union, Washington, D. C., volume 134, 1–35.

Huth, R., C. Beck, A. Philipp, M. Demuzere, Z. Ustrnul, M. Cahynová, J. Kyselý, and O. Tveito,

2008: Classifications of atmospheric circulation patterns: Recent advances and applications. *Annals of the New York Academy of Sciences*, **1146**, 105–152, doi:10.1196/annals.1446.019.

Huth, R., I. Nemesova, and N. Klimperová, 1993: Weather categorization based on the average linkage clustering technique: An application to european mid-latitudes. *International Journal of Climatology*, **13**, 817–835, doi:10.1002/joc.3370130802.

IPCC, 2007: Climate Change 2007: The physical science basis. Working Group I Contribution to the Fourth Assessment Report of the IPCC. Cambridge University Press, Cambridge, United Kingdom and New York, NY, USA.

— 2013: Climate Change 2013: The physical science basis. Contribution of Working Group I to the Fifth Assessment report of the Intergovernmental Panel on Climate Change. Cambridge University Press, Cambridge, United Kingdom and New York, NY, USA.

— 2021: Climate Change 2021: The Physical Science Basis. Contribution of Working Group I to the Sixth Assessment Report of the Intergovernmental Panel on Climate Change. Cambridge University Press, Cambridge, United Kingdom and New York, NY, USA.

Iturbide, M., J. Bedia, and J. M. Gutiérrez, 2018: Tackling Uncertainties of Species Distribution Model Projections with Package mopa. *The R Journal*, **10**, 18.

Iturbide, M., J. Bedia, S. Herrera, J. Baño-Medina, J. Fernández, M. Frías, R. Manzanas, D. San-Martín, E. Cimadevilla, A. Cofiño, and J. Gutiérrez, 2019: The R-based climate4R open framework for reproducible climate data access and post-processing. *Environmental Modelling & Software*, **111**, 42–54, doi:10.1016/j.envsoft.2018.09.009.

Iturbide, M., A. Casanueva, J. Bedia, S. Herrera, J. Milovac, and J. Gutiérrez, 2020a: On the need of bias adjustment for more plausible climate change projections of extreme heat. *Atmospheric Science Letters*, submitted.

Iturbide, M., J. Fernández, J. Gutiérrez, A. Pirani, D. Huard, A. Al Khourdajie, J. Baño-Medina, J. Bedia, A. Casanueva, E. Cimadevilla, A. Cofiño Gonzalez, M. De Felice, J. Diez-Sierra, M. García-Díez, J. Goldie, D. Herrera, S. Herrera, R. Manzanas, J. Milovac, A. Radhakrishnan, D. San-Martín, A. Spinuso, K. Thyng, C. Trenham, and Ö. Yelekçi, 2022: Implementation of FAIR principles in the IPCC: The WGI AR6 Atlas repository. *Scientific Data*, **9**, 629, doi:10.1038/s41597-022-01739-y.

Iturbide, M., J. M. Gutiérrez, L. M. Alves, J. Bedia, R. Cerezo-Mota, E. Cimadevilla, A. S. Cofiño, A. Di Luca, S. H. Faria, I. V. Gorodetskaya, M. Hauser, S. Herrera, K. Hennessy,

H. T. Hewitt, R. G. Jones, S. Krakovska, R. Manzanas, D. Martínez-Castro, G. T. Narisma, I. S. Nurhati, I. Pinto, S. I. Seneviratne, B. van den Hurk, and C. S. Vera, 2020b: An update of ipcc climate reference regions for subcontinental analysis of climate model data: definition and aggregated datasets. *Earth System Science Data*, **12**, 2959–2970, doi:10.5194/essd-12-2959-2020.

Jacob, D., J. Petersen, B. Eggert, A. Alias, O. B. Christensen, L. M. Bouwer, A. Braun, A. Colette, M. Déqué, G. Georgievski, E. Georgopoulou, A. Gobiet, L. Menut, G. Nikulin, A. Haensler, N. Hempelmann, C. Jones, K. Keuler, S. Kovats, N. Kröner, S. Kotlarski, A. Kriegsmann, E. Martin, E. v. Meijgaard, C. Moseley, S. Pfeifer, S. Preuschmann, C. Radermacher, K. Radtke, D. Rechid, M. Rounsevell, P. Samuelsson, S. Somot, J.-F. Soussana, C. Teichmann, R. Valentini, R. Vautard, B. Weber, and P. Yiou, 2014: EURO-CORDEX: new high-resolution climate change projections for European impact research. *Regional Environmental Change*, **14**, 563–578, doi:10.1007/s10113-013-0499-2.

Jacob, D., C. Teichmann, S. Sobolowski, E. Katragkou, I. Anders, M. Belda, R. Benestad, F. Boberg, E. Buonomo, R. M. Cardoso, A. Casanueva, O. B. Christensen, J. H. Christensen, E. Coppola, L. De Cruz, E. L. Davin, A. Dobler, M. Domínguez, R. Fealy, J. Fernandez, M. A. Gaertner, M. García-Díez, F. Giorgi, A. Gobiet, K. Goergen, J. J. Gómez-Navarro, J. J. G. Alemán, C. Gutiérrez, J. M. Gutiérrez, I. Güttler, A. Haensler, T. Halenka, S. Jerez, P. Jiménez-Guerrero, R. G. Jones, K. Keuler, E. Kjellström, S. Knist, S. Kotlarski, D. Maraun, E. van Meijgaard, P. Mercogliano, J. P. Montávez, A. Navarra, G. Nikulin, N. de Noblet-Ducoudré, H.-J. Panitz, S. Pfeifer, M. Piazza, E. Pichelli, J.-P. Pietikäinen, A. F. Prein, S. Preuschmann, D. Rechid, B. Rockel, R. Romera, E. Sánchez, K. Sieck, P. M. M. Soares, S. Somot, L. Srnec, S. L. Sørland, P. Termonia, H. Truhetz, R. Vautard, K. Warrach-Sagi, and V. Wulfmeyer, 2020: Regional climate downscaling over europe: perspectives from the EURO-CORDEX community. *Regional Environmental Change*, **20**, 51, doi:10.1007/s10113-020-01606-9.

James, R., H. Douville, P. J. Kushner, M. Abe, Y. Ait Brahim, A. Alessandri, W. Dong, W. J. Gutowski, R. Haarsma, S. Harari, B.-M. Kim, G. Krinner, S. Li, A. Mariotti, S. McGregor, A. G. Pendergrass, M. Rojas, A. C. Ruane, and T. G. Shepherd, 2021: Future global climate: Scenario-based projections and near-term information. *Climate Change 2021: The Physical Science Basis. Contribution of Working Group I to the Sixth Assessment Report of the Intergovernmental Panel on Climate Change*, V. Masson-Delmotte, P. Zhai, A. Pirani, S. Connors, C. Péan, S. Berger, N. Caud, Y. Chen, L. Goldfarb, M. Gomis, M. Huang,

K. Leitzell, E. Lonnoy, J. Matthews, T. Maycock, T. Waterfield, O. Yelekçi, R. Yu, and B. Zhou, eds., Cambridge University Press, 553–672.

Jenkinson, A. and F. Collison, 1977: An initial climatology of gales over the north sea. synoptic climatology branch memorandum. *Meteorological Office,*, **62**.

Jiang, B., J. Pei, Y. Tao, and X. Lin, 2011: Clustering uncertain data based on probability distribution similarity. *IEEE Transactions on Knowledge and Data Engineering*, **25**, 751–763.

Jones, C., F. Giorgi, and G. Asrar, 2011: The Coordinated Regional Downscaling Experiment: CORDEX, An international downscaling link to CMIP5. *CLIVAR Exchanges*, **56-16(2)**, 34–40.

Jones, P. D., C. Harpham, and K. R. Briffa, 2013: Lamb weather types derived from reanalysis products. *International Journal of Climatology*, **33**, 1129–1139, doi:10.1002/joc.3498.

Jones, P. D., M. Hulme, and K. R. Briffa, 1993: A comparison of Lamb circulation types with an objective classification scheme. *International Journal of Climatology*, **13**, 655–663, doi:10.1002/joc.3370130606.

Jones, R. G., J. M. Murphy, and M. Noguer, 1995: Simulation of climate change over europe using a nested regional-climate model. I: Assessment of control climate, including sensitivity to location of lateral boundaries. *Quarterly Journal of the Royal Meteorological Society*, **121**, 1413–1449, doi:10.1002/qj.49712152610.

Jung, T., M. J. Miller, T. N. Palmer, P. Towers, N. Wedi, D. Achuthavarier, J. M. Adams, E. L. Altshuler, B. A. Cash, I. Kinter, J. L., L. Marx, C. Stan, and K. I. Hodges, 2012: High-Resolution Global Climate Simulations with the ECMWF Model in Project Athena: Experimental Design, Model Climate, and Seasonal Forecast Skill. *Journal of Climate*, **25**, 3155–3172, doi:10.1175/JCLI-D-11-00265.1.
URL https://doi.org/10.1175/JCLI-D-11-00265.1

Jury, M. W., S. Herrera, J. M. Gutiérrez, and D. Barriopedro, 2019: Blocking representation in the ERA-Interim driven EURO-CORDEX RCMs. *Climate Dynamics*, **52**, 3291–3306, doi:10.1007/s00382-018-4335-8.

Kalnay, E., M. Kanamitsu, R. Kistler, W. Collins, D. Deaven, L. Gandin, M. Iredell, S. Saha, G. White, J. Woollen, Y. Zhu, M. Chelliah, W. Ebisuzaki, W. Higgins, J. Janowiak, K. C. Mo, C. Ropelewski, J. Wang, A. Leetmaa, R. Reynolds, R. Jenne, and D. Joseph, 1996: The

NCEP/NCAR 40-Year Reanalysis Project. *Bulletin of the American Meteorological Society*, **77**, 437–472, doi:10.1175/1520-0477(1996)077¡0437:TNYRP¿2.0.CO;2, publisher: American Meteorological Society.

Kang, S. M., Y. Yu, C. Deser, X. Zhang, I.-S. Kang, S.-S. Lee, K. B. Rodgers, and P. Ceppi, 2023: Global impacts of recent southern ocean cooling. *Proceedings of the National Academy of Sciences*, **120**, e2300881120, doi:10.1073/pnas.2300881120.

Kautz, L.-A., O. Martius, S. Pfahl, J. G. Pinto, A. M. Ramos, P. M. Sousa, and T. Woollings, 2022: Atmospheric blocking and weather extremes over the Euro-Atlantic sector – a review. *Weather and Climate Dynamics*, **3**, 305–336, doi:10.5194/wcd-3-305-2022, publisher: Copernicus GmbH.

Kim, Y., J. P. Evans, and A. Sharma, 2024: Correcting Multivariate Biases in Regional Climate Model Boundaries: How Are Synoptic Systems Impacted Over the Australian Region? *Geophysical Research Letters*, **51**, doi:10.1029/2024GL111445.

Kirchmeier-Young, M. C., H. Wan, X. Zhang, and S. I. Seneviratne, 2019: Importance of framing for extreme event attribution: The role of spatial and temporal scales. *Earth's Future*, **7**, 1192–1204, doi:https://doi.org/10.1029/2019EF001253.

Kobayashi, S., Y. Ota, Y. Harada, A. Ebita, M. Moriya, H. Onoda, K. Onogi, H. Kamahori, C. Kobayashi, H. Endo, K. Miyaoka, and K. Takahashi, 2015: The jra-55 reanalysis: General specifications and basic characteristics. *Journal of the Meteorological Society of Japan. Ser. II*, **93**, 5–48, doi:10.2151/jmsj.2015-001.

Kohonen, T., 1982: Self-organized formation of topologically correct feature maps. *Biological cybernetics*, **43**, 59–69, doi:10.1007/BF00337288.

Kullback, S. and R. A. Leibler, 1951: On information and sufficiency. *The annals of mathematical statistics*, **22**, 79–86.

Kushner, P. J., I. M. Held, and T. L. Delworth, 2001: Southern Hemisphere Atmospheric Circulation Response to Global Warming. *Journal of Climate*, **14**, 2238–2249, doi:10.1175/1520-0442(2001)014¡0001:SHACRT¿2.0.CO;2.

Lamb, H., 1972: British isles weather types and a register of daily sequence of circulation patterns 1861-1971. *Meteorological Office, Geophysical Memoir.*, **116**, 1–85.

Lee, C. C. and S. C. Sheridan, 2015: Synoptic Climatology: An Overview. *Reference Module in Earth Systems and Environmental Sciences*, Elsevier.
URL https://www.sciencedirect.com/science/article/pii/B9780124095489094215

Lee, D. Y., M. R. Petersen, and W. Lin, 2019: The Southern Annular Mode and Southern Ocean Surface Westerly Winds in E3SM. *Earth and Space Science*, **6**, 2624–2643, doi:10.1029/2019EA000663.

Liljequist, G. H., 1970: *Klimatologi*. Generalstabens Litografiska anstalt, Stockholm.

Limpasuvan, V. and D. L. Hartmann, 1999: Eddies and the annular modes of climate variability. *Geophysical Research Letters*, **26**, 3133–3136, doi:https://doi.org/10.1029/1999GL010478.

Littmann, T., 2000: An empirical classification of weather types in the mediterranean basin and their interrelation with rainfall. *Theoretical and Applied Climatology*, **66**, 161–171, doi:10.1007/s007040070022.

Lund, I. A., 1963: Map-pattern classification by statistical methods. *Journal of Applied Meteorology and Climatology*, **2**, 56–65, doi:10.1175/1520-0450(1963)002¡0056:MPCBSM¿2.0.CO;2.

Lupo, A. R., 2021: Atmospheric blocking events: a review. *Annals of the New York Academy of Sciences*, **1504**, 5–24, doi:10.1111/nyas.14557, _eprint: https://onlinelibrary.wiley.com/doi/pdf/10.1111/nyas.14557.

Maher, N., S. Milinski, L. Suarez-Gutierrez, M. Botzet, M. Dobrynin, L. Kornblueh, J. Kröger, Y. Takano, R. Ghosh, C. Hedemann, C. Li, H. Li, E. Manzini, D. Notz, D. Putrasahan, L. Boysen, M. Claussen, T. Ilyina, D. Olonscheck, T. Raddatz, B. Stevens, and J. Marotzke, 2019: The max planck institute grand ensemble: Enabling the exploration of climate system variability. *Journal of Advances in Modeling Earth Systems*, **11**, 2050–2069, doi:https://doi.org/10.1029/2019MS001639.

Manabe, S. and R. T. Wetherald, 1967: Thermal equilibrium of the atmosphere with a given distribution of relative humidity. *Journal of the Atmospheric Sciences*, **24**, 241–259.

Mantua, N. J. and S. R. Hare, 2002: The pacific decadal oscillation. *Journal of Oceanography*, **58**, 35–44, doi:10.1023/A:1015820616384.

Manzanas, R., S. Brands, D. San-Martin, A. J. Lucero, C. Limbo, and J. Gutiérrez, 2015: Statistical downscaling in the tropics can be sensitive to reanalysis choice: A case study for precipitation in the philippines. *Journal of Climate*, **28**, doi:10.1175/JCLI-D-14-00331.1.

Maraun, D., 2012: Nonstationarities of regional climate model biases in European seasonal mean temperature and precipitation sums. *Geophysical Research Letters*, **39**, L06706, doi:10.1029/2012GL051210.

— 2016: Bias correcting climate change simulations - a critical review. *Current Climate Change Reports*, **2**, doi:10.1007/s40641-016-0050-x.

Maraun, D., T. G. Shepherd, M. Widmann, G. Zappa, D. Walton, J. M. Gutiérrez, S. Hagemann, I. Richter, P. M. M. Soares, A. Hall, and L. O. Mearns, 2017: Towards process-informed bias correction of climate change simulations. *Nature Climate Change*, **7**, 664–773, doi:10.1038/nclimate3418.

Maraun, D., F. Wetterhall, A. M. Ireson, R. E. Chandler, E. J. Kendon, M. Widmann, S. Brienen, H. W. Rust, T. Sauter, M. Themeßl, V. K. C. Venema, K. P. Chun, C. M. Goodess, R. G. Jones, C. Onof, M. Vrac, and I. Thiele-Eich, 2010: Precipitation downscaling under climate change: Recent developments to bridge the gap between dynamical models and the end user. *Reviews of Geophysics*, **48**, doi:https://doi.org/10.1029/2009RG000314.

Maraun, D. and M. Widmann, 2018: *Statistical Downscaling and Bias Correction for Climate Research*. Cambridge University Press, 1 edition.
URL https://www.cambridge.org/core/product/identifier/9781107588783/type/book

Marshall, G. J., 2003: Trends in the Southern Annular Mode from Observations and Reanalyses. *Journal of Climate*, **16**, 4134–4143, doi:10.1175/1520-0442(2003)016¡4134:TITSAM¿2.0.CO;2, publisher: American Meteorological Society Section: Journal of Climate.

Masato, G., B. J. Hoskins, and T. Woollings, 2013: Winter and Summer Northern Hemisphere Blocking in CMIP5 Models. *Journal of Climate*, **26**, 7044–7059, doi:10.1175/JCLI-D-12-00466.1.

Masato, G., B. J. Hoskins, and T. J. Woollings, 2012: Wave-breaking characteristics of midlatitude blocking. *Quarterly Journal of the Royal Meteorological Society*, **138**, 1285–1296, doi:https://doi.org/10.1002/qj.990.
URL https://rmets.onlinelibrary.wiley.com/doi/abs/10.1002/qj.990

Massei, N. and M. Fournier, 2012: Assessing the expression of large-scale climatic fluctuations in the hydrological variability of daily Seine river flow (France) between 1950 and 2008 using Hilbert–Huang Transform. *Journal of Hydrology*, **448-449**, 119–128, doi:https://doi.org/10.1016/j.jhydrol.2012.04.052.

Matsueda, M., R. Mizuta, and S. Kusunoki, 2009: Future change in wintertime atmospheric blocking simulated using a 20-km-mesh atmospheric global circulation model. *Journal of Geophysical Research: Atmospheres*, **114**, doi:10.1029/2009JD011919.

McFarlane, N., 2011: Parameterizations: representing key processes in climate models without resolving them. *WIREs Climate Change*, **2**, 482–497, doi:https://doi.org/10.1002/wcc.122.

Mcguffie, K. and A. Henderson-Sellers, 2005: *A Climate Modelling Primer*. John Wiley Sons, Ltd, 1-280 pp.

McSweeney, C., R. Jones, R. W. Lee, and D. Rowell, 2015: Selecting CMIP5 GCMs for downscaling over multiple regions. *Climate Dynamics*, **44**, 3237–3260, doi:10.1007/s00382-014-2418-8.

Meehl, G., G. Boer, C. Covey, M. Latif, and S. Ronald, 2000: Cmip coupled model intercomparison project. *Bulletin of the American Meteorological Society*, **81**, 313–318, doi:10.1175/1520-0477(2000)081¡0313:TCMIPC¿2.3.CO;2.

Mellado-Cano, J., D. Barriopedro, R. García-Herrera, R. M. Trigo, and A. Hernández, 2019: Examining the North Atlantic Oscillation, East Atlantic Pattern, and Jet Variability since 1685. *Journal of Climate*, **32**, 6285–6298, doi:10.1175/JCLI-D-19-0135.1, publisher: American Meteorological Society Section: Journal of Climate.

Miró, J., N. Pepin, J. Peña, and J. Martin-Vide, 2020: Daily atmospheric circulation patterns for catalonia (northeast iberian peninsula) using a modified version of jenkinson and collison method. *Atmospheric Research*, **231**, 104674, doi:10.1016/j.atmosres.2019.104674.

Mirones, , J. Bedia, J. A. Fernández-Granja, S. Herrera, S. O. Van Vloten, A. Pozo, L. Cagigal, and F. J. Méndez, 2023: Weather-type-conditioned calibration of Tropical Rainfall Measuring Mission precipitation over the South Pacific Convergence Zone. *International Journal of Climatology*, **43**, 1193–1210, doi:10.1002/joc.7905.

Moss, R. H., J. A. Edmonds, K. A. Hibbard, M. R. Manning, S. K. Rose, D. P. van Vuuren, T. R. Carter, S. Emori, M. Kainuma, T. Kram, G. A. Meehl, J. F. B. Mitchell, N. Nakicenovic, K. Riahi, S. J. Smith, R. J. Stouffer, A. M. Thomson, J. P. Weyant, and T. J. Wilbanks, 2010: The next generation of scenarios for climate change research and assessment. *Nature*, **463**, 747–756, doi:10.1038/nature08823.

Nakicenovic, N., J. Alcamo, A. Grubler, K. Riahi, R. A. Roehrl, H.-H. Rogner, and N. Victor, 2000: *Special Report on Emissions Scenarios (SRES), A Special Report of Working Group III*

of the Intergovernmental Panel on Climate Change. Cambridge University Press, Cambridge, United Kingdom and New York, NY, USA.

Nikulin, G., C. Lennard, A. Dosio, E. Kjellström, Y. Chen, A. Hänsler, M. Kupiainen, R. Laprise, L. Mariotti, C. F. Maule, E. v. Meijgaard, H.-J. Panitz, J. F. Scinocca, and S. Somot, 2018: The effects of 1.5 and 2 degrees of global warming on Africa in the CORDEX ensemble. *Environmental Research Letters*, **13**, 065003, doi:10.1088/1748-9326/aab1b1.

O'Neill, B. C., C. Tebaldi, D. P. van Vuuren, V. Eyring, P. Friedlingstein, G. Hurtt, R. Knutti, E. Kriegler, J.-F. Lamarque, J. Lowe, G. A. Meehl, R. Moss, K. Riahi, and B. M. Sanderson, 2016: The scenario model intercomparison project (scenariomip) for cmip6. *Geoscientific Model Development*, **9**, 3461–3482, doi:10.5194/gmd-9-3461-2016.

Otero, N., J. Sillmann, and T. Butler, 2018: Assessment of an extended version of the Jenkinson-Collison classification on CMIP5 models over Europe. *Climate Dynamics*, 1559–1579, doi:10.1007/s00382-017-3705-y.

Oudar, T., J. Cattiaux, and H. Douville, 2020: Drivers of the northern extratropical eddy-driven jet change in cmip5 and cmip6 models. *Geophysical Research Letters*, **47**, e2019GL086695, doi:10.1029/2019GL086695.

O'Reilly, C. H., S. Minobe, and A. Kuwano-Yoshida, 2016: The influence of the gulf stream on wintertime european blocking. *Climate Dynamics*, **47**, 1545–1567, doi:10.1007/s00382-015-2919-0.

Palmer, T. E., C. F. McSweeney, B. B. B. Booth, M. D. K. Priestley, P. Davini, L. Brunner, L. Borchert, and M. B. Menary, 2023: Performance-based sub-selection of cmip6 models for impact assessments in europe. *Earth System Dynamics*, **14**, 457–483, doi:10.5194/esd-14-457-2023.

Peixoto, J. P., A. H. Oort, C. Covey, and K. Taylor, 1992: Physics of climate. *Physics Today*, **45**, 67–67, doi:10.1063/1.2809772.

Pelly, J. L. and B. J. Hoskins, 2003: A new perspective on blocking. *Journal of the Atmospheric Sciences*, **60**, 743–755, doi:10.1175/1520-0469(2003)060¡0743:ANPOB¿2.0.CO;2.

Pereira, S., A. Ramos, L. Rebelo, R. Trigo, and J. Zêzere, 2018: A centennial catalogue of hydro-geomorphological events and their atmospheric forcing. *Advances in Water Resources*, **122**, 98–112, doi:10.1016/j.advwatres.2018.10.001.

Perez, J., M. Menendez, F. J. Mendez, and I. J. Losada, 2014: Evaluating the performance of CMIP3 and CMIP5 global climate models over the north-east Atlantic region. *Climate Dynamics*, **43**, 2663–2680, doi:10.1007/s00382-014-2078-8.

Perry, A. and J. Mayes, 1998: The lamb weather type catalogue. *Weather*, **53**, 222–229, doi:https://doi.org/10.1002/j.1477-8696.1998.tb06387.x.

Petrie, R., S. Denvil, S. Ames, G. Levavasseur, S. Fiore, C. Allen, F. Antonio, K. Berger, P.-A. Bretonnière, L. Cinquini, E. Dart, P. Dwarakanath, K. Druken, B. Evans, L. Franchistéguy, S. Gardoll, E. Gerbier, M. Greenslade, D. Hassell, A. Iwi, M. Juckes, S. Kindermann, L. Lacinski, M. Mirto, A. B. Nasser, P. Nassisi, E. Nienhouse, S. Nikonov, A. Nuzzo, C. Richards, S. Ridzwan, M. Rixen, K. Serradell, K. Snow, A. Stephens, M. Stockhause, H. Vahlenkamp, and R. Wagner, 2021: Coordinating an operational data distribution network for cmip6 data. *Geoscientific Model Development*, **14**, 629–644, doi:10.5194/gmd-14-629-2021.

Pfahl, S. and H. Wernli, 2012: Quantifying the relevance of atmospheric blocking for co-located temperature extremes in the Northern Hemisphere on (sub-)daily time scales. *Geophysical Research Letters*, **39**, doi:10.1029/2012GL052261.

Philipp, A., J. Bartholy, C. Beck, M. Erpicum, P. Esteban, X. Fettweis, R. Huth, P. James, S. Jourdain, F. Kreienkamp, T. Krennert, S. Lykoudis, S. C. Michalides, K. Pianko-Kluczynska, P. Post, D. R. Álvarez, R. Schiemann, A. Spekat, and F. S. Tymvios, 2010: Cost733cat – A database of weather and circulation type classifications. *Physics and Chemistry of the Earth, Parts A/B/C*, **35**, 360–373, doi:https://doi.org/10.1016/j.pce.2009.12.010.

Pinheiro, M. C., P. A. Ullrich, and R. Grotjahn, 2019: Atmospheric blocking and intercomparison of objective detection methods: flow field characteristics. *Climate Dynamics*, **53**, 4189–4216, doi:10.1007/s00382-019-04782-5.

Poli, P., H. Hersbach, D. P. Dee, P. Berrisford, A. J. Simmons, F. Vitart, P. Laloyaux, D. G. Tan, C. Peubey, J.-N. Thépaut, Y. Trémolet, E. V. Hólm, M. Bonavita, L. Isaksen, and M. Fisher, 2016: ERA-20C: An atmospheric reanalysis of the twentieth century. *Journal of Climate*, **29**, 4083–4097, doi:10.1175/JCLI-D-15-0556.1.

Prein, A. F., M. S. Bukovsky, L. O. Mearns, C. L. Bruyère, and J. M. Done, 2019: Simulating North American Weather Types With Regional Climate Models. *Frontiers in Environmental Science*, **7**, 36, doi:10.3389/fenvs.2019.00036.

Preisendorfer, R. W. and C. D. Mobley, 1988: *Principal component analysis in meteorology and oceanography*. Number 17 in Developments in atmospheric science, Elsevier ; Distributors for

the U.S. and Canada, Elsevier Science Pub. Co, Amsterdam ; New York : New York, NY, U.S.A.

Priestley, M. D. K., D. Ackerley, J. L. Catto, K. I. Hodges, R. E. McDonald, and R. W. Lee, 2020: An Overview of the Extratropical Storm Tracks in CMIP6 Historical Simulations. *Journal of Climate*, **33**, 6315–6343, doi:10.1175/JCLI-D-19-0928.1.

Priestley, M. D. K. and J. L. Catto, 2022: Future changes in the extratropical storm tracks and cyclone intensity, wind speed, and structure. *Weather and Climate Dynamics*, **3**, 337–360, doi:10.5194/wcd-3-337-2022.

Putnikovic, S., I. Tosic, and V. Durdevic, 2016: Circulation weather types and their influence on precipitation in serbia. *Meteorology and Atmospheric Physics*, **128**, doi:10.1007/s00703-016-0432-6.

Qasmi, S. and A. Ribes, 2022: Reducing uncertainty in local temperature projections. *Science Advances*, **8**, eabo6872, doi:10.1126/sciadv.abo6872.

R Core Team, 2020: *R: A Language and Environment for Statistical Computing*. R Foundation for Statistical Computing, Vienna, Austria.
URL https://www.R-project.org/

Ramon, J., L. Lledó, C. A. Ferro, and F. J. Doblas-Reyes, 2024: Uncertainties in the observational reference: Implications in skill assessment and model ranking of seasonal predictions. *Quarterly Journal of the Royal Meteorological Society*, **150**, 897–910, doi:10.1002/qj.4628.

Ramos, A. M., N. Cortesi, and R. M. Trigo, 2014a: Circulation weather types and spatial variability of daily precipitation in the Iberian Peninsula. *Frontiers in Earth Science*, **2**, doi:10.3389/feart.2014.00025.

— 2014b: Circulation weather types and spatial variability of daily precipitation in the Iberian Peninsula. *Frontiers in Earth Science*, **2**, doi:10.3389/feart.2014.00025, 00037.

Ramos, A. M., M. N. Lorenzo, and L. Gimeno, 2010: Compatibility between modes of low-frequency variability and circulation types: A case study of the northwest Iberian Peninsula. *Journal of Geophysical Research: Atmospheres*, **115**, doi:10.1029/2009JD012194.

Rex, D. F., 1950: Blocking action in the Middle Troposphere and its effect upon regional climate. *Tellus*, **2**, 196–211, doi:10.1111/j.2153-3490.1950.tb00331.x.

Riahi, K., D. P. van Vuuren, E. Kriegler, J. Edmonds, B. C. O'Neill, S. Fujimori, N. Bauer, K. Calvin, R. Dellink, O. Fricko, W. Lutz, A. Popp, J. C. Cuaresma, S. Kc, M. Leimbach, L. Jiang, T. Kram, S. Rao, J. Emmerling, K. Ebi, T. Hasegawa, P. Havlik, F. Humpenöder, L. A. Da Silva, S. Smith, E. Stehfest, V. Bosetti, J. Eom, D. Gernaat, T. Masui, J. Rogelj, J. Strefler, L. Drouet, V. Krey, G. Luderer, M. Harmsen, K. Takahashi, L. Baumstark, J. C. Doelman, M. Kainuma, Z. Klimont, G. Marangoni, H. Lotze-Campen, M. Obersteiner, A. Tabeau, and M. Tavoni, 2017: The Shared Socioeconomic Pathways and their energy, land use, and greenhouse gas emissions implications: An overview. *Global Environmental Change*, **42**, 153–168, doi:10.1016/j.gloenvcha.2016.05.009.
URL https://www.sciencedirect.com/science/article/pii/S0959378016300681

Riahi, K., D. Vuuren, E. Kriegler, J. Edmonds, B. O'Neill, S. Fujimori, N. Bauer, K. Calvin, R. Dellink, O. Fricko, W. Lutz, A. Popp, J. Crespo Cuaresma, S. Kc, M. Leimbach, L. Jiang, T. Kram, S. Rao, J. Emmerling, and M. Tavoni, 2016: The shared socioeconomic pathways and their energy, land use, and greenhouse gas emissions implications: An overview. *Global Environmental Change*, **42**, doi:10.1016/j.gloenvcha.2016.05.009.

Ribes, A., S. Qasmi, and N. P. Gillett, 2021: Making climate projections conditional on historical observations. *Science Advances*, **7**, eabc0671, doi:10.1126/sciadv.abc0671.

Rodríguez-Puebla, C., S. M. Ayuso, M. D. Frías, and L. A. García-Casado, 2007: Effects of climate variation on winter cereal production in Spain. *Climate Research*, **34**, 223–232, doi:https://doi.org/10.3354/cr00700.

Rodríguez-Puebla, C., A. H. Encinas, L. A. García-Casado, and S. Nieto, 2010: Trends in warm days and cold nights over the Iberian Peninsula: relationships to large-scale variables. *Climatic Change*, **100**, 667–684, doi:10.1007/s10584-009-9721-0.

Rogers, J. C., 1997: North Atlantic storm track variability and its association to the North Atlantic Oscillation and climate variability of northern Europe. *Journal of Climate*, **10**, 1635–1647, doi:https://doi.org/10.1175/1520-0442(1997)010%3C1635:NASTVA%3E2.0.CO;2.

Rohrer, M., S. Brönnimann, O. Martius, C. C. Raible, M. Wild, and G. P. Compo, 2018: Representation of Extratropical Cyclones, Blocking Anticyclones, and Alpine Circulation Types in Multiple Reanalyses and Model Simulations. *Journal of Climate*, **31**, 3009–3031, doi:10.1175/JCLI-D-17-0350.1.
URL https://doi.org/10.1175/JCLI-D-17-0350.1

Rousi, E., K. Kornhuber, G. Beobide-Arsuaga, F. Luo, and D. Coumou, 2022: Accelerated western European heatwave trends linked to more-persistent double jets over Eurasia. *Nature Communications*, **13**, 3851, doi:10.1038/s41467-022-31432-y, number: 1 Publisher: Nature Publishing Group.

Sarricolea, P., O. Meseguer-Ruiz, J. Martin-Vide, and L. Outeiro, 2018: Trends in the frequency of synoptic types in central-southern chile in the period 1961–2012 using the jenkinson and collison synoptic classification. *Theoretical and Applied Climatology*, **134**, doi:10.1007/s00704-017-2268-5.

Schwierz, C., M. Croci-Maspoli, and H. C. Davies, 2004: Perspicacious indicators of atmospheric blocking. *Geophysical Research Letters*, **31**, doi:https://doi.org/10.1029/2003GL019341.

Seneviratne, S., M. Donat, A. Pitman, R. Knutti, and R. Wilby, 2016: Allowable co2 emissions based on regional and impact-related climate targets. *Nature*, **529**, 477–483, doi:10.1038/nature16542.

Seneviratne, S. and M. Hauser, 2020: Regional climate sensitivity of climate extremes in cmip6 versus cmip5 multimodel ensembles. *Earth's Future*, **8**, e2019EF001474, doi:https://doi.org/10.1029/2019EF001474.

Seneviratne, S., X. Zhang, M. Adnan, W. Badi, A. Luca, S. Ghosh, I. Iskandar, J. Kossin, S. Lewis, F. Otto, I. Pinto, M. Satoh, S. Vicente-Serrano, M. Wehner, B. Zhou, V. Masson-Delmotte, P. Zhai, A. Pirani, S. Connors, C. Péan, S. Berger, N. Caud, Y. Chen, L. Goldfarb, M. Gomis, M. Huang, K. Leitzell, E. Lonnoy, J. Matthews, T. Maycock, T. Waterfield, O. Yelekçi, R. Yu, and B. e. Zhou, 2021: *Climate Change 2021: The physical science basis contribution of Working Group I to the Sixth Assessment Report of the Intergovernmental Panel on Climate Change*, Cambridge University Press. 1513–1766.

Sharma, K. K. and A. Seal, 2019: Modeling uncertain data using monte carlo integration method for clustering. *Expert Systems with Applications*, **137**, 100 – 116, doi:https://doi.org/10.1016/j.eswa.2019.06.050.

Shaw, T. A., J. M. Arblaster, T. Birner, A. H. Butler, D. I. Domeisen, C. I. Garfinkel, H. Garny, K. M. Grise, and A. Y. Karpechko, 2024: Detected climate change signals in atmospheric circulation: mechanisms, puzzles and opportunities. *Authorea Preprints*, doi:https://doi.org/10.22541/essoar.171440118.83921530/v1.

Sillmann, J. and M. Croci-Maspoli, 2009: Present and future atmospheric blocking and its impact on European mean and extreme climate. *Geophysical Research Letters*, **36**, L10702, doi:10.1029/2009GL038259.

Sillmann, J., M. Croci-Maspoli, M. Kallache, and R. W. Katz, 2011: Extreme cold winter temperatures in Europe under the influence of North Atlantic atmospheric blocking. *Journal of Climate*, **24**, 5899–5913, doi:10.1175/2011JCLI4075.1, publisher: American Meteorological Society Section: Journal of Climate.

Soares, P. M. M., D. Maraun, S. Brands, M. W. Jury, J. M. Gutiérrez, D. San-Martín, E. Hertig, R. Huth, A. Belušić Vozila, R. M. Cardoso, S. Kotlarski, P. Drobinski, and A. Obermann-Hellhund, 2019: Process-based evaluation of the value perfect predictor experiment of statistical downscaling methods. *International Journal of Climatology*, **39**, 3868–3893, doi:10.1002/joc.5911.

Sobolowski, S., S. Somot, J. Fernandez, G. Evin, D. Maraun, S. Kotlarski, M. Jury, R. E. Benestad, C. Teichmann, O. B. Christensen, B. Katharina, E. Buonomo, E. Katragkou, C. Steger, S. Sørland, G. Nikulin, C. McSweeney, A. Dobler, T. Palmer, R. Wilke, J. Boé, L. Brunner, A. Ribes, S. Qasmi, P. Nabat, F. Sevault, T. Oudar, and S. Brands, 2023: EURO-CORDEX CMIP6 GCM Selection & Ensemble Design: Best Practices and Recommendations.

Sousa, P. M., R. M. Trigo, D. Barriopedro, P. M. M. Soares, A. M. Ramos, and M. L. R. Liberato, 2017: Responses of European precipitation distributions and regimes to different blocking locations. *Climate Dynamics*, **48**, 1141–1160, doi:10.1007/s00382-016-3132-5.

Spellman, G., 2017: An assessment of the jenkinson and collison synoptic classification to a continental mid-latitude location. *Theoretical and Applied Climatology*, **128**, doi:10.1007/s00704-015-1711-8.

Stensrud, D., 2007: Parametrization schemes. keys to understanding numerical weather prediction models. reprint of the 2007 hardback ed. *Parameterization Schemes: Keys to Understanding Numerical Weather Prediction Models*, doi:10.1017/CBO9780511812590.

Sterl, A., 2004: On the (In)Homogeneity of Reanalysis Products. *Journal of Climate*, **17**, 3866–3873, doi:10.1175/1520-0442(2004)017¡3866:OTIORP¿2.0.CO;2, publisher: American Meteorological Society Section: Journal of Climate.

Strommen, K., I. Mavilia, S. Corti, M. Matsueda, P. Davini, J. von Hardenberg, P.-L. Vidale, and R. Mizuta, 2019: The sensitivity of euro-atlantic regimes to model horizontal resolution.

Geophysical Research Letters, **46**, 7810–7818, doi:https://doi.org/10.1029/2019GL082843.
URL https://agupubs.onlinelibrary.wiley.com/doi/abs/10.1029/2019GL082843

Stryhal, J. and R. Huth, 2017: Classifications of Winter Euro-Atlantic Circulation Patterns: An Intercomparison of Five Atmospheric Reanalyses. *Journal of Climate*, **30**, 7847–7861, doi:10.1175/JCLI-D-17-0059.1.
URL https://doi.org/10.1175/JCLI-D-17-0059.1

Sáenz, J., C. Rodríguez-Puebla, J. Fernández, and J. Zubillaga, 2001: Interpretation of interannual winter temperature variations over southwestern Europe. *Journal of Geophysical Research: Atmospheres*, **106**, 20641–20651, doi:https://doi.org/10.1029/2001JD900247.

Taylor, K. E., R. J. Stouffer, and G. A. Meehl, 2012: An overview of cmip5 and the experiment design. *Bulletin of the American Meteorological Society*, **93**, 485–498, doi:10.1175/BAMS-D-11-00094.1.

Team, C. M. B. T., 2024: Cmip7 assessment fast track diagnostics list for the rapid evaluation framework.

Thomas, J. L., D. W. Waugh, and A. Gnanadesikan, 2015: Southern hemisphere extratropical circulation: Recent trends and natural variability. *Geophysical Research Letters*, **42**, 5508–5515, doi:https://doi.org/10.1002/2015GL064521.

Thompson, D., S. Solomon, P. Kushner, M. England, K. Grise, and D. Karoly, 2011: Signatures of the antarctic ozone hole in southern hemisphere surface climate change. *Nature Geoscience*, **4**, 741–749, doi:10.1038/ngeo1296.

Thompson, D. W. J. and S. Solomon, 2002: Interpretation of recent Southern Hemisphere climate change. *Science (New York, N.Y.)*, **296**, 895–899, doi:10.1126/science.1069270.

Tokarska, K. B., M. B. Stolpe, S. Sippel, E. M. Fischer, C. J. Smith, F. Lehner, and R. Knutti, 2020: Past warming trend constrains future warming in cmip6 models. *Science Advances*, **6**, eaaz9549, doi:10.1126/sciadv.aaz9549.

Tost, H., P. Jöckel, and J. Lelieveld, 2006: Influence of different convection parameterisations in a gcm. *Atmospheric Chemistry and Physics*, **6**, 5475–5493, doi:10.5194/acp-6-5475-2006.
URL https://acp.copernicus.org/articles/6/5475/2006/

Trenberth, K. E., 1997: The definition of el niño. *Bulletin of the American Meteorological Society*, **78**, 2771 – 2778, doi:10.1175/1520-0477(1997)078¡2771:TDOENO¿2.0.CO;2.

Trenberth, K. E. and L. Smith, 2005: The mass of the atmosphere: A constraint on global analyses. *Journal of Climate*, **18**, 864 – 875, doi:10.1175/JCLI-3299.1.

Trigo, R. M. and C. C. DaCamara, 2000: Circulation weather types and their influence on the precipitation regime in Portugal. *International Journal of Climatology*, **20**, 1559–1581, doi:10.1002/1097-0088(20001115)20:13%3C1559::AID-JOC555%3E3.0.CO;2-5.

Trigo, R. M., T. J. Osborn, and J. M. Corte-Real, 2002: The North Atlantic Oscillation influence on Europe: climate impacts and associated physical mechanisms. *Climate Research*, **20**, 9–17, doi:10.3354/cr020009.

Trigo, R. M., D. Pozo-Vázquez, T. J. Osborn, Y. Castro-Díez, S. Gámiz-Fortis, and M. J. Esteban-Parra, 2004: North Atlantic Oscillation influence on precipitation, river flow and water resources in the Iberian Peninsula. *International Journal of Climatology*, **24**, 925–944, doi:https://doi.org/10.1002/joc.1048.

Tuel, A. and E. A. B. Eltahir, 2020: Why is the mediterranean a climate change hot spot? *Journal of Climate*, **33**, 5829 – 5843, doi:10.1175/JCLI-D-19-0910.1.

Turco, M., A. Sanna, S. Herrera, M.-C. Llasat, and J. M. Gutiérrez, 2013: Large biases and inconsistent climate change signals in ENSEMBLES regional projections. *Climatic Change*, **120**, 859–869, doi:10.1007/s10584-013-0844-y.

Turner, A. and H. Annamalai, 2012: Climate change and the south asian monsoon. *Nature Climate Change*, **2**, 587–595, doi:10.1038/nclimate1495.

Tveito, O., R. Huth, A. Philipp, P. Post, M. Pasqui, P. Esteban, C. Beck, M. Demuzere, and C. Prudhomme, 2016: *Harmonization and Application of Weather Type Classifications for European Regions*. Final Scientific Report, COST Action 733, 422 pp.

van den Dool, H. M., S. Saha, and A. Johansson, 2000: Empirical orthogonal teleconnections. *Journal of Climate*, **13**, 1421 – 1435, doi:10.1175/1520-0442(2000)013¡1421:EOT¿2.0.CO;2.

Van Loon, H. and J. C. Rogers, 1978: The seesaw in winter temperatures between greenland and northern Europe. Part I: General description. *Monthly Weather Review*, **106**, 296–310, doi:https://doi.org/10.1175/1520-0493(1978)106¡0296:TSIWTB¿2.0.CO;2.

van Vuuren, D., J. Edmonds, M. Kainuma, K. Riahi, A. Thomson, K. Hibbard, G. Hurtt, T. Kram, V. Krey, J.-F. Lamarque, T. Masui, M. Meinshausen, N. Nakicenovic, S. Smith, and S. Rose, 2011: The representative concentration pathways: an overview. climatic change. this issue. *Climatic Change*, **109**, 5–31, doi:10.1007/s10584-011-0148-z.

Vautard, R., A. Gobiet, S. Sobolowski, E. Kjellström, A. Stegehuis, P. Watkiss, T. Mendlik, O. Landgren, G. Nikulin, C. Teichmann, and D. Jacob, 2014: The European climate under a 2 °C global warming. *Environmental Research Letters*, **9**, 034006, doi:10.1088/1748-9326/9/3/034006.

Vial, J. and T. Osborn, 2012: Assessment of atmosphere-ocean general circulation model simulations of winter northern hemisphere atmospheric blocking. *Climate Dynamics*, **39**, 95–112, doi:10.1007/s00382-011-1177-z.

Voskresenskaya, E. N., V. N. Maslova, A. S. Lubkov, and V. Y. Zhuravskiy, 2022: Present and future changes in winter cyclonic activity in the mediterranean–black sea region in the 21st century based on an ensemble of cmip6 models. *Atmosphere*, **13**, doi:10.3390/atmos13101573.

Wallace, J. M. and D. S. Gutzler, 1981: Teleconnections in the geopotential height field during the Northern Hemisphere winter. *Monthly weather review*, **109**, 784–812, doi:https://doi.org/10.1175/1520-0493(1981)109¡0784:TITGHF¿2.0.CO;2.

Wallace, J. M. and P. V. Hobbs, 2006: *Atmospheric Science: An Introductory Survey*. Elsevier Academic Press, Amsterdam, 2nd edition.

Wallace, J. M., G.-H. Lim, and M. L. Blackmon, 1988: Relationship between Cyclone Tracks, Anticyclone Tracks and Baroclinic Waveguides. *Journal of the Atmospheric Sciences*, **45**, 439–462, doi:10.1175/1520-0469(1988)045¡0439:RBCTAT¿2.0.CO;2.

Wang, X. L., V. R. Swail, and F. W. Zwiers, 2006: Climatology and Changes of Extratropical Cyclone Activity: Comparison of ERA-40 with NCEP–NCAR Reanalysis for 1958–2001. *Journal of Climate*, **19**, 3145–3166, doi:10.1175/JCLI3781.1.
URL https://doi.org/10.1175/JCLI3781.1

Wang, Y. and X. Sun, 2020: Weather type classification and its relation to precipitation over southeastern China. *International Journal of Climatology*, doi:10.1002/joc.6747.

Weijs, S. V., R. van Nooijen, and N. van de Giesen, 2010: Kullback–Leibler Divergence as a Forecast Skill Score with Classic Reliability–Resolution–Uncertainty Decomposition. *Monthly Weather Review*, **138**, 3387–3399, doi:10.1175/2010MWR3229.1.

Wilkinson, M., M. Dumontier, I. J. Aalbersberg, G. Appleton, M. Axton, A. Baak, N. Blomberg, J.-W. Boiten, L. O. Bonino da Silva Santos, P. Bourne, J. Bouwman, A. Brookes, T. Clark, M. Crosas, I. Dillo, O. Dumon, S. Edmunds, C. Evelo, R. Finkers, and B. Mons, 2016: The

fair guiding principles for scientific data management and stewardship. *Scientific Data*, **3**, doi:10.1038/sdata.2016.18.

Williams, D. N., V. Balaji, L. Cinquini, S. Denvil, D. Duffy, B. Evans, R. Ferraro, R. Hansen, M. Lautenschlager, and C. Trenham, 2016: A Global Repository for Planet-Sized Experiments and Observations. *Bulletin of the American Meteorological Society*, **97**, 803–816, doi:10.1175/BAMS-D-15-00132.1.
URL https://journals.ametsoc.org/doi/10.1175/BAMS-D-15-00132.1

WMO, 2017: WMO Guidelines on the Calculation of Climate Normals. Technical Report WMO No. 1203, World Meteorological Organization, ISBN:978-92-63-11203-3.

Woollings, T., M. Drouard, C. O'Reilly, D. Sexton, and C. Mcsweeney, 2023: Trends in the atmospheric jet streams are emerging in observations and could be linked to tropical warming. *Communications Earth & Environment*, **4**, 125 (2023), doi:10.1038/s43247-023-00792-8.

Woollings, T., B. Hoskins, M. Blackburn, and P. Berrisford, 2008: A New Rossby Wave–Breaking Interpretation of the North Atlantic Oscillation. *Journal of the Atmospheric Sciences*, **65**, 609–626, doi:10.1175/2007JAS2347.1.
URL https://doi.org/10.1175/2007JAS2347.1

Wu, J., C. Li, Z. Ma, Z. bin Sun, X. Zhu, and F. Dong, 2020: Influence of meteorological conditions on ozone pollution at shangdianzi station based on weather classification. *Huanjing kexue*, **41**, 4864–4873, doi:10.13227/j.hjkx.202003307.

Xiong, J., J. Yang, and J. Nie, 2020: Possible dependence of climate on atmospheric mass: A convection–circulation–cloud coupled feedback. *Journal of the Atmospheric Sciences*, **77**, 3833 – 3846, doi:10.1175/JAS-D-20-0022.1.

Zaplotnik, Z., M. Pikovnik, and L. Boljka, 2022: Recent Hadley Circulation Strengthening: A Trend or Multidecadal Variability? *Journal of Climate*, **35**, 4157 – 4176, doi:10.1175/JCLI-D-21-0204.1.

Zappa, G., L. C. Shaffrey, and K. I. Hodges, 2013: The Ability of CMIP5 Models to Simulate North Atlantic Extratropical Cyclones*. *Journal of Climate*, **26**, 5379–5396, doi:10.1175/JCLI-D-12-00501.1.

Zappa, G. and T. Shepherd, 2017: Storylines of atmospheric circulation change for european regional climate impact assessment. *Journal of Climate*, **30**, doi:10.1175/JCLI-D-16-0807.1.

Zveryaev, I., 2009: Interdecadal changes in the links between European precipitation and atmospheric circulation during boreal spring and fall. *Tellus A: Dynamic Meteorology and Oceanography*, **61**, 50–56, doi:https://doi.org/10.1111/j.1600-0870.2008.00360.x.